

# **Graphene supported Cu(I) nanocatalysts for application in CuAAC reactions and production of resin/graphene nanocomposites**

## **Dissertation**

zur Erlangung des  
Doktorgrades der Naturwissenschaften (Dr. rer. nat.)

der

Naturwissenschaftlichen Fakultät II  
Chemie, Physik und Mathematik

der Martin-Luther-Universität  
Halle-Wittenberg

vorgelegt

von Herr Ali Shaygan Nia  
geb. am 24.03.1985 in Isfahan (Iran)

Gutachter

1. Prof. Dr. Wolfgang H. Binder

2. Prof. Dr. Rolf Mülhaupt

Verteidigung: 14.06.2016

تو خود حجاب خودی حافظ از میان بر خیز

ایمان نامه را تقدیم می کنم به

پدر (حسن)، مادر (شهناز) و مادر بزرگم (امان ایران)

دربای عشق و محبت

برادرانم، بهنام، ایمان و امین

یاران، همیشگی غائب

دوستانم، پری و حسین

حامیان در غربت

و

نذا، ندای قلم، ندای عزیزم

به خاطر عشق و بودنش

## **Acknowledgment**

First of all I would like to thank my supervisor Prof. Dr. Wolfgang H. Binder for giving me the opportunity to work in his group and perform my PhD in this challenging field. I am grateful for his guidance, time for scientific discussions, his help and encouragement during my work.

I am grateful to Dr. Anja Marinow, Dr. Diana Döhler, Philipp Michael, Dr. Sravendra Rana and Dr. Mathias Schultz for giving me their time for fruitful scientific discussion and their help during my PhD thesis.

Special thanks to Ms. Anke Hassi for her support and help during my time in Halle. I also thank Ms. Sussane Tanner, Mr. Norman Diedrich and Ms. Julia Weichhold for preparing the chemicals and running different measurements.

I would like to thank Prof. Thomas Hahn and his group especially Dr. Daniel Teichmann for allowing me to use their instrument, Prof Michael Bron and his group members especially Eik Koslowski for measuring XRD and RAMAN, and Dr Annete Meister for TEM measurements.

I would like to thank all of my colleagues in the working group of Prof. Binder especially Dr. Parvin Zare, Dr. Bhanuprathab Pulagamatta, Dr. Onur Kir, and Ms. Neda Kargarfard.

Finally, I would like to thank my family for supporting me all these years and making all these possible.

**TABLE OF CONTENTS**

<b>ABSTRACT</b> .....	III
<b>KURZDARSTELLUNG</b> .....	III
<b>ABBREVIATIONS</b> .....	VII
<b>I.INTRODUCTION</b> .....	1
1-Graphene-based materials.....	1
2-Synthesis of graphene materials.....	2
2.1-Bottom-up methods.....	3
2.2-Up-bottom methods.....	4
2.2.1-Chemical exfoliation.....	4
3. Metal(oxide)/graphene catalysts (characterization, synthesis and application).....	7
3.1-Preparation methods of metal(oxide)/graphene catalysts.....	8
4-GO, r-GO and their metal(oxide) composites as initiator/catalyst in polymerization reactions ....	17
4.1-Free radical polymerization.....	17
4.1.1-GO as initiator.....	17
4.1.2-Surface functionalization of GO with radical polymerization initiators.....	19
4.1.3-Catalytic effects of GO and r-GO on FRP.....	20
4.2-Controlled Radical Polymerization (CRL).....	22
4.2.1-Atom Transfer Radical Polymerization (ATRP).....	22
4.2.2-Single Electron Transfer Controlled Radical Polymerization (SET-CRP).....	26
4.2.3-Reversible Addition-Fragmentation Chain Transfer Polymerization (RAFT).....	28
4.2.4-Nitroxide Mediated Polymerization (NMP).....	31
4.3-Ionic polymerization.....	32
4.3.1- Cationic polymerization.....	32
4.3.2-Anionic polymerization.....	33
4.4-Polycondensation reactions.....	34
4.5-Insertion-coordination polymerizations.....	34
4.5.1-Ziegler-Natta polymerization.....	35
4.5.2-Polymerization-filling technique (PFT).....	35
4.5.3-Metallocene polymerization.....	36
4.5.4-Ring Opening Metathesis Polymerization (ROMP).....	38
5-Copper Catalyzed Azide-Alkyne Click cycloaddition reaction (CuAAC).....	38
5.1-CuAAC polymerization reaction.....	43
<b>II.SCOPE OF THE THESIS</b> .....	44
1-Objective.....	44



## TABLE OF CONTENTS

2-Concept .....	45
<b>III.RESULT AND DISCUSSION.....</b>	<b>48</b>
1-Click chemistry promoted by graphene supported copper nanomaterials.....	48
2-Carbon-Supported Copper Nanomaterials: Recyclable Catalysts for Huisgen [3+2] Cycloaddition Reactions .....	60
3-Nanocomposites <i>via</i> a direct graphene-promoted “click”-reaction .....	74
<b>IV.SUMMARY .....</b>	<b>92</b>
<b>V.REFERENCES.....</b>	<b>99</b>
<b>VI.APPENDIX .....</b>	<b>107</b>
1-Synthesis of graphene oxide (GO) and reduced graphene oxide(r-GO) .....	107
2-Experimental part.....	110
2.1-Materials .....	110
2.2-Methods .....	110
2.3-Synthesis .....	110
2.3.1-Graphene oxide (GO) .....	110
2.3.2-Reduction reaction of GO to r-GO.....	112

**ABSTRACT**

One of the most important applications of graphene-based materials is the formation of nanocomposite materials, where graphene in bulk-polymer matrix transfer its properties onto the polymeric material. Control of the polymer/graphene interface is essential to generate nanocomposites, thus avoiding the aggregation of the graphene nanoparticles. The direct use of the graphene materials as either the polymerization catalyst or initiator and as additive not only diminishes the agglomeration of particles in composites, but also reduces the process of composite production to a one facile step.

“CuAAC polymerizations” can be very fast and afford polymeric products with high molecular weights within short reaction times at low temperature. Therefore in the scope of this thesis the development of the new resin (polymer)/graphene nanocomposite for high performance applications was achieved *via* CuAAC crosslinking (polymerization) reaction. The reaction was catalyzed by the Cu(I)/graphene materials itself in order to produce nanocomposites with less aggregation of graphene particles, in turn improving the electrical, thermal conductivities and mechanical properties of final resin materials in a one step reaction.

Accordingly, graphene oxide (GO) and reduced graphene oxide (r-GO) have been chosen as graphene-based materials because of their high catalytic activity achievable *via* low cost graphite as the starting material. In the next step, the immobilization of Cu(I) particles on the surface of r-GO *via* both, the “*ex situ* hybridization”, and the “*in situ* crystallization” methods has been accomplished. Different parameters including the loading effects, the catalytic activity including kinetics studies, the recyclability, the leaching and the feasibility of their production in a large scale applicable for the industrial use have been investigated and compared. The “*in situ* crystallization” method was performed in a two step reaction : firstly GO was reacted with copper(II) acetate ( $\text{Cu}(\text{OAc})_2$ ) exchanging the protons of the carboxylic groups of GO with the Cu(II) particles to immobilize Cu(II) onto the surface of GO (GO-Cu(II)), afterwards GO-Cu(II) was thermally reduced in an oven under the stream of nitrogen at 600 °C to obtain r-GO decorated with Cu(I) nanoparticles (TRGO-Cu<sub>2</sub>O). On the other hand, *N*-heterocyclic carbene (NHC) functional groups had been chosen for functionalization of the surface of r-GO *via* the “*ex situ* hybridization” method. Therefore, the surface of r-GO (reduced by ascorbic acid) was functionalized by the imidazolium groups in a three step reaction, subsequently exchanging the proton of the imidazolium groups with Cu(I) to achieve Cu(I)-NHC bond on the surface of r-GO (CRGO-Ima-Cu(I)). Comparing these two methods for the immobilization of Cu(I), the catalyst obtained by the “*in situ* crystallization” (TRGO-Cu<sub>2</sub>O) exhibited higher loadings of copper together with higher catalytic activities towards the CuAAC reaction. Moreover the synthetic pathway towards TRGO-Cu<sub>2</sub>O catalyst was simpler, and could be produced in a large scale, whereas functionalization of

r-GO with the imidazolium groups and anchoring the Cu (I) particles on the NHC groups required a multi step reaction.

For the CuAAC crosslinking (polymerization) reaction between trivalent azide and trivalent alkyne moieties and the production of high performance resin/graphene composite materials, TRGO-Cu<sub>2</sub>O was chosen as catalyst. *In-situ* DSC and *in-situ* melt-rheology measurements proved that by using 4 wt% (0.5 mol% per functional group) of TRGO-Cu<sub>2</sub>O in the crosslinking reaction, the time and the temperature of the crosslinking were efficiently reduced, now exceeding those of commercial homogenous catalysts. The direct use of TRGO-Cu<sub>2</sub>O (4 wt%) as catalyst and filler in the CuAAC crosslinking reaction led to resin/graphene nanocomposite materials with high dispersion of graphene particles as shown by TEM measurement, in turn improving the mechanical properties as revealed by rheology measurements. Additionally broadband dielectric spectroscopy showed that resin/graphene nanocomposite materials were conductive at 0 °C and TGA proved the high thermal resistance ( $T_d \approx 310$  °C) of the final graphene nanocomposite.

## KURZDARSTELLUNG

Eine der bedeutendsten Anwendungen von Graphen-basierten Materialien ist die Entwicklung von Nanokompositen, wobei die Eigenschaften des Graphens durch das Einbetten in eine Polymermatrix auf das verwendete Polymer übertragen werden. Während der Herstellung von Nanokompositen ist die Kontrolle der Graphen-Polymer-Grenzfläche entscheidend, um die Agglomeration der Graphen-Nanopartikel zu vermeiden. Dabei verringert die direkte Nutzung von Graphen-basierten Materialien als Katalysatoren oder Initiatoren für Polymerisationen oder als Additiv nicht nur eine mögliche Agglomeration der Partikel im Nanokomposit, sondern reduziert außerdem den Herstellungsprozess auf einen entscheidenden Schritt.

Polymerisationen basierend auf der Kupfer(I)-katalysierten Azid-Alkin Klick-Reaktion können sehr schnell verlaufen und innerhalb kurzer Reaktionszeiten bei niedrigen Temperaturen polymere Materialien mit hohen Molekulargewichten liefern. Im Rahmen dieser Dissertation wurden neuartige Graphen-basierte Polymernanokomposite oder Kompositharze für Hochleistungs-Anwendungen entwickelt. Dazu wurden Graphen-basierte Kupfer(I)-Katalysatoren für die Kupfer(I)-katalysierte Azid-Alkin Klick-Polymerisation oder -Vernetzungsreaktion hergestellt, um Nanokomposite mit verringerter Agglomeration und besseren mechanischen Eigenschaften sowie verbesserter elektrischer und thermischer Leitfähigkeit der Kompositharze zu erhalten.

Auf Grund der hohen katalytischen Aktivität und der möglichen, kostengünstigen Massenproduktion ausgehend von Graphit wurde für die Darstellung der Graphen-basierten Materialien Graphenoxid (GO) und reduziertes Graphenoxid (rGO) ausgewählt. Im nächsten Schritt wurde für die Immobilisierung der Kupfer(I)-Partikel auf der Oberfläche des reduzierten Graphenoxids sowohl die *ex situ* Hybridisierung als auch die *in situ* Kristallisation verwendet. Anschließend wurden beide Methoden hinsichtlich der Katalysatorbeladung und -aktivität inklusive kinetischer Studien, Recyclbarkeit und Katalysator-Auswaschung und der Realisierbarkeit der großtechnischen Produktion untersucht und verglichen. Die *in situ* Kristallisation wurde in einer zweistufigen Reaktion durchgeführt, wobei im ersten Schritt Graphenoxid mit Kupfer(II)-Acetat ( $\text{Cu}(\text{OAc})_2$ ) umgesetzt wurde. Dabei wurden die Protonen der Carboxylgruppen des Graphenoxids mit den eingesetzten Kupfer(II)-Partikel ausgetauscht und somit Kupfer(II)-Partikel auf der Graphenoxid-Oberfläche immobilisiert. Danach wurde Kupfer(II)-modifiziertes Graphenoxid in einer Stickstoffatmosphäre bei 600 °C thermisch reduziert, um reduziertes Graphenoxid funktionalisiert mit Kupfer(I)-Nanopartikeln zu erhalten (TRGO-Cu<sub>2</sub>O). Bei der *ex situ* Hybridisierung dagegen wurden *N*-heterocyclische Carbene zur Funktionalisierung der Oberfläche des reduzierten Graphenoxids verwendet. Dafür wurde die Oberfläche des reduzierten Graphenoxids (Reduktion mit Ascorbinsäure) in einer dreistufigen Reaktion mit Imidazol-Gruppen modifiziert und anschließend das Proton der angebrachten Imidazol-Gruppe gegen Kupfer(I) ausgetauscht, um Kupfer(I)-funktionalisiertes, reduziertes Graphenoxids zu

erhalten (CRGO-Ima-Cu(I)). Durch Vergleich der verwendeten Methoden für die Immobilisierung von Kupfer(I) zeigte sich für den durch *in situ* Kristallisation erhaltenen Kupfer(I)-Katalysator (TRGO-Cu<sub>2</sub>O) eine höhere Katalysatorbeladung und -aktivität bezüglich der Kupfer(I)-katalysierten Azid-Alkin Klick-Reaktion. Die Darstellung des TRGO-Cu<sub>2</sub>O Katalysators gestaltete sich einfacher und erlaubt somit perspektivisch eine großtechnische Produktion, wohingegen sich das Aufskalieren der mehrstufigen Funktionalisierung des reduzierten Graphenoxids mit Imidazol-Gruppen und die Verankerung der Kupfer(I)-Partikel an die *N*-heterocyclischen Carbene als schwierig erwies.

Dem entsprechend wurde für die Kupfer(I)-katalysierte Azid-Alkin Klick-Polymerisation oder -Vernetzungsreaktion zwischen trivalenten Azid- und trivalenten Alkin-Verbindungen für die Entwicklung der Graphen-basierten Polymernanokompositen oder Kompositharzen für Hochleistungs-Anwendungen der TRGO-Cu<sub>2</sub>O Katalysator ausgewählt. Durch *in situ* DSC- und Schmelzrheologie-Untersuchungen der Vernetzungsreaktion konnte aufgewiesen werden, dass durch Verwendung von 4 Gew.% (0.5 mol% pro funktionelle Gruppe) TRGO-Cu<sub>2</sub>O sowohl die Reaktionszeit als auch die Reaktionstemperatur effizient gesenkt werden konnte und sich somit die Katalysatorleistung vergleichbar zu kommerziellen, homogenen Kupfer(I)-Katalysatoren darstellt. Demnach zeigten TEM- und Rheologie-Messungen, dass durch die Verwendung von TRGO-Cu<sub>2</sub>O (4 Gew.%) als Katalysator und Füllstoff für die Kupfer(I)-katalysierte Azid-Alkin-Vernetzungsreaktion Graphen-basierte Kompositharze mit feiner Dispergierung der Nanopartikel und verbesserten mechanischen Eigenschaften dargestellt werden konnten. Zusätzlich konnte die Leitfähigkeit der erhaltenen Graphen-basierten Kompositharze bei 0 °C und die hohe thermische Stabilität ( $T_d \approx 310$  °C) durch dielektrische Breitband-Spektroskopie und TGA-Messungen gezeigt werden.

## ABBREVIATIONS

AAS	Atomic absorption spectroscopy
AFM	Atomic force microscopy
AIBN	Azobisisobutyronitrile
Ag	Silver
AgNO <sub>3</sub>	Silver nitrate
AlEt <sub>3</sub>	Triethylaluminium
Al <sub>2</sub> O <sub>3</sub>	Aluminium oxide
APTMS	(3-Aminopropyl)trimethoxysilane
APTS(APTES)	(3-Aminopropyl)triethoxysilane
Au	Gold
BuLi	Butyllithium
BuMgCl	Butylmagnesium chloride
Ce	Cerium
CNT	Carbon nanotubes
Co	Cobalt
CO <sub>2</sub>	Carbon dioxide
Co(OAc) <sub>2</sub> ·4H <sub>2</sub> O	Cobalt(II) acetate
Cp <sub>2</sub> ZrCl <sub>2</sub>	Bis(cyclopentadienyl)zirconium dichloride
Cu	Copper
CuAAC	Copper catalyzed azide-alkyne click cycloaddition reaction
Cu(acac) <sub>2</sub>	Copper (II) acetylacetonate
CuBr	Copper (I) bromide
CuCl <sub>2</sub>	Copper(II) chloride
Cu/C	Copper on charcoal
Cu(NO <sub>3</sub> ) <sub>2</sub> ·3·H <sub>2</sub> O	Copper(II) nitrate trihydrate
Cu <sub>2</sub> O	Copper(I) oxide or cuprous oxide
CuO	Copper(II) oxide or cupric oxide
Cu(OAc) <sub>2</sub>	Copper(II) acetate
Cu(OH) <sub>2</sub>	Copper(II) hydroxide
CuSO <sub>4</sub>	Copper(II) sulfate
CVD	Chemical vapor deposition
DCC	<i>N,N'</i> -Dicyclohexylcarbodiimide
DCM	Dichloromethane
DDS	4,4'-Diaminodiphenylsulfone
DMAP	4-Dimethylaminopyridine
DMF	<i>N,N</i> -Dimethylformamide
DMSO	Dimethyl sulfoxide
DSC	Differential scanning calorimetry
EDTA	Ethylenediaminetetraacetic acid
EDX,EDS,XEDS	Energy-dispersive X-ray spectroscopy
EtOH	Ethanol
EPR	Electron paramagnetic resonance
FAAS	Flame atomic absorption spectroscopy,
fcc	face centered cubic
FeCl <sub>3</sub>	Iron(III) chloride
Fe(NO <sub>3</sub> ) <sub>2</sub> ·9·H <sub>2</sub> O	Iron(III) nitrate nonahydrate
Fe <sub>2</sub> O <sub>3</sub>	Iron(II) oxide
FTIR	Fourier transform infrared spectroscopy
FWHM	Full width at half maximum
GPC	Gel permeation chromatography

HAuCl <sub>4</sub>	Chloroauric acid
HEBrIB	2-Hydroxyethyl 2-bromoisobutyrate
H <sub>2</sub> PdCl <sub>4</sub>	Tetrachloropalladic acid
H <sub>2</sub> PtCl <sub>6</sub>	Chloroplatinic acid
HRTEM	High resolution transmission electron microscopy
ICP	Inductively coupled plasma
ICP-AES	Inductively coupled plasma atomic emission spectroscopy
ICP-MS	Inductively coupled plasma mass spectrometry
IL	Ionic liquid
Ir	Iridium
K <sub>2</sub> CO <sub>3</sub>	Potassium carbonate
KMnO <sub>4</sub>	Potassium permanganate
K <sub>2</sub> PdCl <sub>4</sub>	Potassium tetrachloropalladate(II)
MMA	Methyl methacrylate
MAO	Methyl ammonium oxide
MeOH	Methanol
Mg	Magnesium
Mn	Manganese
Mn(OAc) <sub>2</sub> ·4H <sub>2</sub> O	Manganese(II) acetate tetrahydrate
MW	Microwave irradiation
NaBH <sub>4</sub>	Sodium borohydride
NaH	Sodium hydride
N <sub>2</sub> H <sub>4</sub>	Hydrazine
NHC	<i>N</i> -Heterocyclic carbene
Ni	Nickel
Ni(OAc) <sub>2</sub> ·4H <sub>2</sub> O	Nickel(II) acetate
NMR	Nuclear magnetic resonance
NO <sub>2</sub>	Nitrogen dioxide
N <sub>2</sub> O <sub>4</sub>	Dinitrogen tetroxide
NP	Nanoparticles
PA6	Nylon 6, polycaprolactam, polyamide 6
PAA	Poly(acrylic acid)
PAM	Polyacrylamide
PANI	Polyaniline
PDI	Polydispersity index
Pd	Palladium
PDMA	Poly( <i>N,N</i> -dimethylacrylamide)
Pd(NO <sub>3</sub> ) <sub>2</sub>	palladium nitrate
Pd(OAc) <sub>2</sub>	Palladium(II) acetate
PHEMA	Poly(hydroxyethyl methacrylate)
PMMA	Poly(methyl methacrylate)
PS	Polystyrene
PP	Polypropylene
Pt	Platinum
P4VP	Poly(4-vinylpyridine)
Re	Rhenium
ROMP	Ring-opening metathesis polymerization
Ru	Ruthenium
Ru(acac) <sub>3</sub>	Ruthenium(III) acetylacetonate
RuCl <sub>2</sub> (PPh <sub>3</sub> ) <sub>3</sub>	Tris(triphenylphosphine)ruthenium(II) dichloride
SEM	Scanning electron microscope
Si	Silicon
SiO <sub>2</sub>	Silicon dioxide

## ABBREVIATIONS

SOCl <sub>2</sub>	Thionyl chloride
TEM	Transmission electron microscopy
TGA	Thermogravimetric analysis
THF	Tetrahydrofuran
TiCl <sub>4</sub>	Titanium tetrachloride
TiO <sub>2</sub>	Titanium dioxide
TRGO	Thermally reduced graphene oxide
VO(acac) <sub>2</sub>	Vanadyl acetylacetonate
UV-Vis	Ultraviolet–visible
XPS	X-ray photoelectron spectroscopy
XRD	X-ray diffraction



Part of the introduction has been submitted as “Graphene as initiator/catalyst in polymerization chemistry” (Shaygan Nia, A., and Binder, W. H.).

The results of the Results and Discussion part of this thesis are based on three publications. The first and second sections related to preparation of heterogeneous Cu(I) catalyst on the surface of graphene-based materials refer to “Click chemistry promoted by graphene supported copper nanomaterials”(Shaygan Nia, A., Rana, S., Döhler, D., Noirfalise, X., Belfiore, A. and Binder, W. H. Chem. Commun., 2014. 50, 15374-15377.) and with “Carbon Supported Copper Nanomaterials: Recyclable Catalysts for Huisgen [3+2] Cycloaddition Reaction”(Shaygan Nia, A., Rana, S., Döhler, D., Jirsa, F., Meister, M., Guadagno, L., Koslowski, E., Bron, M. and Binder, W. H. Chem. Eur. J., 2015. 21(30): p. 10763-10770) for the “*in situ* crystallization” and “*ex situ* hybridization” routes, respectively. Text and figures have been adapted with permission from the Royal Society of Chemistry (Copyright 2014) and John Wiley and sons (Copyright 2015).

In the third section of the Results and Discussion part, the application of these heterogeneous catalyst in CuAAC crosslinking reaction for resin/graphene nanocomposite production and their effect on the final physical and mechanical properties of crosslinked resin was investigated , and the results dealing with “Nanocomposites *via* a direct graphene-promoted "click"-reaction” (Shaygan Nia, A., Rana, S., Döhler, D., Osim, W. and Binder, W. H. Polymer., 2015. 79, 21-28)Text and figures have been adapted with permission from Elsevier Ltd. (Copyright 2015).

## I.INTRODUCTION

### 1-Graphene-based materials

Graphene, a single layer of two-dimensional  $sp^2$ -hybridized carbon has attracted a significant research interest due to its unique electrical<sup>[1]</sup> (7200 S/m) and thermal<sup>[2]</sup> ( $4.84\pm 0.44$ ) $\times 10^3$  to ( $5.30\pm 0.48$ ) $\times 10^3$  W/mK) conductivity, including exceptional mechanical (tensile strength :  $130\pm 10$  GPa and Young modulus : 1 TPa)<sup>[3]</sup>, optical<sup>[4]</sup> and chemical properties. These properties endow graphene with a wide range of applications in the field of electronics<sup>[5]</sup>, biomedicine<sup>[6]</sup>, and tribology<sup>[7]</sup>. Of particular importance is the formation of polymer nanocomposite materials, where graphene is intimately mixed with a bulk-polymer matrix, in turn imparting its properties onto the polymeric material. However the difficulties in the producing graphene in a large scale through the mechanical exfoliation of graphite or CVD methods, and its poor processability limited its applications in the polymer composite production. In contrast to a single layer graphene sheet, multi layers (5-6 layers) of graphene oxide (GO) and reduced graphene oxide (rGO) with variety of the defects and oxygen-containing groups on their surfaces are easily available by controlled chemical reactions and can be produced on a large scale. Thus in the past a significant number of the polymer/GO composite materials with properties such as high stiffness and enhanced mechanical properties<sup>[8]</sup>, improved conductivity<sup>[9]</sup> have been developed using GO and r-GO, where the proper distribution of them within the polymer is crucial for its final function. Utilizing graphene-based materials as either the polymerization initiator or catalyst and as an additive not only diminishes the agglomeration of the particles in composites but also reduces the process of the composite production to a one facile step which requires no purification regarding to strong acid initiators and metal particles catalysts.

Graphene-based materials like graphene<sup>[1,10]</sup>, graphene oxide (GO)<sup>[11]</sup> and reduced graphene oxide (r-GO) (Figure 1a) are valuable to be used as the support of the catalyst and as catalyst itself<sup>[12]</sup> due to their special properties like high absorption capacity, large surface area, high thermal<sup>[2]</sup> and electrical conductivity<sup>[1]</sup> and good biocompatibility. For example graphene has high specific surface area near to  $2600\text{ m}^2.\text{g}^{-1}$ <sup>[13]</sup>, which is in turn increasing the dispersion of the metal particles on the surface and the active site of the catalyst. Furthermore, the highly conjugated structure of the graphene materials increases the absorption properties towards the metal(oxide) catalysts<sup>[14]</sup>, and enhances the electron mobility of graphene which facilitates the electron transfer during the catalytic reactions improving its catalytic activity<sup>[15]</sup>. Finally, graphene also exhibits high chemical, thermal, optical and electrochemical stabilities<sup>[16]</sup>, which may improve a lifetime of the catalyst. In general, the two-dimensional graphene and other high-quality graphene materials prepared by the micromechanical exfoliation, the epitaxial growth and the chemical vapor deposition (CVD) possess band gaps equal or close to zero, therefore displaying low catalytic activities<sup>[17]</sup>. However, this problem can be tackled by

doping these graphene materials with different heteroatoms like nitrogen or boron which leads to more active sites and tuning of their band gaps <sup>[18]</sup>. On the other hand, although the residual groups and defects diminish the novel properties of the single layer graphene, they increase the band gap of GO leading to the high catalytic activity of the pristine GO and the GO/metal(oxide) hybrids. Moreover further functionalization on the surface of the GO and r-GO enables to form stable dispersions in the aqueous or organic media, and to be blended and connected with the metal(oxide) nanoparticles to form graphene/metal composites <sup>[12, 18a, 18b, 19]</sup>. Importantly, GO and r-GO can be obtained at relatively low cost on a large scale by using graphite as the starting material <sup>[11, 20]</sup>. Therefore, they are promising support for the catalysts and also attractive components for developing new catalysts.

In addition, defects on the surface of GO and r-GO can create free radicals, and the oxygen-containing groups on the surface of GO and r-GO enable the functionalization of the surface with different residual groups useful for initiation of the different polymerization reactions.

All of these properties make GO, r-GO, and their metal(oxide) hybrids promising materials in the polymerization reactions enabling many polymerization processes from the graphene surface, often even without the need of initiators and catalysts.

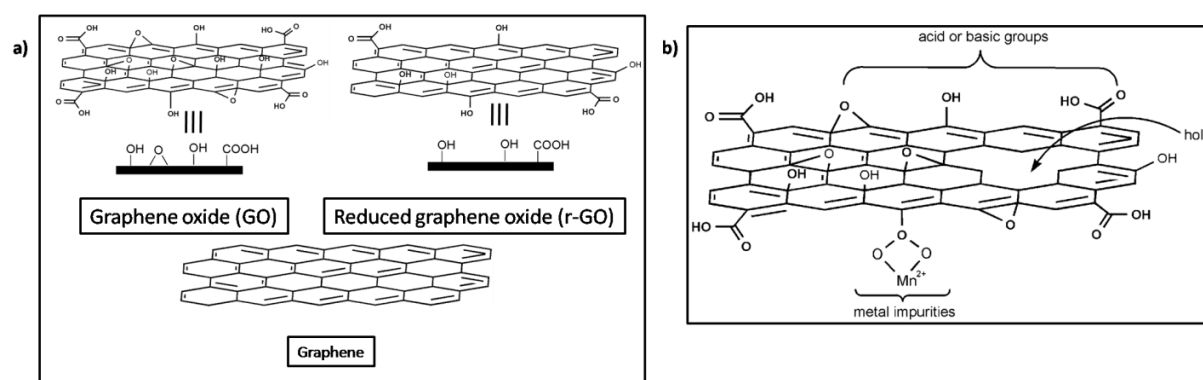


**Figure 1.** a) Different chemical structure of graphene-based materials depending on their mode of preparation b) the defects and residual groups on the surface of graphene materials active in chemical reactions (redrawn from reference <sup>[12b]</sup>)

Critical to this understanding is a closer look onto the exact chemical nature of the graphene material surfaces, which strongly depend on the mode of the preparation creating the functional groups and defects on the surfaces. A schematic picture of different chemical compositions of the graphene surfaces is presented in Figure 1

## 2-Synthesis of graphene materials

Many efforts have been made to synthesize graphene <sup>[1, 10]</sup>, not only in high yields, but also with a quality near to the single layer two-dimensional graphene and with less structural defects. Structural defects (Figure 1b) are mainly related to the formation of sp<sup>3</sup> hybrids and the destruction of sp<sup>2</sup>

hybrids in the structure of the two-dimensional graphene, often reducing the physical properties like electrical conductivity<sup>[21]</sup> and tensile strength<sup>[22]</sup>.

## 2.1-Bottom-up methods

In general the production of graphene can be divided in two main routes: the bottom-up, and up-bottom methodologies. In the bottom-up approach (Figure 2a), graphene is synthesized directly from different carbon sources and precursors like the CVD, graphitization and organic synthesis methods. In contrast, in the up-bottom method (Figure 3a), the synthesis starts from graphite, and the layers of graphite are exfoliated to few layers (1-5) by different forces like the mechanical<sup>[1, 23]</sup>, chemical<sup>[24]</sup>, thermal<sup>[25]</sup> and electrochemical<sup>[26]</sup> forces.

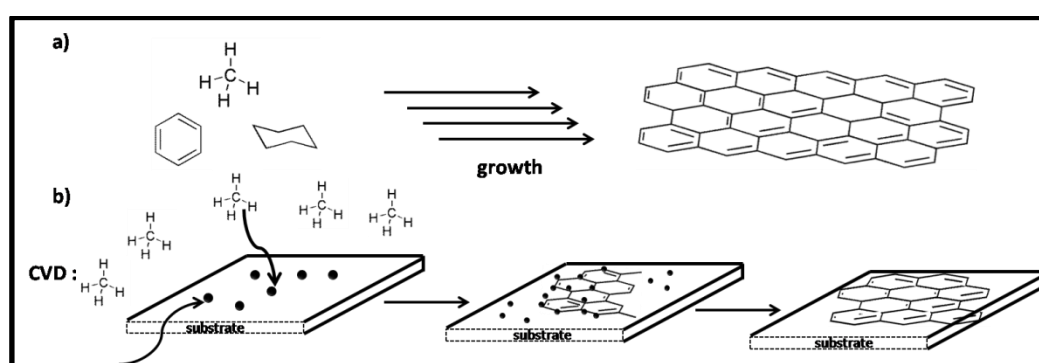


**Figure 2.** a) Bottom-up synthetic method towards graphene-based materials, and b) CVD method (redrawn from reference<sup>[12b]</sup>)

In CVD methods<sup>[27]</sup>, the graphene growth has been obtained *via* a simple thermal decomposition of hydrocarbons such as methane on the surface of the transition metals (Ru, Ir, Co, Re, Ni, Pt, Pd, Cu) which also act as a dehydrogenation catalysts for hydrocarbons. In this process, carbon atoms are dissolved to the metal substrate, and then upon a cooling they segregate from the surface out of a metastable carbon–metal solid solution (Figure 2b). Furthermore the carbon solubility in the metal and the growth conditions determine the deposition mechanism which ultimately also defines the morphology and the thickness of the graphene films. Among transition metals nickel and copper are frequently used as substrates in the CVD method<sup>[27a, 27b]</sup>, since they have a lattice similar to the densely packed hexagonal lattice of graphene and they also have similar lattice constants. Furthermore, the thermal decomposition of SiC(0001) substrate at high temperatures (1000-1600 °C) and the graphitization of detached carbon atoms from Si leads to a single layer graphene<sup>[28]</sup>. In addition to these methods which are based on the application of metal substrates, graphene can be synthesized through the organic synthesis to obtain polyaromatic graphene like materials<sup>[29]</sup> or *via* pyrolysis of the carbonaceous residues which are mainly biopolymers such as polysaccharides and chitosan<sup>[30]</sup>.

## 2.2-Up-bottom methods

Since the van der Waals interaction energy between the layers of graphite is about  $2 \text{ eV/nm}^2$ , the force required to exfoliate the graphite layer is low  $\approx 300 \text{ nN}/\mu\text{m}^2$  [23j]. This low energy can be achieved by simple mechanical forces like rubbing microfabricated arrays of graphite [23g], or even by shear force of an AFM cantilever [23j]. However most of these methods lead to the multilayers of graphene (6-7 layers) with structural defects, which possess different physical properties than a single layer two-dimensional graphene. In 2004, Geim and Novoselov were successful to produce the single layer of graphene from a thick graphite flake by repeatedly cleaving the layers with a scotch tape [1] which led to the Nobel prize in physics in 2010 “ for groundbreaking experiments regarding the two-dimensional material graphene”.

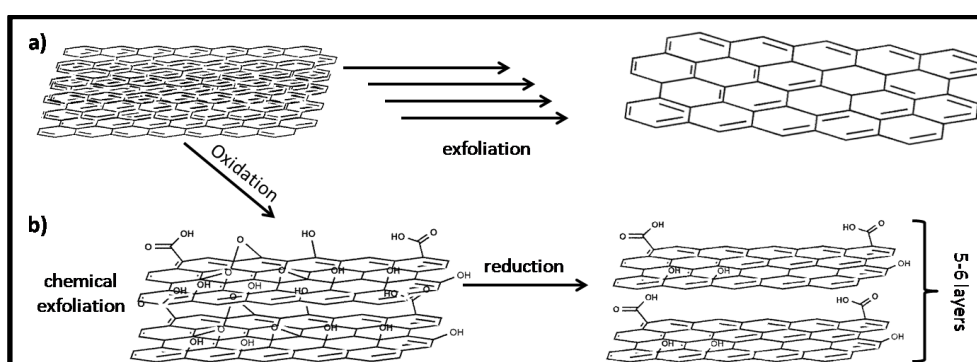


**Figure 3.** a) Up-bottom synthetic methods towards the graphene-based materials and b) chemical exfoliation method

Graphite can be also exfoliated in liquid environments by using ultrasound force including three steps: 1) dispersion of graphite in a liquid environment 2) exfoliation *via* sonication and 3) subsequent purification. In this process, shear forces and cavitations between micrometer bubbles caused by the sonication and graphite sheets induce exfoliation [23i]. The first successful exfoliation was done in NMP (*N*-methyl-2-pyrrolidone) as an organic solvent environment, however the yield was low (1 wt%) and the solubility was nearly  $0.01 \text{ mg/mL}$  [23b]. Even increasing the time of the sonication to 460 h [23d], and changing the solvent to *ortho*-dichlorobenzene [23a], or DMF [23c] did not improve the process due to the aggregation of graphene sheets. However changing the liquid environment to surfactant-assisted solvents [23e, 23f] or ionic liquids could [23h] increase the yield and stability of the final graphene product because of steric and electrostatic repulsions.

### 2.2.1-Chemical exfoliation

**Graphene oxide (GO).** Another way to exfoliate graphite is to oxidize the carbon atoms on the surface, in turn weakening the van der Waals forces between the layers (Figure 3b). The oxidation reaction produces a high pressure gas which increases the interlayer distances, in addition interrupting the  $\pi$ - $\pi$  layer stacking of the graphite sheets by changing the  $sp^2$  lattice with an interlayer spacing of  $0.335 \text{ nm}$  to a  $sp^2$ - $sp^3$  sheet with an interlayer distance of  $0.625 \text{ nm}$  displaying a reduced  $\pi$ -

$\pi$  stacking. Thus a large amount of defects occur in GO compared to the two-dimensional graphene. The product of the oxidation reaction of graphite named graphene oxide (GO) is characterized by the presence of different oxygen containing functional groups such as  $-\text{OH}$ ,  $-\text{COOH}$  and epoxy<sup>[24j, 24k, 24r, 24t, 24v]</sup>. GO was firstly synthesized in 1859 by heating graphite at 60 °C with nitric acid and potassium chlorate and repetition of this reaction several times<sup>[24a]</sup>. In 1898, the oxidation reaction was improved by using a concentrated sulfuric acid in a one-step reaction<sup>[24y]</sup>. Hummers and Offeman presented a safer method in 1958 by an *in situ* production of nitric acid by a mixture of sulfuric acid and sodium nitrate and utilizing potassium permanganate as an oxidation agent<sup>[24aa]</sup>. Recently the less corrosive phosphoric acid was used instead of nitric acid in the Hummers method increasing the yield of the reaction, providing more oxidized form of GO and decreasing the evolution of toxic gases like  $\text{NO}_2$  and  $\text{N}_2\text{O}_4$ <sup>[24n]</sup>.

Hirsch et al.<sup>[24d]</sup> found that GO is not stable at elevated temperatures (50 °C) and more defects are formed by the  $\text{CO}_2$  gas elimination. It was also proved that GO is metastable at room temperature<sup>[24m]</sup>. Therefore in order to decrease the amount of defects on the surface of GO, a longer oxidation time (16 h) at temperatures below 10 °C was applied<sup>[24e]</sup>. However the disadvantage of this method is the low yield of the reaction (1 g of graphite yields 432 mg GO).

The successful oxidation of the graphite sheets and exfoliation of them to a few layers GO can be confirmed *via* different analytical methods like XRD, TGA and RAMAN spectroscopy. In XRD measurement, the sharp peak corresponding to (002) reflection at  $2\theta \approx 26^\circ$  in graphite shifts to  $\approx 14^\circ$  after the oxidation in GO proving the oxidation of the graphite sheets (Figure 4a). Using the Scherrer equation, the number of the layers can be determined by the Lorentzian fitting of the (002) reflection peak, and the Bragg equation calculates the distance between the layers (d-spacing) in the graphene samples<sup>[31]</sup>. The functionalization with the oxygen-containing groups can be monitored by thermogravimetric analysis (TGA) where in contrast to graphite, GO exhibits about 40 % weight loss (Figure 4b)<sup>[24i]</sup>. Most of the weight loss in GO is related to the water molecules connected to the epoxy groups *via* H-bonding<sup>[32]</sup>. Graphite shows two peaks in RAMAN spectra at  $1580\text{ cm}^{-1}$  (G peak) and  $2700\text{ cm}^{-1}$  (2D peak) which are related to the  $\text{sp}^2$  bond. After the oxidation reaction a new peak appears at  $1340\text{ cm}^{-1}$  (D peak, related to  $\text{sp}^3$  hybrid, and defects), and the 2D peak gets broader<sup>[33]</sup> (Figure 4c). Therefore using the intensity ratio of D peak to G peak ( $I_D/I_G$ ) in RAMAN spectra enables to investigate the amount of defects on the surface, however the investigation of the defects in GO is not possible due to the presence of functional groups on the surface, whereby after the reduction reaction and removal of the oxygen containing functional groups the investigation of the defects can be easily probed<sup>[24e, 34]</sup>.

**Reduction reaction.** GO possesses low conductivity and poor electronic properties in comparison to the single layer graphene which is produced by the mechanical exfoliation or by CVD methods.

Therefore a reduction reaction is needed to reduce the amount of oxygen within the material subsequently increasing the current conductivity of the final material. Numerous methods of the reduction have been introduced during the recent years based on the thermal annealing<sup>[24o, 24u]</sup>, using microwave<sup>[24c, 24i]</sup>, and the application of different reducing agents such as hydrazine<sup>[24x]</sup>, ascorbic acid<sup>[24g, 24z]</sup>, hydrohalic acid<sup>[24b, 24p, 24s]</sup>, or sodium borohydride<sup>[24w]</sup>. The successful reduction of GO can be investigated by different methods like XRD and TGA. The reduction reaction of GO changes the interlayer distance and the number of layers in the reduced graphene oxide (r-GO, CCG peaks in Figure 4) which results in a signal shift from  $2\theta \approx 14^\circ$  for GO to  $\approx 23-26^\circ$  for r-GO in the XRD spectra<sup>[31]</sup>. Moreover a weight loss of 70-80 % in comparison to graphite can be observed by TGA. In contrast to GO, the absence of the weight loss at about 200 °C indicates that there are no water molecules on the surface of r-GO.

For example Ajayan et al.<sup>[24i]</sup> oxidized the graphite sheets *via* Hummers' method and reduced GO in three steps by sodium borohydride (CCG1), sulfuric acid (CCG2) and thermally in an oven at 1100 °C (CCG3). The signal shifts in the XRD spectra (Figure 4a) related to graphite, GO and r-GO (CCG peaks), proved the successful oxidation and reduction reactions. TGA and RAMAN spectra related to the product of each reaction steps showed the further evidence of the successful transfer of graphite to GO and r-GO (Figure 4b and 4c).

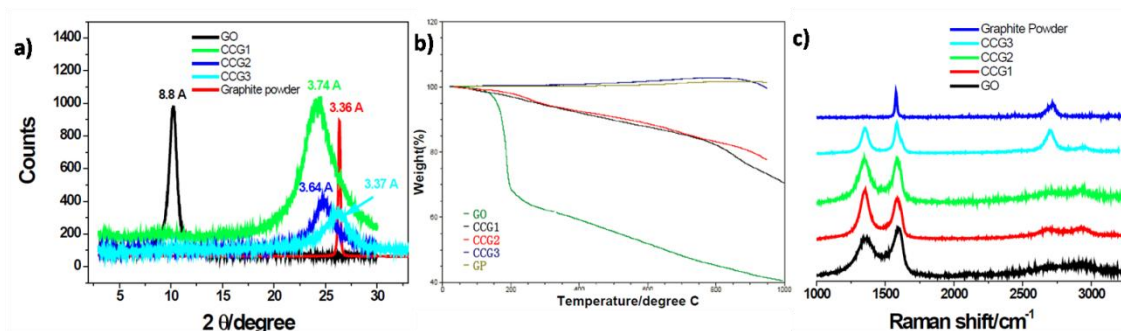


**Figure 4.** The a) XRD b)TGA, and c) RAMAN spectra of graphite, GO and r-GO reduced in three steps by NaBH<sub>4</sub> (CCG1), H<sub>2</sub>SO<sub>4</sub> (CCG2) and in oven (CCG3) ( taken from reference <sup>[24i]</sup>)

The reduction reaction increases the ratio between carbon and oxygen atoms (C/O ratio) in r-GO which in turn leads to products with enhances conductivity. Table 1 describes the efficiency and properties of the reduction reaction for some commonly used methods.

**Table 1.** Comparison of reduction reaction protocols of graphite oxide (GO)

Entry	Reduction method	C/O ratio	Conductivity $\sigma$ ( S/cm)
1 <sup>[24x]</sup>	Hydrazine monohydrate	10.3	2.4
2 <sup>[35]</sup>	Fe/HCl	7.9	2.3
3 <sup>[24h]</sup>	Vitamin C	12.5	8
4 <sup>[24p]</sup>	Hydriodic acid with acetic acid	11.5	304
5 <sup>[24f]</sup>	Aluminum powder	18.6	2.1
6 <sup>[24w]</sup>	NaBH <sub>4</sub>	8.6	4.5



Thus e.g. the traditional hydrazine method increases the C/O ratio from 2.7 for GO to 10.3 for r-GO which increases the conductivity to 2 S/cm for r-GO in comparison to GO with a conductivity of  $5.3 \times 10^{-6}$  S/cm (Table 1, Entry 1). However there is no strict relation between the C/O ratio and the conductivity as the conductivity of r-GO with a C/O ratio of 7.9 reduced by the mixture of Fe/HCl (Table 1, Entry 2) is the same as the one of r-GO reduced by the hydrazine with a C/O ratio of 10.3 (Table 1, Entry 1).

The conductivity of r-GO is mainly related to the defect density on the surface and the size of the distorted area which are created during the oxidation and reduction reactions. As discussed earlier, the reduction reaction removes functional groups on the surface enabling the study of defect formation by RAMAN spectroscopy. Defects increase the intensity ratio of the D peak to the G peak ( $I_D/I_G$ ) and the FWHM of the 2D peak which is about  $32 \text{ cm}^{-1}$  for the two-dimensional graphene (Figure 5a). Plotting of  $I_D/I_G$  vs. the FWHM of 2D bond can be used for the determination of the defects on the surface, where a shift to the left side of the plot with lower  $I_D/I_G$  values is a sign for the high quality r-GO with fewer defects (Figure 5b). Hirsch et al.<sup>[24d, 24e]</sup> probed four different conventional reduction reactions investigating their effect on a defect formation on the surface (Figure 5b), and it was observed that HI-TFA (combination of hydriodic acid and tetrafluoro acetic acid) is the best method leading to fewer defects<sup>[34a]</sup> resulting in a better conductivity than other methods (Table 1, Entry 4).

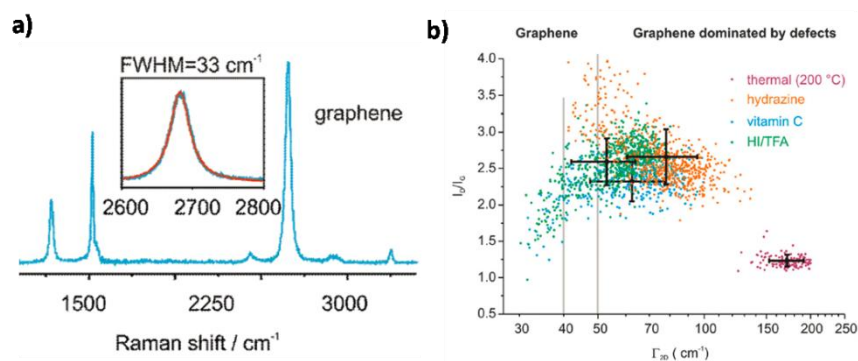


**Figure 5.** a) RAMAN spectrum of r-GO and its FWHM value for 2D peak b)  $I_D/I_G$  ratio vs. FWHM of the 2D peak of r-GO (reduced by different methods) ( taken from references <sup>[24e, 34a]</sup>)

### 3. Metal(oxide)/graphene catalysts (characterization, synthesis and application)

A graphene based metal(oxide)/graphene composite catalyst is a graphene material blended with one or more other metal catalysts, where graphene usually acts as a support material for the immobilization of the metal nanoparticles. Metal(oxide)/graphene composites have been used as catalysts in different types of organic reactions such as coupling reactions<sup>[36]</sup> (like Suzuki, Heck, and Kumuda), whereas most of these reactions can potentially be used as a polymerization reaction. Understanding the synthesis of these materials and their use in organic reactions is a crucial point for their application in polymerization reactions as a catalyst.



The performance of a metal(oxide)/graphene composite catalyst depends on the intrinsic properties, interfacial interaction and synergistic effect of its components. The lifetime of the metal(oxide)/graphene composite is mainly controlled by the stability of the catalyst immobilized on the graphene sheets<sup>[12a, 12c, 12e]</sup>. A lot of efforts have been made to synthesize such metal(oxide)/graphene composite structures with the controlled shape, size and crystallinity prepared *via* the *ex situ* hybridization or *in situ* crystallization methods<sup>[12a]</sup>. In the following section, the synthetic methods towards the graphene based catalysts which have mainly been used in the organic synthesis are outlined.

In general, the characterization and investigation of the metal(oxide)/graphene composite as a catalyst should be done before and after its utilization in an organic reaction. Before application, the properties of the metal particles on the surface of graphene such as the size, distribution, oxidation state, crystalline structure and the amount of the metal on the surface should be investigated knowing the active site of the catalyst running the reaction. After running the reaction for some cycles and deactivation of the catalyst, changes in the metal properties and surface should also be investigated to understand the deactivation process<sup>[36a, 36c, 36u, 36aj, 37]</sup>.

### 3.1-Preparation methods of metal(oxide)/graphene catalysts

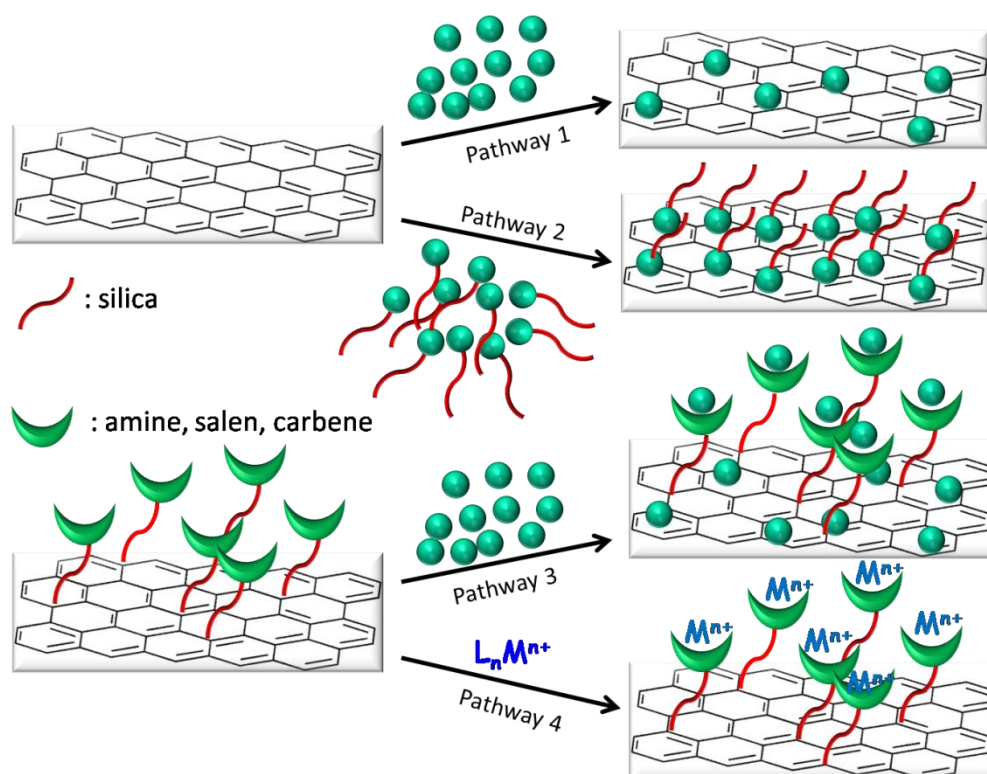


**Figure 6.** *Ex situ* hybridization techniques to synthesize graphene/metal(oxide) composites

***Ex situ* hybridization.** The surface of the graphene-based materials has the affinity to physically absorb the metal nanoparticles<sup>[14]</sup> (Figure 6, Pathway 1). However, surface modification of the either

metal nanoparticles (Figure 6, Pathway 2) or the graphene materials (Figure 6, Pathway 3) before mixing can increase the loading either *via* the non-covalent interaction or by the chemical bonding. For example, Au nanoparticles were treated with r-GO in water to decorate Au nanoparticles on the surface with an average particles size of 5.4 nm and a 1 wt% loading as proved by ICP measurement. Furthermore XPS analysis revealed that the particles are in the metallic state (Au(0)). The obtained r-GO-AuNPs hybrid was used as a catalyst in the benzyl alcohol oxidation with a 65 % conversion and a recyclability of 5 times (Table 2, Entry 1). However, modifying the surface of Au nanoparticles with silica increased the loading to 17.5 wt% with an average particle size of 3.5 nm, whereas XRD confirmed the fcc structure of the metallic gold particles (Au(0)) on the surface. This hybrid was able to catalyze Suzuki coupling and esterification reactions with a high conversion, including a high recyclability (5 times) with a slight reduction in the activity, however after five times recycling some agglomeration of the particles was observed (Table 2, Entry 2). Same methods are used to decorate the silica coated Ag nanoparticles, silica coated-Fe<sub>2</sub>O<sub>3</sub> nanoparticles and Cu nanoparticles on the surface of r-GO which were used in different organic reactions as shown in Table 2 (Entries 3-6). Furthermore nanoparticles can be connected to the electron rich moieties such as pyrene to bind *via* a  $\pi$ - $\pi$  stacking to the surface of the graphene-based materials. Therefore Au-NPs modified with 2-mercaptopyridine were synthesized and mixed with GO and r-GO to bind Au nanoparticles *via* a  $\pi$ - $\pi$  stacking which were subsequently used in the reduction reaction of *o*-nitroaniline (Table 2, Entry 7). The oxygen containing functional groups (-OH and -COOH) give the opportunity to covalently bond functional groups like the chiral salen<sup>[38]</sup>, *N*-heterocyclic carbene<sup>[36t, 36w, 39]</sup>, or amines and ionic liquids<sup>[36ai, 40]</sup> onto the surface of GO and r-GO, thus obtaining novel functionalities which are able to stabilize the metal particles, and their valence on the surface. For example, the surface of GO was firstly modified with the amine groups by the reaction of GO with APTMS, afterwards the obtained amine groups were further reacted with salicylaldehyde to modify the surface with the chiral salen chelating moieties<sup>[38b]</sup>. Subsequent reaction with Cu(NO<sub>3</sub>)<sub>2</sub>·3H<sub>2</sub>O bonded the Cu particles with the salen chelating moieties on the surface (Figure 7). The amount of the copper on the surface was measured by ICP and estimated to be 0.67 wt% (0.1 mmol.g<sup>-1</sup>), whereas the XPS studies showed that the Cu particles are in the second oxidation state. However TEM and XRD did not show any evidence of the Cu particles, because the Cu particles were in the atomic size difficult to visualize *via* these methods. The as-synthesized Cu(salen)-GO catalyst was used in an olefin oxidation with a high conversion and superior recyclability (12 times) without any detectable leaching to the product (Table 2, Entry 8). In another work, the surface of GO was modified with the ionic liquid and amine moieties separately<sup>[40e]</sup>. Afterwards the modified GO sheets were treated with a solution of the asymmetric chiral salen Mn(III) complex to anchor Mn(III) on the surface in a loading of 0.47 mmol.g<sup>-1</sup>. The obtained hybrid was used in the epoxidation of olefins with 7 times recycling without any leaching

(Table 2, Entry 9). Further selected examples on the application of the *ex situ* hybridization method for the synthesis of the graphene/metal(oxide) composites and their subsequent use as the catalyst in an organic reaction are listed in Table 2 (Entries 9-15).

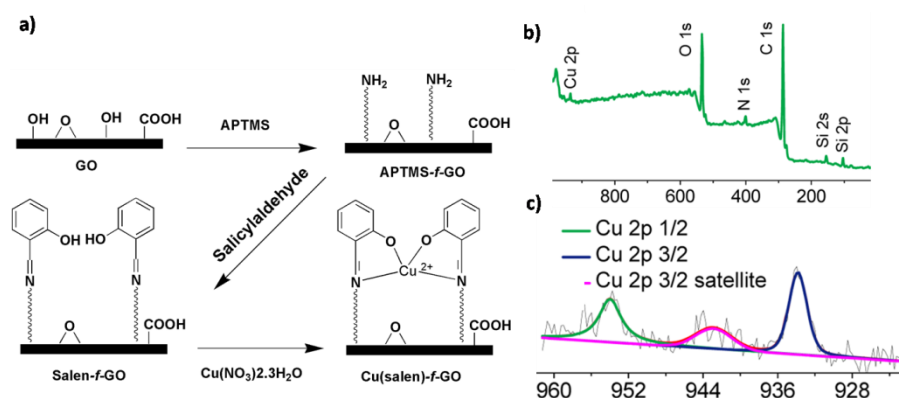


**Figure 7.** a) Modification of GO with salen functional groups, and loading Cu(II) particles on them, b) confirmation of the successful functionalization *via* XPS measurement and c) proving the valence of Cu with high resolution XPS of Cu region. (taken from reference<sup>[38b]</sup>)

**Table 2.** Graphene/metal(oxide) composites synthesized *via ex situ* hybridization and their application in organic synthesis

Entry	Type of graphene	Metal precursor	Characterization	Metal type on surface	Organic reaction	Conversion / recyclability/leaching (agglomeration of particles)
1 <sup>[41]</sup>	r-GO	Au NP	ICP, FAAS: 1 wt% amount of metal on r-GO TEM: average particle size of 5.4 nm XPS: peak at 84.1 eV related to Au(0)	Au(0)	Benzyl alcohol oxidation	65 %/ 5 times/no report
2 <sup>[36aj]</sup>	r-GO	Silica coated Au-NP(Si-Au NP)	ICP, FAAS: 17.5 wt% amount of metal on r-GO TEM: average particle size of 3.5 nm XRD: planes of (111), (200), (220) and (311) detected for Au(0)	Au(0)	Suzuki coupling, esterification	99 %/5 times/agglomeration of particles
3 <sup>[37f]</sup>	r-GO	Silica coated Ag-NP(Si-Ag NP)	TEM: average particle size of 10-12 nm	Ag(0)	A3 coupling, click reaction	A3 : 70 %-98 % / 5 times/ Click : 85 %-99 %/5 times/ agglomeration of particles
4 <sup>[37c]</sup>	r-GO	Silica coated $\gamma$ -Fe <sub>2</sub> O <sub>3</sub> NP	TEM: average particle size of 10-12 nm XRD: planes of (220), (311), (400), (422), (511) and (440) related to the $\gamma$ -Fe <sub>2</sub> O <sub>3</sub> particles	Fe(III)	Oxidation of methyl phenyl Sulfide/ Oxidation of benzyl alcohol/ Click reaction	98 %, 94 %, 92 % (respectively for 3 types of organic reaction)/ 5 times/ no agglomeration of particles
5 <sup>[37e]</sup>	r-GO	Au NP	ICP: 7.1 wt% amount of metal on r-GO TEM: average particle size of 10-20 nm XPS: peaks at 83.9 eV and 87.6 eV related to Au(0)	Au(0)	Ullmann homocoupling	93 % / 6 times/ no report
6 <sup>[42]</sup>	r-GO	Cu NP	TEM: average particle size of 30 nm XRD: peaks at 43.5°(111) and 50.4°(200) related to Cu(0), and peaks at 42.6° and 62.6° related to Cu <sub>2</sub> O	Cu(0), Cu(I)	N-Arylation of phenylurea with aryl halides	82 %-89 % /no report/no report

7 <sup>[43]</sup>	GO, r-GO	Au NP-2-mercapto-pyridine	TEM: average particle size of 20-40 nm ICP, FAAS : 0.67 wt % (0.10 mmol.g <sup>-1</sup> ) of metal on GO	Au(0)	Reduction of <i>o</i> -nitroaniline	The efficiency of catalysts were proved by the reaction under UV lamp
8 <sup>[38b]</sup>	GO-chiral salen	Cu(NO <sub>3</sub> ) <sub>2</sub> ·3H <sub>2</sub> O	TEM: showed no particle (small particle size) XPS: peaks at 933.9 eV and 953.8 eV for Cu 2p, and the peak at 943 eV for Cu 2p <sub>3/2</sub> related to Cu(II) XRD: showed no peak (small particle size)	Cu(II)	Olefin oxidation	High conversion/ 12 times/ no detectable leaching
9 <sup>[40e]</sup>	GO-imidazole	Chiral salen Mn(III)	ICP, FAAS: 0.47 mmol.g <sup>-1</sup> amount of metal on GO	Mn(III)	Asymmetric epoxidation of unfunctionalized olefins	99 %/7 times/ no detectable leaching
10 <sup>[38a]</sup>	GO- chiral salen	Co(NO <sub>3</sub> ) <sub>2</sub> ·6H <sub>2</sub> O, Fe(NO <sub>3</sub> ) <sub>3</sub> ·9H <sub>2</sub> O, VO(acac) <sub>2</sub>	ICP, FAAS: CO = 0.21 mmol.g <sup>-1</sup> / Fe = 0.158 mmol.g <sup>-1</sup> / VO = 0.179 mmol.g <sup>-1</sup> TEM : showed no particle (small particle size) XRD: showed no peak (small particle size)		Styrene epoxidation	93.3 %, 85.3 %, 70.1 % (respectively for 3 different metal catalysts)/ 4 times/ no report
11 <sup>[36u]</sup>	GO-IL	HAuCl <sub>4</sub>	ICP, FAAS: 2.07 wt% amount of metal on GO XPS: peaks at 83.47 eV and 88.27 eV related to Au(0) peaks at 86.84 eV and 90.83 eV related to Au(III) XRD: peaks at 38.0° (111), 44.1° (200), 64.5° (220) and 77.5° (311) related to Au(0)	Au(0), Au(III)	Oxidative A3 coupling	90 %/ 5 times/ no detectable leaching, no agglomeration
12 <sup>[44]</sup>	GO-poly(vinyl imidazole)	CuSO <sub>4</sub>	ICP, FAAS: 2.1 mmol.g <sup>-1</sup> amount of metal on GO		Click reaction	99 %/8 times/slight leaching
13 <sup>[45]</sup>	GO	Mn(OAc) <sub>2</sub> ·4H <sub>2</sub> O	EDTA: 3.2 wt% amount of metal on GO XPS: peak at 641.7 eV for Mn2P related to Mn(II)	Mn(II)	Epoxidation of alkenes	99 %/ 10 times/no detectable leaching
14 <sup>[46]</sup>	GO-amine	RuCl <sub>2</sub> (PP h <sub>3</sub> ) <sub>3</sub>	ICP, FAAS: 1.12×10 <sup>-1</sup> mmol.g <sup>-1</sup> amount of metal on GO XPS: peak at 462.8 eV	RuCl <sub>2</sub> (P Ph <sub>3</sub> ) <sub>3</sub>	Hydrogenation of olefins and ketones	85 %-100 % (olefin), 20 %-89 % (keton)/ 5 times/no leaching
15 <sup>[47]</sup>	GO-amine	Chiral salen Fe(III)/ chiral salen VO(IV)	XPS: peaks 517.1 eV and 524.1 eV related to VO(IV), peaks at 711.8 eV and 725.3 eV related to Fe(III)	VO(IV) Fe(III)	Epoxidation of olefins	80 %-90 %/ 3 times/ with leaching

**In situ crystallization.** Although the *ex situ* hybridization enables the selection of nanostructures by the modification of the surface of GO or metal nanoparticles with special functional groups, it suffers from the low density and non-uniform coverage of the surface of graphene sheet<sup>[43]</sup>. In contrast, the *in situ* crystallization makes it possible to increase the nanoparticles density and achieve an uniform particle size by controlling the nucleation *via* surface modification<sup>[5]</sup>. The reduction reaction is a

method to synthesize the metal nanoparticles from their precursors and salts like  $\text{HAuCl}_4$ ,  $\text{Cu}(\text{OAc})_2$ ,  $\text{AgNO}_3$ . The reduction reaction can proceed thermally, chemically, by microwave-assisted methods or with hydrothermal methods in an autoclave<sup>[48]</sup>. Therefore the *in situ* reduction reaction of the metal precursors in the presence of graphene-based materials leads to the decoration of the metal nanoparticles on the surface (Figure 8). Furthermore the reduction reaction can be used to reduce GO to r-GO as it was discussed previously, and with the simultaneous reduction of the solution of GO and metal precursors, the metal particles can be synthesized and decorated on the surface of r-GO.

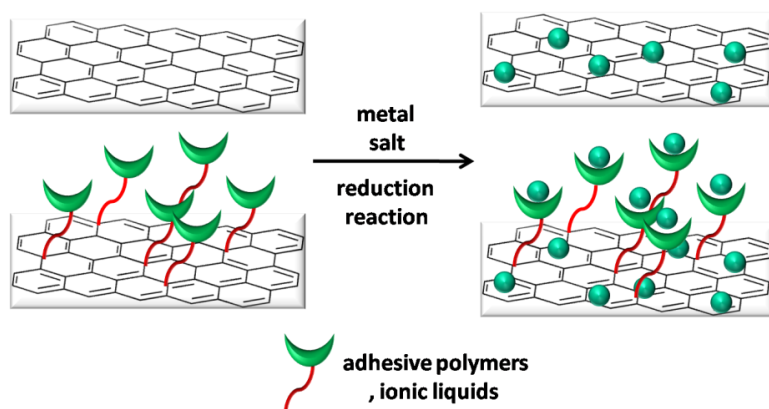


**Figure 8.** The *in situ* crystallization techniques to synthesize graphene/metal(oxide) composites

In the most of the *in situ* crystallization reports, the metal salts and precursors were firstly treated with GO to absorb the metal on the surface *via* an ion-exchange with hydrogen of the hydroxyl and carboxylic groups. Afterwards the GO-metal-ion mixtures were reduced with different methods<sup>[36a, 36f, 37h, 37i, 49]</sup>. Washing of the GO-metal-ions after the first step reaction is a crucial point to remove the excess of the metal salts and precursors which are leading to the agglomeration of the metal nanoparticles after the reduction reaction. These agglomerations decrease the catalytic activity of the metal(oxide)-graphene nanocomposite in the organic reactions and increase the leaching of the metal particles in the organic product.

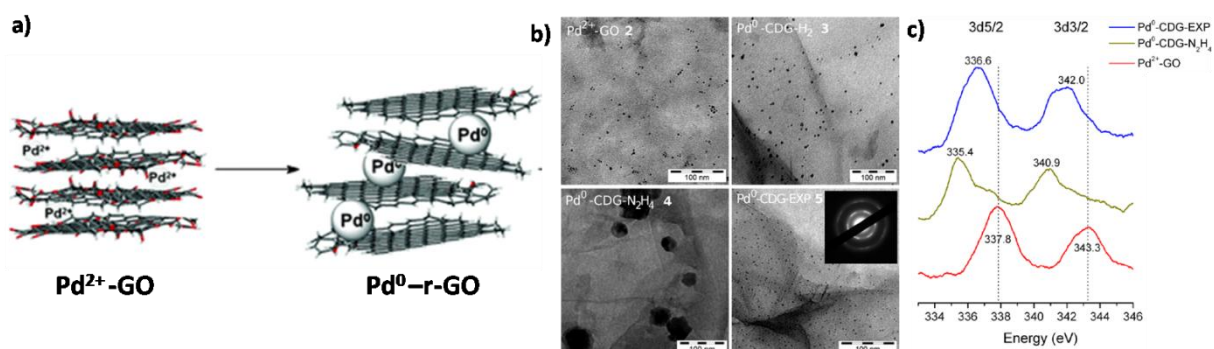


**Figure 9.** a) *In situ* crystallization of palladium particles on the surface of GO and r-GO b) TEM image and c) XPS of GO and r-GO-palladium nanocomposites (taken from reference<sup>[36a]</sup>)

Mülhaupt et al.<sup>[36a]</sup> reported the ion exchange with Pd(II) particles with the hydrogen of the carboxylic groups of GO by dispersing GO and palladium acetate in water obtaining GO-Pd(II). The amount of the



palladium was 3.4 wt% (determined by AAS) with an average particle size of 4 nm and with a high dispersion according to the TEM measurement. Furthermore XPS showed two peaks at 337.8 eV and 343.3 eV, which were related to the Pd(II) metal particles (Table 3, Entry 1). Afterwards the GO-Pd(II) nanocomposite was reduced by different reduction methods like hydrazine (N<sub>2</sub>H<sub>4</sub>), hydrogen gas (H<sub>2</sub>) or thermally in an oven to create the r-GO-Pd(0) nanocomposite (Figure 9a). FAAS measurement showed the 3.5 wt%, 3.4 wt% and 6.0 wt% Pd content for the products reduced with hydrazine, H<sub>2</sub> and thermal reduction, respectively. Also TEM measurement revealed the average particle size of the nanoparticles on the surface which were about 7±2, 54±28, and 3±1 nm for reduction with H<sub>2</sub>, N<sub>2</sub>H<sub>4</sub> and thermal reduction, respectively (Figure 9b). In the XPS measurements the disappearance of the peaks at 337.8 eV and 343.3 eV related to Pd(II), and the appearance of new peaks at 335.4 eV and 340.9 eV corresponding to Pd(0) (Figure 9c) proved the reduction of Pd(II) to Pd(0). The as-prepared graphene-Pd nanocomposites were used as heterogeneous catalysts in the Suzuki reaction (Figure 10a) with a high conversion together with a good recyclability (4 times), furthermore no leaching of the metal particles in the organic product was observed (Table 3, Entry 1). The deactivation of the catalyst was related to the agglomeration and oxidation of the Pd nanoparticles (Figure 10c).

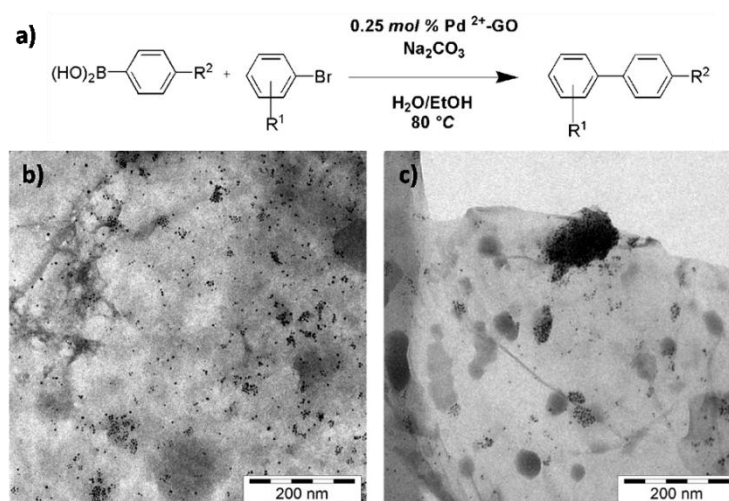


**Figure 10.** a) Suzuki reaction using GO-Pd and r-GO-Pd as catalysts, TEM image of the GO-Pd nanocomposite catalyst b) before c) after four time use in Suzuki reaction (taken from reference<sup>[36a]</sup>)

The same method to decorate the metal nanoparticles on the surface of graphene-based materials like Pd<sup>[36c, 36d, 36f, 36i, 36k-m, 36r, 36s, 36x-aa, 36ad, 36af, 36ah, 36al, 36an-ar, 50]</sup>, Cu<sup>[37h, 51]</sup>, Au<sup>[36b, 36o, 37d, 37g]</sup>, Ag<sup>[37i]</sup> and Ni<sup>[36n, 49b, 49c, 52]</sup> was used in many other works and the obtained metal(oxide)/graphene nanocomposites were evaluated as catalysts in the different organic reactions, the selection of these works is summarized in Table 3.

GO can act as a reduction agent by itself, therefore it was used as an easy and clean synthesis route toward the well dispersed Pd nanoparticles anchored onto the GO surface by mixing GO and a K<sub>2</sub>PdCl<sub>4</sub> aqueous solution, without using any reduction agent<sup>[53]</sup>. With the same method the attachment of the metal nanoparticles on the surface of GO was achieved by stirring of the mixture of the metal

salts ( $\text{AgNO}_3$ ,  $\text{HAuCl}_4$  and  $\text{H}_2\text{PdCl}_4$ ) and GO in water at 0 °C. The TEM results showed an average particle size of 19.3 nm and 3 nm for Au and Pd particles respectively, also the XPS measurements showed the metallic state for all samples. These hybrids were used in the selective reduction of the nitroaromatic compounds (Table 3, Entry 2).<sup>[49a]</sup>

Loading of the metal precursors on the surface of GO, r-GO and graphene sheets and further reduction reaction in order to get the metal nanoparticles onto the surface of the r-GO and graphene nanosheets usually leads to the low metal loading because of the low content of the oxygen containing groups on the surface. However the modification of GO and r-GO sheets with the oxygen-rich moieties like amines, ionic liquids and adhesive polymers can increase the density and dispersibility of the metal nanoparticles on the surface (Table 3, Entries 3-8).

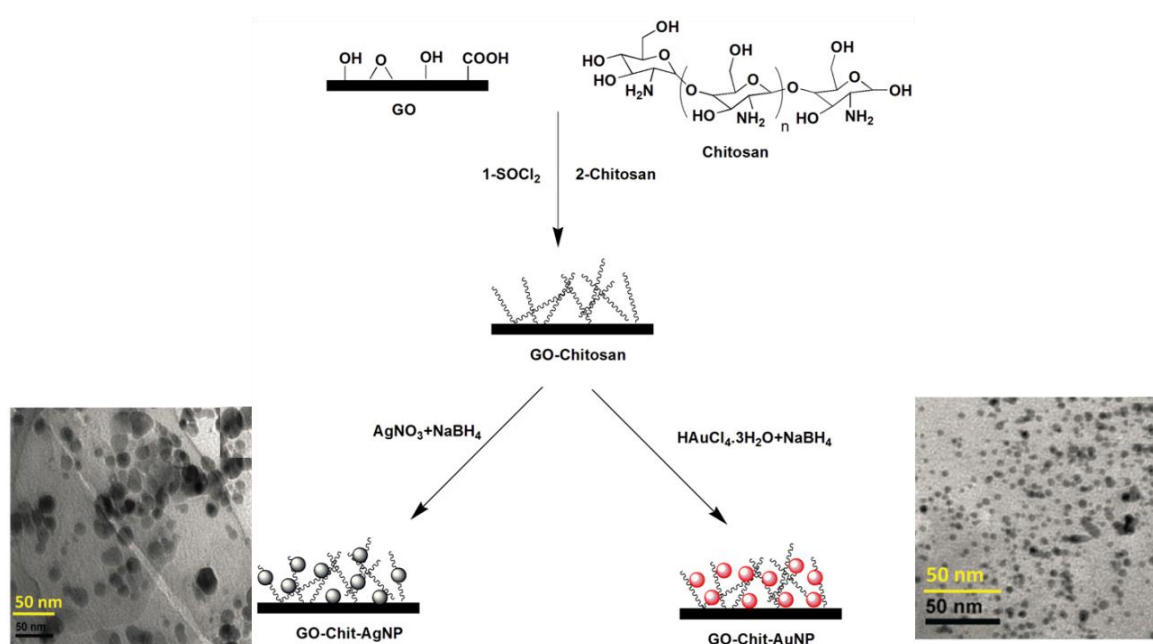


**Figure 11.** Surface modification of GO surface with chitosan, and a reduction reaction to obtain high loading of Ag and Au nanoparticles on the surface (taken from reference <sup>[54]</sup>)

For example the surface of GO was modified with chitosan to increase the absorption of the  $\text{AgNO}_3$  and  $\text{HAuCl}_4$  salts on the surface and subsequently reduce the mixture with  $\text{NaBH}_4$  at room temperature for 24 h<sup>[54]</sup> (Figure 11). The TEM results showed an average particle size of 20 nm and 5 nm for Ag and Au nanoparticles, respectively, furthermore HRTEM and XRD measurements showed the fcc lattice structure of the nanoparticles confirming the metallic state of Ag and Au. The as-prepared metal/graphene catalysts were used in the reduction reaction of nitro groups, degradation of organic azo dyes and reduction reaction of *p*-nitrophenol with a high conversion and reaction rate. Furthermore the heterogeneous catalysts could be recycled for 10 times with a slight loss in the activity (Table 3, Entry 3).

**Table 3.** Graphene/metal(oxide) composites synthesized *via in situ* crystallization and their application in organic synthesis

Entry	Type of graphene	Metal precursor	Characterization	Metal type	Organic reaction	Conversion / recyclability/leaching (agglomeration of particles)
1 <sup>[36a]</sup>	GO r-GO	Pd(OAc) <sub>2</sub>	ICP, FAAS: 3.4 wt% (0.32 mmol.g <sup>-1</sup> ) amount of Pd on GO, and 3.5 wt% - 6.0 wt% amount of Pd on r-GO (reduced by different methods) TEM: average particle size of 4 nm on GO, and average particle size of 7 nm, 54 nm and 3 nm on r-GO (reduced by different methods) XPS: peaks at 337.8 eV and 343.3 eV related to Pd(II) on GO, and peaks at 336.6 eV and 342 eV related to Pd(0) on r-GO	Pd(II) Pd(0)	Suzuki reaction	99 % / 4 times/ not detectable
2 <sup>[49a]</sup>	GO	AgNO <sub>3</sub> , HAuCl <sub>4</sub> , H <sub>2</sub> PdCl <sub>4</sub>	XRD: plane of (200) related to crystal cubic of Ag, plane of (111) related to crystal cubic of Au with 19.3 nm particle size, plane of (111) related to crystal face of cubic of Pd with 0.5-3 nm particle size	Ag (0) Au(0) Pd(0)	Selective reduction of nitroaromatic compounds	99% activity comparison: Pd-RGO > Ag-RGO > Au-RGO
3 <sup>[54]</sup>	GO-chitosan	AgNO <sub>3</sub> HAuCl <sub>4</sub>	TEM : particle size of 20 nm, and 5 nm for Ag and Au, respectively HRTEM : plane of (111), (200), (220), (311) and (222) for Au XRD: peaks at 38.21° (111), 44.31°(200), 64.61°(220) and 77.41°(311) related to fcc plane of Ag, and peaks at 38.31°(111), 44.71°(200), 64.61°(220) and 77.81°(311), related to fcc plane of Au		Reduction of nitro groups, degradation of organic azo-dyes, and reduction of <i>p</i> -nitrophenol	High conversion/ 10 times
4 <sup>[37g]</sup>	r-GO-amine	HAuCl <sub>4</sub>	HRTEM: d-spacing = 0.235 nm related to fcc plane of (111)		Reduction of 4-nitro phenol	High conversion/ 6 times/ no agglomeration
5 <sup>[37d]</sup>	r-GO-amine	HAuCl <sub>4</sub>	TEM : average particle size of 17 nm HRTEM : d-spacing = 0.235 nm related to fcc plane of (111) XPS: peaks at 87.7 eV and 84.0 eV related to Au(0), and peaks at 88.5 eV and 84.8 eV related to Au(I) XRD: peaks at 38.1° (111) and 44.3° (200) related to fcc plane	Au(0) Au(I) (Au(0) /Au(I) =24/1)	Hydrogenation of 4-nitroarenes	High/5 times/ no agglomeration
6 <sup>[36u]</sup>	GO-IL	HAuCl <sub>4</sub>	ICP, FAAS: 2.07 wt% amount of metal on r-GO XPS: peaks at 83.47 eV and 88.27 eV related to Au(0) peaks at 86.84 eV and 90.83 eV related to Au(III) XRD: peaks at 38.0° (111), 44.1° (200), 64.5° (220) and 77.5° (311) related to Au(0)	Au(0), Au(III)	Oxidative A3 coupling	90 %/ 5 times/ no detectable leaching, no agglomeration
7 <sup>[37i]</sup>	GO-amine	AgNO <sub>3</sub>	TEM : particle size between 3 nm to 15 nm		Aerobic oxidation of benzyl alcohol	61 %/5 times/no agglomeration
8 <sup>[51a]</sup>	r-GO-amino acid	CuCl <sub>2</sub>	ICP, FAAS: 8.2 wt%– 10 wt% amount of metal on r-GO TEM: particle size of 10 nm XPS: peak at 932.9 eV related to Cu <sub>2p<sub>3/2</sub></sub> of Cu(0), and Cu(I), and peak at 935.0 eV related to Cu(II)	Cu(0), Cu(I), Cu(II)	<i>N</i> -Arylation	90 %/no report/no report
9 <sup>[37h]</sup>	r-GO	Cu(acac) <sub>2</sub>	ICP, FAAS : 4.37 wt% amount of metal on r-GO TEM : particle size of 26 nm XPS: peaks at 942.4 eV, and 962.6 eV related to Cu <sub>2p<sub>3/2</sub></sub> , and Cu <sub>2p<sub>1/2</sub></sub> of CuO	CuO	A3 coupling	89 %/ 5 times/ agglomeration of particles



10 <sup>[51b]</sup>	r-GO	CuSO <sub>4</sub>	ICP, FAAS: 26.2 wt% amount of metal on r-GO TEM: particle size of 4-5 nm XPS : peaks at 933.6 eV, 935.6 eV and 570.2 eV related to Cu 2p <sub>3/2</sub> of Cu(I) , and peak at 943.5 eV related to Cu(II) XRD : peaks at 43.2°(111), 50.4°(200), 74.1°(220) related to fcc plane of Cu(0), and peaks at 36.4°(111), 42.4°(200), 61.5°(220) related to Cu <sub>2</sub> O	Cu(0), Cu <sub>2</sub> O	N-Arylation of N-heterocycles	83 %-99 %/5 times/ 0.9-1.4 Cu% leaching after each run
11 <sup>[51e]</sup>	r-GO	Cu(NO <sub>3</sub> ) <sub>2</sub> .6H <sub>2</sub> O	ICP, FAAS: 20.73 wt%– 58.04 wt% amount of metal on r-GO TEM: particle size of 27.1 nm - 50.5 nm HRTEM: d-spacing =0.206 nm related to (111) cubic plane XRD: peaks at 43.4°(111), 50.6°(200) and 74.31°(220) related to Cu(0)	Cu(0)	Reduction of 4-nitrophenol	Reaction under UV with high conversion
12 <sup>[36c]</sup>	r-GO	Pd(NO <sub>3</sub> ) <sub>2</sub>	ICP, FAAS: 7.9 wt% amount of metal on r-GO TEM : particle size of 8 nm XPS : peaks at 335.6 eV and 340 eV related to Pd3d <sub>5/2</sub> , and Pd3d <sub>3/2</sub> respectively which proved the mixture of Pd(II), and Pd(0)	Pd(II), Pd(0)	Heck and Suzuki coupling	100 %/10 times/ 300 ppb of leaching, with agglomeration
13 <sup>[36c]</sup>	GO	Pd(NO <sub>3</sub> ) <sub>2</sub>	ICP, FAAS: 6.4 wt% amount of metal on r-GO TEM: particle size of 14 nm XPS: peaks at 337.8 eV, and 343.2 eV related to Pd 3d <sub>5/2</sub> , Pd 3d <sub>3/2</sub> of Pd(II), respectively TEM : particle size of 4.8 ± 2 nm, HRTEM : plane of (111), (222), and (220) for fcc structure of Co <sub>3</sub> O <sub>4</sub>	Pd(II)	Heck and Suzuki coupling	100 %/7 times/ 350 ppb of leaching, with agglomeration,
14 <sup>[37b]</sup>	r-GO	Co(OAc) <sub>2</sub> 4H <sub>2</sub> O	XPS : peaks at 779.8 eV and 781.5 eV related to Co <sup>3+</sup> and Co <sup>2+</sup> respectively XRD: plane of (220), (311), (222), (400), (422), (511), (440) related to fcc structure of Co <sub>3</sub> O <sub>4</sub> TEM : particle size of 5 nm	Co <sub>3</sub> O <sub>4</sub>	Oxidation of olefins and alcohols	94 %-99 %/ 5 times/ no agglomeration
15 <sup>[55]</sup>	r-GO	FeCl <sub>3</sub>	XPS: peaks at 771.5 eV (Fe2p <sub>3/2</sub> ) and 752.2 eV (Fe2p <sub>1/2</sub> ) related to Fe <sub>3</sub> O <sub>4</sub> XRD: peaks at 30.3°(220), 35.4°(311), 42.9°(400), 57.3°(511) and 62.6°(440) related to fcc structure of Fe <sub>3</sub> O <sub>4</sub>	Fe <sub>3</sub> O <sub>4</sub>	Alkyne hydrogenation	70 %-99 %/10 times /no leaching
16 <sup>[56]</sup>	GO	KMnO <sub>4</sub>	EDX: 38.6 wt% amount of Mn on the surface XRD: highly crystalline tetragonal α-phased MnO <sub>2</sub> TEM : particle size of 8 nm	MnO <sub>2</sub>	Oxidation of aromatic amines	50 %-91%/ 6 times/ no report
17 <sup>[49c]</sup>	r-GO	Ni(OAc) <sub>2</sub> ·4 H <sub>2</sub> O	XPS: peaks 852.2 eV and 872.9 eV and their satellite at 857.5 eV and 875.4 eV related to Ni(0) XRD: peaks at 44.8°(111), 52.1°(200), and 77.2°(222) related to fcc structure of Ni(0) crystal	Ni(0)	reduction of 4- nitrophenol	High conversion/ 5 times/no report
18 <sup>[57]</sup>	r-GO	H <sub>2</sub> PtCl <sub>6</sub>	ICP : 39.7 wt% amount of Pt on the surface TEM: particle size of 2-3 nm, HRTEM : d-spacing = 0.228 related to plane of (111) XPS: peaks at 71.5 eV and 74.8 eV XRD: planes of (111),(200), and (220) related to fcc structure of Pt	Pt(0), Pt(I), Pt(II)	hydrogenation	99 %/ no report/ no report
19 <sup>[37a]</sup>	r-GO	Ru(acac) <sub>3</sub>	ICP : 2.99 wt% amount of Pt on the surface TEM : rods with length of 25–30 nm, and diameter of 8–12 nm XPS: peaks at 280.8 eV, 462.5 eV, and 485 eV related to Ru <sup>4+</sup> XRD : peaks at 27.51°(110), 34.91°(101), 39.91°(200) and 57.51°(220) related to RuO <sub>2</sub>	RuO <sub>2</sub> (Ru <sup>4+</sup> )	hydrogenation	99 %/ 4 times/ no significant agglomeration

#### 4-GO, r-GO and their metal(oxide) composites as initiator/catalyst in polymerization reactions

In the formation of polymer/graphene nanocomposite materials, control of the polymer/graphene interface by the attached polymeric interlayers is essential to generate nanocomposites, thus avoiding the aggregation of the graphene nanoparticles. Therefore the direct use of the graphene based materials like GO and r-GO as both, the polymerization initiator or catalyst and additive not only diminishes the agglomeration of the particles in composites but also reduces the process of the composite production to a one facile step. In the following sections, graphene based initiators and catalysts which have been used in the different polymerization reactions are outlined.

#### 4.1-Free radical polymerization

Free radical polymerization (FRP) has many advantages over other polymerization processes, and can be used for the polymerization and copolymerization of a wide range of vinyl monomers. About 50 % of all commercial synthetic polymers such as low density polyethylene, poly(vinyl chloride), polystyrene, polyacrylates, polyacrylamides, poly(vinyl acetate), poly(vinyl alcohol) and many fluorinated polymers are prepared *via* free radical polymerization techniques, like emulsion and suspension polymerization. For this polymerization, a source of the free radical like peroxides or azo compounds are needed to initiate the polymerization<sup>[58]</sup>, for which GO can act as a source.

##### 4.1.1-GO as initiator

The existence of free radicals on the surface of GO has been proved by EPR measurements<sup>[59]</sup> showing that the peak in the EPR spectra is connected to free radicals associated with broken bonds at defects, which can initiate the radical polymerization and can be used as an initiator. In contrast, r-GO does not show any peak in EPR and thus cannot initiate a radical polymerization<sup>[59c]</sup>.

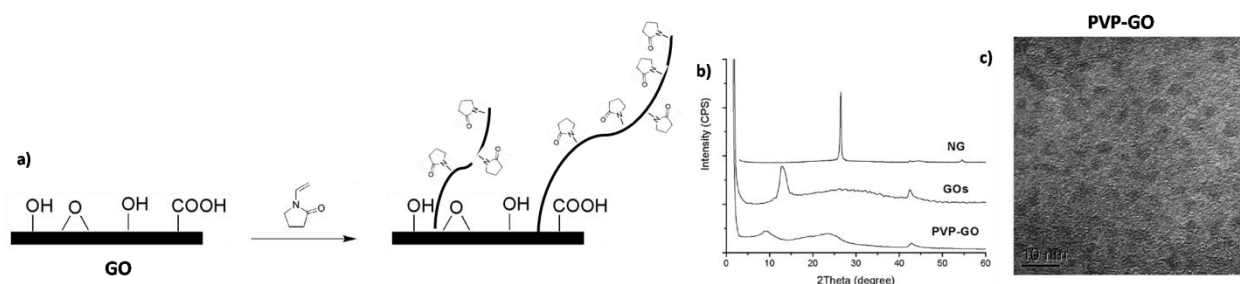


**Figure 12.** a) Free radical polymerization of *N*-vinylpyrrolidone using graphene oxide (GO) as initiator b) XRD measurement of GO before and after the polymerization reaction, c) TEM image of the GO/poly(*N*-vinylpyrrolidone) composite. (taken from reference<sup>[59c]</sup>)

The first report for the use of pristine graphene oxide without any modification as an initiator for a free radical polymerization was done for *N*-vinylpyrrolidone as monomer<sup>[59c]</sup>, where a mixture of GO (2.5 wt%) and *N*-vinylpyrrolidone was dissolved in water and heated at 95 °C for 10 h obtaining poly(*N*-vinylpyrrolidone) grafted GO. Successful functionalization was proven by different methods

such as FTIR, XPS, EDX, elemental analysis, XRD and TEM (Figure 12). The  $M_n$  of the free PVP separated from the product of the GO-initialized polymerization was determined by GPC to be 3.3 *kDa*. Furthermore it was shown that the surface of GO was reduced to r-GO by this surface initiated polymerization, increasing the conductivity to  $4.7 S.m^{-1}$ . The grafting density was calculated to be 46.5 % by measuring the amount of nitrogen atoms on the surface after polymerization *via* XPS. To prove that GO was acting as an initiator, *N*-vinylpyrrolidone was treated at 95 °C in the absence of GO for several hours, and no polymer was obtained. (Table 4, Entry 1).

In other publications<sup>[60]</sup> graphene oxide was used as an oxidation agent in the free radical polymerization of different conducting polymers like polythiophene (PTh), polypyrrole (PPy) and PANI, leading to a simultaneous reduction of GO to r-GO<sup>[60a]</sup>. For this purpose, monomers (thiophene, aniline, and pyrrole) were added to GO as an aqueous solution, and then heated at 90 °C for 10 *min* leading to r-GO-PTh, r-GO-PANI, and r-GO-PPy, respectively (Table 4, Entry2). In the first step of this radical polymerization, the monomer (anilinium, thiophene) approaches the epoxide groups in GO *via* an electrostatic attraction, following by the formation of a new O–H bond and simultaneous cleavage of a C–O bond of an epoxide and the N–H bond of an anilinium ion, yielding hydroxyl group and radical on the GO surface and corresponding monomer radicals (aniline radical cation, and thiophene radical). The so-formed monomer radicals acted as an initiator for the monomers, resulting in the corresponding polymers. The oxidation level of the GO (O/C ratio) played an important role in the polymerization reactions: with an O/C less than 0.4 it was not possible to polymerize the monomers due to the low amount of the epoxy groups. Moreover GO initiated the polymerization at temperatures of more than 80 °C, a suitable temperature for the successful opening of the epoxy ring by attacking of monomers. The modification of r-GO by different conducting polymers was proven by SEM and TEM measurements<sup>[60a]</sup>.

Ce(IV)-alcohol is an effective initiator pair for redox radical polymerization of a variety of water-soluble vinyl monomers. The use of hydroxyl groups on GO, together with Ce(IV) generates an efficient redox polymerization pair<sup>[61]</sup>. In a report the Ce(IV)/HNO<sub>3</sub> and GO pair was used for the polymerization of methyl methacrylate (MMA), acrylonitrile (AN), acrylamide (AM) and styrene (Table 4, Entry 4)<sup>[61b]</sup> at low temperatures (30 °C) (Figure 13a). The polymerization reaction with styrene and acrylonitrile led to lower grafting ratios (23% - 64%) in comparison to the MMA (504%) according to the TGA analysis. Consequently the XRD measurement showed no peak for the GO-grafted-PMMA which clearly demonstrated the disappearance of the regular and periodic structure of the GO sheets, indicating the formation of fully exfoliated structures and the homogeneous distribution of the GO sheets in the polymer matrix (Figure 13c). XRD spectra of GO-PS and GO-PAM possessed a peak at 9.96° and 9.05°, respectively, which were close to the value of GO (10.17°) indicating a low exfoliation of the GO sheets (Figure 13b and 13c).

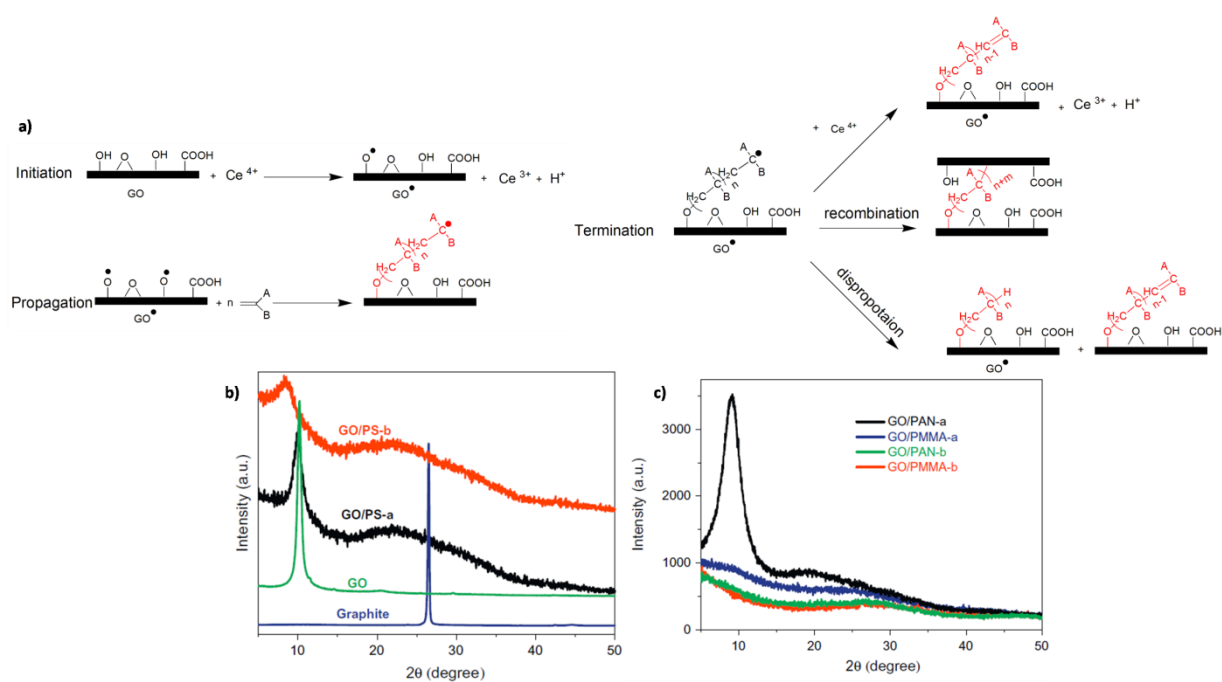


**Figure 13.** Free radical polymerization *via* the Ce(IV)/HNO<sub>3</sub>/graphene oxide pair a) proposed mechanism, and XRD measurements of b) PS/GO, c) PAN/GO and PMMA/GO composites (taken from reference<sup>[61b]</sup>)

The low grafting density of GO with styrene monomer is mainly due to the extremely hydrophilic nature of GO. Therefore in order to increase the hydrophobicity of GO, long chain alkyl amines can be introduced to the surface, thus increasing the compatibility with the organic media such as styrene and apolar solvents. Therefore the surface of GO was modified with the APTS groups in order to increase the hydrophobicity, and in turn using the same method for free radical polymerization of acryl amide under microwave irradiation at 50 °C for 5 min.<sup>[61d]</sup> In contrast to the previous method<sup>[61b]</sup> GO was completely exfoliated by the poly(acrylamide) chains as proven by the XRD measurements, showing a broad peak at 24.8° (Table 4, Entry 5).

#### 4.1.2-Surface functionalization of GO with radical polymerization initiators

Different functional groups on the surface of GO open opportunity to modify the surface with free radical polymerization initiators like azo<sup>[62]</sup> and peroxide<sup>[63]</sup> moieties which subsequently can be used as an initiator for a free radical polymerization. This method enables the efficient polymerization of less polar monomer like styrene from the GO surfaces. The surface of r-GO was modified with the 4,4'-azo bis (4-cyanopentanoic chloride) ABAPC initiator by the conversion of the carboxylic acid groups of r-GO to the amine groups, and subsequent reaction of r-GO-amine with the free radical initiator ABAPC<sup>[62]</sup>. The obtained initiator was then used for the free radical polymerization of acryl amide<sup>[62a]</sup> (Figure 14), and vinyl pyridine<sup>[62b]</sup>. The successful functionalization was proved by XPS, FTIR, TGA, TEM and AFM. The viscosity average molecular weight of the free polymer was determined to be about 1900 kDa for poly(acrylamide) (PAM) and 18.4 kDa for poly(vinylpyridine) (P2VP). AFM

measurements showed a thickness of 4.4 nm for poly(vinylpyridine) on the surface of modified r-GO (Table 4, Entry 6).

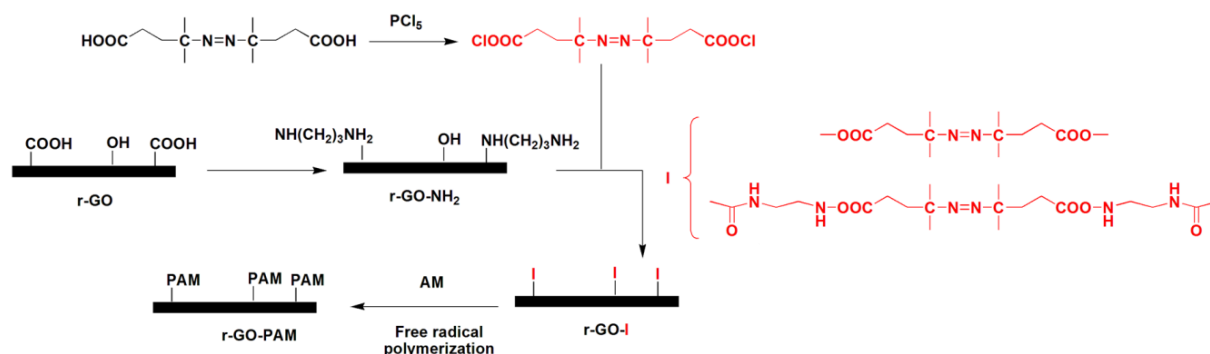


**Figure 14.** Surface modification of r-GO with ABCPC initiator and subsequent free radical polymerization of acrylamide with modified r-GO (taken from reference<sup>[62a]</sup>)

Liu et al.<sup>[63a]</sup> functionalized the surface of GO with the peroxide groups (GPO) by  $\gamma$  irradiation in the presence of oxygen (Figure 15), and proved the existence of peroxides on the surface *via* FTIR, RAMAN, XPS and XRD measurements (Table 4, Entry 7).

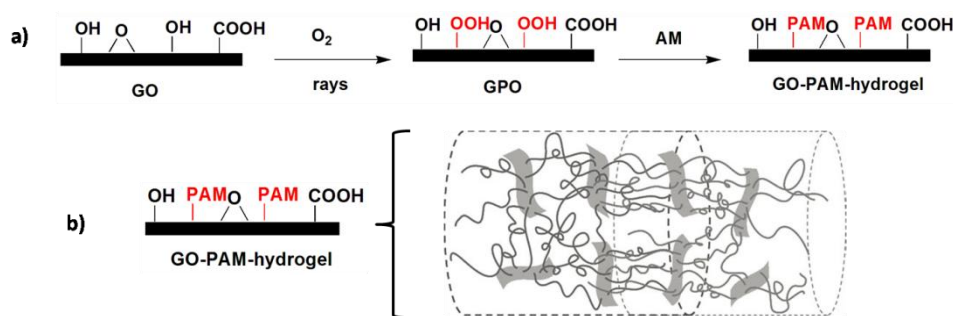


**Figure 15.** a) Surface functionalization of GO with peroxides, and subsequent use of GO-initiator (GPO) in free radical polymerization of acrylamide (taken from reference<sup>[63a]</sup>) b) Schematic illustration of GO-PAM-hydrogel (taken from reference<sup>[63b]</sup>)

The obtained GPO sheets functioned as polyfunctional initiating and crosslinking centers due to the high amount of peroxides on the surface, thus initiating a free radical polymerization of acrylamides with GPO and the formation of GO/hydrogels with good physical and self-healing properties<sup>[63b]</sup>. In another report<sup>[63c]</sup>, the surface of GO was modified<sup>[63c]</sup> with the benzyl peroxide groups as a photoinitiator, polymerizing 2-(dimethylamino) ethyl methacrylate (DMAEMA) from the surface with a nearly 21 wt% grafting density proven by XPS and TGA measurements (Table 4, Entry 8).

#### 4.1.3-Catalytic effects of GO and r-GO on FRP

The catalytic effect of GO and r-GO was studied in a free radical polymerization of 1-naphthylamine<sup>[64]</sup>, and 3-amino-phenylboronic acid (ABA)<sup>[65]</sup>. The polymerization of ABA with  $(\text{NH}_4)_2\text{S}_2\text{O}_8$  (APS) as an initiator was studied in the presence of GO and r-GO by UV measurements. A peak at 514 nm appeared for the polymerization of neat ABA in 60 min, this peak was shifted to 732 nm within 390 min and a new peak appeared at 385 nm indicating the formation of the polymer.

The polymerization was 2.5 to 3.3 times faster in presence of GO and r-GO respectively, and the absorption peak was much more narrow and highly red shifted. The narrow peaks indicated the narrow molecular weight distribution and the red shift revealed the longer conjugation of the obtained polymer (Table 4, Entry 9). In conclusion r-GO exhibited a better catalytic activity in comparison to GO because of its conductivity and larger surface area. Although it was proved that r-GO cannot initiate a radical polymerization, it showed good catalytic effect on the free radical polymerization.

**Table 4.** Application of graphene based materials in free radical polymerization

Entry	Type of graphene	Role of graphene	Reaction condition	Monomer	Characterization
1 <sup>[59c]</sup>	GO	Source of free radical	Monomer, GO (2.5 wt%), water, 95 °C, 10 h	N-Vinylpyrrolidone,	XRD: Complete exfoliation of GO sheets Elemental analysis: 46.5 wt% grafting density GPC : $M_n = 3300 Da$
2 <sup>[60a]</sup>	GO	Oxidation agent	Monomer, GO, water, 90 °C, 10 min	Thiophene, aniline, and pyrrole	Good dispersion proved by TEM and SEM Other measurements : FTIR
3 <sup>[61a]</sup>	GO	Redox agent	Monomer, GO-Ce(IV), water, 50 °C, 8 h	Acrylic acid (AA) N-isopropylacrylamide (NIPAM)	AFM: 1.64 nm (PAA) 2.84 nm (PNIPAM) thickness of polymer on the surface TGA: 45.49 % (PAA) 40.77 % (PNIPAM) Other measurements : FTIR
4 <sup>[61b]</sup>	GO	Redox agent	Monomer, GO-Ce(IV)/HNO <sub>3</sub> , 30 °C	Methyl methacrylate (MMA), acrylonitrile (AN), acrylamide (AM)	XRD :Complete exfoliation with PMMA, partial exfoliation with PAN and PAM AFM: 2.43 nm (GO/PAN) 2.67 nm (GO/PMMA) thickness of polymer on the surface Other measurements : FTIR, TGA
5 <sup>[61d]</sup>	GO-amine	Redox agent	Monomer, GO-Ce(IV), water, 50 °C, 5 min, microwave	Acrylamide (AM)	XRD: Complete exfoliation of GO sheets TGA: 35.34- 68.36 wt% weight loss related to grafted polymer Other measurements : FTIR, RAMAN, SEM, TEM
6 <sup>[62a]</sup>	r-GO-ABCPA	Initiator	Monomer , r-GO-ABCPA, 90 °C, 24 h	Acrylamide (AM), 2-vinyl pyridine (VP)	AFM: 4.4 nm (PVP) thickness of polymer on the surface TGA: PAM: 42 wt% GPC: $M_n$ : P2VP 18.4 kDa, PDI = 2.0/ PAM: 1900 kDa XPS: 3.6 wt% of initiator on the surface of r-GO Other measurements : FTIR, TEM
7 <sup>[63a]</sup>	GO-peroxide	Initiator	Acrylamide , GPO (0.17-1.05 wt%),water, 45 °C, 36 h	Acrylamides	SEM showed the connection between GPO and polymer chains as long fibers Other measurements : FTIR, RAMAN, XPS,
8 <sup>[63c]</sup>	GO-benzyl peroxide	Initiator	Monomer, GO-benzyl peroxide, DMF, reaction under UV (36.12, 72.24, and 108.36 mJ/cm <sup>2</sup> )	2-(Dimethylamino) ethyl methacrylate (DMAEMA)	TGA, XPS: 21-27 wt% grafting density Other measurements : FTIR, RAMAN
9 <sup>[65]</sup>	GO r-GO	Catalyst	ABA monomer (10 mM), KF, fructose, buffer solution, GO or r-GO (0.025 mg), (NH <sub>4</sub> ) <sub>2</sub> S <sub>2</sub> O <sub>8</sub> (APS)	Amino-phenylboronic acid (ABA)	UV: Polymerization run 2.5 and 3.3 times faster with GO, and r-GO respectively

## 4.2-Controlled Radical Polymerization (CRL)

### 4.2.1-Atom Transfer Radical Polymerization (ATRP)

The concept of ATRP was developed independently by Matyjaszewski<sup>[66]</sup> and Sawamoto<sup>[67]</sup> and is based on a dynamic equilibrium between an alkyl halide species (dormant species) and propagating radicals (active species), where the equilibrium is slowly on the side of the alkyl halide (dormant species) to decrease the concentration of radicals, in turn diminishing the termination reaction. This equilibrium is established *via* the homolytic cleavage of an alkyl halogen bond (RX) by a metal complex (Cu and Ru) which generates the radical and higher oxidation state of the metal complex<sup>[68]</sup>. Therefore in a graphene-based ATRP system graphene can play either the role of the catalyst by embedding the transition metals on its surface or as the initiator by surface modification of required initiator with alkyl halides. There are many reports on the embedding Cu<sup>[37h, 38b, 42, 44, 51, 69]</sup> and Ru<sup>[37a, 40b, 46, 70]</sup> metal particles on the surface of graphene, but none of them was used as a catalyst in an ATRP polymerization. However many groups reported on the surface modification of graphene with alkyl halides to initiate the ATRP polymerization of different types of monomers<sup>[71]</sup>, where some of them are summarized in Table 5. In a grafting-from polymerization *via* ATRP often a sacrificial initiator is required, in order to maintain the equilibrium between active/dormant species, in turn leading to a living polymerization<sup>[72]</sup>.

In one of the first reports on the functionalization of graphene-based materials with ATRP initiators, r-GO was treated with diazonium salts and subsequently with bromopropionyl bromide to introduce the ATRP initiator onto the surface<sup>[71a]</sup> (Figure 16a). Afterwards styrene was polymerized *via* an ATRP using the r-GO-grafted initiator and methyl-2-bromopropionate (sacrificial initiator) resulting in the grafted PS and non-grafted PS (Entry 1, Table 5).

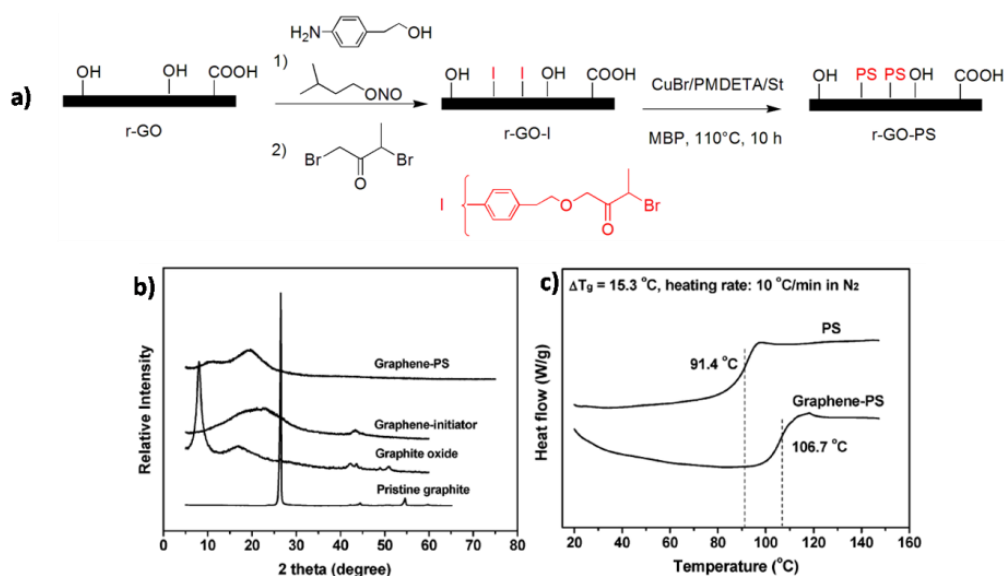


**Figure 16.** a) Surface functionalization of r-GO with ATRP initiator b) XRD of r-GO before and after grafting from polymerization, c) DSC analysis of polystyrene with and without r-GO (taken from reference<sup>[71a]</sup>)



The molecular weight and polydispersity index of the grafted PS chains were determined to be 60 *kDa* and 1.6, respectively, measured *via* GPC of the free polymer resulting from the sacrificial initiator. The successful grafting of PS on the surface was confirmed by FTIR and AFM. The thickness of the PS layer on the surface was measured to be 1 *nm* by AFM, which was more than in a previous report by the free radical polymerization (thickness  $\approx$  0.27 *nm*)<sup>[61b]</sup>. The grafting content of PS was as high as 82 *wt%* measured by TGA and the glass transition temperature ( $T_g$ ) was enhanced by 15 °C measured by DSC (Figure 16c). Furthermore with only 0.9 *wt%* of graphene sheets, the resulting PS composite film showed a 57.2 % and 69.5 % increase in the Young's modulus and tensile strength (relative to the pristine PS film), respectively. In a similar report<sup>[71c]</sup>, GO was modified with an ATRP initiator to polymerize styrene from the surface, in turn exfoliating the GO sheets to the single layers as proven by AFM and TEM. The obtained PS was cleaved from the surface by an acid catalyzed transesterification and the results were compared to the free polymers generated by the sacrificial initiator. The PDI was obtained to be 1.73 and 1.65 for the cleaved PS and free PS, respectively, with molecular weights of the cleaved PS (76.8 *kDa*) being close to that of the free PS (78.8 *kDa*). Moreover, the amount of the initiator was varied by different amounts of the initially used diazonium salt, and the chain length of the polymer on the surface was studied by using different monomer to initiator ratios ( $[M]/[I] = 250-1000$ ), thus proving the livingness of the polymerization initiated from the surface. TEM images showed that the PS dispersed well in the low molecular weight PS-grafted GO, however as the molecular weight increased PS grafted GO started to aggregate as granular domains (Table 5, Entry 2).

Yang et al.<sup>[71b]</sup> introduced the amine groups to the GO sheets followed by grafting an ATRP initiator (2-bromo-2-methylpropionyl bromide) *via* the amine and the hydroxyl groups on the surface. Afterward 2-(dimethylamino)ethyl methacrylate was polymerized from the surface by an ATRP at 60 °C to obtain surface grafted poly-(2-(dimethylamino)ethyl methacrylate) (PDMAEMA) (Figure 17a). GPC of the free polymer chains initiated by the added sacrificial initiator molecules revealed the molecular weight of 27 *kDa* and PDI of 1.72, furthermore the thickness of the polymer on the GO sheets were 4 *nm* proven by AFM analysis (Table 5, Entry 3). In another approach<sup>[71d]</sup>, GO sheets were treated with thionyl chloride to convert the carboxylic acid groups of GO to the acyl chloride groups, subsequently treating the acyl chloride groups with ethylene glycol, followed by attachment of the ATRP initiator moieties by the reaction with 2-bromo-2-methylpropionyl bromide. The ATRP polymerization of MMA was initiated from the modified surface by CuBr/PMDETA at 65 °C in DMF, afterwards the polymer chains were cleaved from the GO sheets using hydrolysis. GPC analysis showed a  $M_n$  of 1170 *Da* and a PDI of 1.09 (Table 5, Entry 4), which is the lowest value achieved in comparison to the other studies. Also the successful surface modification of GO with the initiator and



polymer was confirmed by FTIR, TGA, AFM and TEM, where the presence of dark spots in TEM, and HRTEM (Figure 17b) can be attributed to the polymer brushes on the surface of GO.

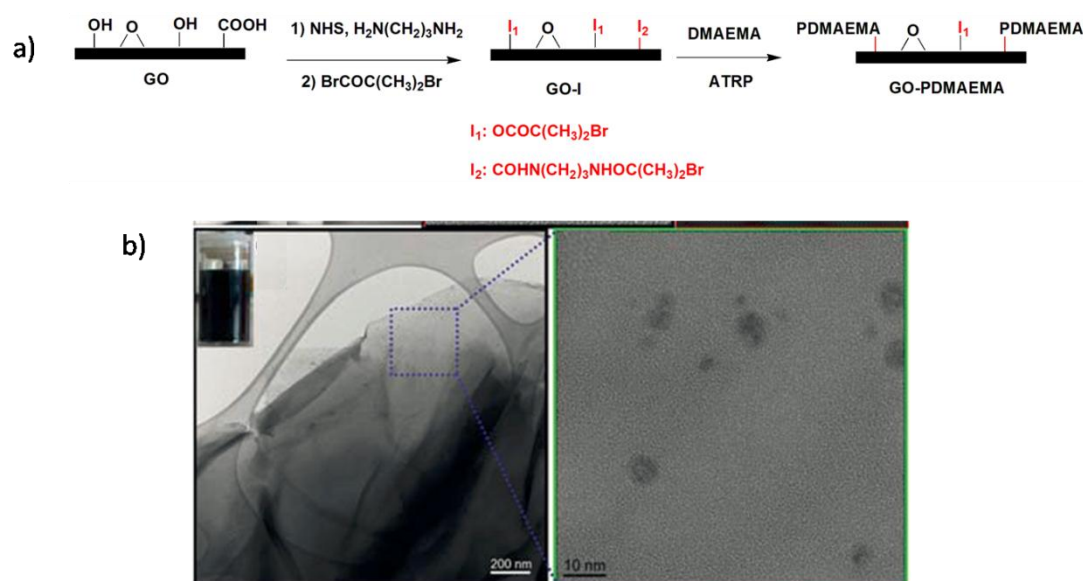


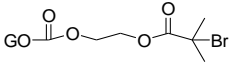
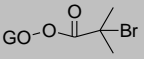
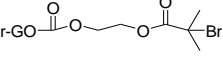
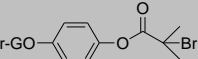
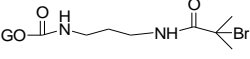
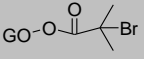
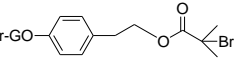
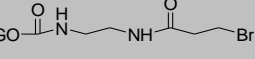
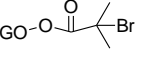
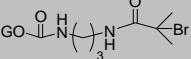
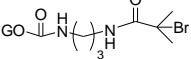
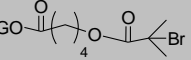
**Figure 17.** a) Surface modification of GO by ATRP initiator (taken from reference<sup>[71b]</sup>) b) PMMA brushes on the surface of GO proven by TEM and HRTEM (taken from reference<sup>[71d]</sup>)

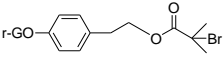
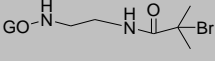
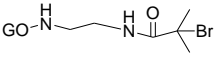
In a direct pathway for the functionalization of GO with an ATRP initiator, the hydroxyl groups on the surface of GO were reacted with bromo isobutyryl bromide to obtain the GO-grafted-ATRP initiator<sup>[71e]</sup>. Methyl methacrylate was successfully polymerized with the achieved GO-grafted-ATRP, and AFM data supported that PMMA increased the thickness of the graphene sheet from 1.2 nm to 2 nm and 4.5 nm due to the polymerization of MMA from initiators at the side and at the basal planes (Table 5, Entry 5). Based on these early studies on the surface initiated ATRP from the graphene-based materials surfaces, different monomers were polymerized by this method like the ionic liquid monomers, [2-(methacryloyloxy)-ethyl]trimethylammonium tetra-fluoroborate ([MATMA] [BF<sub>4</sub>])<sup>[71j]</sup> or *N*-isopropylacrylamide<sup>[71k]</sup>, *N*-hydroxysuccinimide (NHS) styrene derivatives<sup>[71l]</sup>, and *N*-(2-hydroxyphenyl)methacrylamide<sup>[71p]</sup>.

**Table 5.** Modification of GO and r-GO with alkyl halides and application in subsequent ATRP

Entry	Alkyl halide modified GO	Amount of initiator	Reaction condition	monomer	Characterization
1 <sup>[71a]</sup>		---	Styrene, CuBr/PMDETA, MBP, 110 °C, 10 h	Styrene	GPC: $M_n = 60 \text{ kDa}$ , PDI = 1.6 AFM: 1 nm thickness of PS grafted on GO TGA: 82 wt% weight loss DSC: 15 °C increase in $T_g$ with 12 wt% of GO sheets Other measurements: TEM, DMA
2 <sup>[71c]</sup>		1 functional groups per 49 carbon atom	Styrene, CuBr/PMDETA, MBP, 110 °C, 14 h	Styrene	GPC: $M_n = 76.8 \text{ kDa}$ , and PDI = 1.73 AFM: 3.5 nm thickness of PS grafted on GO XRD: Showed no peak, complete exfoliation of GO
3 <sup>[71b]</sup>		0.45 wt% (0.056 mmol/g)	DMAEMA, CuBr, PMDETA, 60 °C, 24 h	2-(Dimethylamino)ethyl methacrylate	GPC: $M_n = 27 \text{ kDa}$ , PDI = 1.72 AFM: 4 nm thickness of polymer grafted on GO Other measurements: FTIR, TEM, XPS

## I. INTRODUCTION

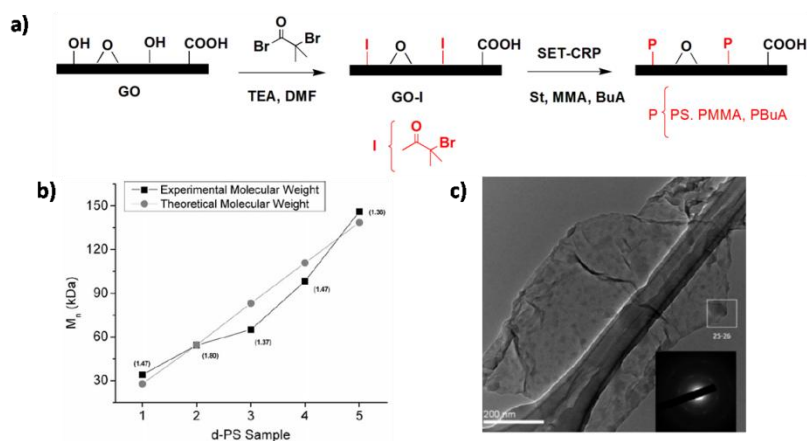
4 <sup>[71d]</sup>		----	Monomer, CuBr/PMDETA DMF, 65 °C, 24 h	MMA	GPC: $M_n = 1.170 \text{ kDa}$ , PDI = 1.09 Polymer brushes confirmed by HRTEM Other measurements : TEM, FTIR, TGA, AFM
5 <sup>[71e]</sup>		----	Monomer, CuCl/PMDETA, DMF, 60 °C, 48 h	MMA	AFM: 2 nm and 4.5 nm thickness of polymer grafted on side, and basal of GO TGA: 21 °C increase in degradation temperature (using 2.5 wt% of GO) Other measurements : FTIR, DSC, DMA, conductivity
6 <sup>[71g]</sup>		----	MMA, CuBr/TMEDA, DMF, 60 °C, 12 h	Styrene, MMA	AFM: 1 nm and 0.73 nm thickness of PS and PMMA respectively grafted on GO Other measurements : FTIR, TEM, RAMAN
7 <sup>[71i]</sup>		----	NIPAM, CuBr/PMDETA, water, 25 °C, 24 h	NIPAM	TGA : 7.5- 37.5 wt% weight loss Other measurements : FTIR, TEM, RAMAN
8 <sup>[71j]</sup>		----	Monomer, CuBr/HMTETA, acetonitrile, 100 °C, 24 h.	[2-(Methacryloyloxy)ethyl]trimethylammonium tetrafluoroborate ([MATMA][BF <sub>4</sub> ])	XRD: Partial exfoliation of GO after polymerization. TEM: Good cover GO by polymer TGA: 50 wt% weight loss Other measurements : FTIR, XPS, RAMAN
9 <sup>[71k]</sup>		1.2 wt%	Monomer, CuBr/PMDETA, ethanol, 65 °C, 50 h	NIPA	XPS: 40 wt% PNIPA in composite AFM: 2.3 nm thickness of Polymer grafted on GO XRD: Partial exfoliation of GO TEM, SEM : Good cover GO by polymer
10 <sup>[71l]</sup>		10 initiators per 1000 graphene carbons	Monomer, CuBr/PMDETA, DMSO, 80 °C, 15 h	2,5-Dioxopyrrolidin-1-yl-4-vinylbenzoate (NHVB)	GPC: ~30 repeat units Other measurements : XPS, RAMAN
11 <sup>[71m]</sup>		----	Monomer, CuBr/PMDETA, DMF, 120 °C, 12 h	Sodium 4-styrenesulfonate	AFM: 5.3 nm thickness of polymer grafted on GO XRD: Complete exfoliation of GO XPS: 15.7 wt% grafting of polymer on GO Other measurements : SEM, TEM
12 <sup>[71n]</sup>		1.3 wt%	Monomer, CuBr/PMDETA, DMF, 60 °C, 24 h	2-N,N-Dimethylaminoethyl methacrylate	XRD: Small exfoliation of GO XPS: 16 wt% grafting of polymer on GO Other measurements : FTIR, TGA
13 <sup>[71o]</sup>		----	Monomer, CuBr/PMDETA, 1,4 dioxane, 80 °C, 48 h	N-Vinyl caprolactam	GPC: $M_n=10 \text{ kDa}$ , PDI=1.47 TGA: 20 wt% grafted polymer Other measurements : FTIR, TEM
14 <sup>[71p]</sup>		8.75 wt%	Monomer, CuBr/PMDETA, 60 °C, 48 h	Tert-butyl acrylate	GPC: $M_n=17.6 \text{ kDa}$ , PDI = 1.33 AFM: 6 nm thickness of polymer grafted on GO AFM: 5-6 nm thickness of polymer TGA: 35 wt% grafted polymer Other measurements : FTIR, XPS, RAMAN
15 <sup>[71q]</sup>		6.23 wt%	Monomer, CuBr/PMDETA, DMF, 110 °C	Styrene	GPC: $M_n=17.77 \text{ kDa}$ , PDI=1.72 DSC: 21 °C increase in $T_g$ with 0.4 wt% of GO initiator XRD: exfoliation of GO sheets by grafted polymer Other measurements : FTIR, XPS, RAMAN, TGA, TEM, SEM

16 <sup>[71s]</sup>		----	Monomer, CuBr/PMDETA, THF, 60 °C, 12 h	<i>N</i> -(2-Hydroxyphenyl)methacrylamide	GPC: $M_n = 17.6 \text{ kDa}$ , PDI = 1.7 TGA: 41 wt% grafted polymer AFM : 3.9 nm thickness of polymer on the surface Other measurements : FTIR, XPS, RAMAN, SEM
17 <sup>[71t]</sup>		----	Monomer, CuBr/PMDETA, DMF, 80 °C, 10-20 h	MMA	GPC: $M_n=43.9 \text{ kDa}$ (10 h) 60 kDa (20 h) AFM : 6.0 nm thickness of polymer grafted on GO TGA. 62 -81 wt% weight loss Other measurements : FTIR, XPS, RAMAN, SEM, TEM
18 <sup>[71u]</sup>		----	Monomer, CuBr/PMDETA, DMF, 110 °C	Styrene	GPC: $M_n=15.98 \text{ kDa}$ , PDI=1.69 XRD: exfoliation of GO sheets by grafted polymer Other measurements : FTIR, XPS, RAMAN, TGA, DSC, SEM, TEM

#### 4.2.2-Single Electron Transfer Controlled Radical Polymerization (SET-CRP)

In 2006 Percec et al.<sup>[73]</sup> reported on a robust and fast polymerization of the acrylates, methacrylates and vinyl chloride at low temperature including the properties of a living polymerization such as a low PDI, high conversion, defined end groups and the capability of preparing block copolymers which was named as Single Electron Transfer Controlled Radical Polymerization (SET-CRP) or Cu(0)-mediated radical polymerization<sup>[74]</sup>. The initiation step was proposed to be mediated by a single electron transfer (SET) from the Cu(0) electron donor (or other donor species) to the electron acceptor alkyl halide. To date there are few reports on the application of GO as an initiator<sup>[75]</sup> in a SET-CRP although the GO functionalized alkyl halides known from the ATRP can be potentially used in the SET-CRP. Furthermore like ATRP, there are no reports on the direct usage of the graphene-based materials as a catalyst, although there are many reports on the decorating of Cu particles on the graphene materials surfaces as mentioned previously.

The group of Bielawski<sup>[75a]</sup> reported a complete study of the successful functionalization of GO with SET-CRP initiators (alkyl halide) and the livingness of the polymerization from its surface. GO was treated with isobutryl bromide in excess of triethylamine in DMF to modify the hydroxyl groups of GO by the SET-CRP initiator in an esterification reaction (Figure 18a). To confirm the attachment of the SET-CRP initiator, the pre- and postfunctionalized graphene oxide samples were analyzed using X-ray photoelectron spectroscopy (XPS) and elemental analysis, which are more promising methods in comparison to FTIR. In the XPS spectra of alkyl halide modified GO, signals attributed to the formation of C-Br bonds appeared in the C atom (285.4 eV) and Br atom area, which were absent in the pristine GO. Furthermore the intensity of the signals attributed to the C-O groups diminished in the alkyl halide modified GO. Collectively, the overall changes reflected a decrease in the quantity of the hydroxyl groups on the surface of GO upon esterification. Moreover elemental analysis showed a 1.2 wt% (0.00115 mmol/mg) alkyl halide initiator on the surface of GO.

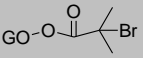
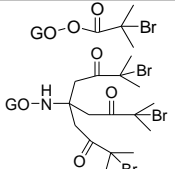
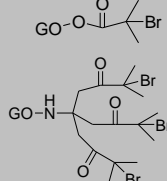
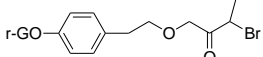
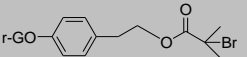


**Figure 18.** a) Surface modification of GO with an alkyl halide and the subsequent SET-CRP polymerization with Cu(0) from the surface, b) the livingness evidence of the SET-CRP polymerization of PS from the surface c) the polymer brushes on the surface of GO proved by TEM (taken from reference<sup>[75a]</sup>)

After the confirmation of the modification of GO with the alkyl halide initiator a series of SET-CRP polymerizations were run using Cu(0) at 80 °C with different monomers like styrene, methyl methacrylate, butyl acrylate and tris(2-aminoethyl)amine (Table 6, Entry 1). It was possible to control the chain lengths of the polymer grown from the surfaces, examined with the different monomer to GO-grafted initiator ratio (1-5 ml of styrene relative to the fix amount (100 mg) of GO-initiator). The grafted polymers were detached from the GO surface *via* saponification with sodium hydroxide in DMF and the molecular weight and PDI were measured by GPC. The molecular weights agreed with the calculated ones (Figure 18b) and showed relatively low polydispersities (PDIs typically less than 1.5) suggesting that the polymerization proceeded in a controlled manner from the GO surface. Moreover TEM results proved the existence of the polymer brushes on the surface (Figure 18c). In another report,<sup>[75c]</sup> GO was reacted with tris(hydroxymethyl) aminomethane (TRIS) as an amine functionality to increase the amount the of hydroxyl groups on the surface and subsequently introduce the alkyl halide to the surface by an esterification reaction between 2-bromo-2-methylpropionyl bromide and the hydroxyl groups of GO (Table 6, Entry 2). XPS and elemental analyses were used to confirm the successful functionalization and revealed one TRIS moiety per seven aromatic rings. The obtained GO-initiator was used in the SET-CRP polymerization of poly(ethylene glycol) ethyl ether methacrylate (PEGEEMA) macromonomer in water/THF solvent mixture at 40 °C using CuBr/tris(2-(dimethylamino)ethyl)amine (Me6TREN) and the sacrificial initiator methyl 2-bromopropionate for 24 h. It is reported that this solvent mixture disproportionates Cu(I) rapidly to Cu(0) and Cu(II) before the activation can occur *via* a Cu(I) ATRP process<sup>[76]</sup>. GPC analysis of the PPEGEEMA initiated by the sacrificial initiator resulted in a  $M_n$  of 8500 Da and a PDI of 1.23. TGA analysis revealed that the PPEGEEMA-GO sheets comprised 45 wt% of the polymer. AFM analysis showed a thickness of 7–9 nm for the polymer on the surface exfoliating the GO completely and made it dispersible in both polar and nonpolar solvents.

The same procedure was used for the SET-CRP polymerization of NIPAM, where the livingness of the surface initiated polymerization was confirmed by using the different ratios of the monomer to GO-initiator ( $[M]/[I]: 1000$  and  $250$ )<sup>[75d]</sup> (Table 6, Entry 3). In other works, tertbutyl methacrylate (tBMA) (Table 6, Entry 4)<sup>[75b]</sup>, and 2-hydroxyethyl acrylate (Table 6, Entry 5)<sup>[75e]</sup> were polymerized by a SET-CRP initiated from the surface of GO.

**Table 6.** Modification of GO and r-GO with alkyl halides and subsequent in SET-CRP

Entry	Alkyl halide modified GO	Amount of initiator	Reaction condition	monomer	Characterization
1 <sup>[75a]</sup>		0.00115 mmol/mg	Monomer, Cu(0), DMF, 80 °C, 18 h	Styrene, methyl methacrylate, butyl acrylate and, tris(2-aminoethyl)amine	GPC: PS: $M_n=17$ kDa, PDI=1.5 TEM : proved the polymer brushed on GO Other measurements: XPS,AFM, TGA, RAMAN
2 <sup>[75c]</sup>		1.338 mmol/g	Monomer, CuBr/tris(2-(dimethylamino)ethyl)amine water/THF, 40 °C	poly(ethylene glycol) ethyl ether methacrylate macromonomer	GPC: $M_n = 8500$ Da, PDI = 1.23 AFM : 7–9 nm thickness of polymer on GO TGA: 45 wt% weight loss Other measurements: AFM, TGA, RAMAN
3 <sup>[75d]</sup>		1.338 mmol/g	Monomer, CuBr/tris(2-(dimethylamino)ethyl)amine, DMF/THF , 25 °C, 24 h	NIPAM	GPC: $M_n =46$ kDa to 140 kDa , PDI = 1.29 and 1.15 AFM: 4-9 nm thickness of polymer on GO TGA: 15-17 wt% weight loss Other measurements: FTIR, RAMAN, TEM
4 <sup>[75b]</sup>		11.5 – 9.7 wt% of Br	Monomer, Cu(0) wire/Me6TREN , DMSO, 25 °C, 24 h	tertbutyl methacrylate (tBMA)	GPC: $M_n = 4500$ Da, PD I=1.12 AFM= 8.3 nm thickness of polymer on r-GO TGA: 71.7 wt% grafted polymer onto r-GO Other measurements: RAMAN, TEM
5 <sup>[75e]</sup>		4.83 wt% of Br	Monomer, Cu(0) wire/Me6TREN DMSO, 25 °C, 2h	2-hydroxyethyl acrylate	GPC: $M_n = 14.8$ kDa , PDI = 1.14 AFM: 6.196 nm thickness of polymer on r-GO TGA: 23.24 wt% grafter polymer of surface Other measurements: FTIR, RAMAN, TEM

#### 4.2.3-Reversible Addition-Fragmentation Chain Transfer Polymerization (RAFT)

The RAFT method relies on the high chain transfer coefficients of the thiocarbonylthio compounds and trithiocarbonates, and requires the addition of a radical initiator, because the chain activation process does not lead to an overall increase in the number of radicals<sup>[77]</sup>. Therefore the GO surface can be easily functionalized with RAFT agents<sup>[78]</sup>, after which, polymerization can be grafted from the surface of GO. Table 7 summarizes selected publications on the modification of GO with RAFT agents and their applications in the RAFT polymerization. In an early report for the grafting of the RAFT agent onto a graphene oxide (GO) surface, GO was reacted with  $\text{SOCl}_2$  to obtain GO-Cl, followed by the reaction of the so-generated GO-Cl with HEBriB to obtain GO-Br. Finally, a reaction between

phenylmagnesium bromide,  $\text{CS}_2$  and GO-Br led to GO-RAFT<sup>[78a]</sup>. As synthesized GO-RAFT was used in the polymerization of methacrylamide monomer from the surface of GO using AIBN as an initiator at 60 °C, proving the successful functionalization by the FTIR, RAMAN and TGA analysis (Table 7, Entry 1). Etmimi et al.<sup>[78b]</sup> attached the RAFT agent, dodecyl isobutyric acid trithiocarbonate (DIBTC), to the surface of GO by a coupling reaction between the hydroxyl groups of GO and DIBTC with the help of DCC and DMAP as coupling catalysts (Figure 19a). The successful functionalization of GO with the RAFT agent was proved by FTIR (Figure 19b) and TGA.

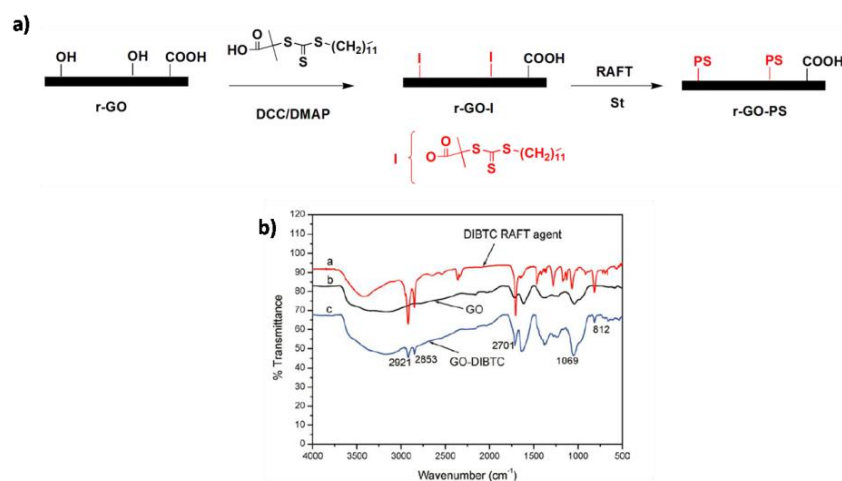


**Figure 19.** a) Surface functionalization of GO with the RAFT agent b) FTIR of GO before and after the functionalization with the RAFT agent (taken from reference<sup>[78b]</sup>)

Furthermore GO-DIBTC was dispersed in the styrene monomer, a surfactant (sodium dodecylbenzene sulfonate) and a hydrophobe (hexadecane) to form miniemulsions for the RAFT assisted emulsion polymerization using AIBN as the initiator to yield encapsulated PS-GO nanocomposites. Different GO-RAFT-agent/monomer ratios (1-7 wt%) with the constant amount of the initiator were used to control the polymerization, obtaining different molecular weights from 28.77 kDa to 67.5 kDa, with PDI between 1.62 and 1.26. The polymer particle size ranged from 150 nm to 180 nm with a narrow size distribution, resulting from the controlled polymerization (Table 7, Entry 2). With the same chemistry S-1-dodecyl-S'-( $\alpha,\alpha'$ -dimethyl- $\alpha''$ -acetic acid) trithiocarbonate was attached as a RAFT agent onto the surface of GO<sup>[78c]</sup>. RAFT polymerization of *N*-vinylcarbazole with the GO-RAFT agent was carried out in THF at 70 °C with AIBN as an initiator. GPC analysis of the detached polymer revealed a  $M_n$  of 8050 Da and a PDI of 1.43, successful grafting was supported by the FTIR, RAMAN spectroscopy and AFM analysis (Table 7, Entry 3), where AFM measurement showed the large thickness (20 nm) of GO-poly(*N*-vinylcarbazole) nanocomposite.

Mülhaupt et al.<sup>[78d]</sup> functionalized the surfaces of GO, the amine functionalized GO (GO-Stearyl) and the thermally reduced GO (TRGO) with different sulfur containing groups such as dithiocarbonates (DTC), dithioester (DTE), and thiols (Figure 20). These modified graphene oxide materials were used as macro chain-transfer agents and RAFT agents in the styrene radical polymerizations. In addition to

previous reports for the preparation of the RAFT agent on the surface of GO such as coupling reactions with DMAP/DCC and Grignard reagent, the hydroxyl groups of GO were deprotonated by different bases and converted either with carbon disulfide or benzyl bromide to benzyldithiocarbonate groups as RAFT agents or by propylene sulfide to thiols as a macro chain transfer agent. It had been proved that the use of stronger bases like BuLi and NaH led to an increase of the grafting density of the polymer on the surface of GO. In contrast to the other reports, the GO initiated RAFT polymerization of styrene was accomplished in bulk (without solvent), and the GPC analysis of the detached polymer from dithiocarbonate linkers showed a molecular weight of 30.4 *kDa* with a polydispersity of 5.0.

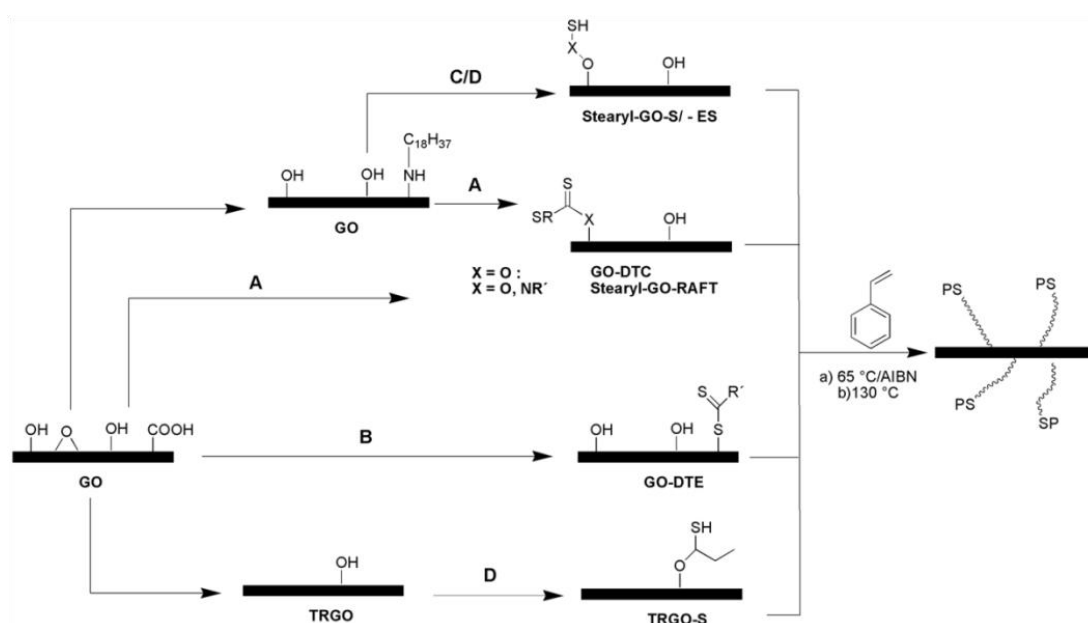


**Figure 20.** Surface functionalization of graphene-based materials with different sulfur containing groups used as initiator for RAFT polymerization (taken from reference<sup>[78d]</sup>)

In another route to attach the RAFT agent<sup>[78g]</sup> on the surface of graphene materials, *r*-GO was functionalized with an alkyne group with diazonium salt of propargyl *p*-aminobenzoate, followed by the click reaction between the alkyne functionalized *r*-GO and *S*-1-dodecyl-*S'*-( $\alpha,\alpha'$ -dimethyl- $\alpha''$ -3-azido-1-propyl acetate) trithiocarbonate. The successful functionalization was proved by FTIR, TGA, XPS and AFM methods, and NIPAM was polymerized with the help of the obtained *r*-GO-RAFT in DMF with AIBN as an initiator. Analysis of the free polymer from the sacrificial RAFT agent showed a  $M_n$  of 19 *kDa* and PDI of 1.77 (Table 7, Entry 4). Using the same method different polymers like PS, PMAA, P4VP, and PDMA were polymerized *via* RAFT from the surface of GO<sup>[78h]</sup> (Table 7, Entry 5). Furthermore the other groups were able to synthesize GO-hydrogels<sup>[78j]</sup> (Table 7, Entry 6), GO-block copolymers (GO-PHEMA-*b*-PAA<sup>[78k]</sup> (Table 7, Entry 7) and GO-PNIPAM-*b*-acryloyloxy)butoxy)coumarin<sup>[78m]</sup>) (Table 7, Entry 9) *via* the RAFT polymerization using GO as an initiator.



**Table 7.** Modification of GO and r-GO with RAFT agents and application in RAFT polymerization

Entry	Type of graphene	Amount of RAFT agent	Reaction condition	monomer	Characterization
1 <sup>[78a]</sup>		----	Monomer, AIBN, 60 °C	Methacrylamide	AFM: 3.70 nm thickness of polymer on GO TGA: 63.15 wt% weight loss Other measurements : RAMAN, FTIR, TEM
2 <sup>[78b]</sup>		32 wt% of RAFT agent	Monomer, AIBN, Surfactant (sodium dodecylbenzene sulfonate)	Styrene	Emulsion polymerization GPC: M <sub>n</sub> = 28.77 to 67.5 kDa, PDI = 1.62 to 1.26 Polymer particle size : 150-180 nm XRD: complete exfoliation of GO sheets Other measurements : RAMAN, FTIR, TEM, TGA
3 <sup>[78c]</sup>		----	Monomer, AIBN, THF, 70 °C, 12 h	N-Vinylcarbazole	GPC: M <sub>n</sub> = 8050 Da, PDI = 1.43 AFM: 20 nm thickness of polymer on GO Other measurements : RAMAN, FTIR, XPS, TEM, TGA
4 <sup>[78g]</sup>		0.34 mmol/g	Monomer, AIBN, DMF, 60 °C, 20 h	NIPAM	GPC: M <sub>n</sub> = 19 kDa, PDI = 1.77 AFM: 1.7-3 nm thickness of polymer on GO TGA: 68 wt% weight loss Other measurements : RAMAN, FTIR, XPS, TEM, TGA
5 <sup>[78h]</sup>		1.35 functional groups per 100 carbons	Monomer, AIBN, DMF, 70 °C, 24 h	Styrene, MMA, 4VP, DMA, ethylene glycol	GPC: PMMA : M <sub>n</sub> = 63.440 kDa, PDI = 1.87/ PS : M <sub>n</sub> = 41.21 kDa, PDI= 1.33/ P4VP : M <sub>n</sub> = 51.560 kDa, PDI= 1.93/ PDMA : M <sub>n</sub> = 72.2 kDa PDI= 2.64 FTIR : 70.9 wt% grafted polymer on surface XRD: partial exfoliation of GO sheets Other measurements : RAMAN, XPS, TEM
6 <sup>[78j]</sup>		----	Monomer, AIBN, dioxane, 75 °C, 7 h	Acrylic acid	Diglycoldimethacrylate as crosslinker to make hydrogel Other measurements : RAMAN, FTIR, TEM, SEM, TGA
7 <sup>[78k]</sup>		----	Monomer, AIBN, DMF, 70 °C, 24 h	2-Hydroxyethyl methacrylate (HEMA), acrylic acid (AA)	GPC: P(HEMA) M <sub>n</sub> = 5100 Da, PDI = 1.18 P(HEMA-b-AA): M <sub>n</sub> = 8800 Da, PDI=1.32 TGA: 35 wt% weight loss related to grafted polymer XRD: exfoliation of GO sheets after polymerization Other measurements : RAMAN, FTIR, SEM
8 <sup>[78l]</sup>		0.75 atom% of S 0.84 RAFT agent per 100 carbons	Monomer, AIBN, 75 °C, 48 h	Styrene	GPC: M <sub>n</sub> = 86.992 kDa, PDI=1.79 TGA: 0.18 polymer chains per 100 carbon atoms AFM: 4.1 nm thickness of polymer on the surface of r-GO, Other measurements : RAMAN, FTIR, XRD, SEM, DSC
9 <sup>[78m]</sup>		----	Monomer, AIBN, DMF, 65 °C, 12 h,	1-NIPAM 2- 7-(4-(Acryloyloxy)butoxy)coumarin (7AC)	GPC: PNIPAM : M <sub>n</sub> = 5.9 kDa, PDI=1.13 Block : 6.4 kDa, PDI=1.16 AFM : 3.15 nm thickness of block-copolymer on GO Other measurements : RAMAN, FTIR, XPS, TGA, TEM

#### 4.2.4-Nitroxide Mediated Polymerization (NMP)

There are some reports<sup>[79]</sup> on the functionalization of the GO surface with 2,2,6,6-tetramethylpiperidine 1-oxyl (TEMPO, T), although only one of them was used as an initiator for the NMP polymerization<sup>[79b]</sup>. In this publication<sup>[79b]</sup>, GO was dispersed in DMF followed by the addition of Br-TEMPO solution drop wise to the dispersion in the presence of triethylamine to obtain TEMPO



functionalized GO (GO-TEMPO). The successful functionalization of GO with TEMPO was proved *via* XPS, where the appearance of a peak at 400.5 eV could be attributed to the presence of the nitrogen from TEMPO. Afterwards styrene and isoprene were polymerized with the help of GO-TEMPO in a NMP polymerization in DMF at 130 °C for 7 h. The obtained GO-polymer composite was analyzed with FTIR, TEM, TGA and XPS. The molecular weight of PS on the surface of GO was estimated to be 370 Da by the mass loss in TGA.

### 4.3-Ionic polymerization

#### 4.3.1- Cationic polymerization

The oxygen-containing functional groups on GO can induce acidity ( $pK_a \sim 3$  in water) to the surface which can be useful for the cationic polymerization. Bielawski et al.<sup>[80]</sup> catalyzed the cationic ring opening polymerization (ROP) of the various cyclic lactones and lactams, such as  $\epsilon$ -caprolactone, d-valerolactone, and  $\epsilon$ -caprolactam, to the corresponding polyesters or polyamides (Figure 21).

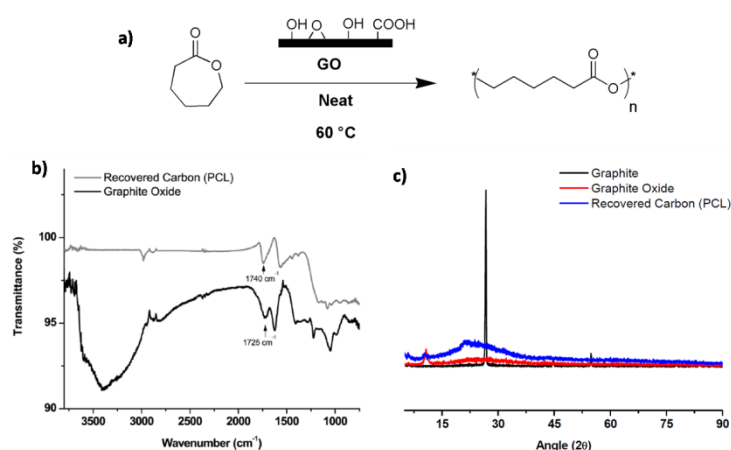


**Figure 21.** a) Cationic polymerization of  $\epsilon$ -caprolactone catalyzed by GO at 60 °C, the b) FTIR and c) XRD of GO before and after the polymerization reaction (taken from reference<sup>[80]</sup>).

In a typical procedure,  $\epsilon$ -caprolactone was heated with GO (2.5 wt%) to obtain poly( $\epsilon$ -caprolactone) (PCL). Subsequent dissolving of the resulted polymer in tetrahydrofuran (THF) and separating from the GO catalyst *via* filtration, GPC revealed a  $M_n$  of 5.1 kDa with a PDI of 2.1, and NMR did not show any side products. Furthermore different amounts of GO (1 wt% - 20 wt%) were used as a catalyst in the polymerization showing that with loadings at or above 2.5 wt% of GO as catalyst the conversion of the monomer was uniformly quantitative, and with more than 2.5 wt% neither the molecular weight nor the PDI did change significantly remaining in the range of 4.8–5.6 kDa for  $M_n$ , and 2.0–2.2 for PDI. The recovered GO from the polymerization was ineffective for the polymerization of  $\epsilon$ -caprolactone under the same conditions, because it was partially reduced to r-GO as proven by the FTIR (Figure 21b), conductivity measurement, elemental analysis and XRD (Figure 21c).

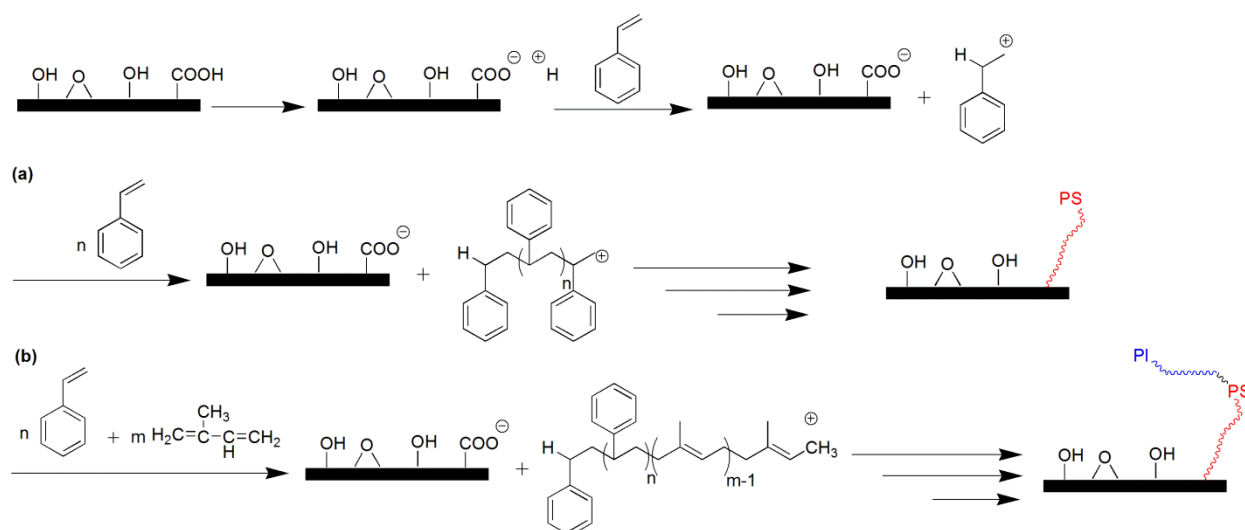


**Figure 22.** Possible reaction mechanism of using GO as the cationic initiator for a) the polymerization of styrene and b) the copolymerization of styrene and isoprene (taken from reference<sup>[81]</sup>)

The same authors reported the polymerization of different olefins such as butyl vinyl ether, *N*-vinylcarbazole, styrene, and sodium 4-styrenesulfonate<sup>[82]</sup> with the same procedure in bulk. In contrast to ROP of the cyclic lactones, the recovered GO was reused in the polymerization of olefins five times with a slight reduction in monomer conversion. Furthermore the analysis of the surface of GO after the polymerization of the cyclic lactones and olefins revealed that the surface was slightly grafted about 12 wt% by the polymer measured by the TGA analysis. They were also able to modify the surface of GO either by the cationic polymerization of styrene or by the cationic copolymerization of styrene and isoprene from the surface (Figure 22)<sup>[81]</sup>.

In another publication,<sup>[83]</sup> the catalytic effect of GO on the cationic ring-opening polymerization of benzoxazine for the formation of a GO/benzoxazine nanocomposite was studied.

#### 4.3.2-Anionic polymerization

Although the surface of GO could be anionized by different techniques (e.g by  $K_2CO_3$  or reduction with hydrazine) there are no reports on the use of the graphene based materials as a direct initiator or catalyst in the anionic polymerization.

Besides the functionalization of GO with BuLi, which potentially can be used in the anionic polymerization<sup>[84]</sup>, in another publication,<sup>[85]</sup> the surface of GO was modified with  $\epsilon$ -caprolactam and used in the anionic polymerization of PA6 in the presence of a caprolactam magnesium bromide as an initiator in combination with a difunctional hexamethylene-1,6-dicarbamoylcaprolactam as an activator and  $\epsilon$ -caprolactam as a monomer (Figure 23). The molecular weights of the so-obtained PA6 matrix in the PA6-GO nanocomposites were in the range of 15 kDa to 21 kDa which were measured

by the dilute solution viscometry. AFM showed the thickness of 4.1 nm for PA6 grafted onto the surface of GO.

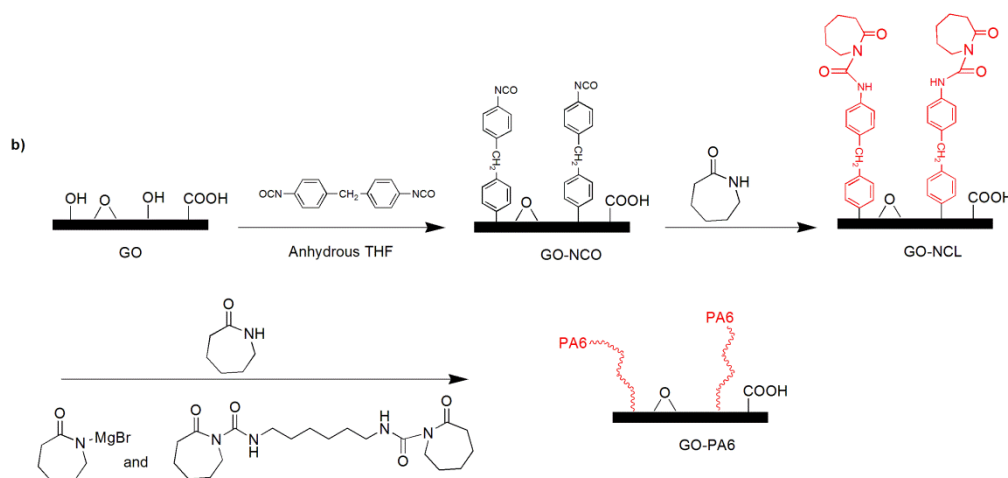


**Figure 23.** Modification of GO with caprolactam and subsequent anionic polymerization from the surface (taken from reference<sup>[85]</sup>)

#### 4.4-Polycondensation reactions

The group of Bielawski successfully polymerized poly(phenylene methylene) from benzyl alcohol in a polycondensation reaction using GO as a catalyst.<sup>[86]</sup> Benzyl alcohol was heated with 10 wt% of GO as the acidic catalyst in a sealed vessel to 200 °C for 14 h under vigorous magnetic stirring, resulting in poly(phenylene methylene) which was dissolved in organic solvents and separated from GO by filtration. GPC showed a  $M_n$  of 2.3 kDa and a PDI of 1.26; NMR proved the full conversion and purity of the product. Furthermore for loadings of GO below 7.5 wt% as the catalyst, GO was unable to completely polymerize benzyl alcohol.

In other reports<sup>[87]</sup>, the catalytic effect of GO on the curing of the epoxy resins<sup>[87a, 87c]</sup>, cyanate ester resin<sup>[87d]</sup> and amino novolac phthalonitrile<sup>[87b]</sup> have been studied. For example, a diglycidyl ether of bisphenol A with isophoronediamine was cured in the presence of different GO amounts. DSC measurements showed an increase in  $T_g$  of the epoxy resin about 30 °C with adding more GO in the composite proving the catalytic effect of GO on the curing reaction between epoxy and amines. Furthermore GO successfully catalyzed the condensation reaction between pyrrole and aldehydes forming a GO/hydrogel composites<sup>[88]</sup>.

#### 4.5-Insertion-coordination polymerizations

Organometallic catalysts are capable of polymerizing different types of monomers (polar to non-polar) by insertion-coordination polymerizations. The oxygen-containing moieties on the surface of GO and r-GO enable the functionalization of their surfaces with organometallic catalysts useful in different organic reactions<sup>[36t, 36u, 36w, 36ai, 36aj, 37c, 37e, 37f, 38-47]</sup> as discussed previously in section 3. In the same vein organometallic catalysts can be prepared for the insertion polymerization reactions.

## 4.5.1-Ziegler-Natta polymerization

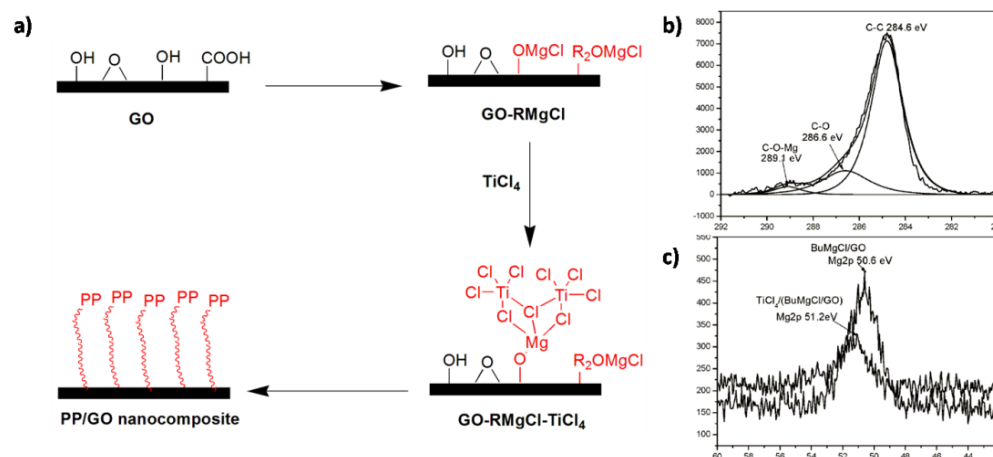


**Figure 24.** a) Immobilization of Ziegler-Natta catalysts on the surface of GO *via ex situ* hybridization, proving the successful functionalization with high resolution XPS region of b) carbon and c) magnesium (taken from reference<sup>[89]</sup>)

GO can be modified by Ziegler-Natta catalysts in a two step reaction<sup>[89]</sup>, firstly treating GO with BuMgCl Grignard reagents in THF, afterwards reacting the BuMgCl/GO product with TiCl<sub>4</sub> to achieve r-GO-Mg-TiCl<sub>4</sub> catalyst (Figure 24). The successful functionalization of the surface by Ziegler-Natta catalyst was proved by XPS and EDX. After the modification of GO with BuMgCl, in XPS measurement, the C1s peak of GO at 286.6 eV vanished, and the band at 289.1 eV related to C-O-Mg bond could be detected (Figure 24b). Furthermore after treatment with TiCl<sub>4</sub>, the Mg 2p band of BuMgCl/GO located at 50.6 eV slightly shifted to higher binding energies (51.2 eV) (Figure 24c). Ziegler-Natta polymerization with this catalyst led to polypropylene with molecular weights in the range of 730 kDa to 810 kDa. Furthermore, the high dispersion of PP in GO was proved by TEM and SEM, and the obtained polypropylene exhibited conductivities of  $9.33 \times 10^{-4} \text{ S/m}$  and  $3.12 \times 10^{-1} \text{ S/m}$  for 1.52 wt% and 4.9 wt% of GO, respectively (Table 8, Entry 1). Using nearly the same method, further works on the immobilization of the Ziegler-Natta catalyst on the surface of GO have been published<sup>[90]</sup> and are listed in Table 8 (Entries 2 and 3).

## 4.5.2-Polymerization-filling technique (PFT)

Mülhaupt et al.<sup>[91]</sup> successfully prepared UHMWPE with an immobilized Cr catalyst on the surface of r-GO : for this purpose r-GO (thermally reduced) was mixed with methyl ammonium oxide (MAO) and dichloro- $\eta^5$ -[3,4,5-trimethyl-1-(8-quinolyl)-2-trimethylsilylcyclopentadienyl]-chromium(III) (Cr1) to immobilize the Cr catalyst on the surface of r-GO. Afterwards ethylene was polymerized in *n*-heptane at 40 °C and 5 bar pressure between 22 and 72 min in a stirred autoclave to produce the nanocomposites with r-GO catalyst filler contents. The resulting polyethylene had the molecular weights of 2000-2400 kDa (UHMWPE) with a PDI of 3.3-3.7. Furthermore it was noted that the homogeneous Cr1/MAO in toluene failed to produce UHMWPE (Table 8, Entry 4). With the same procedure,<sup>[92]</sup> two different catalysts like Cr1 and FeBIP (iron(II) complex) were immobilized on the

surface of r-GO to obtain a dual site catalyst which was useful to synthesize the blend of UHMWPE and HDPE with a shish-kebab morphology inducing reinforcement of the polyethylene matrix (Table 8, Entry 5).

#### 4.5.3-Metallocene polymerization

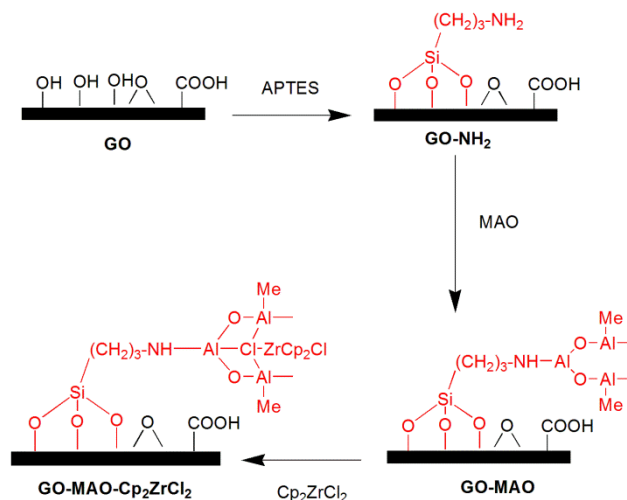


**Figure 25.** Immobilization of the metallocene catalyst on the surface of GO *via* covalent bonding (taken from reference <sup>[93]</sup>).

For the functionalization of the surface of GO with metallocene catalysts, amine groups like aminopropyltriethoxysilane (APTES) were introduced to the surface. Afterwards the mixture of GO or amine-functionalized GO and methyl ammonium oxide (MAO) in toluene were stirred at 50 °C for 3 h, subsequently bis(cyclopentadienyl)zirconium dichloride (Cp<sub>2</sub>ZrCl<sub>2</sub>) was added and stirred for more 3 h to obtain the catalyst<sup>[93]</sup> (Figure 25). The amount of Zr was determined to be between 1.01-1.89 wt% by ICP-AES. The polymer resulting from the metallocene polymerization of ethylene with the so-synthesized catalysts had a molecular weight of 75.4 kDa and 168 kDa for GO and amine-functionalized GO, respectively. Hence by using the unsupported Cp<sub>2</sub>ZrCl<sub>2</sub>/MAO homogenous catalyst PE with a 38.1 kDa molecular weight could be achieved. Further characterizations of the polymer nanocomposites were done by SEM, TEM and DSC measurements (Table 8, Entry 6).

Graphene based materials can also be modified with the metallocene catalyst *via* a  $\pi$ - $\pi$  interaction<sup>[94]</sup>. Thus the reduced graphene oxides which were reduced either thermally (T-r-GO) or by hydrazine (N-r-GO) can be treated with Cp<sub>2</sub>TZrCl<sub>2</sub> or Cp<sub>2</sub>TiCl<sub>2</sub> to achieve the corresponding r-GO/Cp<sub>2</sub>ZrCl or r-GO/Cp<sub>2</sub>TiCl catalysts *via* the  $\pi$ - $\pi$  stacking electronic interactions<sup>[95]</sup>. The amount of the metal on the surface of r-GO, reduced by hydrazine, was higher than the one of thermally reduced graphene oxide measured by ICP-MS. The successful functionalization with the metal catalyst was proven *via* XPS and EDX measurements. Among all of the synthesized catalysts N-r-GO/Cp<sub>2</sub>TiCl (reduced by hydrazine) showed higher activity in the metallocene polymerization and the measured molecular weight (M<sub>w</sub>) by GPC was 3000 kDa with a PDI of 2.9 which is the characteristic molecular weight of UHMWPE (Table 8, Entry 7).

In order to increase the amount of the catalyst loading, the surface of the thermally reduced graphene oxide was modified by multiple reactions with gaseous  $\text{SiCl}_4$  and subsequent hydrolysis with water to modify the surface of r-GO with silica ( $\text{SiO}_2$ ). Afterwards r-GO/ $\text{SiO}_2$  was reacted with MAO and dimethylsilanediyl-bis-(2-methyl-4-phenylindenyl) zirconium dichloride in toluene to obtain the r-GO/ $\text{SiO}_2$ /MAO/Zr catalyst for the metallocene polymerization of ethylene, yielding PE with a molecular weight ( $M_w$ ) of 1830 kDa and a PDI of 3.4<sup>[96]</sup>.

**Table 8.** Graphene/metal(oxide) composites as catalyst in insertion polymerization methods and the final properties of polymer nanocomposites

Entry	Modified graphene	Role of graphene	Reaction condition	Monomer	Characterization
1 <sup>[89]</sup>	r-GO-Mg-TiCl <sub>4</sub>	Ziegler-Natta Catalyst	Monomer, r-GO-Mg-TiCl <sub>4</sub> , AlEt <sub>3</sub> , DDS, 0.5 MPa propylene pressure, hexane, 60 °C, 30 min	Propylene	Viscosity: $M_n$ = of $7.3 \times 10^5 \text{ g.mol}^{-1}$ to $8.1 \times 10^5 \text{ g.mol}^{-1}$ TEM, SEM: well dispersion of PP in GO Conductivity: $9.33 \times 10^{-4} \text{ S/m}$ (1.52 wt%) $3.12 \times 10^{-1} \text{ S/m}$ (4.9 wt%) GPC: $M_w = 33.1 \times 10^4 - 48.4 \times 10^4 \text{ g.mol}^{-1}$ , PDI = 6.6-9.1
2 <sup>[90a, 90b]</sup>	r-GO-Mg-TiCl <sub>4</sub>	Ziegler-Natta Catalyst	Monomer, r-GO-Mg-TiCl <sub>4</sub> , AlEt <sub>3</sub> , DDS, 0.5 MPa propylene pressure, hexane, 60 °C, 30 min	Propylene	TEM, SEM :well dispersion of PP in GO DSC: $T_m = 160.9-162 \text{ }^\circ\text{C}$ Conductivity: $2.51 \times 10^{-8} \text{ S/m}$ (0.09 wt%), $28.5 \text{ S/m}$ (4.1 wt%)
3 <sup>[90c]</sup>	r-GO-Mg-TiCl <sub>4</sub>	Ziegler-Natta Catalyst	Monomer, r-GO-Mg-TiCl <sub>4</sub> , hexane, triisobutylammonium (TIBA)	Ethylene	TGA: decomposition temperature : (467-492 °C) SEM : well dispersion of PE in GO
4 <sup>[91]</sup>	r-GO-MAO-Cr	PFT	Monomer, rGO-MAO-Cr, n-heptane, 40 °C, 5 bar ethylene pressure, for 22 min and 72 min	Ethylene	GPC: $M_n = 2.0 \times 10^6 - 2.4 \times 10^6 \text{ g.mol}^{-1}$ (UHMWPE), PDI= 3.3-3.7 AFM, TEM, SEM : Well dispersion of PP in GO DSC: $T_m = 143.4-143 \text{ }^\circ\text{C}$ Conductivity: $1.5 \times 10^{-2} \text{ S/m}$ (5 wt%), $2 \times 10^{-1} \text{ S/m}$ (10 wt%)
5 <sup>[92]</sup>	rGO-MAO-Cr-Fe	PFT	Monomer, rGO-MAO-Cr-Fe, n-heptane, 40 °C, 5 bar ethylene pressure, for 22 min and 72 min	Ethylene	blend of UHMWPE/HDPE with shish-kebab morphology
6 <sup>[93]</sup>	GO-amine-MAO-Zr	Metallocene	Monomer, GO-amine-MAO-Zr, toluene, 50 °C, 30 min	Ethylene	Viscosity : $M_n = 7.54 \times 10^4 \text{ g.mol}^{-1} - 1.68 \times 10^5 \text{ g.mol}^{-1}$ AFM, TEM, SEM : well dispersion of PP in GO DSC: $T_m = 132.4-135.7 \text{ }^\circ\text{C}$
7 <sup>[95]</sup>	1-T-r-GO-Zr (Thermally reduced) 2-T-r-GO-Ti (Thermally reduced) 3-N-r-GO-Zr (Reduced by hydrazine) 4-N-r-GO-Ti (Reduced by hydrazine)	Metallocene	Monomer, r-GO-Zr, MAO, toluene, 30-90 °C, 1 h	Ethylene	1-GPC: $M_w = 1.07-0.07 \times 10^6 \text{ g.mol}^{-1}$ , PDI= 3.48-2.14, DSC: $T_m = 132-130 \text{ }^\circ\text{C}$ 2-GPC: $M_w = 1.49-0.26 \times 10^6 \text{ g.mol}^{-1}$ , PDI= 2.27-11.63, DSC: $T_m = 131-124 \text{ }^\circ\text{C}$ 3-GPC: $M_w = 1.38-0.08 \times 10^6 \text{ g.mol}^{-1}$ , PDI= 2.58-3.8, DSC: $T_m = 130-133 \text{ }^\circ\text{C}$ 4-GPC: $M_w = 2.97-0.17 \times 10^6 \text{ g.mol}^{-1}$ , PDI = 2.9-2.36, DSC: $T_m = 133-132 \text{ }^\circ\text{C}$

\*PFT: Polymerization-filling technique

Moreover it had been proved that the addition of the pristine graphene based materials to the polymerization reactor of ethylene which was catalyzed with aryliminopyridylnickel chloride could increase the obtained molecular weight. [97]

#### 4.5.4-Ring Opening Metathesis Polymerization (ROMP)

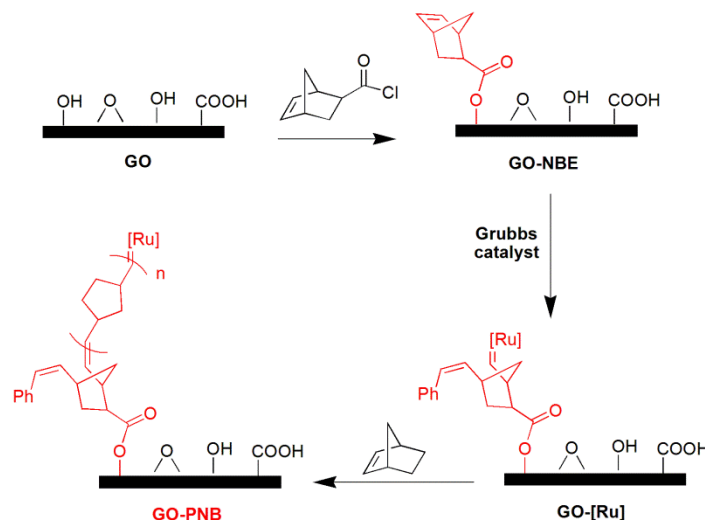


Figure 26. Immobilization of Grubbs catalysts on the surface of GO (taken from reference [98])

Surface of graphene oxide has also been modified by the Grubbs catalyst [98-99] to be utilized in the ROMP polymerization. For this purpose GO was reacted by triethylamine and 5-norbornene-2-acyl chloride in THF to functionalize its surface with norbornene (GO-NBE), subsequently GO-NBE was treated by the Grubbs first and second generation catalysts to immobilize the Grubbs catalysts on the surface (Figure 26). ROMP polymerization of norbornene was run for 30 min at room temperature in THF by the GO-[Ru] catalyst to graft the poly(norbornene) on the surface. The resulting composites were characterized by TGA analysis showing a grafting density of 60 wt%, whereas SEM revealed the high dispersion of poly(norbornene) on the surface of GO. Via the same route [99], the surface of GO was modified with different Grubbs and Hoveyda-Grubbs catalysts enabling a 29% - 59% conversion of 2-norbornene in the ROMP polymerization. The as-synthesized catalysts were embedded in an epoxy matrix, containing microcapsules of the healing agent (mixture of 5-ethylidene-2-norbornene and dicyclopentadiene) for the preparation of the self-healing nanocomposites. The self-healing nanocomposites exhibited nearly a 45% healing efficiency at 60 °C.

#### 5-Copper Catalyzed Azide-Alkyne Click cycloaddition reaction (CuAAC)

Huisgen dipolar cycloaddition [100] between alkynes and terminal azides is a promising reaction in the chemistry mainly due to the fact that the azide and alkyne moieties can be incorporated into the wide range of components making them applicable in different fields like polymer chemistry [101], medicine [102] and electronics. However the non-catalyzed Huisgen reaction between azide and alkyne is usually conducted at elevated temperatures leading to a mixed substitutes of 1,4 and 1,5-triazoles

(Figure 27a). In 2002, Meldal et al.<sup>[103]</sup> and Sharpless et al.<sup>[104]</sup> independently reported the use of the Cu(I) catalyst for the Huisgen dipolar cycloaddition, increasing the reaction rate, reducing the reaction temperature (to room temperature and below), and improving the selectivity to 1,4-substituted 1,2,3-triazole (Figure 27b). These properties include the copper catalyzed Huisgen dipolar cycloaddition reaction in the category of “click” reactions which has been described in 2001 by Sharpless et al.<sup>[105]</sup> namely as copper catalyzed azide-alkyne cycloaddition click reaction (CuAAC). Therefore CuAAC is environmentally friendly, functional-group-tolerant, highly efficient, regioselective, and can be performed under a wide range of solvents and reaction conditions. The copper(I) catalyst can be generated *in situ* from a Cu(II) source with a reducing agent or added directly as Cu(I) salts. However Cu(I) oxidizes easily to Cu(II), therefore adding phosphorous or nitrogen-based ligands during the reaction can stabilize the oxidation state of Cu(I)<sup>[106]</sup>.

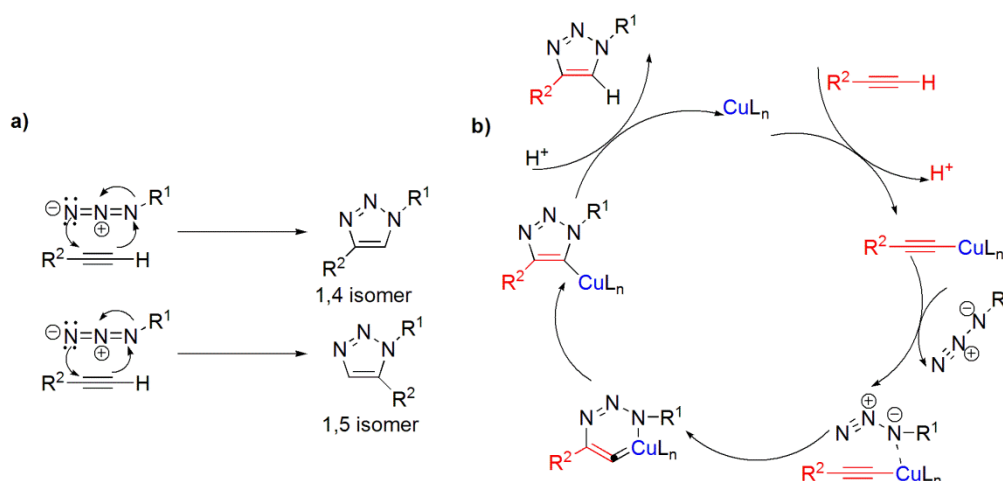


**Figure 27.** Huisgen dipolar cycloaddition conducted a) at elevated temperatures and with b) copper catalyzed (CuAAC) (redrawn from reference<sup>[107]</sup>)

The main disadvantages of these catalytic systems are a significant amount of the toxic and colored copper source, reducing, and oxidation agents which are hampering the utilization of CuAAC, particularly in the area of biology and electronics<sup>[108]</sup>. This problem can be tackled by different methods such as nanofiltration membranes, and metal scavenging iron nanoparticles<sup>[109]</sup> which are expensive, hence using the heterogeneous copper catalyst in the CuAAC reaction can reduce the amount of the copper in the organic product much cheaper. A variety of the recyclable copper-based catalysts have been prepared using resin and polymer based materials bearing different amine groups acting as both a chelating groups and a base<sup>[110]</sup> (Figure 28). The first example for this approach was done on Amberlyst A-21 (dimethylaminomethyl grafted poly(styrene)/divinylbenzene resin) where Cu(I) salts were immobilized *via* chelating with the tertiary amine groups<sup>[111]</sup>. By using 13 mol% of this catalyst, CuAAC was run quantitatively at room temperature with four times of recycling, however small amount of the copper was leached to the organic product. There are also further works using resins and polymers like poly(ethylene-imine) resins, chitosan and tentagel resin bearing



tris(benzyltriazolylmethyl)amine acting as chelating groups for Cu(I) salts in the CuAAC reaction (Figure 28). But these types of the recyclable catalysts are not immobilized on the support materials like zeolites, alumina or carbon materials, therefore they are unstable in an acidic/basic condition or at elevated temperatures; furthermore their synthetic pathways are difficult and expensive.

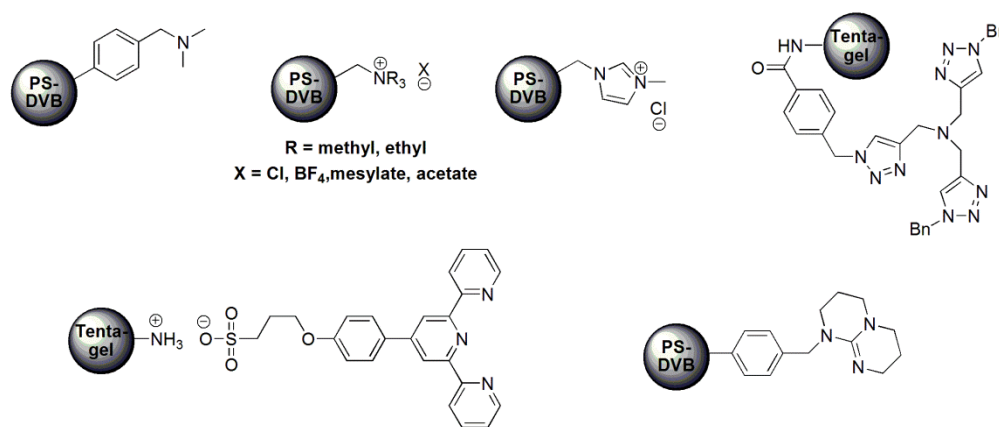


**Figure 28.** Resin and polymer based heterogeneous Cu(I) catalyst used in CuAAC (taken from reference<sup>[110d]</sup>)

The application of some support materials for the copper particles in the heterogeneous catalysis on CuAAC are listed in Table 9. Lipshutz et al.<sup>[112]</sup> used charcoal as the support (Cu/C), and for this purpose activated carbon was treated with Cu(NO<sub>3</sub>)<sub>2</sub>·3H<sub>2</sub>O in water, afterwards the mixture was heated to 200 °C. The copper particles on the surface was characterized by XPS proving the existence of Cu<sub>2</sub>O and CuO structures and ICP-MS showed a 3-5 wt% of the copper loading on the charcoal. The as-synthesized Cu/C was active in CuAAC and gave quantitative yield in 4 h, moreover the amount of the copper on the organic product was too low to be detected with the ICP-MS method (Table 9, Entry 1). Except using activated carbon as a support, recently the application of the other novel carbon-based materials like CNT<sup>[113]</sup> and graphene has increased mostly due to their unique properties. For example, the cuprous oxide particles were immobilized on the surface of r-GO *via* the *in situ* crystallization method<sup>[51c]</sup>, and XRD measurement proved the existence of the Cu<sub>2</sub>O crystal on the surface of r-GO with an average particle size of 5 nm showed by TEM measurement. The prepared r-GO/Cu<sub>2</sub>O catalyst was used in CuAAC with a high conversion and a good recyclability (6 times). TEM analysis of the recycled r-GO/Cu<sub>2</sub>O showed the aggregation of Cu<sub>2</sub>O particles on the surface decreasing the activity of the catalyst (Table 9, Entry 2).

Aluminum oxide also was used as a support for the copper particles. In a report<sup>[114]</sup>, the *in situ* crystallization of the cupric chloride dehydrate in the presence of aluminium tri-*sec*-butoxide decorating the copper particles on the surface of aluminium oxyhydroxide fibers. XPS and ICP measurements revealed that the copper nanoparticles were the mixture of Cu<sub>2</sub>O and CuO with a loading amount of 4 wt% on the surface of aluminium oxyhydroxide. The synthesized catalyst was

able to run the CuAAC reaction five times with a little reduction in the conversion and without leaching in the organic product (Table 10, Entry 4).

**Table 9.** Application of different supported heterogeneous Cu(I) catalyst in CuAAC

Entry	Support material	Characterization of the catalyst	Cu nature	Cu leach-ing	[Cu] in reaction (mol%)	Solvent	T °C	Reaction time	Conversion	Times of cycle
1 <sup>[112]</sup>	Charcoal	ICP, XPS	CuO, Cu <sub>2</sub> O	-	10	Dioxane, H <sub>2</sub> O / dioxane, toluene, EtOH, H <sub>2</sub> O	RT-60	4 min-4 h	Complete	3
2 <sup>[51c]</sup>	r-GO	TEM, XRD	Cu <sub>2</sub> O		no	H <sub>2</sub> O	55	2 h	Complete	6
3 <sup>[115]</sup>	Activated carbon	TEM, EDX, ICP, XPS	CuO, Cu <sub>2</sub> O	-	0.5	H <sub>2</sub> O/EtOH, H <sub>2</sub> O	RT-70	3 h-24 h	Complete	5
4 <sup>[114]</sup>	AlO(OH)	TEM, XPS, ICP-MS	CuO, Cu <sub>2</sub> O	No leach-ing	3	<i>n</i> -Hexane	RT	12 h	Complete	5
5 <sup>[116]</sup>	Al <sub>2</sub> O <sub>3</sub> /TiO <sub>2</sub>	XRD, XPS	Cu(OH) <sub>2</sub>		1.5	Toluene, DMF, propanol	RT-60	7 h 10 min-25 min	99 % in toluene/30 % in DMF/1 % in propanol	4
6 <sup>[117]</sup>	Zeolite				10	Toluene, THF, MeOH	RT	15 h	83% in toluene/62 % in THF and MeOH	5
7 <sup>[118]</sup>	Amino-Silica	TEM, HRTEM, ICP	CuO, Cu(0)	Less than 0.05 wt%	2	THF	RT	6 h	Complete	7
8 <sup>[119]</sup>	SiO <sub>2</sub>	EDS			10	H <sub>2</sub> O	70	12 h	Complete	5
9 <sup>[120]</sup>	SiO <sub>2</sub>	Elemental analysis, XRD, TEM		No leach-ing	8	DCM	RT	16 h	Complete	5
10 <sup>[121]</sup>	SiO <sub>2</sub> -amine	XRD				H <sub>2</sub> O	100		Complete	6
11 <sup>[122]</sup>	SiO <sub>2</sub> -NHC SiO <sub>2</sub> -Fe-NHC	EDS, ICP, TEM			1	H <sub>2</sub> O	RT	18 h	Complete	5/ 9
12 <sup>[123]</sup>	SiO <sub>2</sub> -NHC	ICP		<0.1 ppm	1	Ethanol, DMSO, DMF, H <sub>2</sub> O, toluene, THF, bulk	RT	30 min	Complete	10
13 <sup>[124]</sup>	SiO <sub>2</sub> -NHC	ICP		<0.6 ppm	0.5	DMSO, DMF, H <sub>2</sub> O, ethanol, MeOH acetonitrile, DCM	6	6 h	Complete	6
14 <sup>[125]</sup>	Clay				8	DCM, and in bulk	18	18 h	Complete	5
15 <sup>[126]</sup>	Clay	XPS, XRD	Cu(II)		10	H <sub>2</sub> O/acetonitrile, H <sub>2</sub> O, THF, MeOH, DMF, DMSO	RT	4 h-8 h	Complete	
16 <sup>[127]</sup>	Hydrotalcite					Acetonitrile	RT	6 h-12 h	Complete	
17 <sup>[128]</sup>	porous glass	XPS, ICP	Cu(I)		1.5	Water	MW	2 min	Complete with sodium ascorbate	6

Furthermore other publications immobilized copper hydroxide on the surface of aluminum oxide and titanium oxide ( $\text{Cu}(\text{OH})_x/\text{Al}_2\text{O}_3$  and  $\text{Cu}(\text{OH})_x/3\text{TiO}_2$ )<sup>[116]</sup>. The obtained catalysts had a high catalytic activity and recyclability (4 times) without a detectable leaching on the organic medium (Table 9, Entry 5).

The Cu(I) particles which were decorated on zeolites<sup>[117]</sup> were used in CuAAC with an almost quantitative yield with four times recycling, however only a 20 % conversion was achieved in the fifth cycle, and the amount of the leaching was not reported. Moreover the sufficient characterization of the prepared catalyst before and after reactions has not been reported (Table 9, Entry 6). Silica-based materials are extensively used as the support for Cu(I) heterogeneous catalysis<sup>[118-124]</sup>, for example, the copper nanoparticles were immobilized on the surface of aminopropyl-silica used in CuAAC<sup>[118]</sup>. The obtained hybrid material characterized by TEM and HRTEM proving an average particle size of 2.5 nm, and a lattice distance of 2.1 Å and 2.5 Å related to the Cu(0) and CuO particles. Furthermore this catalyst showed a high catalytic activity in CuAAC together with high conversion up to seventh cycle and with a little leaching to the organic product (0.01-4.8 wt%) confirmed by the ICP measurement (Table 9, Entry 7). Moreover the surface of silica contains the hydroxyl groups enabling the further functionalization of the surface to anchor the metal particles on it. Therefore the surface of the silica nanoparticles and silica coated magnetic nanoparticles were modified by an imidazolium group afterwards the proton of the imidazolium group was exchanged with the Cu(I) making a *N*-heterocyclic carbene-copper bond (NHC-Cu)<sup>[122]</sup>. The presence and the amount of copper on the surface was proved by EDS and ICP measurements, respectively. As-synthesized catalysts were used in CuAAC with a high conversion and the obtained catalyst were recycled 5 times and 9 times without a reduction in the conversion for silica-NHC-Cu(I) and silica-magnetic-NHC-Cu(I), respectively (Table 9, Entry 11).

The surface of the clay materials was immobilized with Cu(I) salts with a 4.6 wt% loading, the CuAAC reaction with this heterogeneous catalyst had a full conversion up to five cycles<sup>[125]</sup>. It should be mentioned that the sufficient characterization of the prepared hybrid before and after the CuAAC reactions has not been reported, furthermore the report regarding to the leaching on the organic product was also missing (Table 9, Entry 14). In another report,<sup>[126]</sup> the Cu(II) was immobilized on the surface of clay by the treatment of the Montmorillonite KSF clay with the copper oligomer, and subsequent calcination of the mixture in an oven at 425 °C, furthermore the valence of the Cu(II) on the surface of clay was proved by XPS, and XRD measurements. In this work the azide moiety was prepared *in situ via* reaction of the boronic acid compound with the sodium azide, which also led to the partial reduction of Cu(II) on the surface of clay to Cu(I) catalyzing CuAAC in a high conversion, however the recyclability report of the catalyst was missing (Table 9, Entry 15). Furthermore other

materials like hydrotalcite<sup>[127]</sup> and porous glass<sup>[128]</sup> can be used as support of Cu(I) catalyst for the CuAAC reaction (Table 9, Entries 16 and 17).

### 5.1-CuAAC polymerization reaction

Shortly after the invention of the copper catalyzed azide-alkyne click cycloaddition reaction (CuAAC), polymer chemists started to utilize this reaction to synthesize poly(triazoles). The “CuAAC polymerizations” can be very fast and afford polymeric products with high molecular weights (396 *kDa*) within a short time.<sup>[129]</sup> The direct use of the nanofillers such as carbon materials, zeolites, alumina and silica as the heterogeneous Cu(I) catalyst in the CuAAC polymerization reaction diminishes the agglomeration of the filler particles in the polymer composites in turn inducing high physical and mechanical properties to the final polymer composites. To date there are very few reports on the application of the heterogeneous Cu(I) catalyst in the CuAAC polymerization reaction.

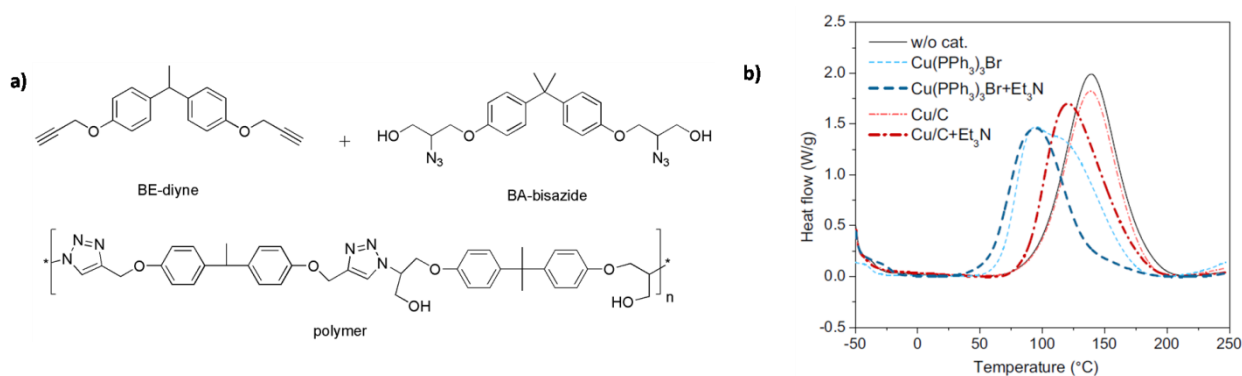


**Figure 29.** a) CuAAC polymerization between a BA-bisazide and a BE-diyne using Cu/C heterogeneous catalyst and comparison its activity to Cu(PPh<sub>3</sub>)<sub>3</sub>Br by DSC measurements (taken from reference<sup>[130]</sup>)

In a report, the group of Kessler used the copper on charcoal (Cu/C) for the bulk CuAAC polymerization reaction between a BA-bisazide and a BE-diyne (Figure 29a), hence the heterogeneous Cu/C<sup>[112]</sup> catalyst was active with the addition of a triethyl amine, and the activation of the catalyst was lower than of a homogenous catalyst Cu(PPh<sub>3</sub>)<sub>3</sub>Br proved by DSC measurements<sup>[130]</sup>. However the final physical properties of polymer nanocomposites with Cu/C had not been characterized.

## II.SCOPE OF THE THESIS

### 1-Objective

The main objective of this thesis was to develop the new resin(polymer)/graphene nanocomposite for high performance applications useful for aerospace and marine industries *via* a direct CuAAC crosslinking(polymerization) reaction, catalyzed by the Cu(I)/graphene materials. Nanocomposites with finely dispersed graphene particles, in turn improving the electrical, thermal conductivities and mechanical properties of the final resin materials, were desired.

In the first step, heterogeneous Cu(I) catalysts supported by graphene-based materials, useful in CuAAC reactions should be developed (Figure 30a). Thus the influence of the method of the catalysts preparation on the catalytic activity including kinetics studies, the recyclability and the leaching should be probed, finally selecting the best catalyst for the CuAAC crosslinking in resin/graphene nanocomposite production.

In the next step, the generation of nanocomposites, *via* a direct CuAAC crosslinking (polymerization) reaction, conducted by the Cu(I)/graphene heterogeneous catalysts was projected to achieve nanocomposites in a short reaction time at low temperatures with increased mechanical properties, electrical and thermal conductivities in a one facile step (Figure 30b). Therefore the effect of Cu(I)/graphene heterogeneous catalysts on the time and the temperature of the crosslinking reaction, together with the optimal final physical properties of the cured resin should be investigated and compared with commercial Cu(I) catalysts checking the visibility for industrial application.

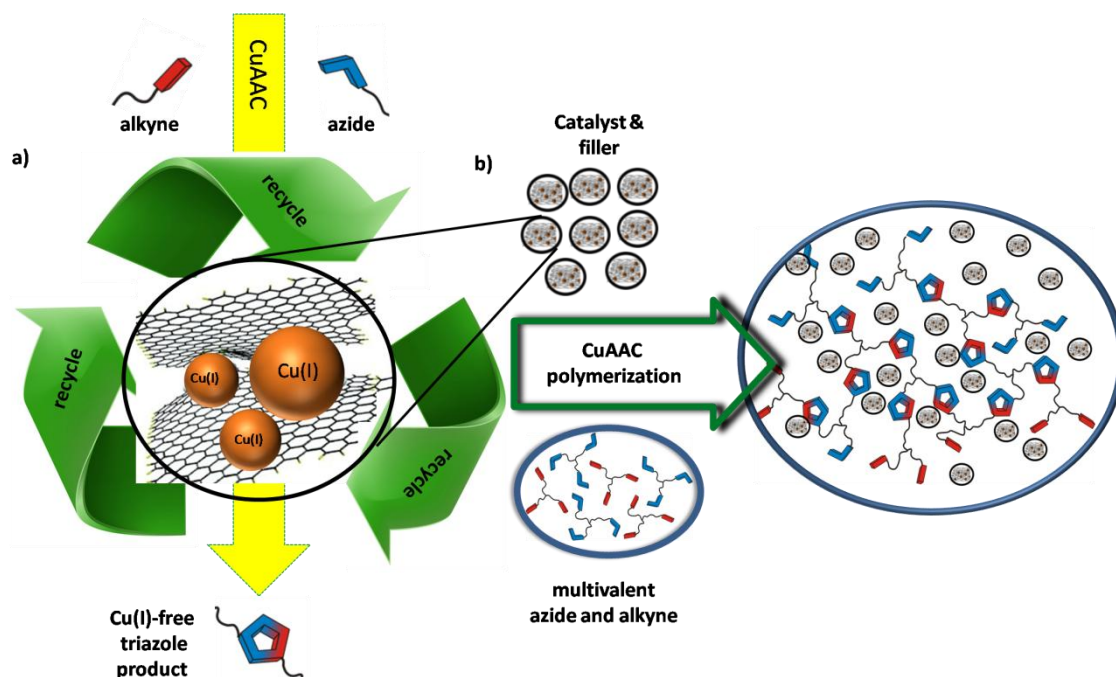


**Figure 30.** a) Recyclable and active heterogeneous Cu(I) catalyst on the surface of graphene-based materials used in the CuAAC reaction achieving Cu(I)-free triazole products b) application of the obtained heterogeneous graphene/Cu(I) catalyst in the CuAAC polymerization for the production of high performance polymer/graphene nanocomposites.

## 2-Concept

For the production of a resin/graphene nanocomposite, the CuAAC crosslinking (polymerization) using Cu(I)/graphene heterogeneous catalyst had been chosen to decrease the time and the temperature of the curing while inducing the novel properties of finely dispersed graphene particles into the final resin material in a one facile step.

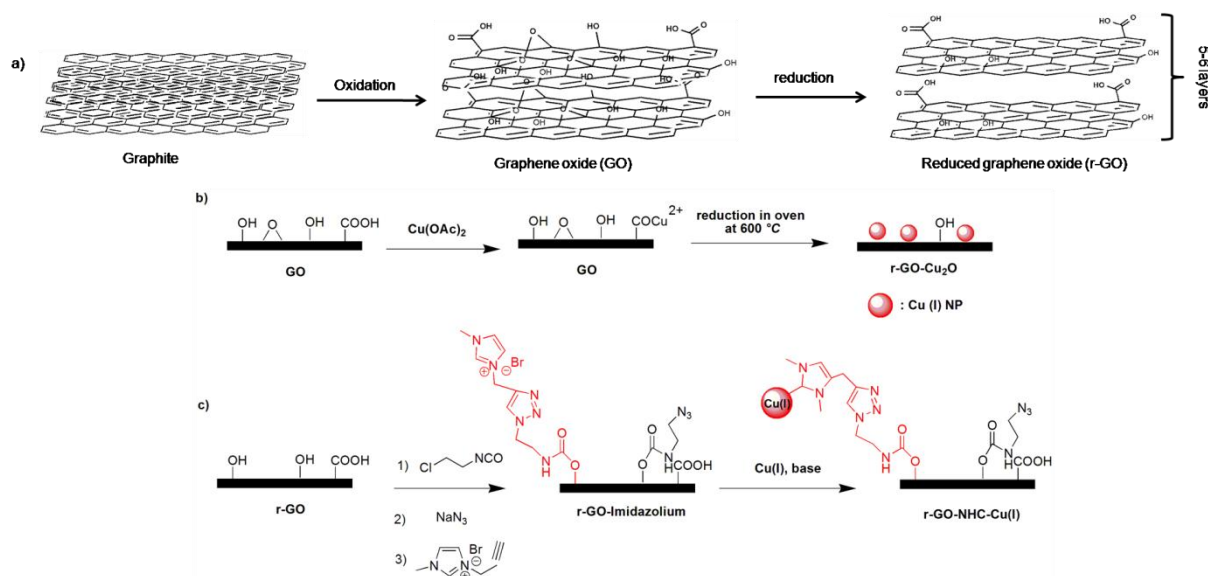


**Figure 31.** a) Graphene-based materials used in this work b) "ex situ hybridization" c) "in situ crystallization" route towards immobilization of Cu(I) on the surface of graphene-based materials

Accordingly, a Cu(I) catalyst was immobilized on the surface of graphene-based materials. For this purpose, graphene oxide (GO) and reduced graphene oxide (r-GO) were chosen (Figure 31a), because GO and r-GO possess residual oxygen containing groups on their surfaces enabling further functionalization, and the defects on their surfaces could increase the catalytic activity by acting as a reaction site and increasing the band gap of graphene-based materials. Finally GO and r-GO can be prepared in a large scale using low cost graphite as the starting material.

Decorating the Cu(I) particles on the surface of reduced graphene oxide has been accomplished *via* both the "ex situ hybridization" (Figure 31b), and the "in situ crystallization" (Figure 31c) methods further investigating and comparing the loading effects, the catalytic activity including kinetics studies, the recyclability, the leaching and the feasibility of their production in a large scale applicable for the industrial use. In the "in situ crystallization" method, firstly GO was reacted with copper(II) acetate ( $\text{Cu}(\text{OAc})_2$ ) to exchange the protons of the carboxylic groups with Cu(II) particles in order to immobilize Cu(II) onto the surface of GO (GO-Cu(II)), afterwards GO-Cu(II) was thermally reduced in an oven under the stream of nitrogen at 600 °C to obtain r-GO decorated with Cu(I) nanoparticles.

On the other hand, *N*-heterocyclic carbene (NHC) functional groups have been chosen for functionalization of the surface of r-GO in the "ex situ hybridization" method. Therefore, the surface of r-GO (reduced by ascorbic acid) was functionalized by the imidazolium groups in three steps of

reaction. In the first step, r-GO was treated with chloroethyl isocyanate to modify the surface with the chlorine groups, afterwards the chlorine groups were exchanged to the azide groups by the reaction with sodium azide and finally a CuAAC reaction between the azide groups on the surface of r-GO and 1-propargyl-3-methylimidazolium bromide functionalized the surface with the imidazolium groups. Subsequently the proton of the imidazolium groups was exchanged with Cu(I) to achieve Cu(I)-NHC bond on the surface of r-GO.

The successful immobilization of the copper particles on the surface of r-GO in both methods was proved *via* different methods such as TEM, HRTEM, STEM-EDXS, XPS, TGA, XRD and RAMAN. The catalytic activity of the synthesized catalysts, as well as the recyclability and the leaching in CuAAC were investigated using different azide and alkyne functionalized molecules. The results of the catalyst preparation methods and their catalytic activity in the CuAAC reaction can be found in the first and second section of the Result and Discussion part of the thesis dealing with the “Click chemistry promoted by graphene supported copper nanomaterials”(Shaygan Nia, A., Rana, S., Döhler, D., Noirfalise, X., Belfiore, A. and Binder, W. H. Chem. Commun., 2014. 50, 15374-15377.) and with “Carbon Supported Copper Nanomaterials: Recyclable Catalysts for Huisgen [3+2] Cycloaddition Reaction”( Shaygan Nia, A., Rana, S., Döhler, D., Jirsa, F., Meister, M., Guadagno, L., Koslowski, E., Bron, M. and Binder, W. H. Chem. Eur. J., 2015. 21(30): p. 10763-10770) for the “*in situ* crystallization” and the “*ex situ* hybridization” routes, respectively.

After the preparation of Cu(I)/graphene catalyst, the as-prepared catalyst was utilized in the production of the resin/graphene nanocomposites *via* a direct CuAAC crosslinking reaction (Figure 32). For the formation of a covalent network, the sufficient molecular mobility is required, in order to keep the diffusion high while getting to a high monomer conversion together with a high molecular weight of the resulted polymer. Therefore a low molecular weight trivalent azide and alkyne were synthesized.

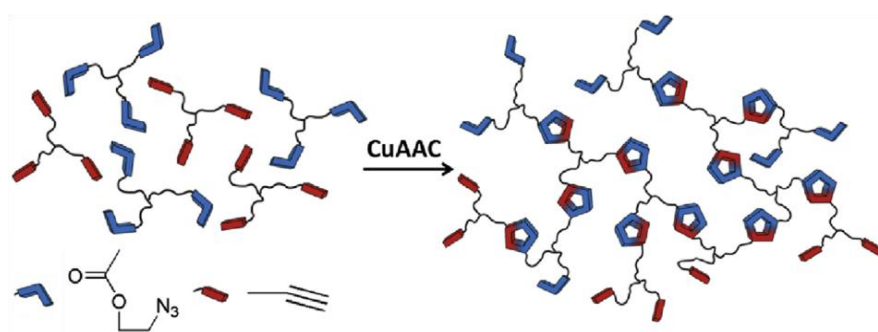


**Figure 32.** CuAAC crosslinking reaction between trivalent azide and alkyne moieties

The kinetics of the CuAAC crosslinking reaction was investigated by *in-situ*-DSC and *in-situ* melt-rheology measurements using the Cu(I)/graphene as catalyst, and the activity of the Cu(I)/graphene catalyst was compared to different commercially available heterogeneous and homogeneous catalysts.



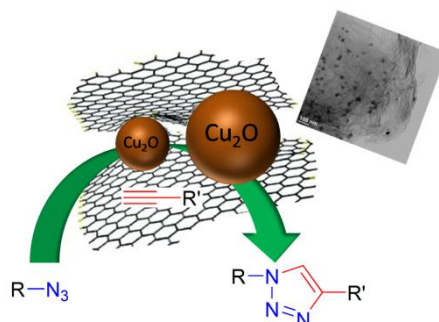
## II.SCOPE OF THE THESIS

The final physical and mechanical properties of the cured resin/graphene nanocomposite were studied by different methods. Broadband dielectric spectroscopy (BDS) was conducted to determine the conductivity of the final resin materials, systematically investigating the influence of the added amounts of the Cu(I)/graphene catalyst. Thermogravimetric analysis (TGA) was performed to assess the thermal stability of the resulting resin materials. In addition, the physical properties of the final resin materials were also investigated by melt rheology, and the dispersion of the graphene nanoparticles into the resin matrix was tested by TEM measurements. The corresponding results of this investigation can be found in the third section of the result and discussion part of the thesis dealing with “Nanocomposites *via* a direct graphene-promoted "click"-reaction” (Shaygan Nia, A., Rana, S., Döhler, D., Osim, W. and Binder, W. H. *Polymer.*, 2015. 79, 21-28).



### III.RESULT AND DISCUSSION

#### 1-Click chemistry promoted by graphene supported copper nanomaterials

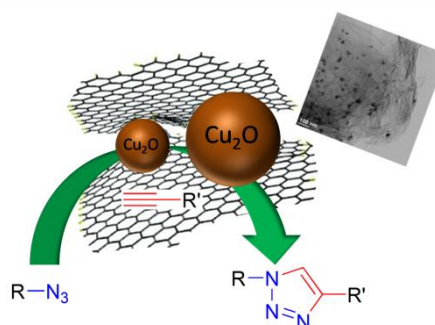


#### Abstract

A facile and robust approach is provided for the synthesis of highly dispersed copper nanoparticles immobilized onto graphene nanosheets, useful as a recyclable and reusable heterogeneous catalyst with excellent catalytic activity to achieve Cu(I)-catalyzed [3+2] cycloaddition 'click' chemistry.

Since its development by Sharpless<sup>1,2</sup> and Meldal,<sup>3,4</sup> the Cu(I)-catalyzed [3+2] cycloaddition reaction<sup>5</sup> between terminal acetylenes and azides ("click" reaction (CuAAC)) has emerged as a strategy for the rapid and efficient assembly of molecules with diverse functionality on both laboratory and production scales.<sup>6-9</sup> Click reactions are modular, tolerant of a wide range of functional groups, simple to perform, insensitive to reaction solvents irrespective to their polar/non-polar or protic/aprotic character.<sup>10,11</sup> However, in order to enhance the catalytic activity, the presence of a co-catalyst is required such as bases (mainly amines), auxiliary ligands, and oxidizing or reducing agents depending on the used Cu sources (CuI/CuO). Furthermore, the recyclability, reusability, and easy removal of the copper catalyst are often severely limited. Therefore, the development of recyclable and stable heterogeneous copper catalysts with improved catalytic activity devoid of any oxidizing/reducing agents is highly desirable.

Herein, we report a facile and robust approach for the synthesis of highly dispersible, recyclable, and reusable Cu(I) nanoparticles decorated onto graphene nanosheets, useful as a catalyst for "click" chemistry without any co catalyst (Scheme 1). Graphene, a single layer of two dimensional sp<sup>2</sup>-hybridized carbon has attracted significant research interest due to its unique electrical and thermal conductivity, including exceptional mechanical, optical and chemical properties.<sup>12-14</sup>



**Scheme 1** Schematic illustration of click chemistry promoted by graphene supported copper nanoparticles.

In contrast to single layer graphene sheets conveniently prepared by mechanical exfoliation, graphene oxide (GO) and reduced graphene oxide (rGO)<sup>15,16</sup> are easily available by controlled chemical reactions and can be produced on a large scale. Also due to the presence of functional groups on GO and rGO surfaces, further chemical reaction onto their surfaces is possible. On account of their large surface area, their unique interaction with metal particles,<sup>17,18</sup> and their performance for electron capture, transport, as well as prevention of supported nanoparticles agglomeration due to their scaffold behavior, graphene supported catalysts have represented outstanding catalytic activity compared to other carbon supported catalysts.<sup>19</sup> Several reports for the preparation of different metal particles-GO heterostructures and their wide range of applications from photocatalytic hydrogen production to lithium ion batteries have been discussed.<sup>20,21</sup> Recently, few reports have appeared regarding the preparation

### III.RESULT AND DISCUSSION

of Cu–GO nanoconjugates and their relevance in hydrogen generation, supercapacitors, as well as in other applications.<sup>22–25</sup> However according to our knowledge their application in CuAAC catalyzed “click” chemistry has not been explored yet.

For the preparation of graphene oxide (GO), Hummers’ method was applied,<sup>26</sup> whereas ion exchange with Cu<sup>2+</sup> was achieved by dispersing GO in water,<sup>27</sup> followed by addition of copper(II) acetate under vigorous stirring for overnight. Afterwards Cu(II)–GO was reduced under Ar at 600 °C in an oven to obtain TRGO/Cu(I). We first investigated the morphology and chemical composition of our nanoconjugates by TEM, EDX, XPS, and FAAS.

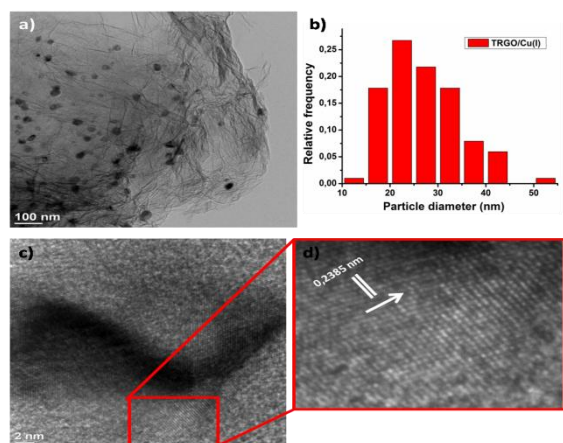


**Fig. 1** (a) TEM image of the TRGO/Cu(I) catalyst. (b) Copper particles size and distribution. (c, d) HRTEM of TRGO/Cu(I) and calculation of the lattice plane distance.

Fig. 1a shows the TEM image of TRGO–Cu(I) conjugates, where highly dispersed uniformly sized Cu nanoparticles on the surface of graphene nanosheets were obtained. From the TEM images the average particle size is about 25 nm for Cu particles (Fig. 1b). HRTEM was performed to measure the lattice plane distance in a single Cu nanoparticle (Fig. 1c and d), where  $0.2385 \pm 0.01$  nm as a lattice plane distance was obtained, that could be due to the presence of CuO(110)<sup>28</sup> or Cu<sub>2</sub>O(111),<sup>29</sup> indicative that for the TRGO–Cu conjugates the Cu is in the form of Cu(I) or Cu(II). To confirm the existing form of Cu, quantitation of nanoparticles was also achieved by STEM-EDXS (Fig. S1, ESI<sup>†</sup>) indicating that Cu and O are present in a ratio of 68.8 : 31.2 ( $\approx 2 : 1$ ), which strongly supports that the particles consist of Cu<sub>2</sub>O, and the valence of Cu is Cu(I) as required for their use in “click” chemistry. Further evidence of the chemical

composition of the nanoconjugates was obtained by X-ray photoelectron spectroscopy (XPS) (Fig. 2a), where the peaks correspond to C 1s (285.1 eV), O 1s (531.6 eV) and Cu 2p. The high-resolution XPS (Fig. 2b) reveals that Cu 2p<sub>3/2</sub> peaks located at 932.37 eV and 952.31 eV correspond to the peak energy of Cu(I).<sup>30</sup> Also there are no peak satellites at 942 eV and 962 eV and no peaks at 934.8 eV which would be related to Cu(II). The Cu content of the sample was also determined by analysis on a flame atomic absorption spectroscopy (FAAS) as  $7.55 \times 10^{-7}$  mol mg<sup>-1</sup> loading.

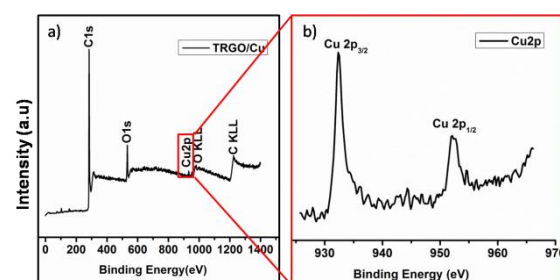


**Fig. 2** (a) X-ray photoelectron spectroscopy of TRGO/Cu(I). (b) High resolution XPS of elemental Cu

The catalytic activity of the TRGO/Cu(I) catalyst was investigated in the azide/alkyne click chemistry between benzyl azide and phenyl acetylene under different reaction conditions in high yields (up to 99%) as a model system. Also the model reaction for commercial available Cu on charcoal (Cu/C)<sup>31</sup> and Cu<sub>2</sub>O powder as a reference was done, but a very low click conversion was obtained by these commercial catalysts (Table 1).

**Table 1.** Performance of various of Cu-catalysts at different reaction conditions

Entry	Conditions	Conversion%
1	TRGO without copper, in THF, 40 °C, 48 h	0
2	Copper on charcoal (2 mol%), in THF, 40 °C, 48 h	3
3	Cu <sub>2</sub> O (2 mol%), in THF, 40 °C, 48 h	0
4	TRGO/Cu (2 mol%), in THF, 40 °C, 48 h	99
5	TRGO/Cu (2 mol%), in THF, room temperature, 48 h	70
6	Recycled catalyst in air	99
7	Repeat 6, forth use in air	55
8	TRGO/Cu, 1:1 water/methanol, room temperature, 24 h	99

The recyclability of the catalyst was studied using the same alkyne/azide click model reactants. After four repetitions, a reduction ( $\sim 30\%$ ) of the reaction yield was observed (Fig. 3a), whereas the washing and recycling of the catalyst was accomplished in open air environment, supportive of the stability and recyclability of the synthesized catalyst (Table 1, Fig. 3a). The reduction of reaction yield after several repetitions could be due to agglomeration of Cu particles, as observed by TEM (Fig. 3b).

### III. RESULT AND DISCUSSION

For kinetic investigation, NMR studies have been performed. Therefore aliquots were taken at intervals from the reaction, filtered to remove the catalyst and conversion of the reaction was determined by the resonance of the CH<sub>2</sub>-moiety of benzyl azide (educt) in comparison to the CH<sub>2</sub> moiety of the click product (Fig. S2, ESI<sup>†</sup>). Eqn (1)<sup>32</sup> was used for the kinetic study and calculation yielded  $k' = 1.33 M^{-1.3} h^{-1}$ , which was in the same range as those reported previously by Finn et al.<sup>33</sup> using CuSO<sub>4</sub> and sodium ascorbate as catalytic system.

$$\text{Rate} = k'[\text{alkyne}]^{1.3 \pm 0.2}[\text{azide}]^{1 \pm 0.2} \quad (k' = k[\text{Cu}]^2) \quad (1)$$

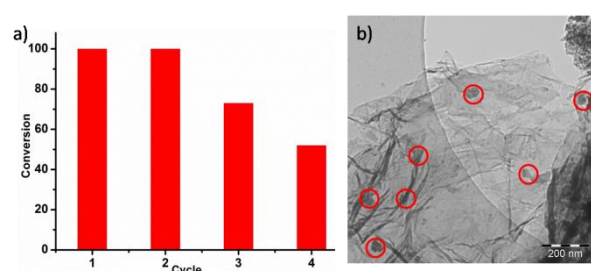


**Fig. 3** (a) Catalyst recycling and stability in four cycles of click chemistry. (b) TEM image of Cu particles after the fourth run.

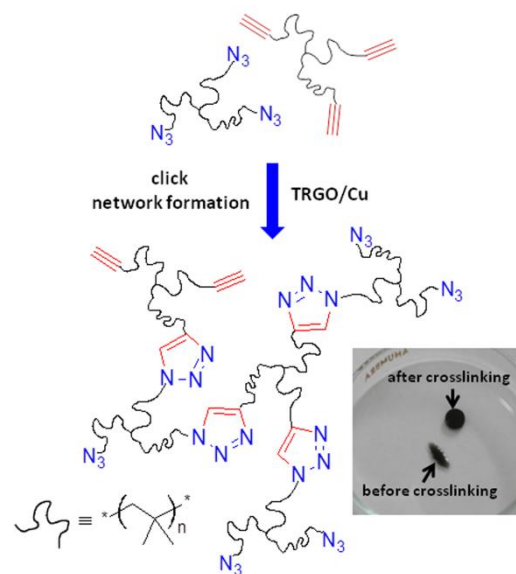
Furthermore Table 2 shows the different types of click reactions with different alkynes for TRGO/Cu(I) catalyst, and even with a highly sterically hindered alkyne (entry 3) and linear hydroxyl alkynes (entry 4) a high conversion was achieved.

**Table 2** Click reaction of benzyl azide with different alkynes with 2 mol% TRGO/Cu(I) at 40 °C after 48 h

Entry	Alkyne	Azide	Conversion (%)
1			99
2			90
3			97
4			90
5			95

To evaluate the performance of synthesized TRGO/Cu(I) catalyst for bulk click chemistry including high molecular weight molecules, melt rheology was carried out for trivalent azide- and alkyne-functionalized polyisobutylenes (PIBs,  $M_n$  5500 g mol<sup>-1</sup> and 6900 g mol<sup>-1</sup> respectively)

(Scheme 2), suitable for crosslinking *via* “click” chemistry at room temperature, being designed for self healing materials.<sup>9</sup>



**Scheme 2** Schematic illustration of the bulk click reaction of PIB azide and PIB-alkyne with TRGO/Cu(I) at 20 °C *via* melt rheology

For crosslinking experiments an azide-functionalized trivalent PIB and an alkyne functionalized trivalent PIB were mixed with the TRGO/Cu(I) catalyst (2 mol%, 0.7 mass%) and crosslinking was investigated on a rheometer plate. Fig. S3a<sup>†</sup> shows the rheology result of the “click” reaction of polymers at 20 °C, where at the beginning of the reaction, the sample clearly possesses liquid like character; the loss modulus is higher than the storage modulus ( $G'' > G'$ ). After some time (520 minutes), both moduli increase and a crossover was observed (gel point), which is indicative of network formation. The structure of polymer/TRGO–Cu(I) mixtures before and after crosslinking was investigated using FT-IR measurements (Fig. S3b, ESI<sup>†</sup>), where after crosslinking a complete disappearance of the azide peak (2097 cm<sup>-1</sup>) confirms the complete crosslinking of the polymer. In contrast, in experiments with Cu/C and without catalyst no gel point was observed even after 1000 minutes, which again supports the high activity of the synthesized TRGO/Cu(I) catalyst.

In summary, we have presented a facile and robust approach for the immobilization of Cu(I) catalyst onto graphene nanosheets obtaining a highly active TRGO/Cu(I) catalyst for the Cu(I)-catalyzed alkyne-azide “click” cycloaddition reaction. The TRGO/Cu(I) catalyst shows high stability at

### III.RESULT AND DISCUSSION

standard reaction conditions (air) with excellent recyclability and reusability. Furthermore, the TRGO/Cu(I) catalyst shows excellent performance for bulk click reactions as proven *via* melt-rheology. Thus, Cu nanoparticles immobilized onto graphene nanosheets can function as an effective catalyst in click chemistry under both solvent and bulk conditions, including low and high molecular weight molecules.

We gratefully acknowledge the financial support from the EU-IASS project: Improving the Aircraft Safety by Self-Healing Structure and Protecting Nanofillers, European Union Seventh Framework Programme (FP7/20072013), Grant Agreement No. 313978 as well as the grant DFG-BI 1337/8-1 and DFG-BI 1337/8-2 within the SPP 1568 ("Design and Generic Principles of Self-Healing Materials).

#### Notes and references

1. H. C. Kolb, M. G. Finn and K. B. Sharpless, *Angew. Chem. Int. Ed.*, 2001, **40**, 2004-2021.
2. V. V. Rostovtsev, L. G. Green, V. V. Fokin and K. B. Sharpless, *Angew. Chem. Int. Ed.*, 2002, **41**, 2596-2599.
3. M. T. Meldal, C. W., in *Proceedings of the Second International and the Seventeenth American Peptide Symposium*, 2001, pp. 263-264.
4. C. W. Tornøe, C. Christensen and M. Meldal, *J. Org. Chem.*, 2002, **67**, 3057-3064.
5. *Proceedings of the Chemical Society*, 1961, 357-396.
6. W. H. Binder and R. Zirbs, in *Encyclopedia of Polymer Science and Technology*, John Wiley & Sons, Inc., 2002.
7. W. H. Binder and R. Sachsenhofer, *Macromol. Rapid Commun.*, 2007, **28**, 15-54.
8. B. Uszczynska, T. Ratajczak, E. Frydrych, H. Maciejewski, M. Figlerowicz, W. T. Markiewicz and M. K. Chmielewski, *Lab on a Chip*, 2012, **12**, 1151-1156.
9. D. Döhler, P. Michael and W. H. Binder, *Macromolecules*, 2012, **45**, 3335-3345.
10. R. K. Iha, K. L. Wooley, A. M. Nyström, D. J. Burke, M. J. Kade and C. J. Hawker, *Chem. Rev.*, 2009, **109**, 5620-5686.
11. J.-F. Lutz, *Angew. Chem. Int. Ed.*, 2007, **46**, 1018-1025.
12. X. Huang, X. Qi, F. Boey and H. Zhang, *Chem. Soc. Rev.*, 2012, **41**, 666-686.
13. K. S. Novoselov, A. K. Geim, S. V. Morozov, D. Jiang, Y. Zhang, S. V. Dubonos, I. V. Grigorieva and A. A. Firsov, *Science*, 2004, **306**, 666-669.
14. S. Yang, R. E. Bachman, X. Feng and K. Müllen, *Acc. Chem. Res.*, 2012, **46**, 116-128.
15. S. Eigler, S. Grimm, F. Hof and A. Hirsch, *J. Mater. Chem. A*, 2013, **1**, 11559-11562.
16. S. Eigler and A. Hirsch, *Angew. Chem. Int. Ed.*, 2014, **53**, 7720-7738.
17. S. Yang, J. Dong, Z. Yao, C. Shen, X. Shi, Y. Tian, S. Lin and X. Zhang, *Sci. Rep.*, 2014, **4**, 4501.
18. R. Wang, Z. Wu, C. Chen, Z. Qin, H. Zhu, G. Wang, H. Wang, C. Wu, W. Dong, W. Fan and J. Wang, *Chem. Commun.*, 2013, **49**, 8250-8252.
19. G. M. Scheuermann, L. Rumi, P. Steurer, W. Bannwarth and R. Mülhaupt, *J Am Chem. Soc.*, 2009, **131**, 8262-8270.
20. J. Qin, W. Lv, Z. Li, B. Li, F. Kang and Q.-H. Yang, *Chem. Commun.*, 2014.
21. T. Jia, A. Kolpin, C. Ma, R. C.-T. Chan, W.-M. Kwok and S. C. E. Tsang, *Chem. Commun.*, 2014, **50**, 1185-1188.
22. P. D. Tran, S. K. Batabyal, S. S. Pramana, J. Barber, L. H. Wong and S. C. J. Loo, *Nanoscale*, 2012, **4**, 3875-3878.
23. S. K. Movahed, M. Dabiri and A. Bazgir, *Appl. Catal., A*, 2014, **481**, 79-88.
24. C. Hong, X. Jin, J. Tottleben, J. Lohrman, E. Harak, B. Subramaniam, R. V. Chaudhari and S. Ren, *J. Mater. Chem. A*, 2014, **2**, 7147-7151.
25. X. Dong, K. Wang, C. Zhao, X. Qian, S. Chen, Z. Li, H. Liu and S. Dou, *J. Alloy. Compd.*, 2014, **586**, 745-753.
26. W. S. Hummers and R. E. Offeman, *J. Am. Chem. Soc.*, 1958, **80**, 1339-1339.
27. T. Kyotani, K.-y. Suzuki, H. Yamashita and A. Tomita, *TANSO*, 1993, **1993**, 255-265.
28. O. García-Martínez, R. M. Rojas, E. Vila and J. L. M. de Vidales, *Solid State Ionics*, 1993, **63-65**, 442-449.
29. M. L. Foo, Q. Huang, J. W. Lynn, W.-L. Lee, T. Klimczuk, I. S. Hagemann, N. P. Ong and R. J. Cava, *J. Solid. State. Chem.*, 2006, **179**, 563-572.
30. S. Suzuki, M. Saito, S. C. Kang, K. T. Jacob and Y. Waseda, *Mater. Trans., JIM*, 1998, **39**, 1024-1028.
31. B. H. Lipshutz and B. R. Taft, *Angew. Chem. Int. Ed.*, 2006, **45**, 8235-8238.
32. V. O. Rodionov, V. V. Fokin and M. G. Finn, *Angew. Chem.*, 2005, **117**, 2250-2255.
33. V. O. Rodionov, S. I. Presolski, S. Gardinier, Y.-H. Lim and M. G. Finn, *J. Am. Chem. Soc.*, 2007, **129**, 12696-12704.

## Supporting information

### 1. Materials

All chemicals and solvents, which were used for the synthesis were purchased from Sigma-Aldrich and used as received unless otherwise stated. Deuterated tetrahydrofuran (THF- $d_8$ , 95%) was purchased from AMAR chemicals and phenyl acetylene from MERK. Graphite flakes (KFL 99.5, *min* 20% > 100  $\mu m$ ) was received from Kropfmühl AG. Tetrahydrofuran (THF) for recycling experiment was pre-dried over potassium hydroxide for several days, refluxed over sodium/benzophenone and freshly distilled under an argon atmosphere before use.

### 2. Methods

#### TEM, STEM and EDXS

The high-resolution transmission electron microscopy (HRTEM) analyses were performed on a FEI Titan<sup>3</sup> 80-300 electron microscope with a  $c_s$ -image aberration corrector (FEI Company) at 300 kV acceleration voltage. Using the same instrument, scanning TEM (STEM) employing a high-angle annular dark field (HAADF) detector (Fischione Model 3000, camera length: 145 mm) was accomplished. STEM in combination with energy-dispersive X-ray spectroscopy (EDXS), performed with a dedicated, high-solid angle (0.7 sr) detector system (Super-X EDX analysis system, FEI Company) allowed to achieve distribution mappings of different elements of chosen samples, using the commercially available software Esprit (Bruker Company). Element distribution mappings were derived by evaluating the lateral distribution of the peak intensity, i.e., the area underlying the  $K_\alpha$  edges of the analyzed elements, with an automatic routine provided by the software. In an attempt to evaluate the oxidation state of Cu in the copper-oxide nanoparticles, an EDXS quantification was also performed with the help of the same software, evaluating the peaks of the K-lines of the respective elements Cu and O. Since only the element ratio of Cu and O was of interest for this specific question, all other peaks in the respective EDXS spectra, which originate from other elements of the sample (e.g., Cl, B and S) were only deconvoluted, but disregarded for quantification. A special Ni grid instead of a standard Cu grid was used for sample preparation to keep Cu quantification errors as low as possible.

#### XPS

XPS analysis was performed using a XPS PHI Versa Probe 5000 spectrometer. The pressure in the analysis chamber was typically  $1.10^{-9}$  Torr. The XPS measurements were performed using a monochromatic AlK  $\alpha$  radiation at 1486.6 eV. A neutralizer with a Ar gun was used during the XPS analysis to compensate charging effects. The analysis of the TRGO-Cu(I) sample show the presence of C1s (88.78 atom%), O1s (9.3 atom%), Cu(0.34 atom%), Si(1.58 atom%) (pass energy: 187.85 eV). Also the high resolution XPS spectra of each element recorded with a pass energy of 23.5 eV and an energy step 0.2 eV.

#### NMR

All NMR spectra were recorded on a Varian spectrometer (Gemini 400) at 400 MHz at 27 °C. THF- $d_8$  and DMSO- $d_6$  (Armar AG, 99.8 Atom %D) was used as solvent and tetramethylsilane as internal standard. The coupling constants were given in Hz and the chemical shifts in ppm and referred to the



### III.RESULT AND DISCUSSION

solvent residue peak [THF- $d_8$  1.72 and 3.58 ppm and DMSO- $d_6$  2.5 ppm ( $^1H$ )]. For the interpretation of the spectra, MestReNova v. 6.0.2–5475 was used.

#### Rheology

Rheological measurements were performed on an oscillatory plate rheometer MCR 501/SN 80753612 from Anton Paar (Physica). For all measurements a PP08 measuring system (parallel plated, diameter 8 mm) was used. Measurements were performed at 20 °C and the sample temperature was regulated by thermoelectric heating and cooling. For evaluation of data the RheoPlus/32 software (V 3.40) and OriginPro7 was used. For sample preparation a 1:1 mixture of an azido-functionalized polymer and an alkyne-functionalized polymer was placed in a flask (ca. 100.0 mg) and was dissolved in THF (approximately 3.0 mL). The solvent was removed and the sample was dried in high vacuum. TRGO/Cu(I) catalyst (0.02 equiv per functional group) was suspended in  $CHCl_3$  (40.0  $\mu L$ ) and was added to the polymer mixture. Subsequently, the reaction mixture was mixed with a spatula and was immediately put on the rheometer plate. Measurements were performed with a strain  $\gamma$  of 0.1% and with an angular frequency  $\omega$  ranging from 100 to 1 rad/s. A frequency sweep was performed every 10 min. All samples were measured at 20 °C. The gelation time was determined as crossover of the storage ( $G'$ ) and loss modulus ( $G''$ ) at 10 rad/s. Measurements were stopped after a total time (26.7 h) when the values of the storage and the loss modulus stayed constant (second decimal place) for at least 60 min.

#### IR

ATR-IR spectra were performed on a Bruker Tensor VERTEX 70 equipped with a Golden Gate Heated Diamond ATR Top-plate. Opus 6.5 was used for analyzing data.

### 3. Characterization

#### 3.1-STEM-EDXS

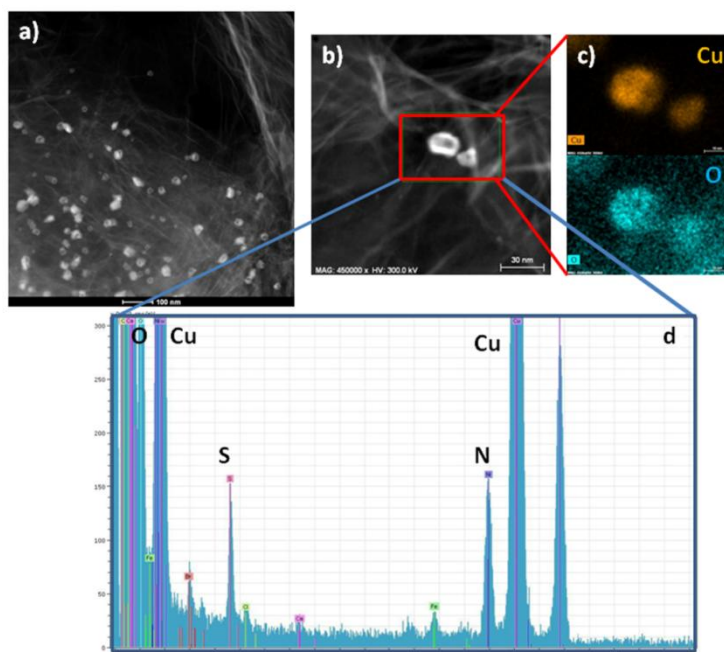


**Fig. S1** a) STEM-EDXS spectrum of TRGO/Cu(I), b) selected particle area for STEM-EDXS analysis, c) STEM spectrum of selected particle, d) EDXS spectrum of selected particle.

### 3.2- Kinetic study

In a 10 mL schlenk flask, benzyl azide (0.0751 mmol), phenyl acetylene (0.0826 mmol, 1.1eq) and TRGO/Cu(I) (1.8 mg, 2 mol%) were dissolved in 1.5 mL of deuterated THF. Afterwards the mixture was degassed by freeze-thaw cycle (2 times). Then the mixture was sonicated (bath sonicator) for some seconds to disperse the catalyst, and the reaction was run at 40 °C. The aliquots taken at different intervals from the reaction, filtered to remove the catalyst and <sup>1</sup>H NMR study was performed to calculate the conversion according to equation S1 (Fig S2a,b). The equation (1) which was evaluated by Fokin and Finn et al.<sup>1</sup> was used for calculation of k' as below:

$$\text{rate} = k' [\text{alkyne}]^{1.3} [\text{azide}]^1 \quad (k' = k[\text{Cu}]^2) \quad \text{equation 1}$$

$$\text{Conversion} = \frac{\text{integration}_{\text{CH}_2\text{-moiety of click product}}}{\text{integration}_{\text{CH}_2\text{-moiety of click product}} + \text{integration}_{\text{CH}_2\text{-moiety of benzyl azide}}} \quad \text{equation S1}$$

- 1- [Cu]=constant. As the catalyst was highly dispersible in the reaction mixture, so we assumed that the catalyst concentration did not change while taking the aliquots.
- 2- [alkyne]=[azide]=C.
- 3- C<sub>0</sub>= concentration of azide in the beginning      C<sub>0</sub>=0.0534 M
- 4- C<sub>t</sub>= concentration of azide at time t              C<sub>t</sub>=0.0524×(1-Conversion) M
- 5- Rate =  $\frac{-d[\text{azide}]}{dt} = \frac{-d[C]}{dt}$

$$\frac{-dC}{dt} = k' C^{2.3} \longrightarrow \int_{C_0}^{C_t} \frac{-dC}{dt} = \int_0^t k' t \longrightarrow C_t^{-1.3} - C_0^{-1.3} = kt$$

- 6- The slope of (C<sub>t</sub><sup>-1.3</sup> - C<sub>0</sub><sup>-1.3</sup>) vs. t is k' (Fig. S2c)

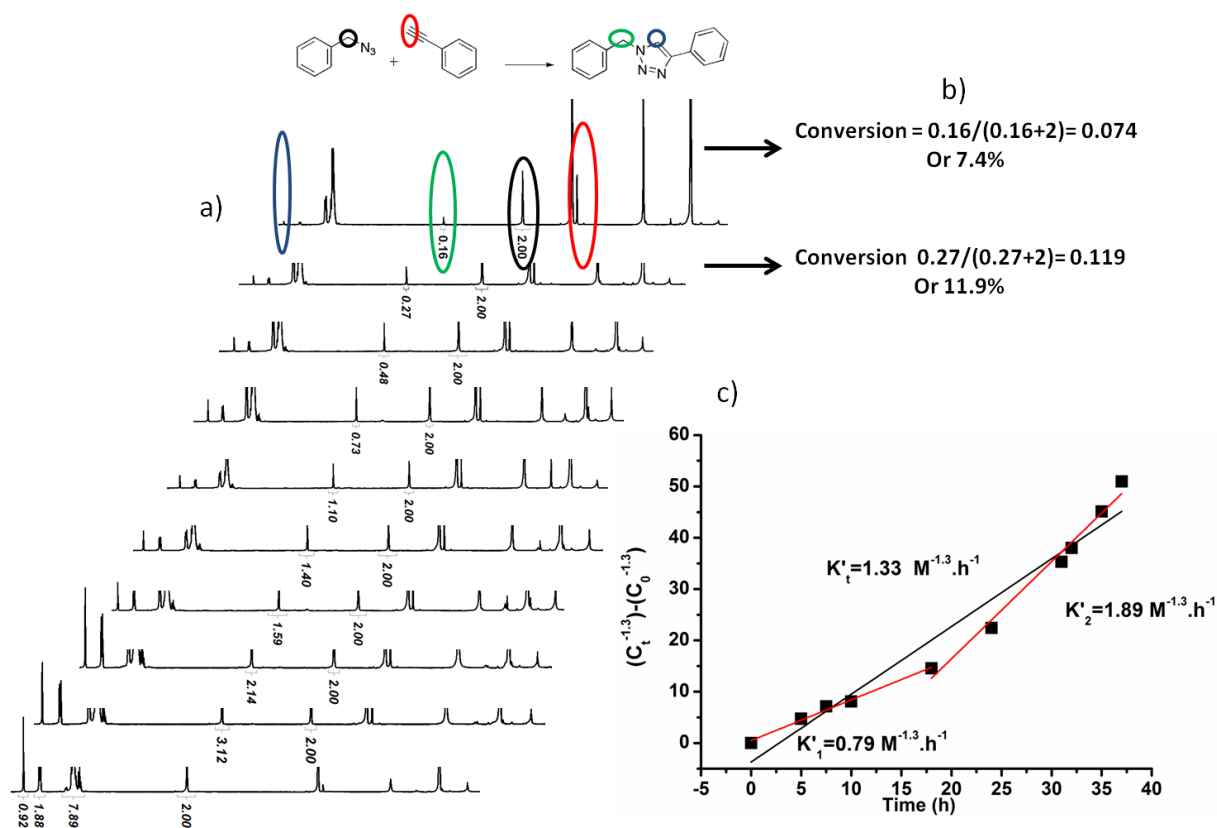


**Fig. S2** Kinetic study of model click reaction with TRGO/Cu(I) as catalyst a) <sup>1</sup>H NMR measurements at different time intervals, b) calculation of conversion (%) c) different k' values of reaction derived from graph.

### III. RESULT AND DISCUSSION

Two different  $k'$  are calculated ( $k'_1=0.79 M^{-1.3}.h^{-1}$ ,  $k'_2=1.89 M^{-1.3}.h^{-1}$ ) by linear fit (Fig. S2c). Increment in  $k'$  value is explainable by autocatalytic effect caused by the formed triazole moieties and the subsequent complexation by the Cu(I)-ions.<sup>1</sup> However in order to compare the current work with Finn et al.<sup>2</sup>, a single linear fit was used to calculate  $k'_t = 1.33 M^{-1.3}.h^{-1}$ .

#### 3.3-Rheology and IR of polymer mixture

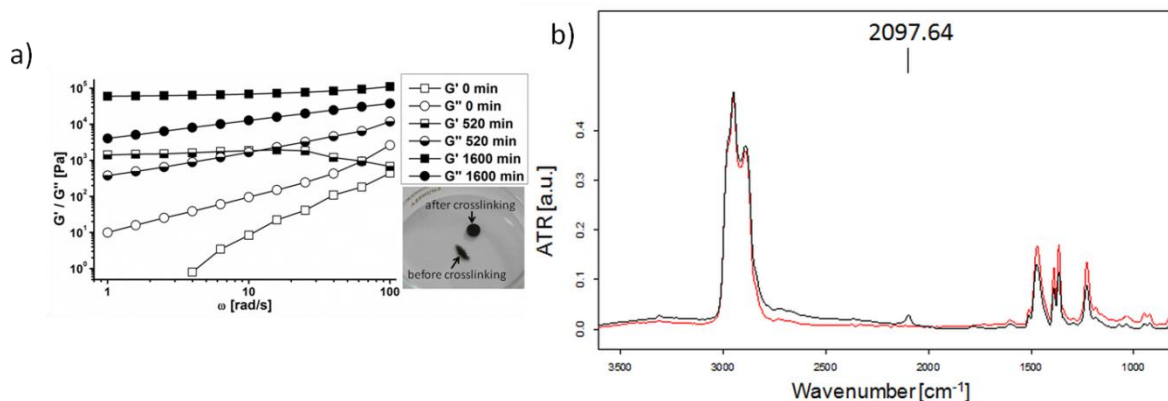


**Fig. S3 a)** Typical graphs derived from an *in-situ* rheological measurement by reaction of PIB-azide and PIB-alkyne with TRGO/Cu(I) conjugate at 20 °C **b)** IR spectrum of polymer mixture with TRGO/Cu(I) before (black curve) and after crosslinking (red curve).

#### 4. Recycling experiment

In a 10 mL schlenk flask, benzyl azide (0.0751 mmol), phenyl acetylene (0.0826 mmol, 1.1 eq) and TRGO/Cu(I) (1.8 mg, 2 mol%) were dissolved in 1.5 mL of THF. Afterwards the mixture was degassed by freeze-thaw cycle (2 times). Then the mixture was sonicated (bath sonicator) for few seconds to disperse the catalyst and the reaction was run at 40 °C for 55 h. Afterwards the reaction mixture was filtered and washed by 10-15 mL of THF. The solvent of the filtrate was evaporated under reduced pressure (200 mbar was used as the minimum pressure to avoid flashing of starting materials). The recovered catalyst was dried under high vacuum for 30 min and used for next cycle.

#### 5. Synthesis

##### 5.1-Synthesis of graphene oxide (GO)

Graphite (3 g) was stirred in concentrated sulfuric acid (117 mL) at room temperature (RT), and sodium nitrate (1.5 g) was added, afterwards the mixture was cooled to 0 °C and potassium permanganate (9 g) was added during 30 min to 1 h in order to avoid the increment in internal temperature of the reaction mixture. After 2 h, the green slurry was allowed to come to RT, and after being stirred for 3 h (during this time the viscosity of mixture was increased) the whole batch was carefully poured into a 700 mL beaker filled with ice-cold water (distilled). Subsequently, hydrogen peroxide (3%) was added in excess and the mixture was stirred overnight and then filtered. Workup was accomplished by several washings with a mixture of HCl/H<sub>2</sub>O<sub>2</sub> (1:1, 5%) and filtration was followed by several washings with water and centrifugation until the supernatant did not show anymore precipitation with AgNO<sub>3</sub> solution. The obtained GO carefully powdered in a ball mill, with pre cooling by liquid nitrogen. (For more detail see Appendix 2.3.1)



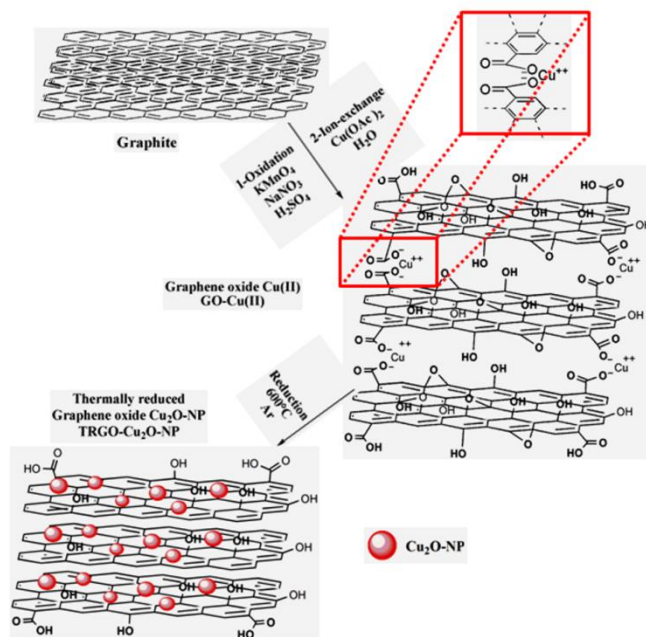


Fig. S4 Synthesis of Cu catalyst immobilized graphene nanosheets.

## 5.2-Synthesis of different click product

In a 10 mL schlenk flask, benzyl azide (0.0751 mmol), different alkynes (0.0826- 0.09763 mmol, 1.1- 1.3 eq) and TRGO/Cu(I) (1.8 mg, 2 mol%) were dissolved in 1.5 mL of deuterated THF. Afterwards the mixture was degassed by freeze-thaw cycle (2 times). Then the mixture was sonicated (bath sonicator) for some seconds to disperse the catalyst. The reaction was run at 40 °C for 48 h. Afterwards the reaction mixture was filtered and the  $^1\text{H}$  NMR of filtrate showed the conversion of the reaction like kinetic measurements. The  $^1\text{H}$  NMR's of the products were measured without any purification and they just filtered to remove the graphene catalyst. Therefore the traces of excess alkyne and unreacted azide are visible in some spectra (Figures S5-S9). Furthermore the  $^1\text{H}$  NMRs of these products are in agreeing with the previous works.<sup>3-6</sup>

### 5.2.1- 1-Benzyl-4-phenyl-1H-1,2,3-triazole (Fig. S5)

$^1\text{H}$  NMR (400 MHz, THF- $d_8$ )  $\delta$  ppm 5.81 (s, 2H), 7.39-7.21 (m, 7H), 7.82 (m, 2H), 8.08 (s, 1H)

### 5.2.2- 1-Benzyl-4-(4-chlorobutyl)-1H-1,2,3-triazole (Fig. S6)

$^1\text{H}$  NMR (400 MHz, THF- $d_8$ )  $\delta$  ppm 1.84-1.74 (m, 3H), 2.67 (t,  $J = 6.87, 6.87$  Hz, 2H), 3.56 (t,  $J = 9.10, 9.10$  Hz, 2H), 5.49 (s, 2H), 7.39-7.21 (m, 5H), 7.49 (s, 1H)

### 5.2.3- 2-(1-Benzyl-1H-1,2,3-triazol-4-yl)butan-2-ol (Fig. S7)

$^1\text{H}$  NMR (400 MHz, THF- $d_8$ )  $\delta$  ppm 0.78 (t,  $J = 7.43, 7.43$  Hz, 3H), 1.46 (s, 3H), 1.88-1.74 (m, 2H), 3.97 (s, 1H), 5.50 (s, 2H), 7.42-7.19 (m, 5H), 7.55 (s, 1H),

### 5.2.4- 1-(1-Benzyl-1H-1,2,3-triazol-4-yl)pentan-1-ol (Fig. S8)

$^1\text{H}$  NMR (400 MHz, THF- $d_8$ )  $\delta$  ppm 0.89 (t,  $J = 7.12, 7.12$  Hz, 3H), 1.37 (m 4H), 2.58 (s, 2H), 4.23 (s, 1H), 4.70 (s, 1H), 5.50 (s, 2H), 7.46-7.18 (m, 5H), 7.59 (s, 1H)

### 5.2.5- 2-(1-Benzyl-1H-1,2,3-triazol-4-yl)propan-2-ol (Fig. S9)

$^1\text{H}$  NMR (400 MHz, THF- $d_8$ ) ppm 1.48 (s, 6H), 2.07 (s, 1H), 5.49 (s, 2H), 7.45-7.11 (m, 5H), 7.56 (s, 1H)

### III.RESULT AND DISCUSSION

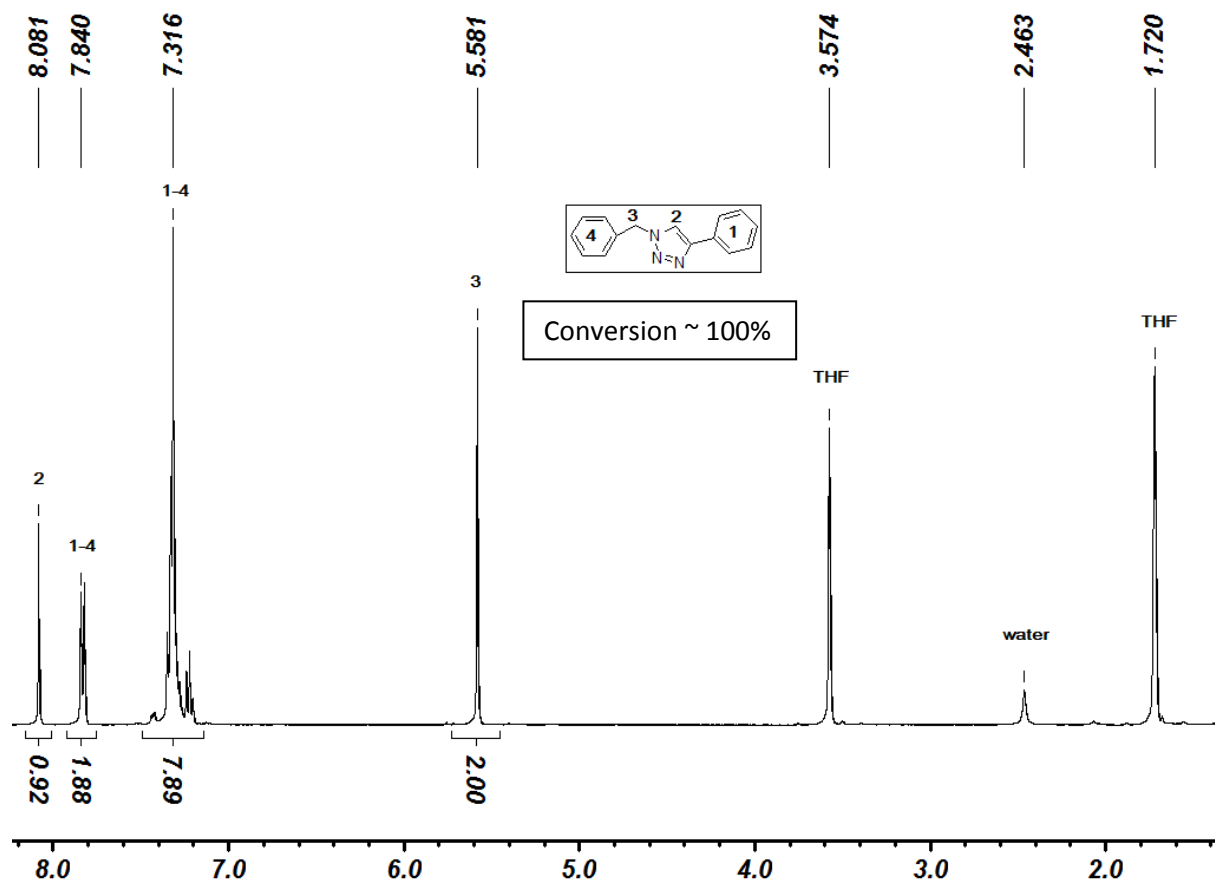


Fig. S5 <sup>1</sup>H NMR of 1-benzyl-4-phenyl-1H-1,2,3-triazole

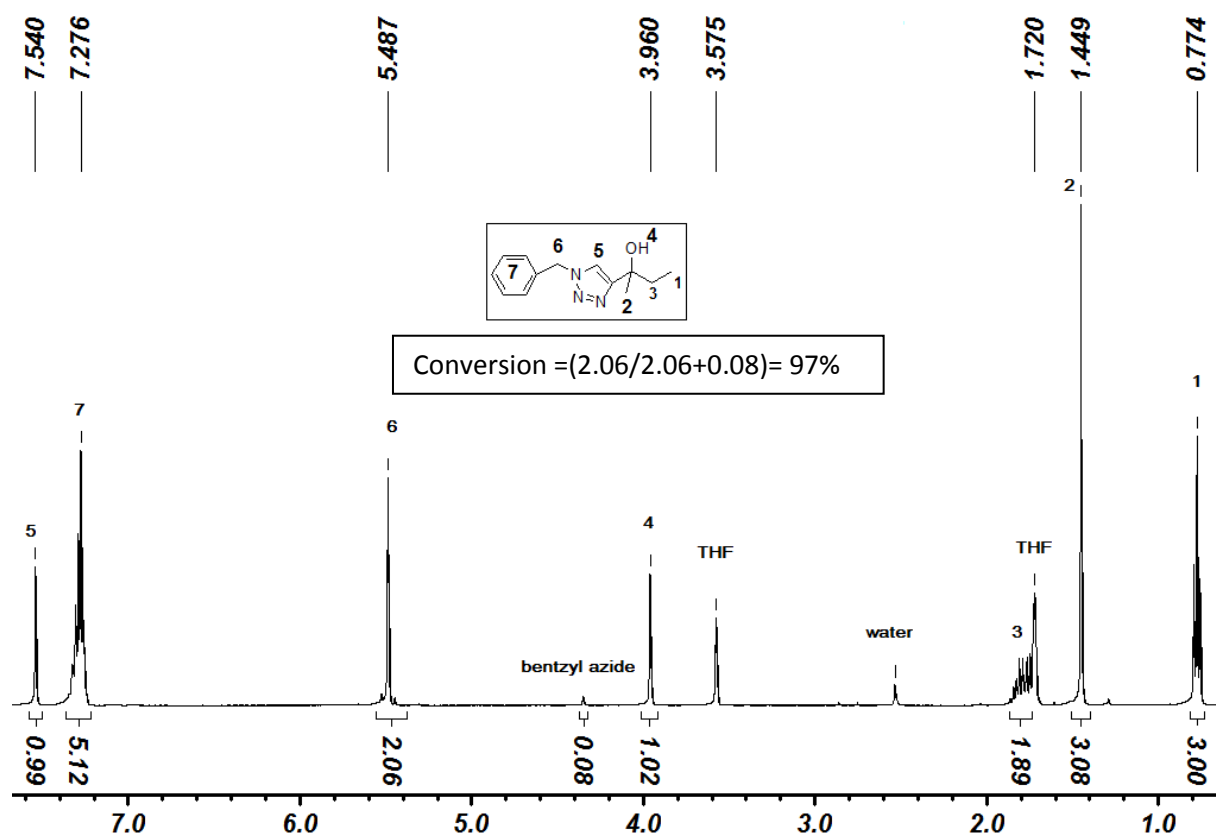


Fig. S6 <sup>1</sup>H NMR of 1-benzyl-4-(4-chlorobutyl)-1H-1,2,3-triazole

### III.RESULT AND DISCUSSION

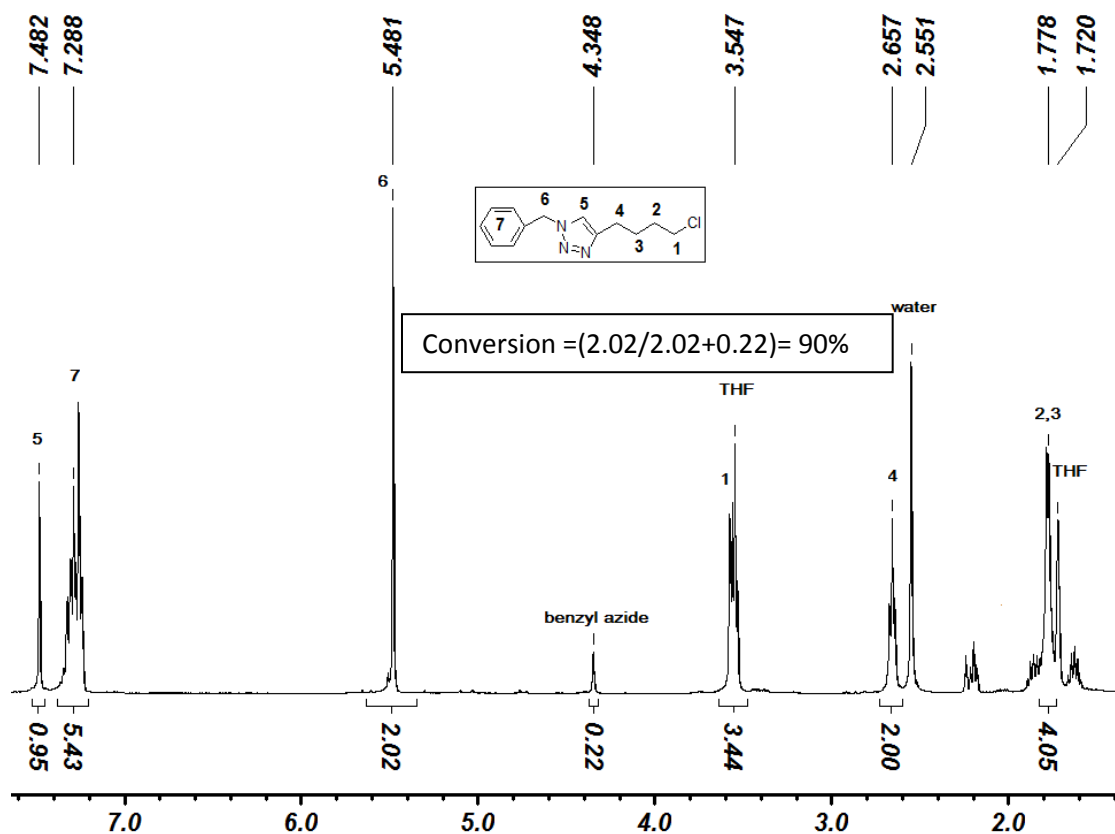


Fig. S7 <sup>1</sup>H NMR of 2-(1-benzyl-1H-1,2,3-triazol-4-yl)butan-2-ol

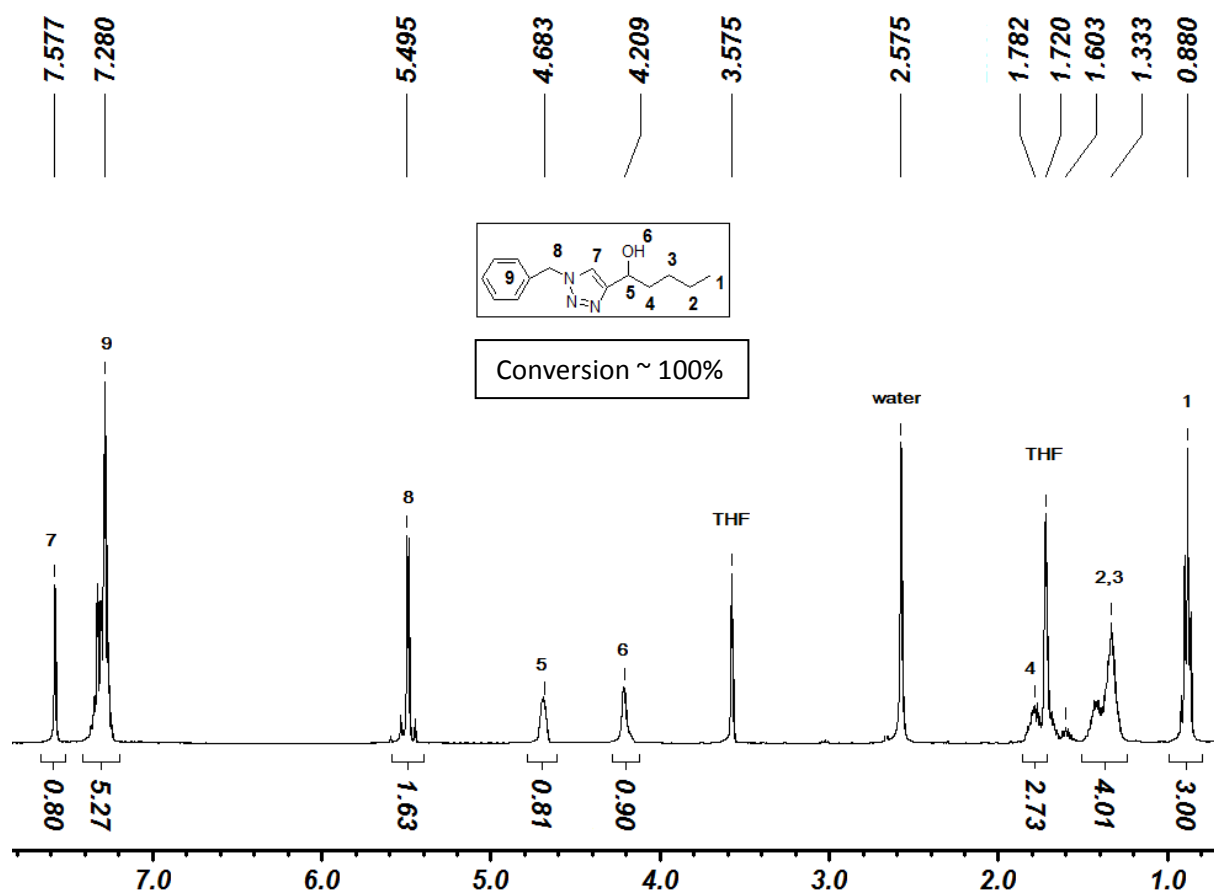
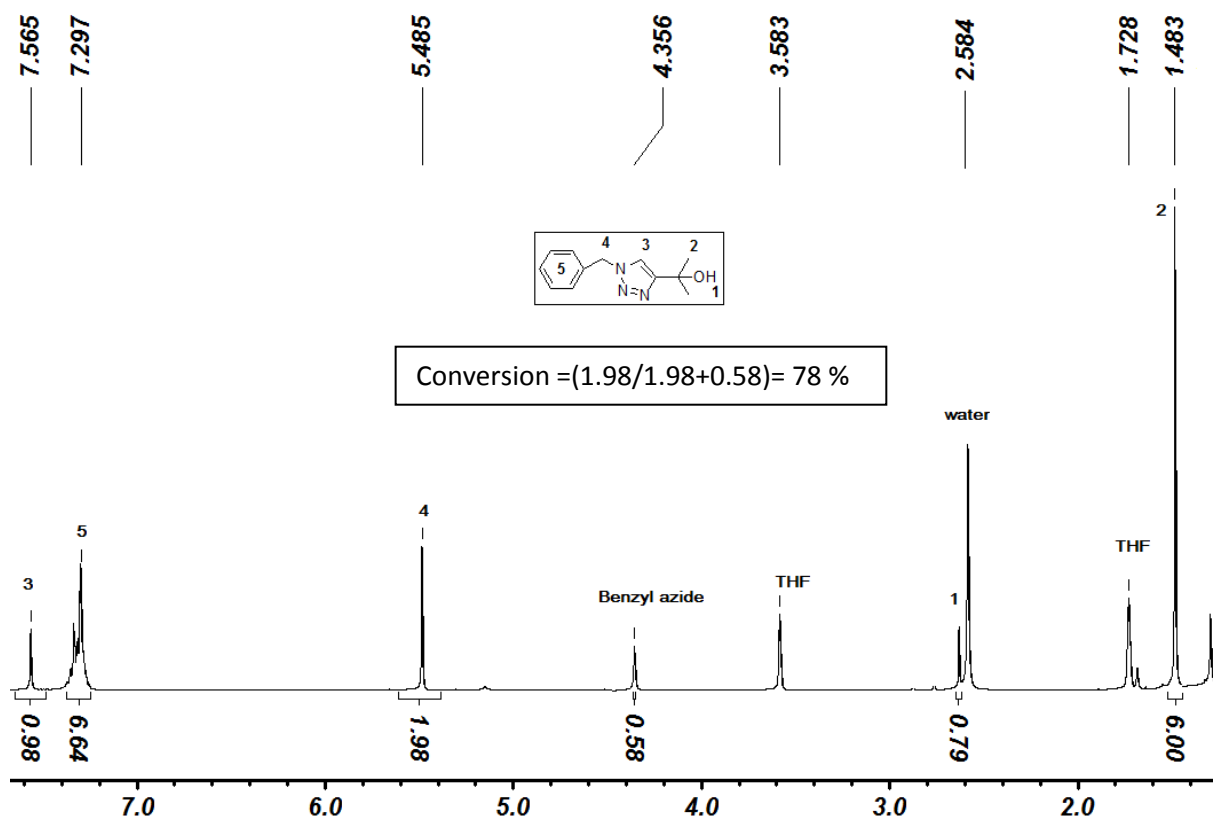


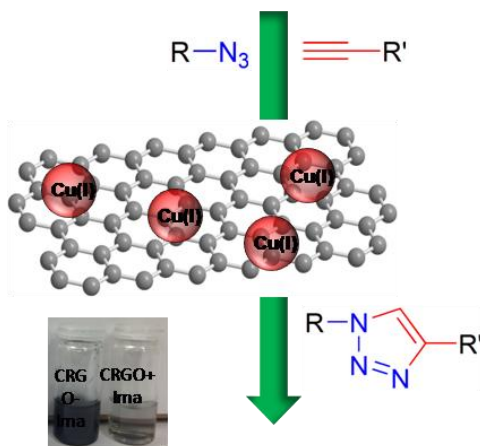
Fig. S8 <sup>1</sup>H NMR of 1-(1-benzyl-1H-1,2,3-triazol-4-yl)pentan-1-ol

### III.RESULT AND DISCUSSION



1. V. O. Rodionov, V. V. Fokin and M. G. Finn, *Angew. Chem.*, 2005, **117**, 2250-2255.
2. V. O. Rodionov, S. I. Presolski, S. Gardinier, Y.-H. Lim and M. G. Finn, *J. Am. Chem. Soc.*, 2007, **129**, 12696-12704.
3. B. H. Lipshutz and B. R. Taft, *Angew. Chem. Int. Ed.*, 2006, **45**, 8235-8238.
4. L. Zhang, X. Chen, P. Xue, H. H. Y. Sun, I. D. Williams, K. B. Sharpless, V. V. Fokin and G. Jia, *J. Am. Chem. Soc.*, 2005, **127**, 15998-15999.
5. P. Appukkuttan, W. Dehaen, V. V. Fokin and E. Van der Eycken, *Org. Lett.*, 2004, **6**, 4223-4225.
6. V. V. Rostovtsev, L. G. Green, V. V. Fokin and K. B. Sharpless, *Angew. Chem. Int. Ed.*, 2002, **41**, 2596-2599.

## 2-Carbon-Supported Copper Nanomaterials: Recyclable Catalysts for Huisgen [3+2] Cycloaddition Reactions



### Abstract

Highly disperse copper nanoparticles immobilized on carbon nanomaterials (CNMs; graphene/carbon nanotubes) were prepared and used as a recyclable and reusable catalyst to achieve Cu<sup>I</sup>-catalyzed [3+2] cycloaddition click chemistry. Carbon nanomaterials with immobilized N-heterocyclic carbene (NHC)-Cu complexes prepared from an imidazolium-based carbene and Cu<sup>I</sup> show excellent stability including high efficiency at low catalyst loading. The catalytic performance evaluated in solution and in bulk shows that both types of Cu-CNMs can function as an effective recyclable catalysts (more than 10 cycles) for click reactions without decomposition and the use of external additives.

### Introduction

The copper(I)-catalyzed azide–alkyne cycloaddition (CuAAC, click reaction)<sup>[1]</sup> has drawn extensive attention for the rapid and efficient assembly of molecules, and it has found application in a broad range of disciplines, in particular in organic, bioorganic, and materials science.<sup>[2]</sup> Click reactions are environmentally friendly, functional-group-tolerant, highly efficient, regioselective, and can be performed under a wide range of solvents and reaction conditions.<sup>[3]</sup> The click reaction accelerated by catalytically active Cu<sup>I</sup> species (CuAAC) involves the reduction of Cu<sup>II</sup> to Cu<sup>I</sup>, or the oxidation of Cu<sup>0</sup> to Cu<sup>I</sup> by addition of sacrificial reducing/oxidizing agents. Often complete removal of the applied copper catalysts or the used oxidizing/reducing agents in the CuAAC click reaction remains the main challenge hampering the utilization of click chemistry, particularly in the area of biology and electronics.<sup>[4]</sup> Also, Cu<sup>I</sup> catalysts are easily oxidized to Cu<sup>II</sup>, and/or disproportionate to Cu<sup>0</sup> and Cu<sup>II</sup> owing to thermodynamic-

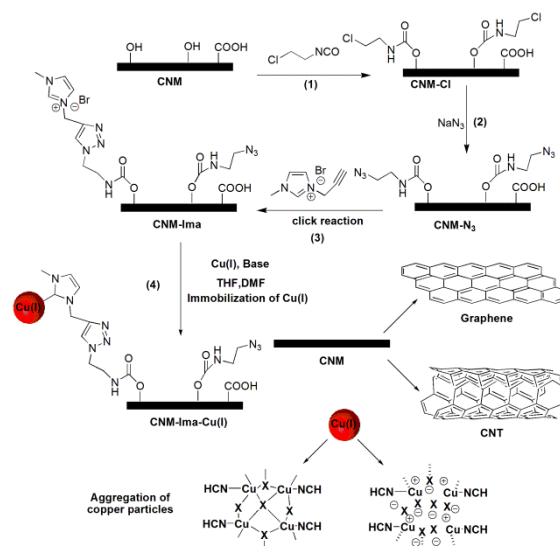
Instability.<sup>[5]</sup> Therefore, the synthesis of a new generation of catalysts including high activity, stability, and recyclability is highly desirable. A variety of recyclable heterogeneous copper-based catalysts have been prepared on the basis of commercially available supporting matrices, including charcoal,<sup>[6]</sup> chitosan,<sup>[7]</sup> resins,<sup>[8]</sup> and cross-linked polymers,<sup>[9]</sup> where the separation of the catalyst from the reaction mixture is strongly facilitated. However a low number of catalytic cycles, the high catalyst loadings required, and the necessity of an external ligand or base often limit their applicability.

Metal catalysts supported by carbon nanomaterials (CNMs) have excellent characteristic properties, owing to their high surface area, thermal stability, and porous surface, which acts as a scaffold to prevent the agglomeration of the immobilized metal particles.<sup>[10]</sup> In the past decade, the advantages of CNMs (carbon nanotubes (CNTs),<sup>[11]</sup> graphene<sup>[12]</sup>) in various fields of science reflect the use of these materials for realizing different innovative and prolific scientific works around the globe, including a variety of applications such as

electronics, biomedical engineering, and gene therapy.<sup>[12, 13]</sup> Furthermore, a number of reports show a higher catalytic activity by using CNT as a scaffold material,<sup>[14]</sup> with however limited importance of CNTs, as their catalytic activity depends on the diameter of CNTs as well as on the applied metal deposition method (outside/inside) including high cost of production.<sup>[15]</sup> Owing to their large-scale production, as well as the presence of plenty of functional groups on their surface, graphene oxide (GO)<sup>[16]</sup> has been acknowledged as one of the most promising supporting material. A good CNM support system can only be achieved by stable dispersion of nanomaterials. However, owing to strong intermolecular  $\pi$ - $\pi$  interactions, these nanoobjects form densely packed bundles<sup>[17]</sup> and thus it is quite a challenge to establish the most suitable atomic organization on their surfaces. To overcome this issue, the dispersibility of nanomaterials has been improved by covalent and non-covalent functionalization.<sup>[18]</sup> Ionic liquids (ILs), and in particular imidazolium-based ILs, have received a great deal of interest as they have been employed for the functionalization of nanomaterials with excellent dispersibility.<sup>[19]</sup> Herein we discuss a detailed investigation for the immobilization of copper particles onto both chemically reduced graphene oxide (CRGO) and CNTs acting as nanocatalysts for click chemistry, and highlight the performance of CRGO- and CNT-supported Cu catalysts. CRGO was chosen over GO as the defect sites in CRGO act as a trap for organic molecules and are useful to enhance the activity of supported catalyst.<sup>[20]</sup> The synthesis of highly stable *N*-heterocyclic carbene (NHC)-stabilized Cu<sup>I</sup>-catalyst immobilized graphene/CNT nanoconjugates was achieved through highly dispersible imidazolium functionalized CRGO/CNTs. NHCs are strong  $\sigma$ -donors but poor  $\pi$ -acceptor ligands and bind strongly to the metal center to improve the catalyst stability with promising catalytic activity.<sup>[21]</sup> Furthermore, the imidazolium group acts as an ionic liquid moiety that is able to improve the dispersibility of the CRGO/CNTs. The catalytic study shows that both types of Cu-CNMs (Cu-CRGO/Cu-CNT) conjugates can function as effective recyclable catalysts for click chemistry in solution and in bulk without decomposition, also without the use of any external ligand or base.

## Results and Discussion

Copper nanoparticles were immobilized onto the surface of CNMs as shown in Scheme 1, based on the formation of Cu<sup>I</sup> nanoparticles. Hummers' method was applied to prepare graphene oxide (GO),<sup>[22]</sup> whereas ascorbic acid was employed as a reducing agent to obtain chemically reduced graphene oxide (CRGO).<sup>[23]</sup>



**Scheme 1.** The synthesis of CNMs-Ima-Cu<sup>I</sup> nanoparticles. 1) and 2) substitution reaction for chlorination and azidation, 3) azide-alkyne click reaction to add imidazolium moiety on the surfaces, 4) exchanging the proton of the carbene with Cu<sup>I</sup>.

The number of OH groups on CRGO were determined using the method reported earlier by Mülhaupt et al.,<sup>[13c]</sup> where titration with phenyl isocyanate and TGA analysis estimates the number of OH groups on CRGO (Supporting Information, Figure S1). The modification of CRGO-OH with azide functionalities (CRGO-N<sub>3</sub>) was accomplished by a reported procedure.<sup>[24]</sup> To attach the imidazolium moiety acting as an ionic liquid on the surface of CRGO (CRGO-Ima, step 3), the Cu<sup>I</sup>-catalyzed azide alkyne click reaction was employed between the azide-functionalized CRGO (CRGO-N<sub>3</sub>) and 1-propargyl-3-methylimidazolium bromide.<sup>[25]</sup> The efficiency of the click reaction onto the surfaces of CRGO was optimized by different reaction conditions and the best click functionalization was obtained using water/*t*BuOH as a solvent and CuSO<sub>4</sub>/ sodium ascorbate as the catalytic system (Supporting Information, Figure S2, Table S1). Furthermore, the content of the modified surface after each step of reaction was calculated from thermogravimetric analysis (TGA; Figure 1a, Table 1). For the synthesis of CNT-Ima, first, OH groups

### III.RESULT AND DISCUSSION

were grafted on the surface of pristine multi-walled carbon nanotubes by a reported procedure,<sup>[26]</sup> afterwards we have applied the same reaction conditions as discussed in Scheme 1 and the results are given in the Supporting Information, Sections S1.3 and S1.4.

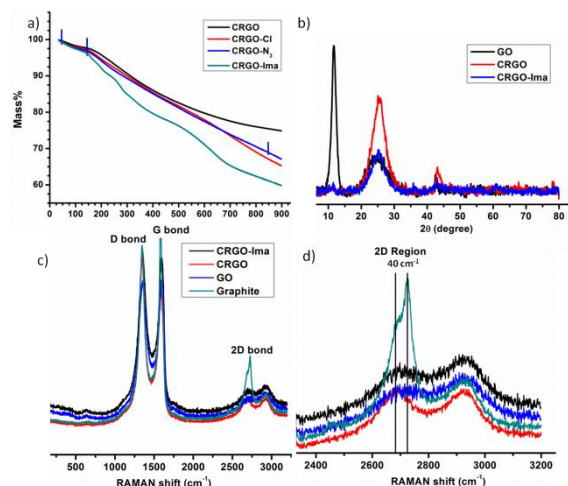


**Figure 1.** a) TGA analysis of functionalized CRGOs. b) XRD spectra of GO, CRGO, and CRGO-Ima. c) Raman spectra of pristine graphite, GO, CRGO, and CRGO-Ima. d) Enlargement of the 2D peak region in the Raman spectra.

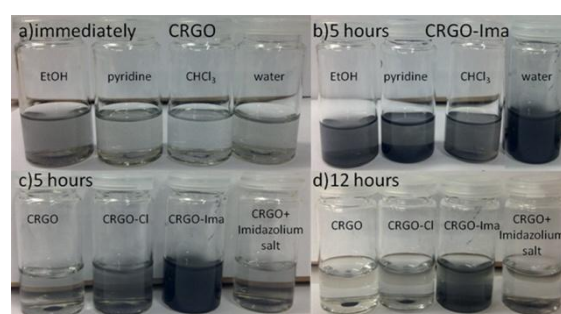
Raman spectroscopy was performed to analyze the ratio between carbon atoms with  $sp^2$  (G-band,  $I_G$ ) and  $sp^3$  (D-band,  $I_D$ ) hybridization in the graphite lattice, GO, and CRGO including each functionalization step. Pristine graphite shows two peaks at  $1583\text{ cm}^{-1}$  and  $2680\text{ cm}^{-1}$ , corresponding to the G-band and the 2D-band, respectively. During the oxidation step (conversion of graphite to GO) the appearance of a new band at  $1348\text{ cm}^{-1}$  (D-band) confirms structural defects on the GO surface. The intensity ratio between the D-band and the G-band was used to analyze the amount of defects on the surfaces (Table 1, Figure 1c).

Table 1. TGA, FAAS, and RAMAN results of CNM surfaces.				
Sample	TGA Mass [%]	Amount of loading [mmol $mg^{-1}$ ] <sup>[a]</sup>	Cu amount [mmol $mg^{-1}$ ] <sup>[b]</sup>	$I_D/I_G$ RAMAN
GO	40			0.98
CRGO	21			1.18
CRGO-Cl	28	$4.9 \times 10^{-4}$		1.21
CRGO-N <sub>3</sub>	28	$4.9 \times 10^{-4}$		1.19
CRGO-Ima	33	$3.4 \times 10^{-4}$	$1.5 \times 10^{-5}$	1.17
CRGO-Ima-Cu <sup>[c]</sup>			$3.1 \times 10^{-3}$	1.22
CRGO-Ima-Cu <sup>[d]</sup>			$2.8 \times 10^{-4}$	
CNT-Ima-Cu <sup>[c]</sup>			$3.1 \times 10^{-3}$	
CNT-Ima-Cu <sup>[d]</sup>			$5.9 \times 10^{-4}$	

[a] Calculated with respect to CRGO. [b] FAAS analysis. [c] Before washing with ammonium chloride. [d] After washing with ammonium chloride.

In contrast to the reactions with C=C bond of the graphene sheets (for example, free radicals or

dienophiles), which result in high amounts of defects onto the surface ( $I_D/I_G \approx 2$ ),<sup>[18a]</sup> we observed relatively few defects (ca. 1–1.2) even after 3–4 steps of modifications. Furthermore, a shift in the 2D-band (ca.  $40\text{ cm}^{-1}$ ) was observed during the modification of graphite to GO and CRGO, which can be related to a reduction in the number of graphene layers.<sup>[27]</sup> However, during the surface modification from CRGO to CRGO-Ima, a pronounced shift of the 2D band was not observed, which suggests that imidazolium-based functional groups do not have any effect on the number of layers (Figure 1d). The study was further supported by X-ray diffraction (XRD), where no significant change in the interlayer distance of CRGO ( $3.51\text{ \AA}$ ) and CRGO-Ima ( $3.55\text{ \AA}$ ) was observed (Figure 1b). The effect of the functionalization steps on the dispersibility of CRGO was also studied. CRGO and CRGO-Ima were dispersed in ethanol, pyridine, chloroform, and water ( $0.1\text{ mg mL}^{-1}$ ; Figure 2a,b). CRGO fails to disperse and agglomeration starts immediately after sonication (sonicator bath, 10 min). However for the CRGO-Ima a stable dispersion was observed up to 12 h in water, being the best solvent for the dispersion of functionalized CRGO. Compared to CRGO-Cl and a physical mixture of CRGO with 1-propargyl-3-methylimidazolium bromide, CRGO-Ima has shown better dispersibility, which is related to the hydrophilic behavior of bound imidazolium moieties. This effect can stabilize the dispersion electrostatically thus preventing the agglomeration of graphene nanosheets.<sup>[18a, 19d]</sup>



**Figure 2.** Dispersion of a) CRGO ( $0.1\text{ mg mL}^{-1}$ ) and b) CRGO-Ima ( $0.1\text{ mg mL}^{-1}$ ) in different solvents. c), d) Dispersion of CRGO, CRGO-Cl, CRGO-Ima, and a mixture of CRGO with 1-propargyl-3-methylimidazolium bromide (1:3) in water after 5 and 12 h.

Additionally, CNT-Ima also shows a good dispersibility behavior in different solvents, but agglomeration started already after 3 h (Supporting Information, Figure S4). This behavior can be due to advantages of CRGO over CNT such as high



### III.RESULT AND DISCUSSION

surface area, and less tendency to tangle, as discussed earlier.<sup>[28]</sup>

To obtain the *N*-heterocyclic carbene (NHC)-stabilized Cu<sup>I</sup> catalyst (CRGO-Ima-Cu<sup>I</sup>; Scheme 1, step 4), the proton of the imidazolium moiety was exchanged with a Cu<sup>I</sup> salt. To remove the excess of the copper salt, a soluble Cu<sup>I</sup> salt, tetrakis (acetonitrile)-copper(I) hexafluorophosphate, was used. The amount of the immobilized Cu content for CRGO-Ima-Cu<sup>I</sup> was determined by flame atomic absorption spectroscopy (FAAS), showing  $3.15 \times 10^{-3} \text{ mmol mg}^{-1}$  loading. However, residual copper particles were observed by transmission electron microscopy (TEM) analysis (Figure 3a), even after several washing steps with different solvents (DMF, THF, H<sub>2</sub>O). Therefore, the product was washed with a saturated solution of ammonium chloride to get rid of unbound or agglomerated Cu particles. After washing with ammonium chloride solution, highly dispersed Cu particles were observed in TEM images (Figure 3b), which could be due to a neutral Cu-Cu complex formation (Scheme 1), as discussed earlier by Flower et al.<sup>[29]</sup> Furthermore, a significant difference in the Cu loading was observed by FAAS showing  $2.83 \times 10^{-4} \text{ mmol mg}^{-1}$  loading. The same behavior was observed for CNT-Ima-Cu<sup>I</sup>, where  $3.1 \times 10^{-3} \text{ mmol mg}^{-1}$  and  $5.9 \times 10^{-4} \text{ mmol mg}^{-1}$  Cu amount was obtained before and after washing with ammonium chloride solution (Table 1).

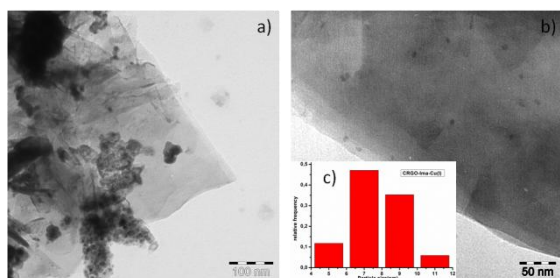


**Figure 3.** TEM image of the CRGO-Ima-Cu<sup>I</sup> catalysts a) before and b) after washing with NH<sub>4</sub>Cl solution. c) Copper particle size and distribution.

To further illustrate the successful functionalization of CNMs with ILs and Cu particles, X-ray photoelectron spectroscopy (XPS) was performed. From Figure 4 (XPS for CRGO-Ima-Cu<sup>I</sup>) the peaks at 284.68 eV and 531.6 eV correspond to C1s and O1s, respectively, and the peak at 285.93 eV corresponds to the C-N bonds (from the triazole rings<sup>[30]</sup> and the imidazolium moieties).<sup>[27, 31]</sup> The XPS measurement also confirms the presence of the existing form of the Cu before and after

washing with ammonium chloride solution. Before washing, the Cu 2p<sub>3/2</sub> peaks show three different Cu satellites, where the contributions at 932.37 eV and 952.31 eV are related to Cu<sup>I</sup>, and that at 934.6 eV is related to Cu<sup>II</sup> (Supporting Information, Figure S6). However, after washing, no peak satellites were observed at 934.6 eV, supporting the absence of Cu<sup>II</sup>, as already confirmed by TEM and FAAS measurements. After confirming the immobilized amount and the actual present form of Cu (Cu<sup>I</sup>) in the CNMs conjugates, the catalytic activity of the CNM-Ima-Cu<sup>I</sup> catalysts was investigated. Therefore a click model reaction between benzyl azide and phenyl acetylene under different reaction conditions was studied (Table 2).

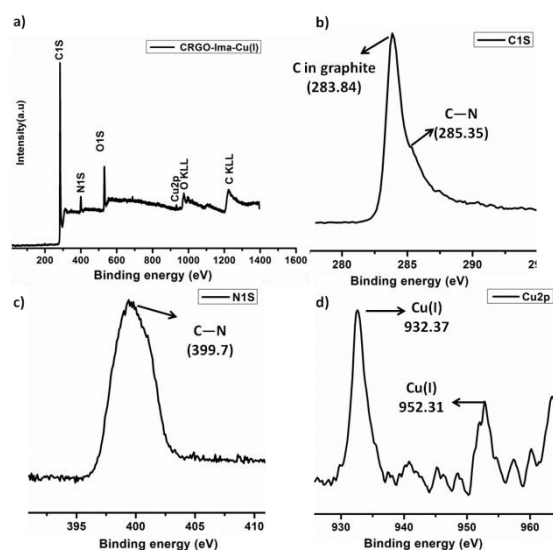


**Figure 4.** a) Survey XPS data for CRGO-Ima-Cu<sup>I</sup>, and high resolution data for the b) C 1s, c) N 1s, and d) Cu 2p areas.

A 99% reaction yield was achieved for the CRGO-Ima-Cu<sup>I</sup> catalyst with only 2 mol% catalyst loading in THF, whereas only 30% conversion was obtained for the CNT-Ima-Cu<sup>I</sup> catalyst even after 5 mol% catalyst was employed. The reaction yield was improved up to 60 %, when a little amount of methanol was added (THF/MeOH, 30:1). The observed higher efficiency for CRGO-Ima-Cu<sup>I</sup> might be due to the higher surface area as well as the better dispersibility of the nanoparticles.<sup>[32]</sup> The model reaction was also investigated using commercially available tetrakis (acetonitrile)-copper(I) hexafluorophosphate catalyst, where the click reaction was completed within 24 h (Table 2, entry 2), however catalyst recycling was not possible (Table 2, entry 3). For further analyzing the importance of CNMs immobilized catalysts, the model reaction was carried out using a physical

### III.RESULT AND DISCUSSION

mixture of CRGO and tetrakis (acetonitrile)-copper(I) hexafluorophosphate (1:1) (Table 2, entries 4 and 5), where during recycling a very small amount of click product was obtained, which is presumably due to physical adsorption of catalyst onto the porous structure of CRGO.<sup>[33]</sup> A similar phenomenon was observed for the commercial available imidazolium ligand-based Cu<sup>I</sup> catalyst chloro[1,3-bis(2,4,6 trimethylphenyl)imidazol-2-ylidene]copper(I) (Table 2, entries 6 and 7). Finally heterogeneous copper on charcoal (Cu/C)<sup>[6]</sup> was used, but only a very low conversion towards the click product was obtained (Table 2, entry 8).

Table 2. Performance of different Cu-catalysts: benzylazide (0.0751 mmol) and phenylacetylene (0.0826 mmol) with different reaction conditions.		
Entry	Conditions	Conversion [%]
1	CRGO without copper, in THF, 40 °C, 72 h	0
2	[Cu(CH <sub>3</sub> CN) <sub>4</sub> ]PF <sub>6</sub> (8 mol%) in THF, 40 °C, 24 h	99
3	[Cu(CH <sub>3</sub> CN) <sub>4</sub> ]PF <sub>6</sub> (8 mol%) in THF, 40 °C, 24 h (first cycle)	2
4	CRGO/[Cu(CH <sub>3</sub> CN) <sub>4</sub> ]PF <sub>6</sub> (1:1) (8 mol%) in THF, 40 °C, 24 h	99
5	CRGO/[Cu(CH <sub>3</sub> CN) <sub>4</sub> ]PF <sub>6</sub> (1:1) (8 mol%) in THF, 40 °C, 24 h (first cycle)	10
6	C <sub>21</sub> H <sub>24</sub> ClCuN <sub>2</sub> (8 mol%) in THF, 40 °C, 24 h	99
7	C <sub>21</sub> H <sub>24</sub> ClCuN <sub>2</sub> (8 mol%) in THF, 40 °C, 24 h (first cycle)	3
8	Copper on charcoal (8 mol%), in THF, 40 °C, 72 h	3
9	CRGO-Ima-Cu <sup>I</sup> (2 mol%), in THF, 40 °C, 72 h	99
10	CRGO-Ima-Cu <sup>I</sup> (8 mol%), in THF, 40 °C, 24 h	99
11	Recycled CRGO-Ima-Cu <sup>I</sup> (8 mol%), catalyst in air (first cycle)	97
12	Recycled CRGO-Ima-Cu <sup>I</sup> (8 mol%) catalyst in air (tenth cycle)	91
13	Pristine CNT without copper in THF, 40 °C, 120 h	0
14	CNT-Ima-Cu <sup>I</sup> (2 mol%), in THF, 40 °C, 96 h	30
15	CNT-Ima-Cu <sup>I</sup> (8 mol%), in THF/MeOH (30:1), 40 °C, 24 h	60
16	CNT-Ima-Cu <sup>I</sup> (8 mol%), in THF/MeOH (30:1) (tenth cycle)	45

The recyclability of the catalysts was also studied using the same azide–alkyne click model reaction. After ten repetitions, a slight reduction of the reaction yield was observed (Figure 5), whereas washing and recycling of the catalysts were accomplished under open air environment. Metal leaching for reaction product (after 4, 7, and 10 cycles) was studied by FAAS measurements; however, the detectable amount of Cu was too low for accurate detection. Although the reactivity of CNT-Ima-Cu<sup>I</sup> was lower than that CRGO-Ima-Cu<sup>I</sup>,

the recyclability was similar, supporting the stability and recyclability of the carbene-stabilized CNM-immobilized copper particles.

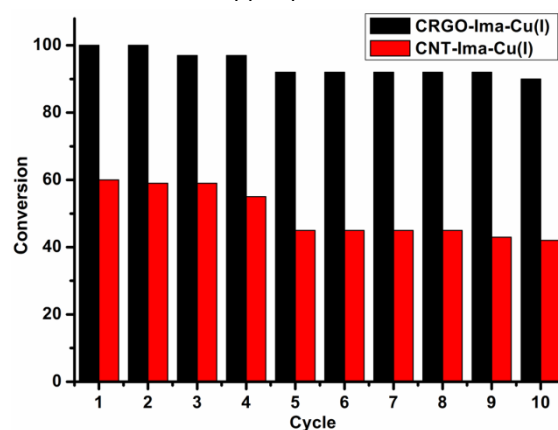


Figure 5. Catalyst recycling within ten reaction cycles for CRGO-Ima-Cu<sup>I</sup> and CNT-Ima-Cu<sup>I</sup> (8 mol% catalyst, benzylazide (0.0751 mmol) and phenyl acetylene (0.0826 mmol)).

$$\text{rate} = k' [\text{alkyne}]^{1.3 \pm 0.2} [\text{azide}]^{1 \pm 0.2} \quad (k' = k[\text{Cu}]^2) \quad (1)$$

For kinetic investigation with 2 mol% of catalyst, <sup>1</sup>H NMR studies have been performed, where aliquots were taken from the reaction at defined intervals and filtered to remove the catalyst. Conversion of the reaction was determined by comparing the resonance of the CH<sub>2</sub> moiety of benzyl azide and the resonance of the CH<sub>2</sub> moiety of the click product (Figure 6).

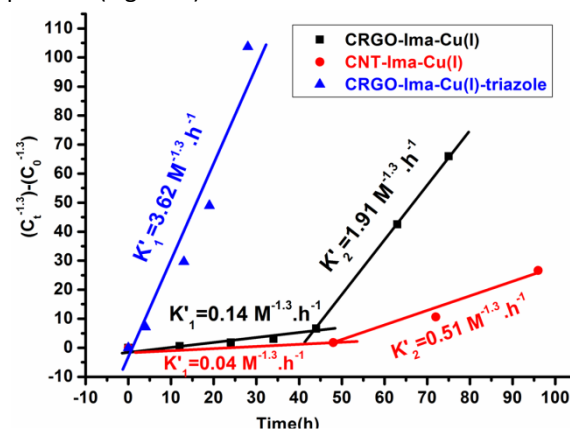
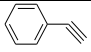
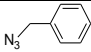
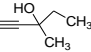
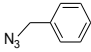
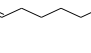
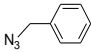
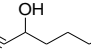
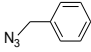


Figure 6. Kinetic study of CRGO-Ima-Cu<sup>I</sup> (black line), CRGO-Ima-Cu<sup>I</sup> with 1-benzyl-4-phenyl-1H-1,2,3-triazole (blue line), and CNT-Ima-Cu<sup>I</sup> (red line). Straight lines are guides for the eyes and are used for estimation of the indicated rate constants.

Equation (1)<sup>[34]</sup> was used for calculation of rate constants  $k'$ . During the kinetic analysis for CRGO Ima-Cu<sup>I</sup>, only 14% conversion was observed after 40 h, where the rate of the reaction increased rapidly afterwards and the reaction was completed within the next 24 h. The same phenomenon was observed for the CNT-Ima-Cu<sup>I</sup> catalyst, however, only 30% conversion was obtained, as discussed earlier. The enhancement of the reaction yield

### III.RESULT AND DISCUSSION

after a certain period of time can be explained by autocatalytic effects caused by the formed triazole moieties, as observed from our earlier investigations<sup>[35]</sup> and those reported by Fokin et al.,<sup>[5]</sup> where it is claimed that the N-ligands of the newly formed triazole act as the source of autocatalysis. To confirm the autocatalytic effect, kinetic measurements were performed by adding 0.7 equiv of 1-benzyl-4-phenyl-1H-1,2,3-triazole (click product) together with the CRGO-Ima-Cu<sup>I</sup> catalyst, observing a higher reaction rate (Figure 6, blue line). The activity of the CRGO-Ima-Cu<sup>I</sup> catalyst was also examined with different alkynes and the catalyst worked well with a sterically hindered alkyne and with alkynes with long alkyl chains (Table 3).

Entry	Alkyne	Azide	Conversion [%]
1			99
2			85
3			99
4			87

[a] Conditions: 2 mol% CRGO-Ima-Cu<sup>I</sup>, 40 °C, 72 h

To evaluate the performance of recycled (after first cycle) catalysts for bulk click chemistry, melt rheology was carried out for three-arm star-shaped azide- and alkyne-functionalized polyisobutylenes (PIBs,  $M_n$  5500  $g\ mol^{-1}$  and 6300  $g\ mol^{-1}$  respectively),<sup>[36]</sup> suitable for cross-linking *via* click chemistry under ambient conditions.<sup>[37]</sup>

For cross-linking experiments an azide-functionalized trivalent PIB and an alkyne-functionalized trivalent PIB were mixed with the prepared catalysts (2 mol% for CRGO-Ima-Cu<sup>I</sup>), and cross-linking was immediately measured on a rheometer plate. Figure 7 shows the rheology result of the click reaction of polymers at 40 °C, where at the beginning of the reaction, the sample clearly possesses liquid like character; the loss modulus is higher than the storage modulus ( $G'' > G'$ ). After some time (1632 min), both moduli increase and a crossover was observed (gel point), indicative of network formation. For CNT-Ima-Cu<sup>I</sup> (5 mol%), even after five days no gel point was observed, however almost 30% conversion was detected *via* FTIR analysis. In contrast in the

experiments with Cu/C and without catalyst, no gel point was observed.

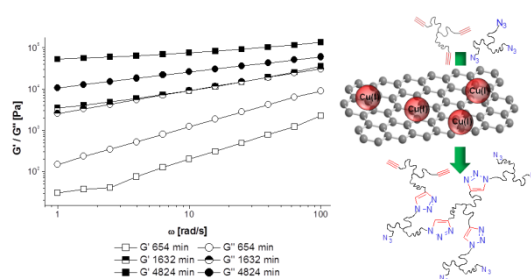


Figure 7. Graphs derived from an *in situ* rheological measurement by reaction of PIB-azide and PIB-alkyne with CRGO-Ima-Cu<sup>I</sup> conjugate at 40 °C.

### Conclusion

We have developed highly dispersible, recyclable, and reusable carbon nanomaterials (graphene/carbon nanotubes) for Cu<sup>I</sup> catalyzed [3+2] cycloaddition click chemistry. The *N*-heterocyclic carbene stabilized copper particles show excellent stability at standard reaction conditions, performed in solution and bulk without adding any external ligand or base. Furthermore, a comparative study between graphene and CNT supported catalyst indicates that the graphene-supported catalyst exhibits a superior catalytic activity in comparison to CNT-supported catalyst, with significantly more than 10 cycles of reuse and only marginal loss of activity, thus significantly exceeding currently known supported Cu catalysts for click reactions. The thus-generated catalysts form the basis for future nanocomposites with inherent restorable properties, where the catalytic activity of the CRGO-Ima-Cu<sup>I</sup> forms the basis for self-healing properties.

### Experimental Section

#### Materials and methods

All chemicals and solvents used for the synthesis of samples were purchased from Sigma–Aldrich and used as received unless otherwise stated. Deuterated tetrahydrofuran ([D<sub>8</sub>]THF, 95%) was purchased from AMAR chemicals and phenyl acetylene from MERCK. Graphite flakes (KFL 99.5, min 20% > 100 μm) were received from Kropfmühl AG. Tetrahydrofuran (THF) was predried over potassium hydroxide for several days, refluxed over sodium/benzophenone and freshly distilled under an argon atmosphere before use. DMF was dried over CaH<sub>2</sub>.

### III.RESULT AND DISCUSSION

TEM: The samples (CRGO-Ima-Cu<sup>I</sup> and CNT-Ima-Cu<sup>I</sup>) were dispersed in *iso*-propanol using a sonicator bath and spread onto a Cu grid coated with a Carbon-film. After 1 *min*, excess liquid was blotted off with filter paper. The dried specimens were examined with an EM 900 transmission electron microscope (Carl Zeiss Microscopy GmbH, Oberkochen, Germany). Micrographs were taken with a SSCCD SM-1k-120 camera (TRS, Moorenweis, Germany).

XRD measurement were performed using a Bruker AXS D8 advanced X-ray diffractometer with Cu<sub>Kα</sub> ( $\lambda = 0.15406 \text{ nm}$ ) radiation in the  $2\theta$  range between 5–80° with a scan rate of 2 ° *min*<sup>-1</sup>.

Raman spectra were obtained at room temperature with a Renishaw inVia spectrometer equipped with a Leica DM2500M confocal microscope using a Cobalt CW DPSS Laser. The Raman scattering was excited using 532 *nm* as excitation wavelength and detected with a CCD camera. Spectra were recorded in the 100–3200 *cm*<sup>-1</sup> Raman shift range.

XPS analysis was performed using a XPS PHI Versa Probe 5000 spectrometer. The pressure in the analysis chamber was typically 1.10<sup>-9</sup> Torr. The XPS measurements were performed using a monochromatic AlK $\alpha$  radiation at 1486.6 eV. A neutralizer with an Ar gun was used during the XPS analysis to compensate charging effects (pass energy: 187.85 eV). The high resolution XPS spectra of each element were recorded with a pass energy of 23.5 eV and an energy step of 0.2 eV.

All NMR spectra were recorded on a Varian spectrometer (Gemini 400) at 400 MHz at 27 °C. [D<sub>8</sub>]THF and [D<sub>6</sub>]DMSO (Armar AG, 99.8 Atom %D) were used as solvents and tetramethylsilane as internal standard. The coupling constants were given in Hz and the chemical shifts in ppm and referred to the solvent residue peak [[D<sub>8</sub>]THF 1.73 and 3.58 ppm and [D<sub>6</sub>]DMSO 2.5 ppm (<sup>1</sup>H)]. For the interpretation of the spectra, MestReNova v. 6.0.2–5475 was used.

Rheological measurements were performed on an oscillatory plate rheometer MCR 501/SN 80753612 from Anton Paar (Physica). For all measurements a PPO8 measuring system (parallel plated, diameter 8 mm) was used. Measurements were performed at 40 °C and the sample temperature was regulated by thermoelectric heating and cooling. For evaluation of data the RheoPlus/32 software (V 3.40) and OriginPro7 was used. For sample

preparation a 1:1 mixture of an azido-functionalized polymer and an alkyne-functionalized polymer was placed in a flask (ca. 50.0 mg) and was dissolved in CHCl<sub>3</sub> (ca. 3.0 mL). The solvent was removed and the sample was dried in high vacuum. CRGO-Ima-Cu<sup>I</sup> catalyst (0.02 equiv per functional group) and CNT-Ima-Cu<sup>I</sup> catalyst (0.05 equiv per functional group) was suspended in CHCl<sub>3</sub> (30 mL) and was added to the polymer mixture. Subsequently, the reaction mixture was mixed with a spatula and was immediately put on the rheometer plate. Measurements were performed with a strain  $\gamma$  of 0.1% and with an angular frequency  $\omega$  ranging from 100 to 1 *rad s*<sup>-1</sup>. A frequency sweep was performed every 10 *min*. The gelation time was determined as crossover of the storage (*G'*) and loss modulus (*G''*) at 10 *rad s*<sup>-1</sup>.

#### Kinetic study

In a 10 mL Schlenk flask, benzyl azide (0.0751 mmol), phenyl acetylene (0.0826 mmol, 1.1 equiv), and the catalyst (CRGO-Ima-Cu<sup>I</sup> (2 mol%, 5.2 mg), CNT-Ima-Cu<sup>I</sup> (5 mol%, 7.4 mg)) were dissolved in 1.5 mL of deuterated THF. Afterwards the mixture was degassed by freeze thaw cycles (2 times). Then the mixture was sonicated (sonicator bath) for some seconds to disperse the catalyst. The reaction was run at 40 °C. Aliquots were taken at intervals from the reaction, filtered to remove the catalyst, and a <sup>1</sup>H NMR study was performed to calculate the conversion of the reaction by the resonance of CH<sub>2</sub> moiety of benzyl azide adjacent to the CH<sub>2</sub> moiety of click product.

#### Recycling experiment

In a 10 mL Schlenk flask, benzyl azide (0.0751 mmol), phenyl acetylene (0.0826 mmol, 1.1 equiv), and the catalyst (CRGO-Ima-Cu<sup>I</sup> (20 mg, 8 mol%), CNT-Ima-Cu<sup>I</sup> (12 mg, 8 mol%)) were dissolved in THF (1.5 mL). Afterwards the mixture was degassed by freeze–thaw cycles (2 times). The mixture was then sonicated (bath sonicator) for few seconds to disperse the catalyst and the reaction was run at 40 °C for 80 h. Afterwards the reaction mixture was filtered and washed by 10–15 mL of THF. The solvent of the filtrate was evaporated under reduced pressure. The catalyst on the filter paper was dried under high vacuum (for 30 *min*) and



### III.RESULT AND DISCUSSION

recycled by washing with THF (2–3 mL). The resulting suspension was used for the same click reaction

#### Catalyst synthesis

**CRGO-Cl**<sup>[24]</sup>: Reduced graphene oxide (CRGO, 200 mg) was dispersed *via* bath sonicator in anhydrous *N,N*-dimethylformamide (DMF, 40–50 mL). 2-chloroethyl isocyanate (10 mmol, 1.055 g) was added to the CRGO suspension in a 100 mL round-bottom flask and the mixture was stirred under nitrogen. After 24 h, the product (CRGO-Cl) was filtered and washed several times with DCM (5×50 mL), and dried under high vacuum.

**CRGO-N<sub>3</sub>**: CRGO-Cl (100 mg) was dispersed by bath sonicator in DMSO (40–50 mL) in a 50 mL round bottom flask. Afterwards sodium azide (12 mmol, 780 mg) was added, and then the mixture was stirred for 48 h at 50 °C. The product was filtered and washed several times with water (5×50 mL) and DCM (5×50 mL) and dried under high vacuum.

**CRGO-Ima**: CRGO-N<sub>3</sub> (50 mg) was dispersed by bath sonicator into a mixture of H<sub>2</sub>O/*t*BuOH (2:1, 3 mL). 1-Propagyl-3-methylimidazolium bromide (0.5 mmol, 100 mg), sodium ascorbate (0.16 mmol, 30 mg), and CuSO<sub>4</sub> (0.07 mmol, 10 mg) were added to the solution, which was then stirred at room temperature for 3 days. Afterwards, the mixture was filtered and washed with water (5×50 mL) and DCM (5×50 mL). Finally it dried under high vacuum.

**CRGO-Ima-Cu<sup>I</sup>**: CRGO-Ima (70 mg), tetrakis (acetonitrile) copper (I) hexafluorophosphate (0.53 mmol, 196 mg), and K<sub>t</sub>BuO (0.53 mmol, 59 mg) was added to a 10 mL Schlenk flask and degassed by vacuum and nitrogen. Afterwards a mixture of anhydrous THF/ DMF (1:1, 3 mL) was added to the mixture and it was dispersed by sonicator bath. The mixture was stirred at room temperature for 48 h. For workup procedure the reaction mixture was washed three times by DMF (3×50 mL), H<sub>2</sub>O (3×50 mL), THF (3×50 mL), and ammonium chloride (NH<sub>4</sub>Cl) solution (50 mL) (all solvents were degassed by nitrogen for 15 min before use), and the product was separated by centrifugation ( 10 min, 5000 rpm) and dried under high vacuum.

#### Different click reactions

In a 10 mL Schlenk flask, benzyl azide (0.0751 mmol), alkyne (0.0826 mmol, 1.1 eq), and CRGO-

Ima-Cu<sup>I</sup> (5.2 mg, 2 mol%) were dissolved in 1.5 mL of deuterated THF. Afterwards the mixture was degassed by freeze–thaw cycles (two times). Then the mixture was sonicated (sonicator bath) for some seconds to disperse the catalyst. The reaction was run at 40 °C for 80 h. Afterwards the reaction mixture was filtered and the <sup>1</sup>H NMR spectra of filtrate showed the conversion of the reaction by the resonance of CH<sub>2</sub> moiety of benzyl azide in comparison to the CH<sub>2</sub> moiety of click product.

**1-Benzyl-4-phenyl-1H-1,2,3-triazole**: <sup>1</sup>H NMR (400 MHz, [D<sub>8</sub>]THF): d=5.81 (s, 2H), 7.39–7.21 (m, 7H), 7.82 (m, 2H), 8.08 ppm (s, 1H).

**1-Benzyl-4-(4-chlorobutyl)-1H-1,2,3-triazole**: <sup>1</sup>H NMR (400 MHz, [D<sub>8</sub>]THF):d=1.84–1.74 (m, 4H), 2.67 (t, J=6.87, 6.87 Hz, 2H), 3.56 (t, J=9.10, 9.10 Hz, 2H), 5.49 (s, 2H), 7.39–7.21 (m, 5H), 7.49 ppm (s, 1H); <sup>13</sup>C NMR (101 MHz, [D<sub>8</sub>]THF):d=25.81, 27.75, 33.32, 45.49, 54.18, 121.68, 128.80, 128.98, 129.66, 137.61, 148.32 ppm.

**2-(1-Benzyl-1H-1,2,3-triazol-4-yl)butan-2-ol**: <sup>1</sup>H NMR (400 MHz, [D<sub>8</sub>]THF): d=0.78 (t, J=7.43, 7.43 Hz, 3H), 1.46 (s, 3H), 1.88–1.74 (m, 2H), 3.97 (s, 1H), 5.50 (s, 2H), 7.42–7.19 (m, 5H), 7.55 ppm (s, 1H); <sup>13</sup>C NMR (101 MHz, [D<sub>8</sub>]THF): d=8.75, 29.15, 30.8, 36.95, 54.19, 121.07, 128.86, 128.97, 129.66, 137.83, 156.84 ppm.

**1-(1-Benzyl-1H-1,2,3-triazol-4-yl)pentan-1-ol**: <sup>1</sup>H NMR (400 MHz, [D<sub>8</sub>]THF): d=0.89 (t, J=7.12, 7.12 Hz, 3H), 1.37 (m 4H), 1.79 (m, 2H), 4.23 (s, 1H), 4.70 (s, 1H), 5.50 (s, 2H), 7.46–7.18 (m, 5H), 7.59 ppm (s, 1H); <sup>13</sup>C NMR (101 MHz, [D<sub>8</sub>]THF): d=14.65, 23.72, 28.8, 38.69, 54.25, 121.29, 128.9, 129, 129.59, 137.59, 154.31 ppm.

#### Acknowledgements

This project has received funding from the European Union's Seventh Framework Program for research, technological development and demonstration under grant agreement no. 313978 as well as the grant DFG-BI 1337/8–1 and DFG-BI 1337/ 8-2 within the SPP 1568 ("Design and Generic Principles of Self Healing Materials") and the SFB TRR 102 (project A3).

Keywords: carbon nanotubes · click chemistry · copper nanoparticles · graphene · heterogeneous catalysis

[1] a) H. C. Kolb, M. G. Finn, K. B. Sharpless, Angew. Chem. Int. Ed. 2001, 40, 2004; Angew. Chem. 2001, 113, 2056; b) M. T.

### III.RESULT AND DISCUSSION

- Meldal, C. W. Tornøe, in Proceedings of the Second International and the Seventeenth American Peptide Symposium, American Peptide Society, San Diego, 2001, pp. 263; c) C. W. Tornøe, C. Christensen, M. Meldal, *J. Org. Chem.* 2002, 67, 3057.
- [2] a) V. V. Rostovtsev, L. G. Green, V. V. Fokin, K. B. Sharpless, *Angew. Chem. Int. Ed.* 2002, 41, 2596; *Angew. Chem.* 2002, 114, 2708; b) W. H. Binder, R. Sachsenhofer, *Macromol. Rapid Commun.* 2007, 28, 15; c) W. H. Binder, R. Zirbs in *Encyclopedia of Polymer Science and Technology*, Wiley, 2014, 3, 186; d) W. H. Binder, R. Sachsenhofer, *Macromol. Rapid Commun.* 2008, 29, 952.
- [3] R. K. Iha, K. L. Wooley, A. M. Nyström, D. J. Burke, M. J. Kade, C. J. Hawker, *Chem. Rev.* 2009, 109, 5620.
- [4] C. Deraedt, N. Pinaud, D. Astruc, *J. Am. Chem. Soc.* 2014, 136, 12092.
- [5] T. R. Chan, R. Hilgraf, K. B. Sharpless, V. V. Fokin, *Org. Lett.* 2004, 6, 2853.
- [6] B. H. Lipshutz, B. R. Taft, *Angew. Chem.* 2006, 118, 8415.
- [7] M. Chtchigrovsky, A. Primo, P. Gonzalez, K. Molvinger, M. Robitzer, F. Quignard, F. Taran, *Angew. Chem. Int. Ed.* 2009, 48, 5916; *Angew. Chem.* 2009, 121, 6030.
- [8] C. Girard, E. Önen, M. Aafort, S. Beauviere, E. Samson, J. Herscovici, *Org. Lett.* 2006, 8, 1689.
- [9] L. Bonami, W. Van Camp, D. Van Rijckegem, F. E. Du Prez, *Macromol. Rapid Commun.* 2009, 30, 34.
- [10] a) S. Sarkar, M. L. Moser, X. Tian, X. Zhang, Y. F. Al-Hadeethi, R. C. Haddon, *Chem. Mater.* 2014, 26, 184; b) X. Gu, W. Qi, W. X. Xu, Z. Sun, L. Zhang, W. Liu, X. Pan, D. Su, *Nanoscale* 2014, 6, 6609; c) G. M. Scheuermann, L. Rumi, P. Steurer, W. Bannwarth, R. Mülhaupt, *J. Am. Chem. Soc.* 2009, 131, 8262.
- [11] S. Iijima, *Nature* 1991, 354, 56.
- [12] K. S. Novoselov, A. K. Geim, S. V. Morozov, D. Jiang, Y. Zhang, S. V. Dubonos, S. V. Grigorieva, A. A. Firsov, *Science*, 2004, 306, 666.
- [13] a) X. Huang, X. Qi, F. Boey, H. Zhang, *Chem. Soc. Rev.* 2012, 41, 666; b) J. Bartelmess, B. Ballesteros, G. de La Torre, D. Kiessling, S. Campidelli, M. Prato, T. Torres, D. M. Guldi, *J. Am. Chem. Soc.* 2010, 132, 16202; c) A.-K. Appel, R. Thomann, R. Mülhaupt, *Macromol. Rapid Commun.* 2013, 34, 1249.
- [14] H. Sharghi, M. H. Beyzavi, A. Safavi, M. M. Doroodmand, R. Khalifeh, *Adv. Synth. Catal.* 2009, 351, 2391.
- [15] a) J. Zhang, Y. Cheng, S. Lu, L. Jia, P. K. Shen, S. P. Jiang, *Chem. Commun.* 2014, 50, 13732; b) W. Chen, X. Pan, X. Bao, *J. Am. Chem. Soc.* 2007, 129, 7421; c) R. M. M. Abbaslou, J. Soltan, A. K. Dalai, *Appl. Catal. A* 2010, 379, 129.
- [16] a) S. Yang, R. E. Bachman, X. Feng, K. Müllen, *Acc. Chem. Res.* 2013, 46, 116; b) S. Eigler, S. Grimm, F. Hof, A. Hirsch, *J. Mater. Chem. A* 2013, 1, 11559; c) S. Eigler, A. Hirsch, *Angew. Chem. Int. Ed.* 2014, 53, 7720; *Angew. Chem.* 2014, 126, 7852.
- [17] a) D. Konatham, A. Striolo, *Nano Lett.* 2008, 8, 4630; b) G. R. Kasaliwal, S. Pegel, A. Gödel, P. Pötschke, G. Heinrich, *Polymer* 2010, 51, 2708.
- [18] a) V. Georgakilas, M. Otyepka, A. B. Bourlinos, V. Chandra, N. Kim, K. C. Kemp, P. Hobza, R. Zboril, K. S. Kim, *Chem. Rev.* 2012, 112, 6156; b) N. G. Sahoo, S. Rana, J. W. Cho, L. Li, S. H. Chan, *Prog. Polym. Sci.* 2010, 35, 837.
- [19] a) W. Osim, A. Stojanovic, J. Akbarzadeh, H. Peterlik, W. H. Binder, *Chem. Commun.* 2013, 49, 9311; b) A. P. Saxena, M. Deepa, A. G. Joshi, S. Bhandari, A. K. Srivastava, *ACS Appl. Mater. Interfaces* 2011, 3, 1115; c) P. Tamilarasan, S. Ramaprabhu, *J. Mater. Chem. A* 2014, 2, 14054; d) B. Kerscher, A. K. Appel, R. Thomann, R. Mülhaupt, *Macromolecules* 2013, 46, 4395.
- [20] C. Su, K. P. Loh, *Acc. Chem. Res.* 2013, 46, 2275.
- [21] a) D. Wang, K. Wurst, M. R. Buchmeiser, *Chem. Eur. J.* 2010, 16, 12928; b) J. D. Egbert, C. S. J. Cazin, S. P. Nolan, *Catal. Sci. Technol.* 2013, 3, 912.
- [22] W. S. Hummers, R. E. Offeman, *J. Am. Chem. Soc.* 1958, 80, 1339.
- [23] M. J. Fernandez-Merino, L. Guardia, J. I. Paredes, S. Villar-Rodil, A. Sol.-Fernandez, n.-A. A, J. M. D. Tascon, *J. Phys. Chem. C* 2010, 114, 6426.
- [24] Z. Wang, Z. Ge, X. Zheng, N. Chen, C. Peng, C. Fan, Q. Huang, *Nanoscale* 2012, 4, 394.
- [25] P. Zare, A. Stojanovic, F. Herbst, J. Akbarzadeh, H. Peterlik, W. H. Binder, *Macromolecules* 2012, 45, 2074.
- [26] M. Kim, C. K. Hong, S. Choe, S. E. Shim, *J. Polym. Sci. Part A* 2007, 45, 4413.
- [27] T. Kim, H. Lee, J. Kim, K. S. Suh, *ACS Nano* 2010, 4, 1612.
- [28] a) Y. T. Shieh, H. F. Jiang, *J. Electroanal. Chem.* 2015, 736, 132; b) Y. Fan, L. Wang, J. Li, J. Li, S. Sun, F. Chen, L. Chen, W. Jiang, *Carbon* 2010, 48, 1743.
- [29] M. Saif, K. Flower, *Transition Met. Chem.* 2013, 38, 113.
- [30] M. Castelain, G. Martinez, P. Merino, J. A. Martin-Gago, J. L. Segura, G. Ellis, H. J. Salavagione, *Chem. Eur. J.* 2012, 18, 4965.
- [31] H. Yang, C. Shan, F. Li, D. Han, Q. Zhang, L. Niu, *Chem. Commun.* 2009, 3880.
- [32] H. Peng, Z. Mo, S. Liao, H. Liang, L. Yang, F. Luo, H. Song, Y. Zhong, B. Zhang, *Sci. Rep.* 2013, 3, 1765.
- [33] B. F. Machado, P. Serp, *Catal. Sci. Technol.* 2012, 2, 54.
- [34] V. O. Rodionov, V. V. Fokin, M. G. Finn, *Angew. Chem.* 2005, 117, 2250.
- [35] a) D. Döhler, P. Michael, W. H. Binder, *Macromolecules* 2012, 45, 3335; b) M. Schunack, M. Gragert, D. Döhler, P. Michael, W. H. Binder, *Macromol. Chem. Phys.* 2012, 213, 205.
- [36] F. Herbst, S. Seiffert, W. H. Binder, *Polym. Chem.* 2012, 3, 3084.
- [37] D. Döhler, P. Zare, W. H. Binder, *Polym. Chem.* 2014, 5, 99

## Supporting information

### 1. Synthesis

#### 1.1. Synthesis of graphene oxide (GO)

Graphite (3 g) was stirred in concentrated sulfuric acid (117 mL) at room temperature (RT), and sodium nitrate (1.5 g) was added. The mixture was cooled to 0 °C and potassium permanganate (9 g) was added during 30 min to 1 h in order to avoid the increasing in internal temperature of the reaction mixture. After 2 h, the green slurry was allowed to come to RT, and after being stirred for 3 h (during this time the viscosity of the mixture increased) the whole batch was carefully poured into a 700 mL beaker filled with ice-cold distilled water. Subsequently, hydrogen peroxide (3%) was added in excess and the mixture was stirred overnight and then filtered. Workup was accomplished by several washings with a mixture of HCl/H<sub>2</sub>O<sub>2</sub> (1:1, 5%) and filtration followed by several washings with water and centrifugation until the supernatant did not show anymore precipitation with AgNO<sub>3</sub> solution. The obtained GO was carefully powdered in a ball mill, with pre-cooling by liquid nitrogen. (For more detail see Appendix 2.3.1)

#### 1.2. Synthesis of chemically reduced graphene oxide (CRGO)

GO powders were chemically reduced using ascorbic acid as reducing agent to obtain chemically reduced graphene oxide (CRGO). 0.5 g of GO were placed in a 200 mL three-neck flask and then 50 mL of de-ionized water were added, till GO powders in water were completely dispersed. 0.5 g of ascorbic acid was added to the GO dispersion and the mixture was allowed to react under agitation at 100 °C for 24 h. The CRGO powders slowly precipitated as a black solid. This product was centrifugated, washed with de-ionized water and finally dried at 60 °C for 24 h in an oven. (For more detail see Appendix 2.3.2)

##### 1.2.1. Titration of hydroxyl group of CRGO (CRGO-Phi)<sup>[1]</sup>

In a 10 mL one-necked flask, CRGO (150 mg) was dispersed in 3 mL of dry toluene using bath sonicator. Afterwards phenyl isocyanate (1.5 mL) was added, and the reaction was run for 3 days at 50 °C. After completion of the reaction, the reaction mixture was washed several times with chloroform (2×200 mL), and dried in high vacuum at 100 °C. TGA data shows a mass loss of about 6 wt%, which is related to phenyl isocyanate groups reacted with hydroxyl groups of CRGO. The data supports the presence of hydroxyl groups on CRGO ( $5 \times 10^{-4}$  mmol/mg).

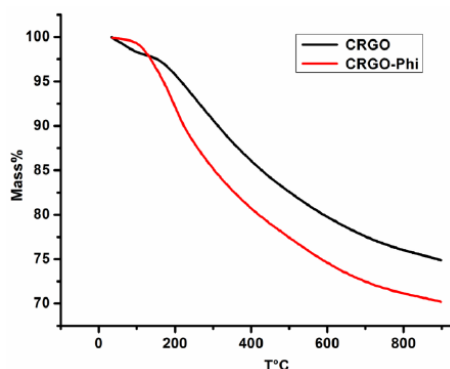


Figure S1-TGA spectrum to analyze the titration of CRGO with phenyl isocyanate.



### 1.3 Synthesis of azide functionalized CNTs

For this purpose commercially available multi-wall carbon nanotubes Nanocyl™ CN3100 (Thin MWNT 95+% C purity) have been used. First hydroxyl groups modified CNTs were prepared, where MWNTs (200 mg) and 100 mL DCM were added into a 250 mL flask, and the mixture was dispersed by ultrasonication (bath sonicator) for 15 min in the flask. Tetrabutylammonium bromide (TBABr) (1 g) being dissolved in 10 mL H<sub>2</sub>O, 10 mL acetic acid, and KMnO<sub>4</sub> solution (0.25 g KMnO<sub>4</sub> dissolved in 5 mL H<sub>2</sub>O) were added in the flask. The mixture was stirred vigorously at 25 °C for 24 h. The mixture was washed with HCl and filtered with methanol through Teflon Filter. The methanol washing step was repeated at least four times. After vacuum drying the filtrate, 180 mg hydroxyl group functionalized CNTs (CNTs-OH) were achieved. In order to obtain azide functionalization, CNTs bearing OH groups on their surface are used. CNT-OH (50 mg) was placed in a 50 mL round-bottom flask in 15 mL of anhydrous *N,N*-dimethylformamide (DMF). After dispersion, 2-chloroethyl isocyanate (0.85 g, 2 mmol) was added in order to form the desired product by in situ generation of the diazonium salt. After completeness of reaction, the obtained CNT-Cl was then filtered, washed with DMF until the liquid filtrate was colourless and dried under vacuum. The azide group was introduced on the CNT-Cl sheets *via* nucleophile substitution reaction of alkyl halide with sodium azide in DMSO. The final product (CNT azide, CNT-N<sub>3</sub>) was obtained after filtration as a black powder and dried under vacuum.

### 1.4 Synthesis of Cu (I) catalyst immobilized CNTs (CNT-Ima-Cu (I))

Azide functional groups decorated MWNTs (50 mg) were dispersed in a mixture of H<sub>2</sub>O/ tBuOH (2:1, total 30 mL) by water bath sonication. 1-propargyl-3-methylimidazole bromide (100 mg), CuSO<sub>4</sub> (10 mg), sodium ascorbate (30 mg), were added to the solution, which was then stirred at 50 °C temperature for 60 h. After completion the reaction, the mixture was filtered using PTFE membrane, and washed several times with water and CH<sub>2</sub>Cl<sub>2</sub>, obtained CNT-Ima. The synthesized CNT-Ima (50 mg) was further added to a 20 mL schlenk flask containing the solvent (DMF/THF, 1:1, total 10 mL) and degassed by nitrogen. Tetrakis (acetonitrile) copper (I) hexafluorophosphate was added in excess to the mixture and the mixture was stirred at room temperature over night. For workup procedure the reaction mixture was washed 5-6 times by dry DMF, THF and ammonium chloride solution (NH<sub>4</sub>Cl).

## 2. Characterization

### 2.1 effect of different reaction conditions for the preparation of imidazolium bromide modified CRGO

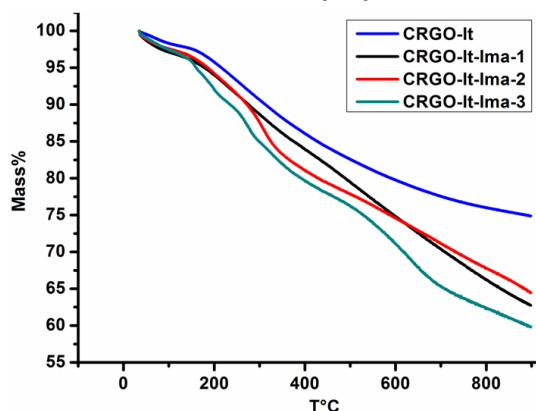


**Figure S2**-TGA spectrum to analyse the effect of different reaction conditions for the preparation of imidazolium bromide modified CRGO (CRGO-Ima)

**Table S1.** TGA analysis of different click reaction condition between CRGO-N<sub>3</sub> and 1-Propagyl-3-methylimidazolium bromide

Entry	Click reaction condition	Compound	TGA (mass%)	Loading (mmol.mg <sup>-1</sup> )
1	-----	CRGO	20.94	-----
2	THF/H <sub>2</sub> O/Cu(PPh <sub>3</sub> ) <sub>3</sub> Br/TBTA	CRGO-Ima-1	31.32	3.144×10 <sup>-4</sup>
3	H <sub>2</sub> O/ <sup>t</sup> BuOH/Cu(PPh <sub>3</sub> ) <sub>3</sub> Br/TBTA	CRGO-Ima-2	29.75	2.6684×10 <sup>-4</sup>
4	H <sub>2</sub> O/ <sup>t</sup> BuOH/CuSO <sub>4</sub> , sodium ascorbate	CRGO-Ima-3	32.24	3.429×10 <sup>-4</sup>

## 2.2-Analysis of imidazolium bromide modified CNT (CNT-Ima) (TGA, Raman and dispersibility)

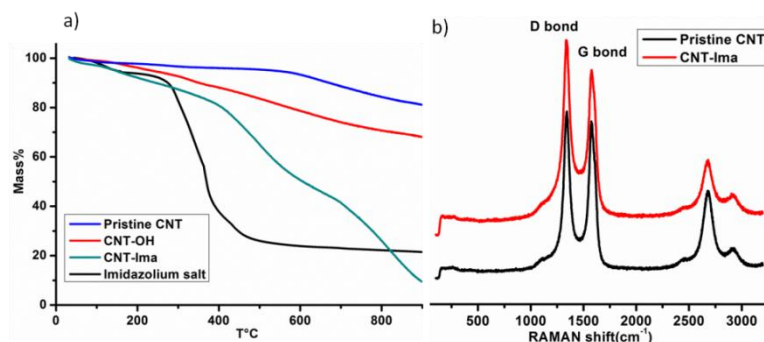


**Figure S3- a)** TGA analysis of imidazolium bromide modified CNT (CNT-Ima) **b)** Raman spectrum of pristine and imidazolium bromide modified CNT

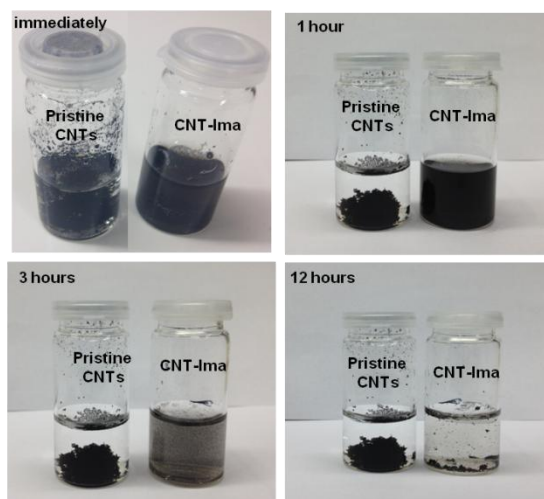


**Figure S4-** Dispersion of pristine and modified CNTs in water

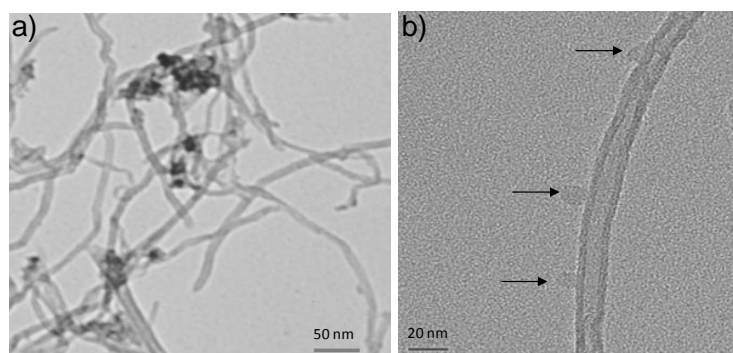


**Figure S5-** TEM images of modified CNTs (CNT-Ima-Cu(I)); a) before washing with ammonium chloride, and b) after washing with ammonium chloride

### III.RESULT AND DISCUSSION

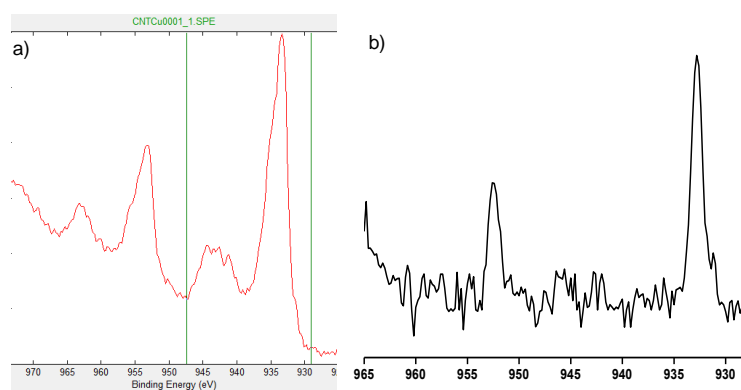


**Figure S6-** XPS analysis of modified CNTs (CNT-Ima-Cu(I)); a) before washing with ammonium chloride, b) after washing with ammonium chloride

### 2.3. $^1\text{H}$ NMR Spectra of click products obtained in CuAAC using CRGO-Ima-Cu(I) as catalyst

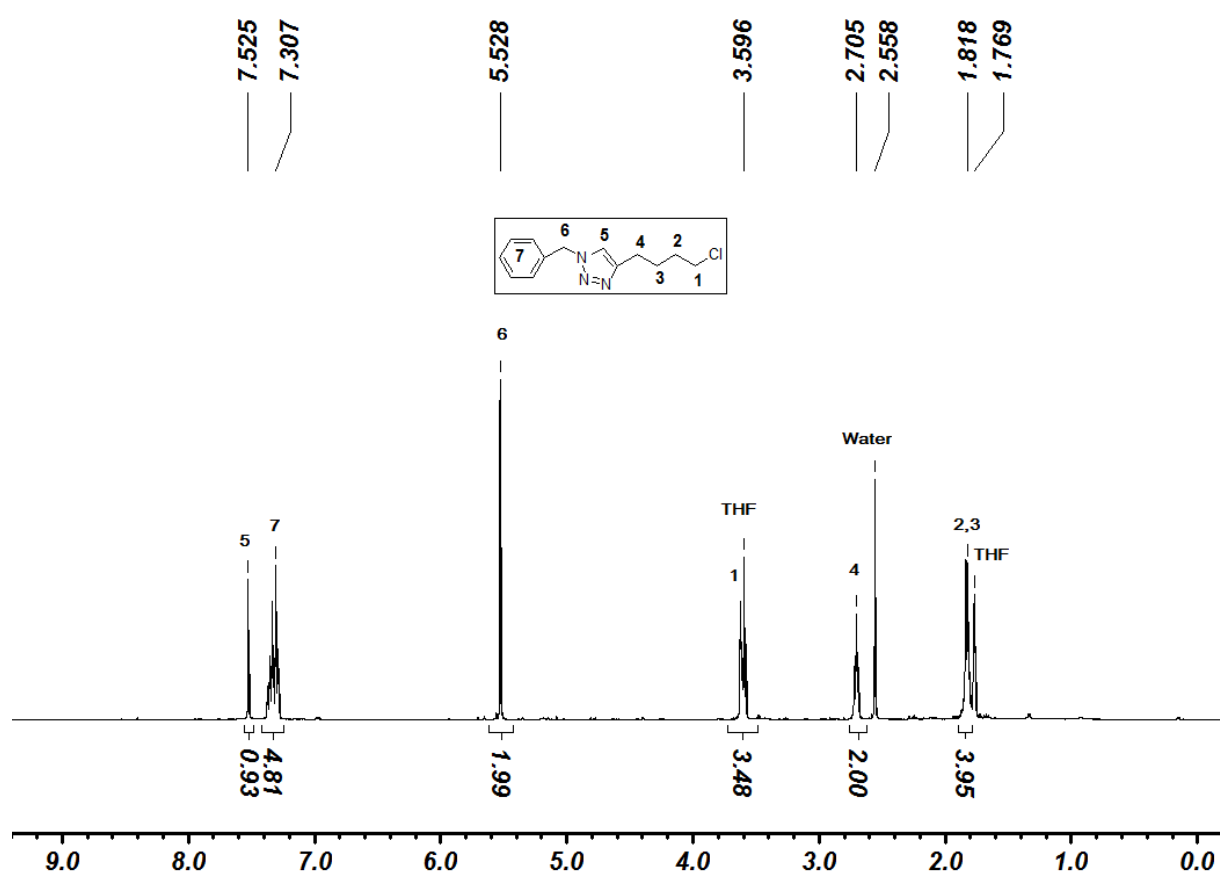


**Figure S7-**  $^1\text{H}$  NMR spectra of 1-benzyl-4-(4-chlorobutyl)-1H-1,2,3-triazole

### III.RESULT AND DISCUSSION

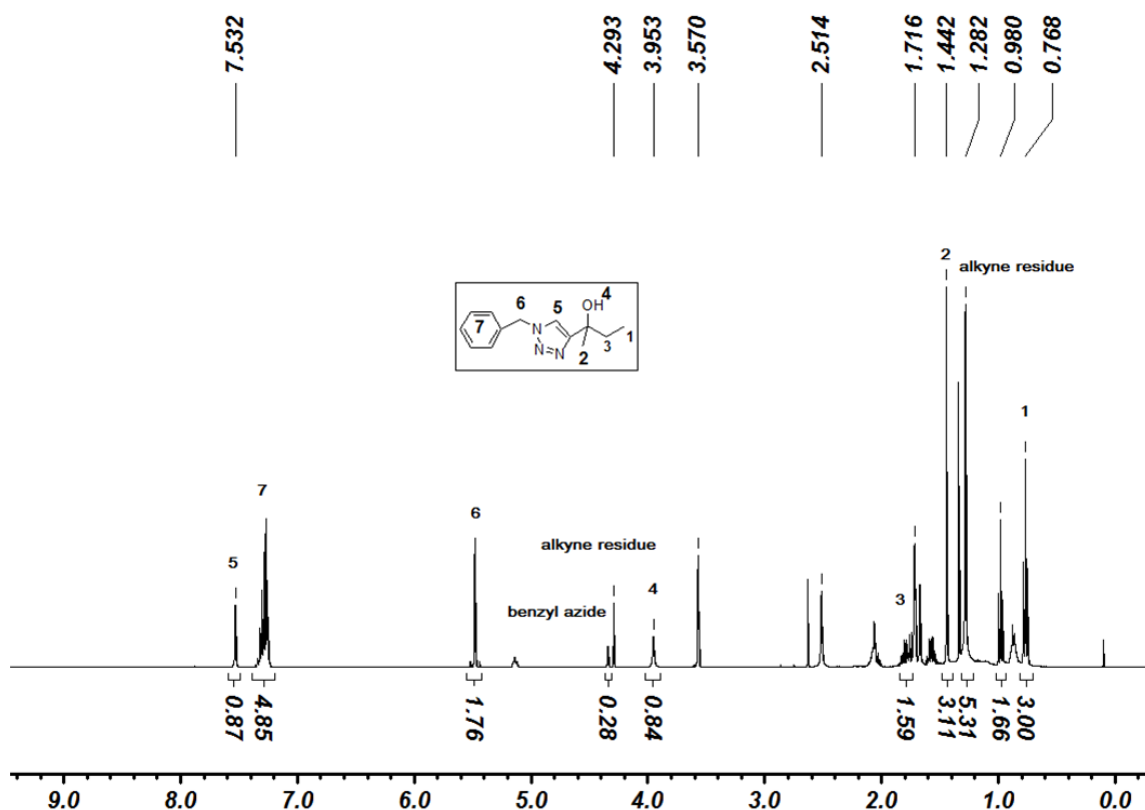


Figure S8-  $^1\text{H}$  NMR spectra of 2-(1-benzyl-1H-1,2,3-triazol-4-yl)butan-2-ol

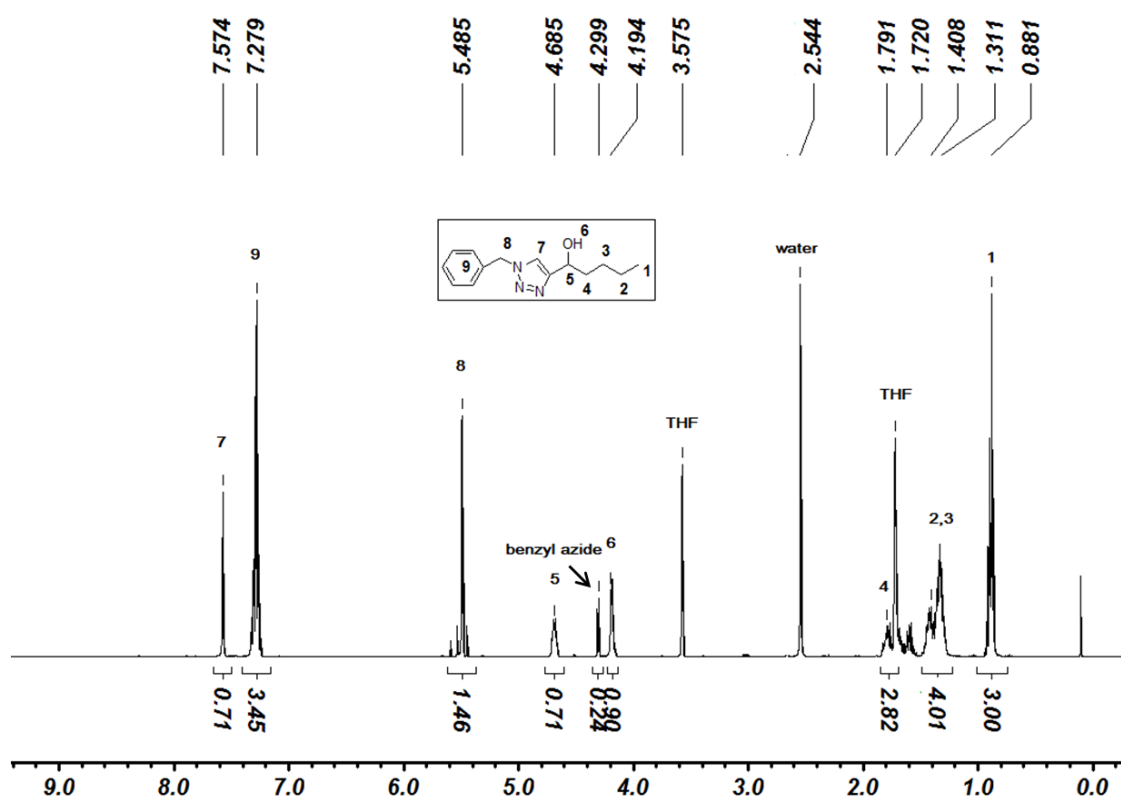
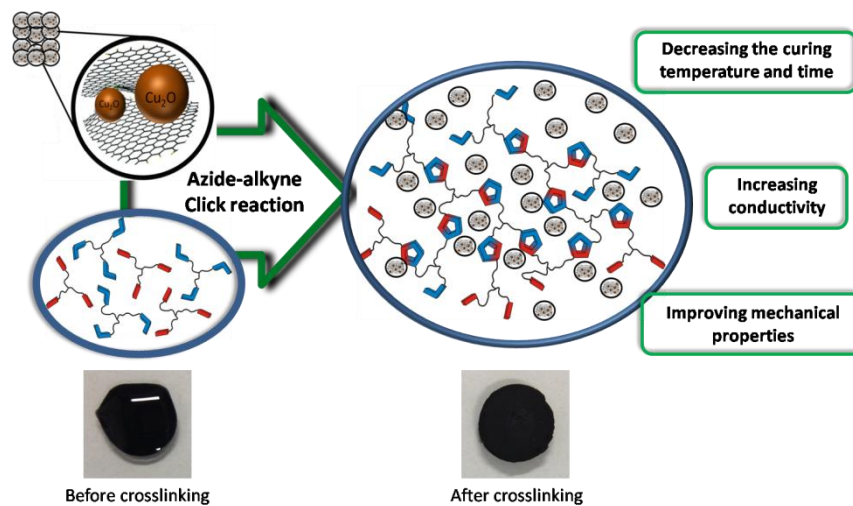


Figure S9-  $^1\text{H}$  NMR spectra of 1-(1-benzyl-1H-1,2,3-triazol-4-yl)pentan-1-ol

[1] A.-K. Appel, R. Thomann, R. Mülhaupt, *Polymer* **2012**, *53*, 4931.

### 3-Nanocomposites *via* a direct graphene-promoted “click”-reaction



#### Abstract

The generation of graphene nanocomposites by curing of a new resin material *via* the Cu(I) catalyzed azide-alkyne click reaction (CuAAC) has been investigated by using graphene supported copper nanoparticles (TRGO-Cu<sub>2</sub>O) as catalyst directly embedded into the curing resin. Low molecular weight trivalent azide and alkyne were used as resin-components for “click” crosslinking by graphene supported copper nanoparticles (TRGO-Cu<sub>2</sub>O) in comparison to different commercially available homo- and heterogeneous copper catalysts. The kinetics of the crosslinking process were investigated by differential scanning calorimetry (DSC) and melt rheology, proving the superior performance of the (TRGO-Cu<sub>2</sub>O). Additionally the physical and mechanical properties of the finally cured resins were studied *via* melt rheology, broadband dielectric spectroscopy (BDS) and thermogravimetric analysis (TGA), proving the outstanding catalytic activity of the TRGO-Cu<sub>2</sub>O catalyst performing “click” crosslinking without addition of base or oxidizing/reducing agents. Along with its catalytic performance, TRGO-Cu<sub>2</sub>O acts as reinforcing filler, significantly improving the mechanical and physical properties, as well as the conductivity and the thermal stability of the final resin material.

#### 1. Introduction

Graphene, a single layer of two-dimensional sp<sup>2</sup>-hybridized carbon has attracted significant research interest due to its unique electrical [1] and thermal conductivity [2], including exceptional mechanical [3], optical [4] and chemical properties [5]. The advantages of graphene in various fields of science reflect use of this material in numerous innovative and prolific scientific works around the globe, as its honey comb structure is considered to be even more promising than 1-dimensional nanotubes and 0-dimensional fullerenes towards potential applications such as memory devices [6], energy storage [7], solar cells [7], fuel cells [8], and heterogeneous catalysis [9,10]. In contrast to single layer graphene sheets which are usually prepared by mechanical exfoliation, graphene oxide (GO)-

[11,12] and reduced graphene oxide (rGO) are easily available by controlled chemical reactions and can be produced in a larger scale. Furthermore, they demonstrate promising properties as catalyst supporting material for the preparation of heterogeneous catalysts [13], as well as a filler towards preparing polymer based resin/composite materials [14,15].

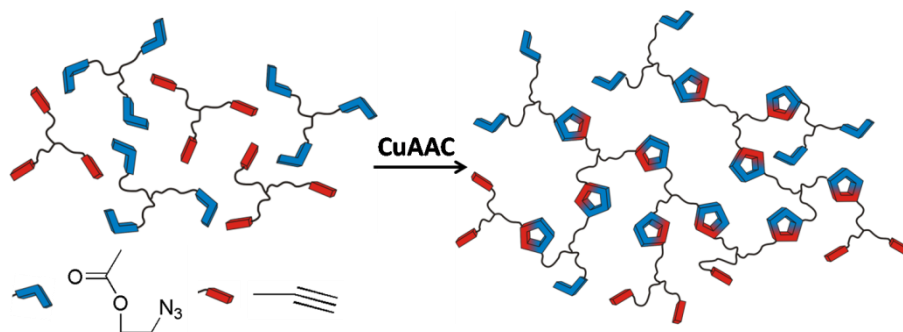
Resins are important thermosetting polymers typically used in the production of composites for high performance applications like aerospace [16], automotive [17], and marine industry [18], therefore placing the final physical and mechanical properties of these materials in the limelight of interest. To improve the mechanical and physical properties, fiber reinforced materials like fiberglass, Kevlar® and carbon materials have been incorporated during the curing process [19]. Thus

## III.RESULT AND DISCUSSION

in turn curing kinetics is one of the main criteria influencing the processing time and the final physical properties of the resins, especially in e.g. Resin Transfer Molding (RTM) processes [16,20]. In many cases curing proceeds under harsh conditions in the autoclave using high temperature and pressure [21]. Therefore, reducing the reaction time and temperature is one of the key challenges in industry to trim down the cost of production. Kessler et al. [22] reported low temperature curing of dicyclopentadiene *via* ring-opening metathesis polymerization (ROMP) using Grubbs catalysts, and investigated the kinetics of the curing reaction *via* differential scanning calorimetry (DSC). However, high cost and stability issues of the required Grubbs catalysts limit the utilization of ROMP based resin curing. Another approach to reduce the cost of the curing process was to use highly efficient Cu(I) catalyzed azide-alkyne click reactions (CuAAC) [23-27] which lead to high yields of the product within short reaction times at low temperature. The kinetics of the Cu(I) catalyzed bulk click polymerization reaction and the effect of different catalysts was briefly studied earlier [28,29], furthermore the crosslinking and curing of multivalent azide and alkyne moieties *via* copper free azide-alkyne click reaction conducted at elevated temperatures has been discussed earlier [30-33], however investigations on the kinetics of bulk Cu(I) catalyzed click crosslinking is rare. Nanofillers which can act as a curing catalyst while being useful to enhance the conducting and mechanical properties may be very advantageous in the production of resin materials.

attractive as support for heterogeneous catalysts [34,35]. Recently our group [36] reported the synthesis of thermally reduced graphene oxide supported copper nanoparticles (TRGO-Cu<sub>2</sub>O), a catalyst which enables a CuAAC at low temperatures in solution and in bulk without the addition of any base or oxidizing/reducing agent. Thus, the synthesized catalyst (TRGO-Cu<sub>2</sub>O) can reduce the required curing time and temperature, while being helpful to improve the mechanical and physical properties, including conductivity and the thermal stability of the final resin material.

Herein, we report on the kinetics of the bulk click crosslinking of trivalent azide and alkyne compounds using TRGO-Cu<sub>2</sub>O as catalyst (see Scheme 1). Mechanistically, for the formation of a covalent network, sufficient molecular mobility is required. In order to keep diffusion high, liquid components based on trivalent azide and alkyne with high mobility (low molecular weights) were prepared, in turn investigating the kinetics of the CuAAC crosslinking reaction by *in-situ*-DSC and *in-situ* melt-rheology measurements. Broadband dielectric spectroscopy (BDS) was conducted to determine the conductivity of the final resin materials systematically investigating the influence of the added TRGO-Cu<sub>2</sub>O. Finally, to assess the thermal stability of the resulting resin materials, thermogravimetric analysis (TGA) was performed. In addition, the crosslinking kinetics, including the physical properties for the resin materials were also investigated using different commercially available homogeneous (Cu(PPh<sub>3</sub>)<sub>3</sub>Br and Cu(PPh<sub>3</sub>)<sub>3</sub>F) and heterogeneous (Cu/C) [37] copper-



**Scheme 1.** Cu(I) catalyzed azide-alkyne bulk click reaction for a low temperature curing system

On account of their large surface area, and unique interactions with metal particles, graphene nanosheets supported catalysts have represented outstanding catalytic activity compared to other carbon supported catalysts making them extremely

catalysts. The obtained results demonstrate a higher catalytic activity of TRGO-Cu<sub>2</sub>O compared to commercially available catalysts, along with the proven activity, it acts as a reinforcing filler for the-



### III. RESULT AND DISCUSSION

preparation of high performance composites with enhanced conductivity and mechanical properties.

## 2. Experimental

### 2.1. Materials

All used chemicals and solvents, were purchased from Sigma-Aldrich and were used as received unless otherwise stated. Tetrahydrofuran (THF) was predried over potassium hydroxide for several days, refluxed over sodium/benzophenone and freshly distilled under an argon atmosphere before use. *N,N'* dimethylformamide (DMF) was dried over  $\text{CaH}_2$  and freshly distilled under argon atmosphere before use.

### 2.2. Instrumentation

#### 2.2.1. Differential scanning calorimetry (DSC)

DSC measurements were performed on a differential scanning calorimeter 204F1/ASC Phoenix from Netzsch. Crucibles and lids made of aluminum were used. Measurements were performed in a temperature range from  $-20$  to  $250$  °C using heating rates of 5, 10, 15 and 20 *K/min*. As purge gas a flow of dry nitrogen (20 *mL/min*) was used for all experiments. For evaluation of data the Proteus Thermal Analysis Software (Version 5.2.1) and OriginPro7 was used. For sample preparation a 1:1 mixture (molar ratio) of the triazide compound (1) and the trialkyne compound (2) was placed in a flask (50 mg) and the catalyst (1-2 *mol%* per functional group) was added to the mixture which was mixed with a spatula and immediately put in a crucible and closed with a pinhole pricked lid. The mixture with the catalyst was put in a freezer at  $-20$  °C and was used in a period of 2 *h* for a series of measurements.

#### 2.2.2. Rheology

Rheological measurements were performed on an oscillatory plate rheometer MCR 101 from Anton Paar (Physica). For all measurements a PP08 measuring system (parallel plated, diameter 8 *mm*) was used. Measurements were performed at 20 °C, 40 °C or 70 °C and the sample temperature was regulated by thermoelectric heating and cooling. For evaluation of data the RheoPlus/32 software (V 3.40) and OriginPro7 was used. For sample preparation a 1:1 mixture (molar ratio) of the

triazide compound (1) and the trialkyne compound (2) were placed in a flask (100 *mg*) and the catalyst (1 *mol%* per functional group) was added to the mixture. Subsequently, the reaction mixture was mixed with a spatula and immediately put on the rheometer plate. Measurements were performed with a strain  $\gamma$  of 1.0% and with an angular frequency  $\omega$  ranging from 100 to 1 *rad/s*. A frequency sweep was performed every 5 *min*. The gelation time was determined as crossover of the storage ( $G'$ ) and the loss modulus ( $G''$ ). Measurements were stopped, when the values of the storage and the loss modulus stayed constant (second decimal place) for at least 60 *min*.

#### 2.2.3. Nuclear magnetic resonance (NMR)

All NMR spectra were recorded on a Varian spectrometer (Gemini 400) at 400 *MHz* at 27 °C.  $\text{CDCl}_3$  (Armar AG, 99.8 Atom %D) was used as solvent. The coupling constants were given in *Hz* and the chemical shifts in ppm and referred to the residual solvent peak [ $\text{CDCl}_3$  7.26 *ppm* ( $^1\text{H}$ ) and 77.16 *ppm* ( $^{13}\text{C}$ )]. For the interpretation of the spectra, MestReNova v. 6.0.2-5475 was used.

#### 2.2.4. Thermogravimetric analysis (TGA)

TGA was performed on a Netzsch TG tarsus 209 instrument. The samples were heated in a Pt pan under a dry flow of nitrogen (250 *mL/min*) over a temperature range of 25-900 °C, with a heating rate of 10 °C/*min*.

#### 2.2.5. Electrospray ionization time of flight mass spectrometry (ESI-TOF-MS)

Mass spectrometry measurements were obtained on a microTOF Focus by Bruker Daltonics with an electrospray ionization source (ESI source). Samples were dissolved in THF (HPLC grade) as solvent and injected with a 180 *mL/h* flow rate at 180 °C.

#### 2.2.6. Broadband dielectric spectroscopy (BDS)

A NOVOCONTROL Alpha analyzer equipped with a Quatro temperature controller was used for dielectric spectroscopy experiments. The experiments were performed on thin films obtained after crosslinking reaction under rheometer with a thickness of 400-500  $\mu\text{m}$  and  $\sim 7$ -8 *mm* diameter. All the measurements were



### III. RESULT AND DISCUSSION

conducted using a measuring cell in which the sample was placed between two parallel, disc like, gold plated electrodes. Isothermal frequencies in the range of  $0.01 \text{ Hz} < f < 1 \text{ MHz}$  were applied at  $25 \text{ }^\circ\text{C}$  and at  $0 \text{ }^\circ\text{C}$ . All the measurements were performed under a controlled nitrogen gas.

#### 3. Synthesis of trivalent azide and alkyne moieties

##### 3.1. Synthesis of trimethylolpropane-1-azidobutan-2-yl-acetate ether (1)

The azidation of trimethylolpropanetri glycidyl ether was done according to literature with slight modification [38] (see Scheme 2). Trimethylolpropanetri glycidyl ether ( $0.033 \text{ mol}$ ,  $10.0 \text{ g}$ ,  $8.64 \text{ mL}$ ) was added to a  $250 \text{ mL}$  round bottom flask containing methanol ( $150 \text{ mL}$ ). Ammonium chloride ( $0.165 \text{ mol}$ ,  $8.8 \text{ g}$ ) and sodium azide ( $0.165 \text{ mol}$ ,  $10.7 \text{ g}$ ) were added to the reaction flask, and the mixture was heated to reflux for  $12 \text{ h}$ . After completion of the reaction, the solvent was removed under vacuum and the crude product was purified by washing with water ( $3 \times 100 \text{ mL}$ ), brine ( $1 \times 50 \text{ mL}$ ) and again with water ( $2 \times 50 \text{ mL}$ ), followed by extraction with chloroform to give the slight yellow liquid product (yield: 92%)  $^1\text{H}$  NMR ( $400 \text{ MHz}$ ,  $\text{CDCl}_3$ )  $\text{ppm}$  3.92 (dd,  $J = 9.97, 5.27 \text{ Hz}$ , 3H), 3.41 (m, 18H), 3.17 (s, 3H), 1.36 (m, 2H), 0.83 (t,  $J = 7.57 \text{ Hz}$ , 3H);  $^{13}\text{C}$  NMR ( $100 \text{ MHz}$ ,  $\text{CDCl}_3$ )  $\text{ppm}$  72.6, 72.3, 69.5, 53.4, 43.3, 23.3, 7.6.

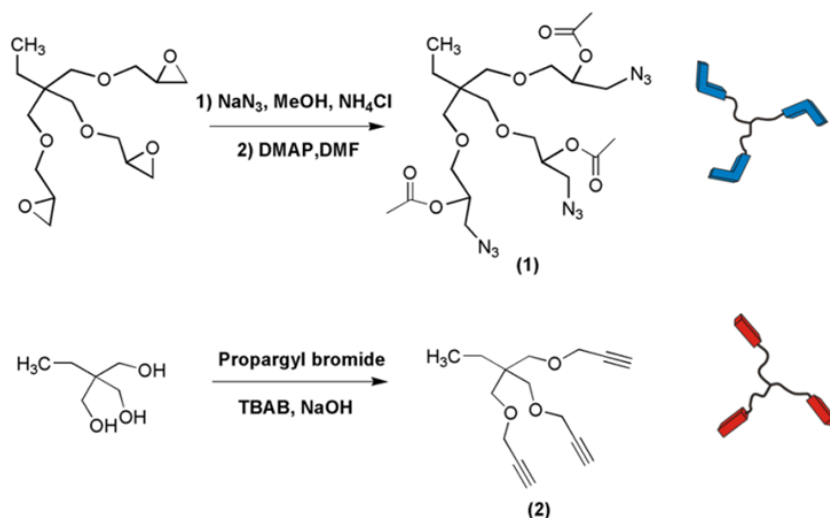
For the acetylation reaction, trivalent azide with hydroxyl ( $0.232 \text{ mmol}$ ,  $100.0 \text{ mg}$ ) and 4-dimethylaminopyridine ( $0.046 \text{ mmol}$ ,  $5.6 \text{ mg}$ ) were placed in a  $5 \text{ mL}$  round bottom flask containing freshly distilled DMF ( $3 \text{ mL}$ ). The reaction mixture was stirred for  $10 \text{ min}$  followed by the addition of acetic anhydride ( $0.695 \text{ mmol}$ ,  $70.9 \text{ mg}$ ) at room temperature. The reaction mixture was then allowed to stir for an additional  $1 \text{ h}$  at room temperature. After completion of the reaction, the solvent was removed under vacuum and the crude product was purified by flash chromatography using chloroform. NMR analysis indicated that the purified product (slight yellow liquid) was 90% tri- and 10% of bivalent substituted. The purity of the product (slight yellow liquid) was confirmed by NMR. (yield: 98%)  $^1\text{H}$  NMR ( $400 \text{ MHz}$ ,  $\text{CDCl}_3$ )  $\text{ppm}$  5.06 (m, 3H), 3.46-3.54 (m, 12H), 3.27 (s, 6H), 2.09 (s, 9H), 1.35 (d,  $J = 7.58 \text{ Hz}$ , 2H), 0.82 (d,  $J = 7.50 \text{ Hz}$ , 3H);  $^{13}\text{C}$  NMR ( $100 \text{ MHz}$ ,  $\text{CDCl}_3$ )  $\text{ppm}$  162.5, 71.6,

69.5, 50.9, 36.4, 31.4, 22.9, 20.9, 7.5. ESI-TOF-MS, Measured:  $558.21 \text{ Da}$  and  $580.19 \text{ Da}$  Simulated:  $558.26 \text{ Da}$   $[\text{C}_{21}\text{H}_{35}\text{N}_9\text{O}_9+\text{H}]^+$  and  $580.24 \text{ Da}$   $[\text{C}_{21}\text{H}_{35}\text{N}_9\text{O}_9+\text{Na}]^+$ .

#### 4. Results and discussion

Dynamic scanning calorimetry (DSC) analysis imparts good knowledge about the relationship between the extent of the reaction and the time of curing at certain temperatures, essential to optimize the performance of resin materials at minimum costs, while furthermore providing information about kinetic parameters and reaction modeling. Thus, DSC analysis is helpful to obtain a wide range of data related to the crosslinking reaction such as the enthalpy of the reaction ( $\Delta H$ ), the onset temperature ( $T_{\text{onset}}$ ), the temperature at the maximum of the DSC curve ( $T_p$ ), the activation energy of the reaction ( $E_a$ ), the variation of the activation energy with conversion, the reaction model, and the order of the reaction. As a simple reference reaction, a DSC measurement was run using phenylacetylene and benzylazide with  $1 \text{ mol}\%$  of  $\text{Cu}(\text{PPh}_3)_3\text{Br}$  as catalyst in a CuAAC reaction and a  $\Delta H$  value of  $262 \text{ kJ/mol}$  was obtained, which is analogous to the reported values in literature for click reactions ( $210\text{-}270 \text{ kJ/mol}$ ) [39]. The click crosslinking reaction conversion can be estimated with respect to the determined reference value ( $262 \text{ kJ/mol}$ ), a maximum  $\Delta H$  value for the reference click reaction quantitatively forming one triazole unit, representative of one successful "click" reaction. The activity of TRGO- $\text{Cu}_2\text{O}$  towards CuAAC reaction was compared with different commercially available homogenous ( $\text{Cu}(\text{PPh}_3)_3\text{Br}$  and  $\text{Cu}(\text{PPh}_3)_3\text{F}$ ) and heterogeneous ( $\text{Cu}/\text{C}$ ) [37] copper catalysts. DSC thermograms at  $5 \text{ }^\circ\text{C}/\text{min}$  for different catalysts are plotted in Fig. 1a ( $1 \text{ mol}\%$  of catalyst per functional group) and the results are summarized in Table 1. For the uncatalyzed reaction (W/O cat) (Table 1, Entry 1), the observed enthalpy was  $144 \text{ kJ/mol}$  which corresponds to 55% conversion with respect to the enthalpy for 100% click conversion ( $262 \text{ kJ/mol}$ , reference reaction). Furthermore, for the W/O based click reaction, crosslinking happened at a high temperature with a  $T_{\text{onset}}$  at  $99.1 \text{ }^\circ\text{C}$  and a  $T_p$  at  $133 \text{ }^\circ\text{C}$ . The TRGO- $\text{Cu}_2\text{O}$  catalyst (Table 1, Entry 2) enhanced the reaction dramatically and -

## III. RESULT AND DISCUSSION



Scheme 2. Synthetic pathway for the trivalent azide (1) and trivalent alkyne (2).

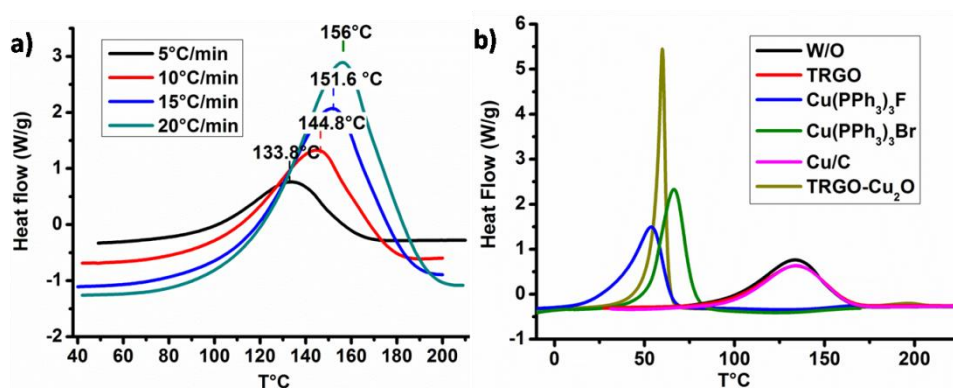


Fig. 1. DSC measurements for the bulk click reaction a) with different catalysts at 5 °C/min heating rate and b) without catalyst at different heating rates.

**Table 1** Summary of thermal properties, like reaction temperatures ( $T_{\text{onset}}$  and  $T_p$ ), the enthalpy ( $\Delta H$ ) and the activation energy ( $E_a$ ) of click crosslinking reactions with different catalysts

Entry	Catalyst	mol%	mass%	$T_{\text{onset}}$ (°C)	$T_p$ (°C)	$\Delta H$ (KJ/mol)	$E_a$ (KJ/mol)	Reaction conversion (%)
1	W/O cat			99 ± 3	133 ± 4	144 ± 7	83 ± 3	55
2	TRGO/Cu <sub>2</sub> O	1	7.6	55 ± 6	59 ± 6	153 ± 8	71 ± 3	58
3	TRGO/Cu <sub>2</sub> O	2	13.6	67 ± 4	72 ± 4	148 ± 9	75 ± 4	56
4	TRGO		7.4	97	134	137	80 ± 5	52
5	TRGO		14.2	99	134	146 ± 5	83 ± 4	56
6	Cu(PPh <sub>3</sub> ) <sub>3</sub> Br	1	3.5	52 ± 1	66	158 ± 1	78 ± 5	60
7	Cu(PPh <sub>3</sub> ) <sub>3</sub> Br	2	7.1	49 ± 3	63 ± 2	149 ± 4	73 ± 6	57
8	Cu(PPh <sub>3</sub> ) <sub>3</sub> F	1	3.3	37 ± 6	53 ± 7	139 ± 8	78	53
9	Cu(PPh <sub>3</sub> ) <sub>3</sub> F	2	6.4	23 ± 6	42 ± 7	122 ± 7	70 ± 2	46
10	Cu/C	1	8.7	100	134	136 ± 4	74	52
11	Cu/C	2	13.2	99	134	130 ± 3	75	49

All results related to the experiments with 5 °C/min heating rate.

$$\ln\left(\frac{\beta}{T_p^2}\right) = \ln\left(\frac{AR}{E}\right) - \frac{E}{RT_p} \quad (1)$$

$$\log \beta = -\frac{0.4567E_a}{RT_i} + A' \quad (2)$$

reduced the reaction temperatures to 55 °C ( $T_{\text{onset}}$ ) and 59 °C ( $T_p$ ), respectively. Additionally, the enthalpy of the reaction increased to 153 kJ/mol (58% conversion), indicative of a higher crosslinking density.

However, pure graphene without copper nanoparticles (TRGO) (Table 1, Entries 4 and 5) did not show any effect on DSC thermograms, so that the values are similar to the obtained values for the uncatalyzed reaction (Table 1, Entry 1). A lower  $T_{\text{onset}}$  (52 °C) and  $T_p$  (66 °C) with 158 kJ/mol enthalpy (60% conversion), was observed for the homogenous catalyst (Cu(PPh<sub>3</sub>)<sub>3</sub>Br), which possesses comparable results with TRGO-Cu<sub>2</sub>O

## III. RESULT AND DISCUSSION

(Table 1, Entry 6). A much lower  $T_{\text{onset}}$  (37 °C) and  $T_p$  (53 °C) was observed for another homogeneous catalyst ( $\text{Cu}(\text{PPh}_3)_3\text{F}$ ), although an enthalpy of 139 kJ/mol (53% conversion) was obtained (Table 1, Entry 8), indicating a lower amount of triazole formation. This phenomenon can be related to the early formation of the network, in turn decreasing the diffusion of monomers and the catalyst [22] thus reducing the effective number of possible click crosslinks in the later stages of the reaction. No significant change was observed for the commercially available heterogeneous copper catalyst copper on charcoal (Cu/C) [37] (Table 1, Entry 10). A  $T_{\text{onset}}$  (100 °C) and  $T_p$  (134 °C) including an enthalpy of 136 kJ/mol (52% conversion) was observed for Cu/C. The obtained results confirm that the synthesized heterogeneous catalyst TRGO-Cu<sub>2</sub>O and the homogeneous catalyst  $\text{Cu}(\text{PPh}_3)_3\text{Br}$  provide improved crosslinking activity with respect to all other probed catalysts. Increasing the amount of catalysts to 2 mol% per functional group for  $\text{Cu}(\text{PPh}_3)_3\text{Br}$  and  $\text{Cu}(\text{PPh}_3)_3\text{F}$  diminished the  $T_{\text{onset}}$  and  $T_p$  temperatures (Table 1, Entries 7 and 9), but the  $\Delta H$  values were reduced about 10-20 kJ/mol, again explainable by the early network formation. Though using higher amounts of TRGO-Cu<sub>2</sub>O catalyst no significant effect was observed on the enthalpy ( $\Delta H$ ), and reaction temperatures ( $T_{\text{onset}}$  and  $T_p$ ) (Table 1, Entry 3). In literature, an activation energy ( $E_a$ ) of 85-90 kJ/mol for click reactions has been reported [39]. The addition of a catalyst thus should reduce the activation energy ( $E_a$ ) and in turn enhance the rate of the reaction. With a relatively low activation energy of 70 kJ/mol, the reaction can occur at low temperatures, even at room temperature [33]. From DSC thermograms we observed that a high heating rate shifts the peak temperatures ( $T_p$ ) to higher values (Fig. 1b).

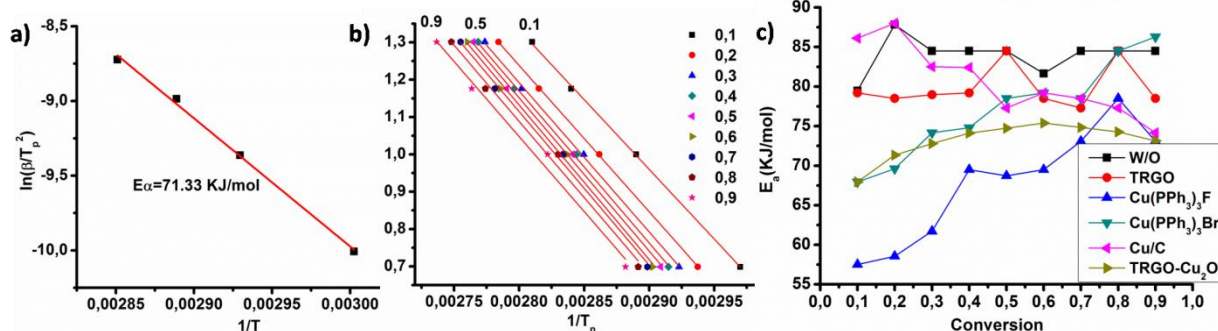


**Fig. 2.** a) Kissinger and b) Ozawa plot for the calculation of the activation energy in the crosslinking reaction between (1) and (2) using TRGO Cu<sub>2</sub>O as catalyst, c) activation energy vs. conversion for the crosslinking reaction between (1) and (2) with different Cu(I) catalysts and without Cu(I) catalyst.

The  $E_a$  for the click reaction can be determined using Kissinger's equation [40] (Eq. (1)) with the slope of  $(\beta/T_p^2)$  vs.  $(1/T_p)$  (Fig. 2a), where  $\beta$  is the heating rate.

The observed  $E_a$  for the catalyst free crosslinking reaction (W/O cat) was 83 kJ/mol (Table 1, Entry 1), while a reduced  $E_a$  was detected for the click reaction using TRGO-Cu<sub>2</sub>O (71 kJ/mol, Table 1, Entry 2). A higher  $E_a$  was determined for  $\text{Cu}(\text{PPh}_3)_3\text{Br}$  and  $\text{Cu}(\text{PPh}_3)_3\text{F}$  catalysts with 78 kJ/mol (Table 1, Entry 6 and Entry 8). Using 2 mol% of catalysts lowered the activation energy for  $\text{Cu}(\text{PPh}_3)_3\text{Br}$  (Table 1, Entry 7) and  $\text{Cu}(\text{PPh}_3)_3\text{F}$  (Table 1, Entry 9), however was increased in the case of TRGO-Cu<sub>2</sub>O (Table 1, Entry 3). The results show that the use of higher amounts of nanofiller catalyst can enhance the reaction kinetics and increase the activation energy  $E_a$  due to a reduction in the mobility of the monomers, as discussed earlier. To further investigate the effect of different catalysts on the activation energy, the relation between the activation energy and the reaction conversion was determined by the Ozawa equation (Eq. (2), Fig. 2c) [41,42], where  $\beta$  is the heating rate and  $E_a$  is the activation energy at the temperature ( $T_i$ ) for a given conversion ( $\alpha$ ). For the reaction without catalyst (W/O cat) and with pure graphene (TRGO) a constant  $E_a$  was observed regardless to the reaction conversion. However, the  $E_a$  increases with conversion for  $\text{Cu}(\text{PPh}_3)_3\text{Br}$  and  $\text{Cu}(\text{PPh}_3)_3\text{F}$  (Fig. 2c). As discussed earlier, this behavior can be explained by an elevated network density at high conversion which reduces the mobility for monomers and catalysts.

The activation energy of TRGO-Cu<sub>2</sub>O increases slightly up to 60% conversion, after which it remains constant. The lower and constant activation energy for TRGO-Cu<sub>2</sub>O might be attributable to a good dispersibility of the copper particles immobilized graphene sheets, where the -

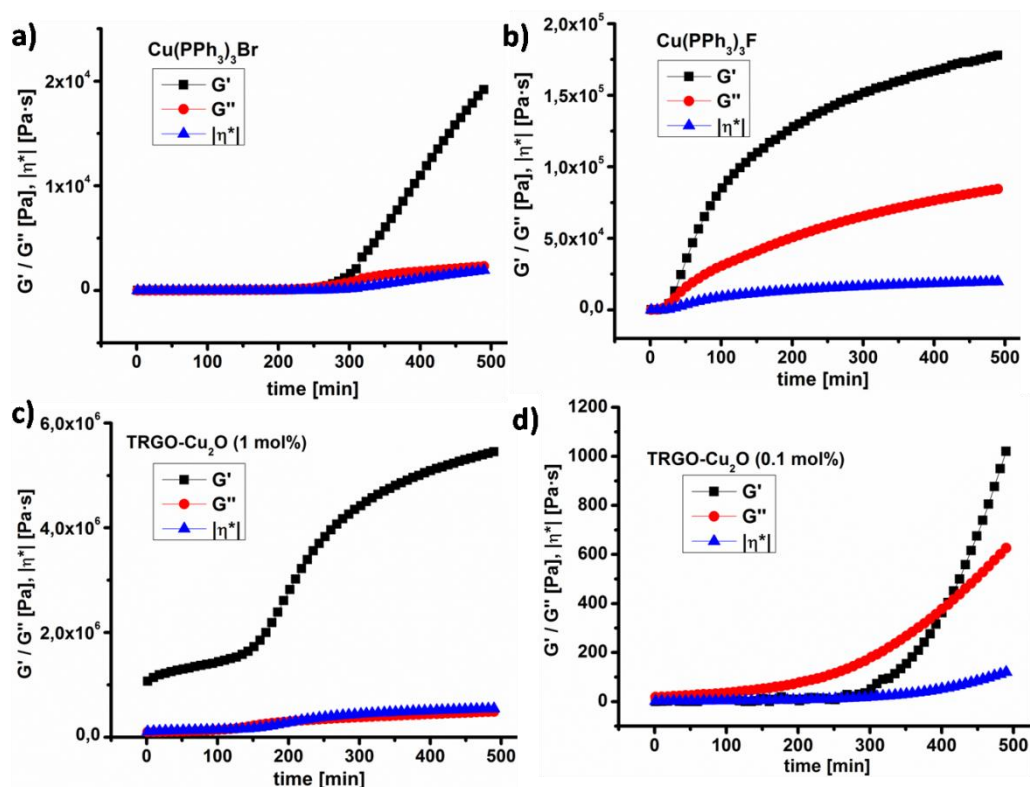
## III.RESULT AND DISCUSSION

**Table 2** Results of simulation models for crosslinking reaction with different catalysts.

Entry	Best Model reaction	Catalyst <sup>a</sup>	A	m	n	K <sub>cat</sub>	Reaction order (m+n)
1	F1	W/O Cat	5.9E9	-	1	-	1
2	F1	TRGO	8.0E8	-	1	-	1
3	PT	TRGO-Cu <sub>2</sub> O	9.0E11	1.5	1.2	-	2.7
4	PT	Cu(PPh <sub>3</sub> ) <sub>3</sub> F	8.9E11	0.21	0.93	-	1.14
5	Cn	Cu(PPh <sub>3</sub> ) <sub>3</sub> F	6.1E11	-	0.92	0.43	0.92
6	PT	Cu(PPh <sub>3</sub> ) <sub>3</sub> Br	5.2E11	0.72	1.23	-	1.95
7	F1	Cu/C	3.4E8	-	1	-	1

<sup>a</sup> 1 mol% per functional group.**Table 3** Crossover time study and physical-mechanical properties like storage modulus, viscosity, conductivity, and the decomposition temperature of final resin materials cured by different catalysts at 20 °C.

Entry	Catalyst	mol%	mass%	crossover time [min]	G' [Pa]	G'' [Pa]	η*  [Pa.s]	Conductivity (σ <sub>0</sub> ) (S/m)	T <sub>d</sub> (T°C)
1	Cu(PPh <sub>3</sub> ) <sub>3</sub> Br	1	3.5	270	7.4E+4	1.4E+4	7.5E+3	2.8E-11	296
2	Cu(PPh <sub>3</sub> ) <sub>3</sub> F	1	3.3	35	3.3E+5	2.3E+5	4.0E+4	1.5E-10	291
3	TRGO-Cu <sub>2</sub> O	1	7.6	-	8.6E+6	1.8E+6	8.7E+5	2.2E-4(1.6E-4) <sup>c</sup>	300
4	TRGO	-	7.4	-	3.2E+5	6.4E+4	3.2E+4	-	-
5	TRGO-Cu <sub>2</sub> O	0.1	0.8	409 <sup>a</sup>	1.9E+5	5.5E+4	1.9E+4	5.7E-11	-
6	TRGO-Cu <sub>2</sub> O	0.2	1.6	118 <sup>b</sup>	7.9E+5	5.9E+3	7.9E+4	5.0E-10	-
7	TRGO-Cu <sub>2</sub> O	0.3	2.5	10 <sup>b</sup>	1.5E+6	2.7E+4	1.4E+5	1.8E-10	-
8	TRGO-Cu <sub>2</sub> O	0.5	4.1	- <sup>b</sup>	1.4E+6	5.6E+4	1.4E+5	4.9E-6(4.5E-6) <sup>c</sup>	-
9	Cu/C	1	8.7	-	1.2E+1	1.3E+1	1.74	-	-

<sup>a</sup> 40 °C<sup>b</sup> 70 °C<sup>c</sup> 0 °C**Fig. 3.** In-situ rheological behavior of triazide (1) and trialkyne (2) with 1 mol% of a) Cu(PPh<sub>3</sub>)<sub>3</sub>Br b) Cu(PPh<sub>3</sub>)<sub>3</sub>F c) TRGO-Cu<sub>2</sub>O and d) 0.1 mol% of TRGO-Cu<sub>2</sub>O and determination of the crossover time.

## III.RESULT AND DISCUSSION

agglomeration of copper nanoparticles is prevented due to the high porosity and scaffold behavior of the graphene sheets as evidence by the uniform dispersion displayed in the TEM image of Fig. S9.

A model fitting was also applied to investigate the reaction kinetics and the reaction order according to the literature [22] (see Supporting information Section S7). Table 2 summarizes the kinetic parameters for all bulk click crosslinking reactions between triazide compound (1) and trialkyne compound (2). For the reaction without catalyst (Table 2, Entry 1) the best fitting equation was a first order function (F1) (Figure S10a). The reaction with pure TRGO also represents the same reaction order (Table 2, Entry 2), which again proves that pure TRGO (devoid of Cu nanoparticles) does not possess any catalytic behavior. The TRGO-Cu<sub>2</sub>O catalyst fits very well to the Prout Tompkins equation (PT), with the reaction order ( $m + n$ ) of "2.7", which indicates a high catalytical efficiency of TRGO-Cu<sub>2</sub>O (Figure S10b, Table 2, Entry 3). The Prout Tompkins equation also fits for Cu(PPh<sub>3</sub>)<sub>3</sub>F and Cu(PPh<sub>3</sub>)<sub>3</sub>Br catalysts (Table 2, Entries 4 and 6) with a reaction order ( $m + n$ ) of "1.95" and "1.14", respectively. Furthermore the pre-exponential factor (A) of TRGO-Cu<sub>2</sub>O possessed higher value in comparison to other catalysts showing faster reaction rate ( $A = 9.0E11$ ). The results favor higher catalytic activity of TRGO-Cu<sub>2</sub>O in comparison with Cu(PPh<sub>3</sub>)<sub>3</sub>Br and Cu(PPh<sub>3</sub>)<sub>3</sub>F. However, no catalytic effect was observed for Cu/C (Table 2, Entry 7).

The obtained kinetic results are comparable to results earlier reported by Finn and Fokin et al. [43] where a reaction order of "2.3 ± 0.4" was observed for a solution based CuAAC reaction between phenylacetylene and benzylazide.

## 4.1. Rheology measurements

Rheological measurements coupled with curing kinetics modeling provides information about the gelation time, the evolution of the viscosity during the reaction and the buildup of viscoelastic properties of the finally obtained networks. Therefore, the isothermal click crosslinking reaction between triazide compound (1) and trialkyne compound (2) was done on a rheometer plate at 20 °C using different Cu(I) catalysts. Mixtures containing homogenous catalysts (Cu(PPh<sub>3</sub>)<sub>3</sub>F and Cu(PPh<sub>3</sub>)<sub>3</sub>Br) (Table 3, Entries 1 and 2), clearly possess liquid like character at the beginning, and the loss modulus was higher than the storage modulus ( $G'' > G'$ ).

After some time (270 and 35 min for Cu(PPh<sub>3</sub>)<sub>3</sub>Br and Cu(PPh<sub>3</sub>)<sub>3</sub>F respectively), both moduli increased and a crossover of  $G'$  and  $G''$  (gelation time) was observed (Fig. 3a and b). It was difficult to determine the crossover when applying TRGO-Cu<sub>2</sub>O (1 mol% catalyst per functional group) (Table 3, Entry 3), as it acts as catalyst and nanofiller and the rheological percolation threshold of graphene nanofillers is reached. However the moduli ( $G'$  and  $G''$ ) increased significantly (Fig. 3c), and, a solid product was obtained at the end. To find out the crossover time and rheological percolation threshold for TRGO-Cu<sub>2</sub>O as catalyst for click crosslinking and nanofiller respectively, the amount of the TRGO-Cu<sub>2</sub>O was reduced to 0.1, 0.2, 0.3 and 0.5 mol% per functional group (Table 3, Entries 5-8). The reaction with 0.1 mol% per functional group was run at 40 °C (Table 3, Entry 5), and the crossover time was observed at 490 min (Fig. 3d). Although the amount of the TRGO-Cu<sub>2</sub>O was 10 times reduced, the gelation time was still in the -

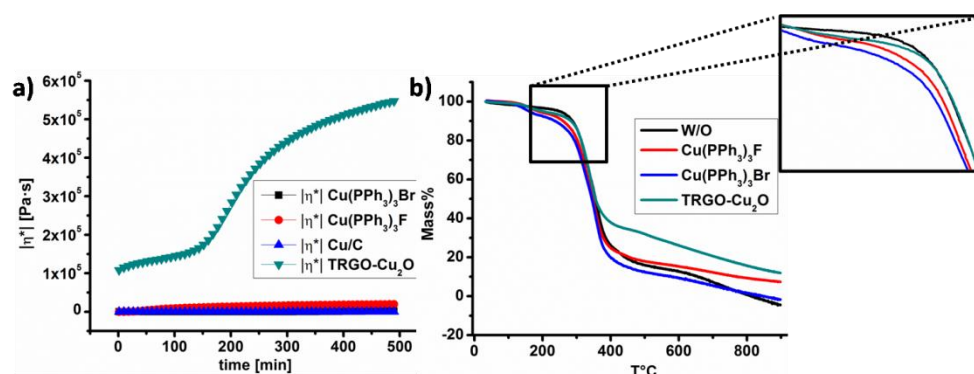


Fig. 4. a) Evolution of viscosity during the isothermal curing at 20 °C by different catalysts, and b) thermal degradation of the final resin materials which were cured with different catalysts.



## III. RESULT AND DISCUSSION

range of commercially available homogeneous catalysts ( $\text{Cu}(\text{PPh}_3)_3\text{Br}$ ), which further supports a higher catalytic activity of TRGO- $\text{Cu}_2\text{O}$ . Furthermore it was observed that with more than 0.3 mol% of TRGO- $\text{Cu}_2\text{O}$  catalyst per functional group, (2.5 mass%) it was difficult to study the gelation time and the  $G'$  was higher than  $G''$  ( $G' > G''$ ) in the beginning of measurement (Table 3, entries 3, 7, and 8). This effect is due to the network formation of graphene filler within the resin considered as rheological percolation threshold [44]. Pure TRGO does not influence the modulus of the final resin (Table 3, Entry 4) as it is not active as a catalyst. Moreover, Fig. 4a describes the viscosity evolution during the reaction for different types of catalysts, where the fastest viscosity increment was observed for the TRGO- $\text{Cu}_2\text{O}$  catalyst

#### 4.2. Physical and mechanical properties of finally cured resins.

Along with its catalytic properties, TRGO- $\text{Cu}_2\text{O}$  can act as nanofiller therefore improving the physical properties like the conductivity, the storage modulus and the strength of the final resin material. The physical and mechanical properties of the cured resins were measured *via* rheology, thermogravimetric analysis (TGA) and broadband dielectric spectroscopy (BDS), and the results are summarized in Table 3. Compared to resins cured with  $\text{Cu}(\text{PPh}_3)_3\text{Br}$  and  $\text{Cu}(\text{PPh}_3)_3\text{F}$  (Table 3, Entries 1 and 2), the resin which was cured by TRGO- $\text{Cu}_2\text{O}$  (Table 3, Entry 3) clearly possesses a higher storage modulus and a higher viscosity, even when the resin was cured with a low amount of TRGO- $\text{Cu}_2\text{O}$  (0.2-0.5 mol%) (Table 3, Entries 6-8).

A good thermal stability was observed for the final resin materials (Fig. 4b, Table 3), emphasizing their utilization for high performance applications. However, the thermal stability was independent -

from the nature of the used catalyst, where almost the same decomposition temperature  $T_d$  was observed for all the resins crosslinked using different catalysts.

Fig. 5 shows the frequency dependence of the conductivity of the final resin materials which were cured by adding different amounts of TRGO- $\text{Cu}_2\text{O}$  catalyst and commercially available homogenous catalysts ( $\text{Cu}(\text{PPh}_3)_3\text{Br}$  and  $\text{Cu}(\text{PPh}_3)_3\text{F}$ ) measured at 25 °C and 0 °C. The plateau in the real part of the complex conductivity function,  $\sigma'$  in the broadband dielectric spectroscopy (BDS) measurement corresponds to  $\sigma_0$ , the value of the conductivity in the dc limit [45].

For the measurements at 25 °C (Fig. 5a) all resins showed a plateau and the values of  $\sigma_0$  are listed in Table 3. The resin cured with 1 mol% TRGO- $\text{Cu}_2\text{O}$  (Table 3, Entry 3) demonstrates conducting behavior ( $5.4\text{E-}4 \text{ S/m}$ ), whereas insulating behavior was observed for the resin materials cured by ( $\text{Cu}(\text{PPh}_3)_3\text{F}$  and  $\text{Cu}(\text{PPh}_3)_3\text{Br}$ ) (Table 3, Entries 1 and 2). For further investigating the effect of TRGO- $\text{Cu}_2\text{O}$  on the conductivity of the final resin and electrical percolation threshold, broadband dielectric spectroscopy measurements were conducted for the resins cured with 0.1-0.5 mol% of TRGO- $\text{Cu}_2\text{O}$  (Table 3, Entries 5-8). The conductivity curves can be divided into two groups, corresponding to the resins cured with more and with less than 0.3 mol% (2.5 mass%) of TRGO- $\text{Cu}_2\text{O}$  where the latter ones show a frequency dependent conductivity at high frequencies. However, when the amount of TRGO- $\text{Cu}_2\text{O}$  increased to 0.5 mol% (4 mass%) and more, the conductivity was completely frequency independent and the dc conductivity plateau shows a higher value which can be considered as a electrical percolation threshold for graphene based nanofillers [46]. This value is in the same range of rheological percolation threshold. All measurements were repeated at 0 °C (Fig. 5b) and-

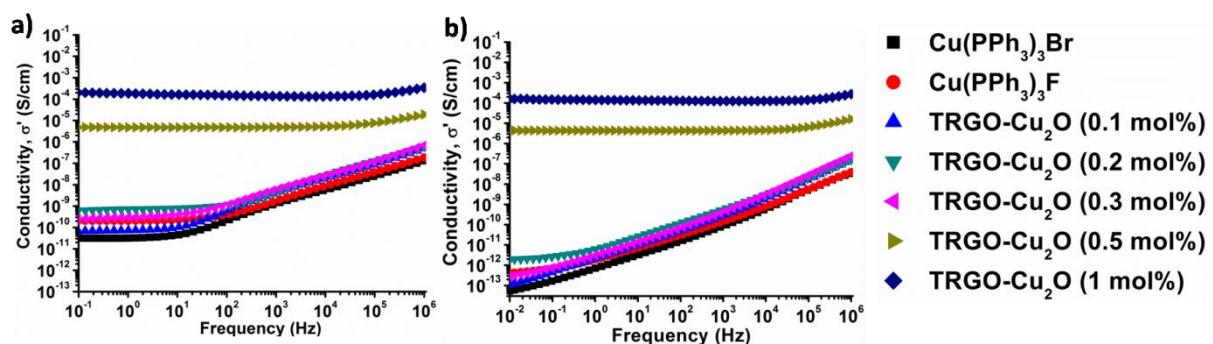


Fig. 5. Frequency dependence of the conductivity of final resin materials which were cured with different commercially available catalysts and different amount of TRGO- $\text{Cu}_2\text{O}$  measured by BDS at a) 25 °C and b) 0 °C.

### III. RESULT AND DISCUSSION

the samples which were cured with homogenous catalysts or with less than 0.5 *mol%* (4 *mass%*) of the TRGO-Cu<sub>2</sub>O catalyst showed a clear frequency dependence of the conductivity over the whole frequency range and thus, no dc conductivity plateau was observed. In contrast, the conductivity of resins cured with more than 0.5 *mol%* (4 *mass%*) of TRGO-Cu<sub>2</sub>O was frequency independent showing a dc conductivity plateau similar to the measurements at 25 °C (Table 3, Entries 3 and 8). In conclusion, a low temperature conductive resin material with improved mechanical properties can be prepared while using 0.5 *mol%* of TRGO-Cu<sub>2</sub>O per functional group (4 *mass%* in total).

#### 5. Conclusions

Graphene supported Cu(I) catalyst (TRGO-Cu<sub>2</sub>O) was used in a CuAAC crosslinking reaction between a triazide (1) and trialkyne (2) to form a new nanocomposite/resin materials with a strong reduction in curing-time and temperature, including a significant improvement in physical, mechanical and conductive properties of the finally cured resin. Study of the crosslinking reaction between (1) and (2) by DSC and rheology proved that TRGO-Cu<sub>2</sub>O displays a higher catalytic activity in comparison to the commercially available homogenous (Cu(PPh<sub>3</sub>)<sub>3</sub>Br and Cu(PPh<sub>3</sub>)<sub>3</sub>F) and heterogeneous (Cu/C) catalysts. In the DSC measurement, TRGO-Cu<sub>2</sub>O displayed lower reaction temperatures ( $T_{\text{onset}}$  and  $T_p$ ), higher reaction enthalpies,  $\Delta H$  (corresponding to higher crosslinking densities), and lower activation energies ( $E_a = 70 \text{ kJ/mol}$ ) independent of reaction conversion. Modeling studies did prove the autocatalytic behavior, the higher reaction order and faster reaction rate of TRGO-Cu<sub>2</sub>O in comparison to other homogenous and heterogeneous catalysts. Investigations on the crossover time was accomplished for different amount of TRGO-Cu<sub>2</sub>O (0.1-1 *mol%*) and for 1 *mol%* of homogenous commercially available catalyst (Cu(PPh<sub>3</sub>)<sub>3</sub>Br and Cu(PPh<sub>3</sub>)<sub>3</sub>F) directly on the rheometer plate at low temperatures (20-40 °C). Even with low amounts of TRGO Cu<sub>2</sub>O catalyst (0.1 *mol%*) the gelation time was comparable with 1 *mol%* of homogenous catalyst (Cu(PPh<sub>3</sub>)<sub>3</sub>Br), moreover the rheological percolation threshold of TRGO-Cu<sub>2</sub>O filler was observed around 0.3-0.5 *mol%* (3-4 *mass%*). The physical and mechanical

properties of finally cured resins were measured by rheology, BDS and TGA. Resins cured by TRGO-Cu<sub>2</sub>O (0.2-1 *mol%*) displayed a higher storage modulus and a higher viscosity in comparison to resins cured by 1 *mol%* of commercially available catalysts. Also BDS measurement showed that using more than 0.5 *mol%* (4 *mass%*) of TRGO-Cu<sub>2</sub>O, considered as electrical percolation factor of filler, the resin show the conductive behavior even at 0 °C. Thus, high performance resin materials have been prepared while using a low amount (4 *mass%*) of an easy to synthesize and cheap TRGO-Cu<sub>2</sub>O catalyst also being a favorable choice from industrial point of view. As TRGO-Cu<sub>2</sub>O can be prepared in a large scale in the laboratory using a facile synthetic route including low production cost, it now presents a viable material for industrial usage, generating nanocomposites with a high value.

#### Acknowledgments

This project has received funding from the European Union's Seventh Framework Program for research, technological development and demonstration under grant agreement no 313978 as well as the grant DFG-BI 1337/8-1 and DFG-BI 1337/8-2 within the SPP 1568 ("Design and Generic Principles of Self-Healing Materials"). We also gratefully thank Tamoor Babur for BDS measurements.

#### References

- [1] K.S. Novoselov, A.K. Geim, S.V. Morozov, D. Jiang, Y. Zhang, S.V. Dubonos, I.V. Grigorieva, A.A. Firsov, *Science* 306 (2004) 666-669.
- [2] A.A. Balandin, S. Ghosh, W. Bao, I. Calizo, D. Teweldebrhan, F. Miao, C.N. Lau, *Nano Lett.* 8 (2008) 902-907.
- [3] C. Lee, X. Wei, J.W. Kysar, J. Hone, *Science* 321 (2008) 385-388.
- [4] R.R. Nair, P. Blake, A.N. Grigorenko, K.S. Novoselov, T.J. Booth, T. Stauber, N.M.R. Peres, A.K. Geim, *Science* 320 (2008) 1308.
- [5] C.N.R. Rao, A.K. Sood, K.S. Subrahmanyam, A. Govindaraj, *Angew. Chem. Int. Ed.* 48 (2009) 7752-7777.
- [6] X.-D. Zhuang, Y. Chen, G. Liu, P.-P. Li, C.-X. Zhu, E.-T. Kang, K.-G. Noeh, B. Zhang, J.-H. Zhu, Y.-X. Li, *Adv. Mater.* 22 (2010) 1731-1735.
- [7] L.L. Zhang, R. Zhou, X.S. Zhao, *J. Mater. Chem.* 20 (2010) 5983-5992.
- [8] X. Zhou, J. Qiao, L. Yang, J. Zhang, *Adv. Energy. Mater.* 4 (2014) 1301523.
- [9] S. Navalon, A. Dhakshinamoorthy, M. Alvaro, H. Garcia, *Chem. Rev.* 114 (2014) 6179-6212.
- [10] B.F. Machado, P. Serp, *Catal. Sci. Technol.* 2 (2012) 54-75.
- [11] S. Yang, R.E. Bachman, X. Feng, K. Müllen, *Acc. Chem. Res.* 46 (2012) 116-128.



### III.RESULT AND DISCUSSION

- [12] S. Eigler, S. Grimm, F. Hof, A. Hirsch, J. Mater. Chem. A 1 (2013) 11559-11562.
- [13] C. Huang, C. Li, G. Shi, *Energy Environ. Sci.* 5 (2012) 8848-8868.
- [14] Y. Zhu, S. Murali, W. Cai, X. Li, J.W. Suk, J.R. Potts, R.S. Ruoff, *Adv. Mater.* 22 (2010) 3906-3924.
- [15] R. Sengupta, M. Bhattacharya, S. Bandyopadhyay, A.K. Bhowmick, *Prog. Polym. Sci.* 36 (2011) 638-670.
- [16] Susanna Laurenzi, M. Marchetti, in: N. Hu (Ed.), *Composite and Their Properties*, 2012.
- [17] L.A. Carlson, *Thermoplastic Composite Materials*, Florida Atlantic University, 1991.
- [18] A. Yousefpour, M.N. Ghasemi Nejjhad, *J. Compos. Mater.* 38 (2004) 1701-1732.
- [19] D. Bhattacharyya, S. Fakirov, *Synthetic Polymer-polymer Composites*, 2012.
- [20] Woo Il Lee, G.S. Springer, *J. Compos. Mater.* 21 (1987) 1017-1055.
- [21] V. Antonucci, M. Giordano, S. Inerraimparato, L. Nicolais, *Polym. Compos.* 22 (2001) 613-620.
- [22] M.R. Kessler, S.R. White, *J. Polym. Sci. Part A Polym. Chem.* 40 (2002) 2373-2383.
- [23] V.V. Rostovtsev, L.G. Green, V.V. Fokin, K.B. Sharpless, *Angew. Chem. Int. Ed.* 41 (2002) 2596-2599.
- [24] M. Meldal, C.W. Tornøe, in: *Proceedings of the Second International and the Seventeenth American Peptide Symposium*, 2001, pp. 263-264.
- [25] W.H. Binder, R. Sachsenhofer, *Macromol. Rapid Commun.* 28 (2007) 15-54.
- [26] W.H. Binder, R. Sachsenhofer, *Macromol. Rapid Commun.* 29 (2008) 952-981.
- [27] W.H. Binder, R. Zirbs, in: *Encyclopedia of Polymer Science and Technology*, John Wiley & Sons, Inc., 2002.
- [28] X. Sheng, T.C. Mauldin, M.R. Kessler, *J. Polym. Sci. Part A Polym. Chem.* 48 (2010) 4093-4102.
- [29] X. Sheng, D.M. Rock, T.C. Mauldin, M.R. Kessler, *Polymer* 52 (2011) 4435-4441.
- [30] L. Wan, Y. Luo, L. Xue, J. Tian, Y. Hu, H. Qi, X. Shen, F. Huang, L. Du, X. Chen, *J. Appl. Polym. Sci.* 104 (2007) 1038-1042.
- [31] C. Besset, J. Bernard, E. Fleury, J.-P. Pascault, P. Cassagnau, E. Drockenmuller, R.J.J. Williams, *Macromolecules* 43 (2010) 5672-5678.
- [32] R. Pötzsch, B. Voit, *Macromol. Rapid Commun.* 33 (2012) 635-639.
- [33] I.E. Gorman, R.L. Willer, L.K. Kemp, R.F. Storey, *Polymer* 53 (2012) 2548-2558.
- [34] A. Shaygan Nia, S. Rana, D. Döhler, F. Jirsa, A. Meister, L. Guadagno, E. Koslowski, M. Bron, W.H. Binder, *Chem. Eur. J.* 21 (2015) 10763-10770.
- [35] G.M. Scheuermann, L. Rumi, P. Steurer, W. Bannwarth, R. Mülhaupt, *J. Am. Chem. Soc.* 131 (2009) 8262-8270.
- [36] A. Shaygan Nia, S. Rana, D. Döhler, X. Noirfalise, A. Belfiore, W.H. Binder, *Chem. Commun.* 50 (2014) 15374-15377.
- [37] B.H. Lipshutz, B.R. Taft, *Angew. Chem.* 118 (2006) 8415-8418.
- [38] S. kantheti, P.S. Sarath, R. Narayan, K.V.S.N. Raju, *React. Funct. Polym.* 73 (2013) 1597-1605.
- [39] J.E. Hein, V.V. Fokin, *Chem. Soc. Rev.* 39 (2010) 1302-1315.
- [40] H.E. Kissinger, *Anal. Chem.* 29 (1957) 1702-1706.
- [41] T. Ozawa, *Bull. Chem. Soc. Jpn.* 38 (1965) 1881-1886.
- [42] T. Ozawa, *J. Therm. Anal.* 2 (1970) 301-324.
- [43] V.O. Rodionov, V.V. Fokin, M.G. Finn, *Angew. Chem.* 117 (2005) 2250-2255.
- [44] M. Martin-Gallego, M.M. Bernal, M. Hernandez, R. Verdejo, M.A. Lopez-Manchado, *Eur. Polym. J.* 49 (2013) 1347-1353.
- [45] J.R. Sangoro, A. Serghei, S. Naumov, P. Galvosas, J. Kärger, C. Wespe, F. Bordusa, F. Kremer, *Phys. Rev. E* 77 (2008) 051202.
- [46] Y. Jinhong, H. Xingyi, W. Chao, J. Pingkai, *IEEE Trans. Dielectr. Electr. Insul.* 18 (2011) 478-484.

## Supporting information

### 1. Materials

Graphite flakes (KFL 99.5, min 20 % > 100  $\mu\text{m}$ ) was received from Kropfmühl AG

### 2. Methods

#### TEM

The samples were dispersed in *iso*-propanol using bath sonicator and spread onto a Cu grid coated with a Carbon-film. After 1 *min* excess liquid was blotted off with filter paper. The dried specimens were examined with an EM 900 transmission electron microscope (Carl Zeiss Microscopy GmbH, Oberkochen, Germany). Micrographs were taken with a SSCCD SM-1k-120 camera (TRS, Moorenweis, Germany).

#### XPS

XPS analysis was performed using a XPS PHI Versa Probe 5000 spectrometer. The pressure in the analysis chamber was typically  $1.10^{-9}$  Torr. The XPS measurements were performed using a monochromatic AlK  $\alpha$  radiation at 1486.6 eV. A neutralizer with a Ar gun was used during the XPS analysis to compensate charging effects. Also the high resolution XPS spectra of each element recorded with a pass energy of 23.5 eV and an energy step 0.2 eV.

### 3- Synthesis of graphene supported copper nanoparticles

#### 3.1-synthesis of graphene oxide (GO)

Graphite (10 g) was stirred in concentrated sulfuric acid (390 mL) at room temperature (RT), and sodium nitrate (5 g) was added, afterwards the mixture was cooled to 0 °C and potassium permanganate (30 g) was added during 30 *min* to 1 *hour* in order to avoid the increment in internal temperature of the reaction mixture. After 2 *h*, the green slurry was allowed to come to RT, and after being stirred for 3 *h* (during this time the viscosity of mixture was increased) the whole batch was carefully poured into a 2 L beaker filled with ice-cold water (distilled). Subsequently, hydrogen peroxide (3 %) was added in excess and the mixture was stirred overnight and then filtered. Workup was accomplished by several washings with a mixture of HCl/H<sub>2</sub>O<sub>2</sub> (1:1, 5 %) and filtration was followed by several washings with water and centrifugation until the supernatant did not show anymore precipitation with AgNO<sub>3</sub> solution. The obtained GO carefully powdered in a ball mill, with pre cooling by liquid nitrogen. (For more detail see Appendix 2.3.1)

#### 3.2- Synthesis of graphene oxide immobilized Cu(II) (GO-Cu(II))

GO (1g) was dispersed in water (300 mL) by ultrasonication (30 % amplitude, 30 *min*). Subsequently, copper (II) acetate (300 mg, 1.65 mmol) was added and the mixture was vigorously sonicated for 5 *min* with 30% amplitude, and stirred at room temperature overnight. After several washing steps with water (5×200 mL) and acetone (5×200 mL) the graphene oxide (GO) bearing adsorbed Cu(II) at the surface was dried in high vacuum at 40 °C (GO-Cu(II)). Then GO-Cu(II) was carefully powdered in a ball mill, with pre-cooling by liquid nitrogen.

### 3.3- Synthesis of graphene supported copper nanoparticles (TRGO-Cu<sub>2</sub>O)

GO-Cu(II) (1.2 g) was placed in quartz flask of the oven and flashed for 40 min with nitrogen. Then it was heated to 600 °C with 10 K/min as heating rate and kept at 600 °C for 2 min. Afterwards the oven was cooled down to room temperature under nitrogen atmosphere to obtain TRGO/Cu<sub>2</sub>O.

## 4- Characterization of graphene supported copper nanoparticles (TRGO-Cu<sub>2</sub>O)

### 4-1-TEM

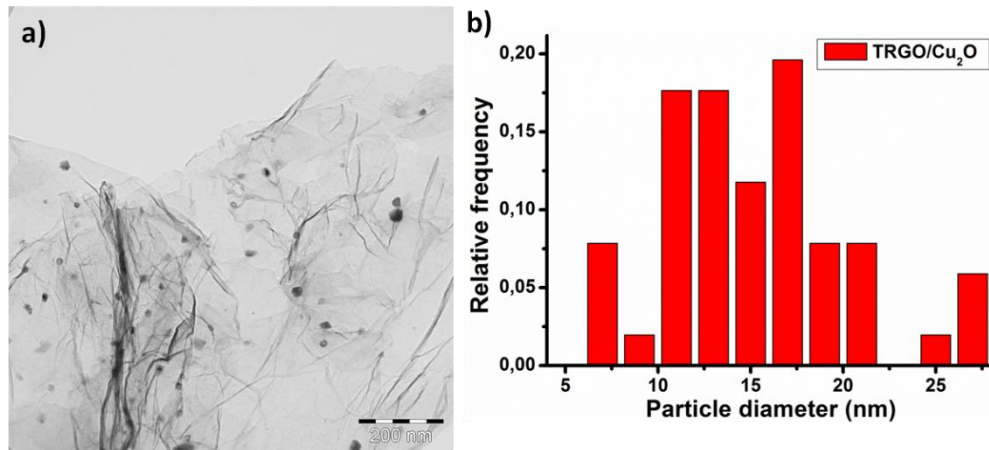


Figure S1. a) TEM image of the catalysts, c) copper particles size and distribution

Figure S1a shows the TEM image of TRGO/Cu<sub>2</sub>O conjugates, where uniform in size Cu<sub>2</sub>O nanoparticles with the average size of 15 nm (Figure S1b) are dispersed well onto the surface of graphene nanosheets.

### 4-2- XPS and FAAS

The chemical composition of TRGO/Cu<sub>2</sub>O was also obtained by X-ray photoelectron spectroscopy (XPS) (Figure S2a), where the peaks correspond to C 1s (285.1 eV), O 1s (531.6 eV) and Cu2p. The high-resolution XPS spectra (Figure S2b) reveals that Cu 2p<sub>3/2</sub> peaks located at 932.37 eV and 952.31 eV related to the peak energy of Cu (I). Also there are no peak satellites at 942 eV and 962 eV neither a peak at 934.8 eV which are related to Cu(II). The Cu content of the sample was also determined by a flame atomic absorption spectroscopy (FAAS) with  $4.72 \times 10^{-7}$  mol/mg loading.

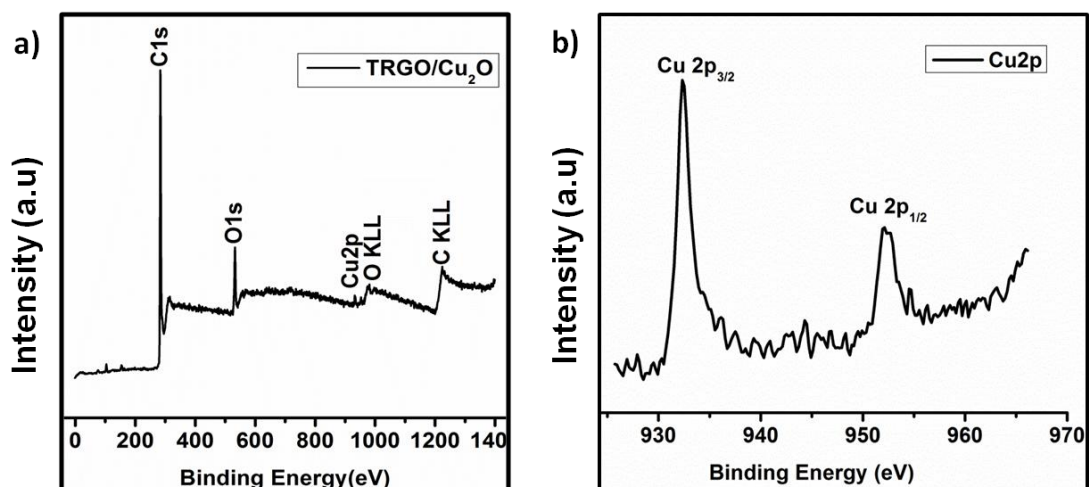


Figure. S2 a) X-ray photoelectron spectroscopy of TRGO/Cu<sub>2</sub>O, b) high resolution XPS of Cu element.

III.RESULT AND DISCUSSION

5- <sup>1</sup>H and <sup>13</sup>C NMR and ESI-TOF-MS spectra of trivalent azide (1) and trivalent alkyne (2) moieties

5-1- Trivalent azide

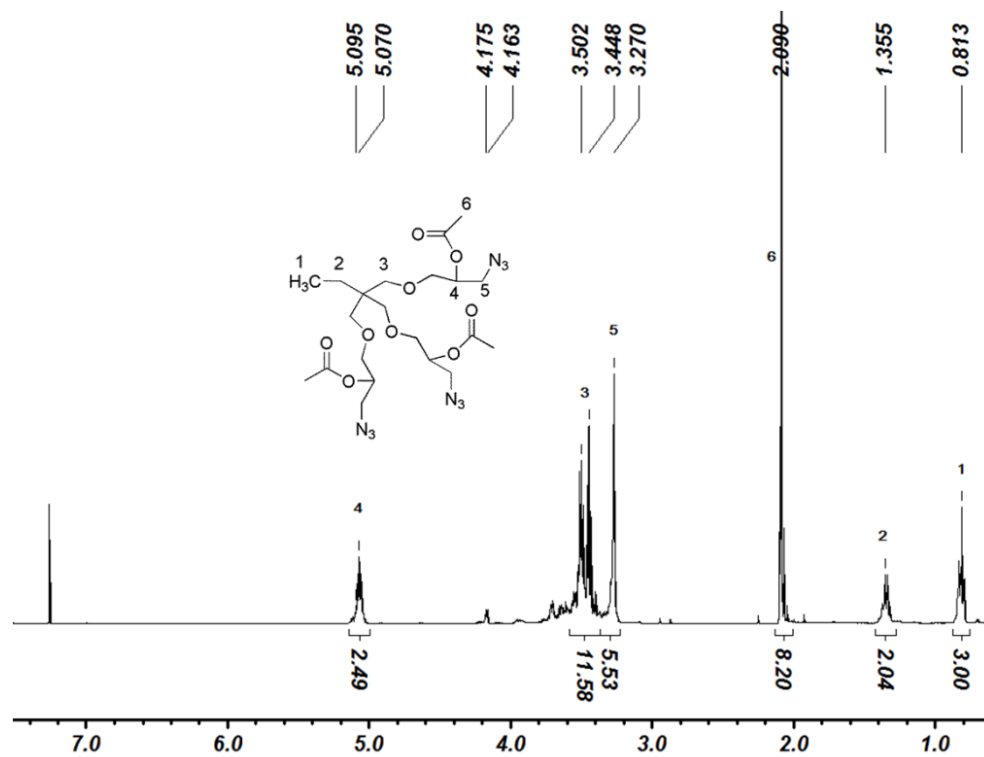


Figure S3. <sup>1</sup>H NMR of triazide compound (1)

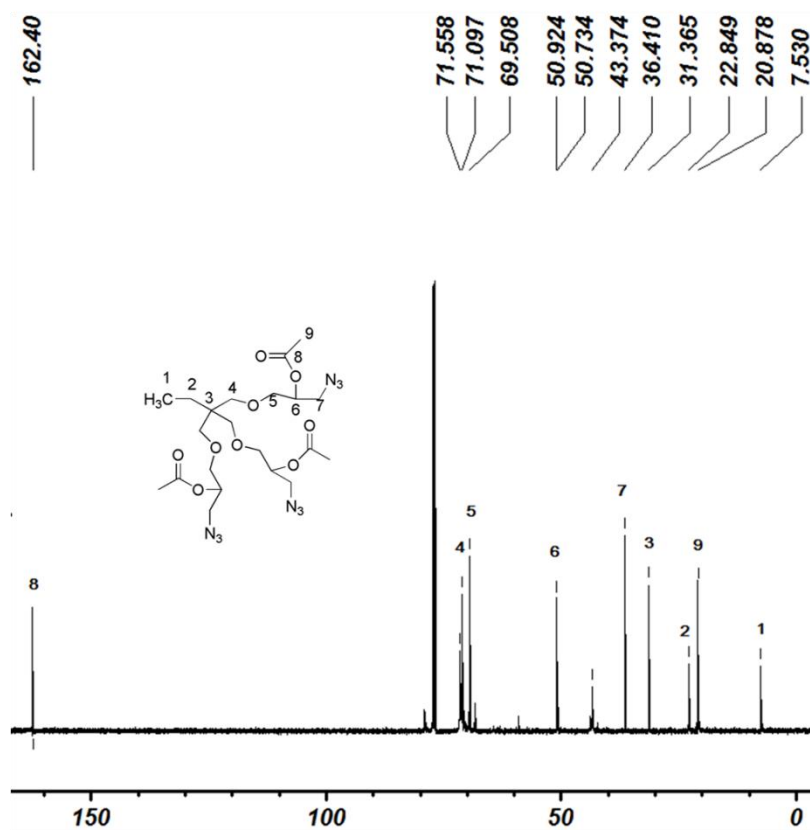
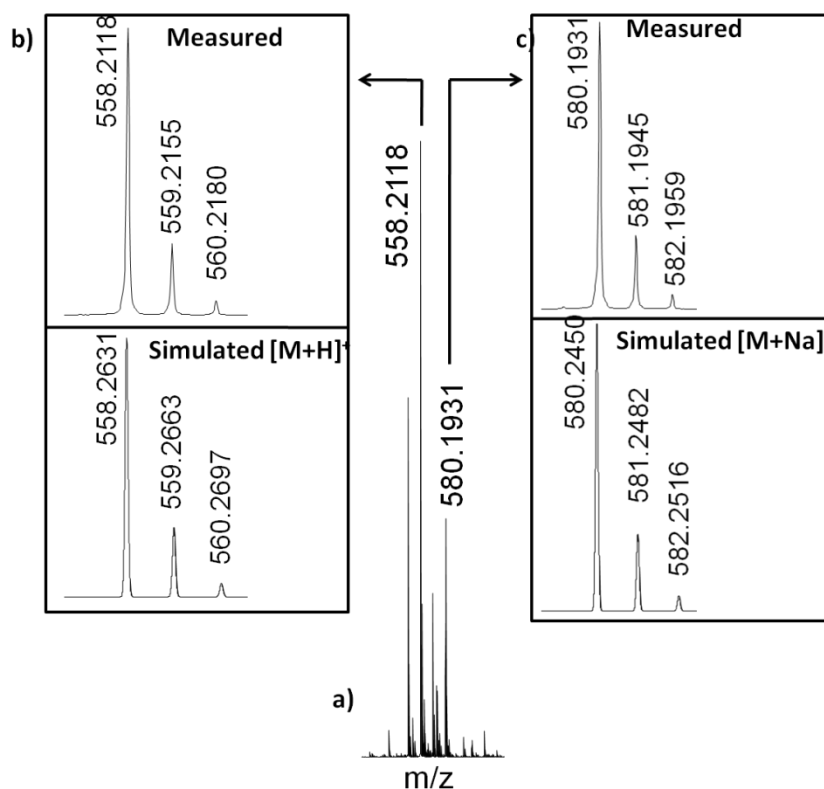


Figure S4. <sup>13</sup>C NMR of triazide compound (1)

## III. RESULT AND DISCUSSION



**Figure S5.** a) ESI-TOF-MS spectrum of compound (1), measured (top) and simulated (bottom) isotopic pattern of (1) b) with proton adduct ( $M = C_{21}H_{35}N_9O_9$ ,  $[M+H]^+$ ) and c) with sodium adduct ( $M = C_{21}H_{35}N_9O_9$ ,  $[M+Na]^+$ )

### 5-2- Trivalent alkyne (2)

**Synthesis of 1-(prop-2-ynyloxy)-2,2-bis(prop-2-ynyloxy)methyl)butane (2).** The synthesis followed a procedure with minor modification of previously reported procedures.<sup>1,2</sup> Trimethylolpropane (0.050 mol, 6.7 g) was weighted into a dry 100 mL round bottom flask equipped with a magnetic stir bar and septum. Sodium hydroxide (0.300 mol, 12.0 g), water (2.0 mL), and tetrabutylammonium bromide (TBAB) (2.482  $\mu$ mol, 0.8 g) were added and the mixture was degassed with nitrogen for 20 minutes. Afterwards propargyl bromide (0.300 mol, 45.0 g, 33.7 mL, 80 wt% solution in toluene) was added drop wise over the course of 1 h, and the temperature was slowly raised to 60°C over the course of 1 h followed by stirring for another 22 h at 60°C. The reaction mixture was then cooled and diluted with dichloromethane (150 mL), washed five times with 150 mL water and the organic phase was dried over sodium sulphate, filtered and the solvent was evaporated under reduced pressure. Further purification was done with flash column chromatography using chloroform: methanol, 30:1. (yield: 85 %) <sup>1</sup>H-NMR (400 MHz, CDCl<sub>3</sub>) ppm 4.11 (d,  $J = 2.41$  Hz, 6H), 3.39 (s, 6H), 2.39 (t,  $J = 2.38$  Hz, 3H), 1.42 (q,  $J = 7.58$  Hz, 2H), 0.87 (t,  $J = 7.58$  Hz, 3H); <sup>13</sup>C-NMR (100 MHz, CDCl<sub>3</sub>) ppm 80.1, 73.7, 70.3, 58.6, 42.8, 22.8, 7.5. ESI-TOF-MS, Measured: 271.11 Da Simulated: 271.13 Da [C<sub>12</sub>H<sub>20</sub>O<sub>3</sub>+Na]<sup>+</sup>.

III.RESULT AND DISCUSSION

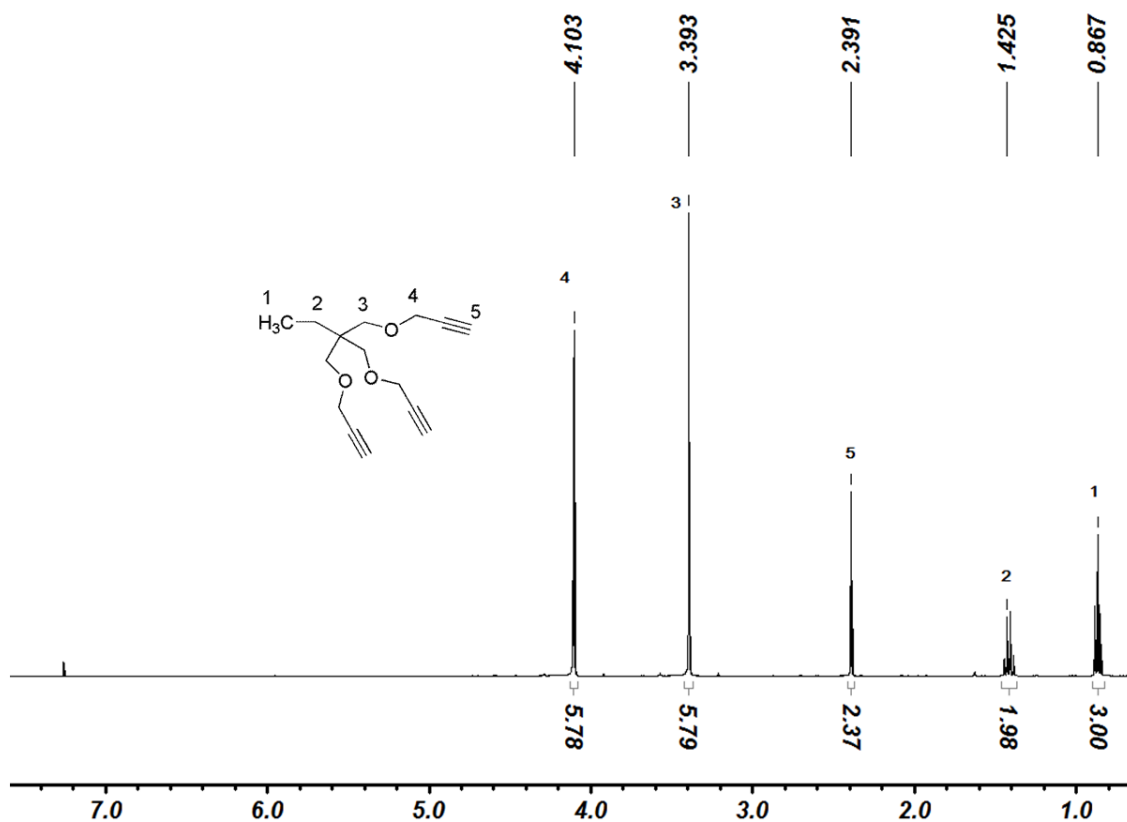


Figure S6. <sup>1</sup>H NMR of trialkyne compound (2)

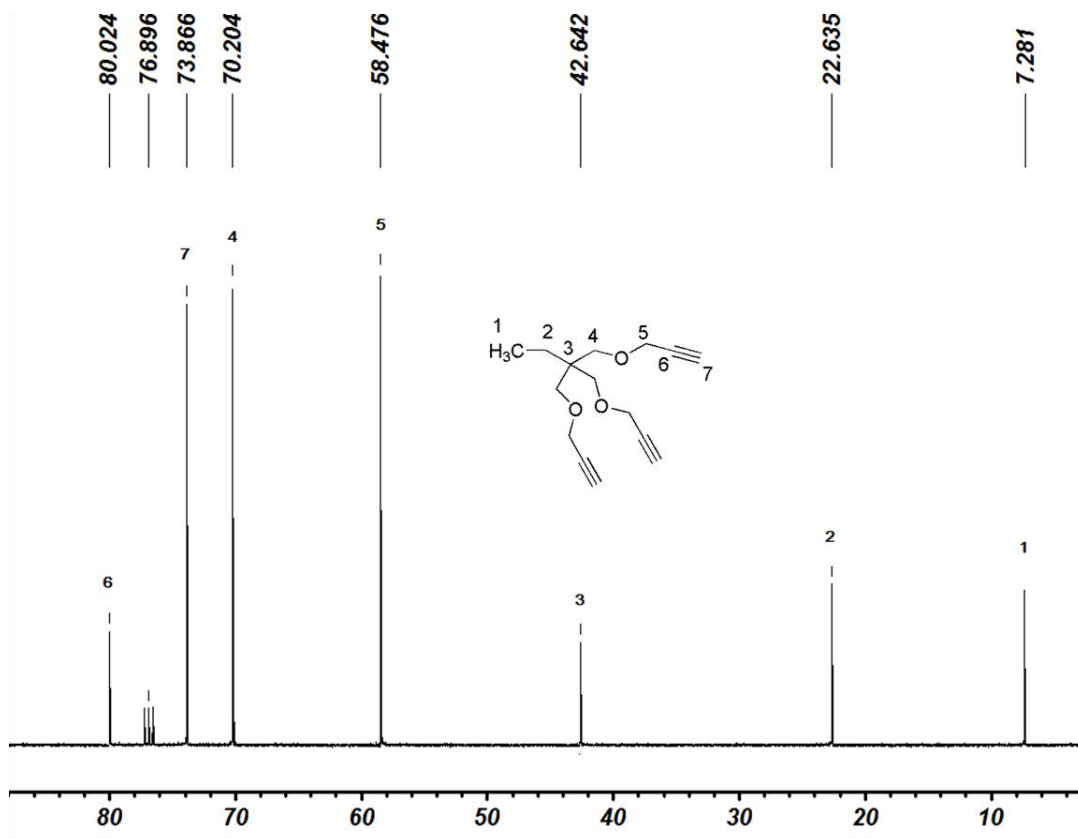
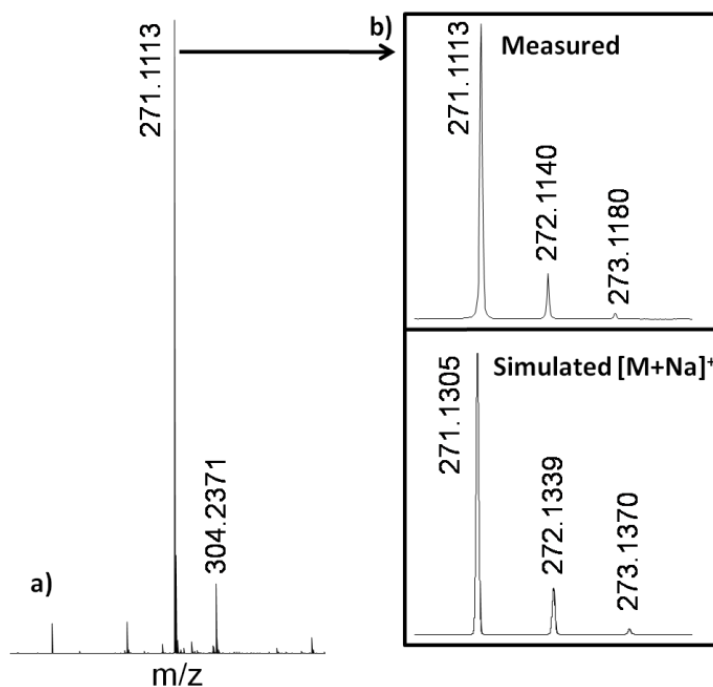
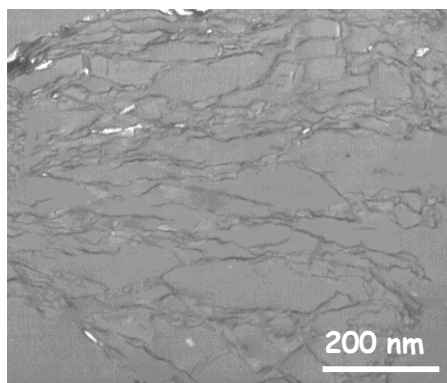


Figure S7. <sup>13</sup>C NMR of trialkyne compound (2)



**Figure S8.** a) ESI-TOF-MS spectrum compound of (2), measured (top) and simulated (bottom) isotopic pattern of (1) b) with sodium adduct ( $M = C_{12}H_{20}O_3$ ,  $[M+Na]^+$ )

#### 6-TEM image of dispersion of TRGO-Cu<sub>2</sub>O in resin materials.



**Figure S9.** TEM image of TRGO-Cu<sub>2</sub>O (1 mass%) dispersion in cured resin materials

#### 7-Equations and reaction models for model fitting of click crosslinking reaction with different catalysts

The DSC measurement indicates further details of the reaction kinetics through model fitting. The rate of the reaction ( $\frac{d\alpha}{dt}$ ) described by two separable functions,  $K(T)$  and  $f(\alpha)$  in equation (Eq.S1)

$$\frac{d\alpha}{dt} = K(T) \cdot f(\alpha) \quad (\text{Eq.S1})$$

**Table S1.** Reaction models which are used for fitting the experimental results.

Reaction model	Model symbol	$f(\alpha)$	Parameters
First order	F1	$(1 - \alpha)$	A
Second order	F2	$(1 - \alpha)^2$	A
nth order	Fn	$(1 - \alpha)^n$	A, n
nth order with autocatalysis	Cn	$(1 - \alpha)^n (+K_{cat}\alpha)$	A, n, $K_{cat}$
Prout-Tompkins equation (autocatalytic)	PT	$(1 - \alpha)^n \alpha^m$	A, n, m



## III.RESULT AND DISCUSSION

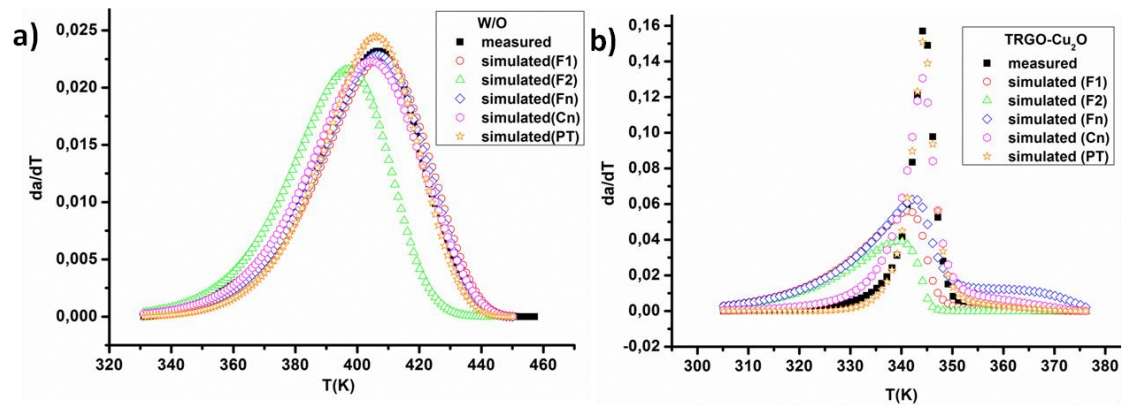


**Figure S10.** Model fits of DSC data for the CuAAC crosslinking reaction a) without catalyst and b) TRGO-Cu<sub>2</sub>O (1 mol% per functional group, 5 °C/min heating rate).

Where  $\left(\frac{d\alpha}{dt}\right)$  is the rate of the reaction,  $\alpha$  is the conversion,  $T$  is the absolute temperature in  $K$ ,  $f(\alpha)$  is a function related to the reaction type and conversion (Table S1), and  $K(T)$  is the temperature-dependent rate constant described by the Arrhenius equation (Eq. S2)

$$K(T) = A \cdot \exp\left(-\frac{E_a}{RT}\right) \text{ (Eq.S2)}$$

where  $R$  is the universal gas constant,  $E_a$  is the activation energy, and  $A$  is the pre-exponential factor. For experiments in which samples are heated at a constant rate, equation S2 can be rewrite like this,

$$\frac{d\alpha}{dt} = \frac{A}{\beta} \cdot \exp\left(-\frac{E_a}{RT}\right) \cdot f(\alpha) \text{ (Eq.S3)}$$

Where  $\beta = \frac{dT}{dt}$ . To simplify the calculation, the constant value of activation energy ( $E_a$ ) from Kissinger's analysis is taken as an approximation to replace the  $E_a$  in equation S3. The pre-exponential factor  $A$  and reaction orders ( $n$  and  $m$ ) are determined by the best fitting results.

1. M. Schunack, M. Gragert, D. Döhler, P. Michael and W. H. Binder, *Macromol. Chem. Phys.*, 2012, **213**, 205-214.
2. I. E. Gorman, R. L. Willer, L. K. Kemp and R. F. Storey, *Polymer*, 2012, **53**, 2548-2558.

## IV.SUMMARY

The main objective of this thesis was to develop the new resin (polymer)/graphene nanocomposite for high performance applications useful in the aerospace and marine industries while the unique physical and mechanical properties of graphene such as high tensile strength, thermal and electrical conductivity incorporated to the final resin(polymer)/graphene composite. Therefore, a CuAAC crosslinking (polymerization) reaction using Cu(I)/graphene heterogeneous catalyst had been chosen to decrease the time and the temperature of the curing process while inducing the novel properties of graphene and achieving better dispersion of graphene particles into the final resin material in a one facile step.

Accordingly, the Cu(I) catalyst was immobilized on the surface of graphene-based materials. For this purpose, graphene oxide (GO) and reduced graphene oxide (r-GO) were chosen because GO and r-GO possess the residual oxygen containing groups on their surfaces which enable further functionalization, and the defects on their surfaces are increasing the catalytic activity by acting as a reaction site, and by increasing the band gap of the graphene-based materials. Finally GO and r-GO can be prepared in a large scale using low cost graphite as the starting material. Thus graphite was oxidized to graphene oxide (GO) by Hummers' method. Subsequently GO was reduced to reduced graphene oxide (r-GO) both thermally in an oven at high temperatures, and chemically using different reducing agents like hydrazine, sodium borohydride, ascorbic acid and ammonia/sodium mixture.

The immobilization of the Cu(I) particles on the surface of reduced graphene oxide (r-GO) was accomplished *via* both the "ex situ hybridization", and the "in situ crystallization" methods to investigate and compare the loading effects, the catalytic activity including kinetics studies, the recyclability, the leaching and the feasibility of their production in a large scale. Finally, the catalyst with the higher activity was chosen to be used in a CuAAC crosslinking reaction for the resin/graphene nanocomposite production.

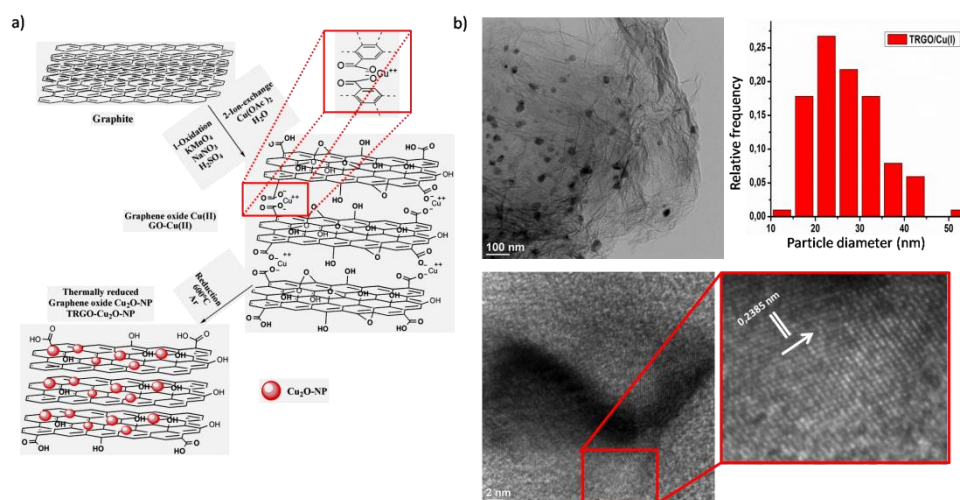


**Figure 33.** a) *In situ* crystallization method towards graphene/Cu(I) catalyst b) TEM, particle size distribution and HRTEM of graphene/Cu(I) hybrid

In the “*in situ crystallization*” method, GO was reacted with copper(II) acetate ( $\text{Cu}(\text{OAc})_2$ ) to exchange the protons of the carboxylic groups of GO with Cu(II) particles in order to immobilize Cu(II) onto the surface of GO (GO-Cu(II)), afterwards GO-Cu(II) was thermally reduced in an oven under the stream of nitrogen at 600 °C to obtain r-GO decorated with the Cu(I) nanoparticles (Figure 33a). The morphology and the chemical composition of the nanoparticles on the surface were investigated using TEM, HRTEM, STEM-EDXS, XPS and FAAS methods. TEM and HRTEM revealed the highly dispersed copper particles on the surface of r-GO with an average particle size of 25 nm and a lattice distance of  $0.2385 \pm 0.01$  nm which can be related to CuO or  $\text{Cu}_2\text{O}$  (Figure 33b). Therefore, STEM-EDXS method was applied to study the composition of the nanoparticles in detail, and it was observed that Cu and O atoms were existed in a ratio of 68.8:31.2 (2:1) for the selected particles on the surface confirming that the copper particles were present in the  $\text{Cu}_2\text{O}$  crystal form (Figure 34a).

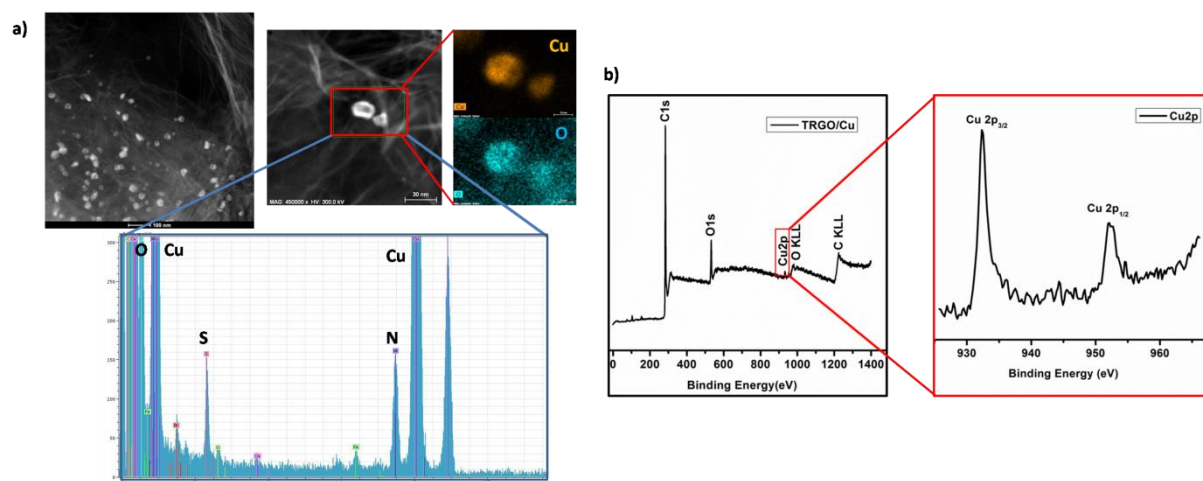


**Figure 34.** a) STEM-EDXS spectra of the selected particle on the surface b) the survey XPS and the high resolution XPS of the Cu 2P region

Furthermore, the overall valence of the copper nanoparticles on the surface was studied *via* the high resolution XPS measurement for Cu 2P area (Figure 34b), where peaks located at 932.37 eV and 952.31 eV corresponded to the peak energy of the Cu(I). Also there were no peak satellites at 942 eV and 962 eV and no peak at 934.8 eV which would be related to the Cu(II). All of these investigations strongly supported that the particles were  $\text{Cu}_2\text{O}$  crystals, and the oxidation state of the Cu was the Cu(I) required for a CuAAC reaction. The Cu content of the sample was also determined by the flame atomic absorption spectroscopy (FAAS) as  $7.55 \times 10^{-7} \text{ mol.mg}^{-1}$  loading. The obtained catalyst named as TRGO- $\text{Cu}_2\text{O}$  was highly active in the CuAAC reaction of different azide and alkyne functional molecules, and most of the reactions reached the complete conversion in 48 h at 20 °C to 40 °C. The kinetics measurement of the CuAAC reaction between phenyl acetylene and benzyl azide using TRGO- $\text{Cu}_2\text{O}$  as the catalyst exhibited the rate constant of  $k' = 1.33 \text{ M}^{-1.3} \cdot \text{h}^{-1}$ , which was in the same range of the CuAAC reaction using  $\text{CuSO}_4$  and sodium ascorbate as the catalytic system. Moreover TRGO- $\text{Cu}_2\text{O}$

was recyclable up to 4 times, and the deactivation of the catalyst was related to the aggregation of  $\text{Cu}_2\text{O}$  on the surface not to the leaching.

For the “*ex situ hybridization*” method, *N*-heterocyclic carbene (NHC) functional groups had been chosen for the functionalization of the surface of r-GO. Therefore, the surface of r-GO (reduced by ascorbic acid) was modified by the imidazolium groups in a three step reaction (Figure 35a) : firstly the surface of r-GO was treated with chloroethyl isocyanate to functionalize the surface by the chlorine groups (CRGO-Cl), subsequently the chlorine groups on the surface were inverted to the azide groups by sodium azide (CRGO- $\text{N}_3$ ), finally in a CuAAC reaction between the azide functional groups of r-GO and 1-propargyl 3-methylimidazolium, the imidazolium moieties were added to the surface (CRGO-Ima). The successful functionalization in each step of the reaction was proved by XRD, RAMAN, XPS and TGA measurements, where in the latter one the amount of the imidazolium groups on the surface of r-GO was measured to be  $3.4 \times 10^{-4} \text{ mmol.mg}^{-1}$  (Figure 35b). The XPS measurement after the CuAAC reaction on the surface showed no peak of the azide groups on the surface proving the completion of the click reaction. Furthermore no additional defects were added to the surface of r-GO by any step of the reaction as proven by the RAMAN spectra. This amount of the imidazolium functional groups on the surface was able to stabilize r-GO in most of the organic solvents such as ethanol, pyridine and chloroform (Figure 35c), furthermore the solution of CRGO-Ima in water was stable up to 12 h (Figure 35d). This dispersibility property could increase the catalytic activity of the catalyst in solution.

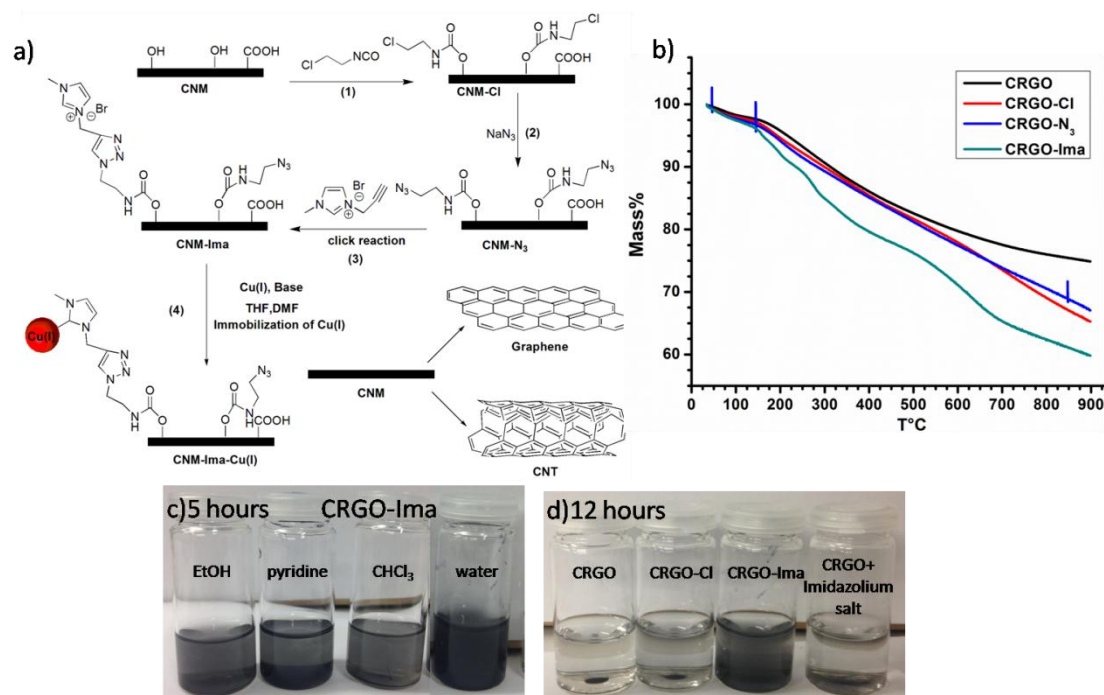


**Figure 35.** a) Synthetic route towards NHC-Cu(I) immobilized graphene-based materials b) TGA measurement after each step of reactions c) the dispersibility of CRGO-Ima in different solvents d) the dispersibility of CRGO-Ima in water

Afterwards the proton of the imidazolium groups was exchanged with the  $\text{Cu(I)}$  to achieve the NHC-Cu(I) bond on the surface of r-GO (CRGO-Ima-Cu(I)) (Figure 35a, route 4). The high resolution XPS

measurement revealed that the valence of the copper on the surface is the Cu(I) (Figure 36a)(peaks at 932.37 eV and 952.31 eV corresponded to the peak energy of Cu(I)), TEM measurement showed the existence of the small copper nanoparticles with an average size of 7 nm (Figure 36b) related to the aggregations of the copper clusters (Figure 36c) and the copper content on the surface was  $2.8 \times 10^{-7} \text{ mol.mg}^{-1}$  as measured by the FAAS.

The CuAAC reactions between different azide and alkyne functionalized molecules using CRGO-Ima-Cu(I) as the catalyst were completed in 72 h at 40 °C. The kinetics measurement of the CuAAC reaction between phenyl acetylene and benzyl azide using CRGO-Ima-Cu(I) as the catalyst exhibited two rate constants of  $k_1' = 0.14 \text{ M}^{-1.3} \cdot \text{h}^{-1}$  (between the reaction time of 0-48 h), and  $k_2' = 1.91 \text{ M}^{-1.3} \cdot \text{h}^{-1}$  (between the reaction time of 48-72 h). Moreover as-synthesized catalyst exhibited the high recyclability up to 10 times with the slight reduction in conversion and without leaching to the organic product.

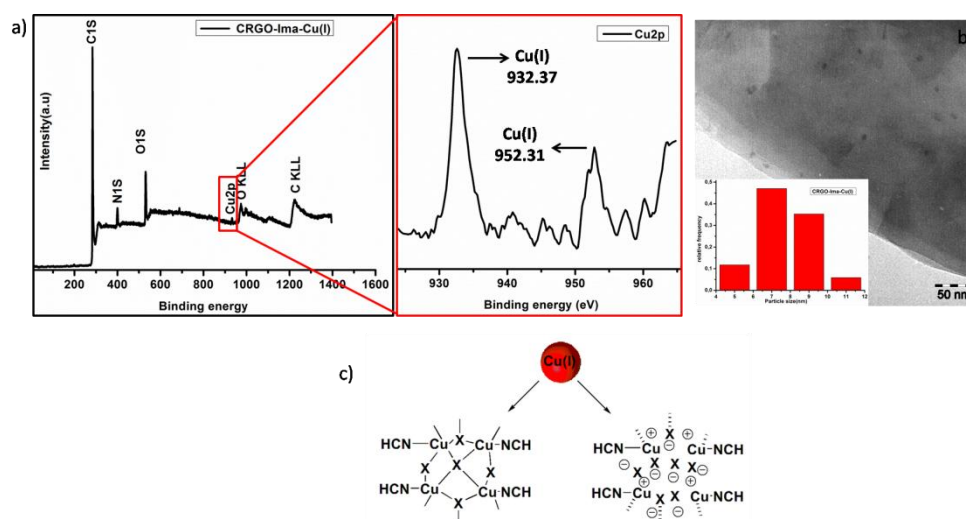


**Figure 36.** a) XPS and b) TEM measurements of CRGO-Ima-Cu(I) c) proposed aggregation of copper particles on the surface

Comparing these two methods for the immobilization of Cu(I), the catalyst achieved by the “*in situ* crystallization” (TRGO-Cu<sub>2</sub>O) exhibited higher loadings of copper together with higher catalytic activities towards the CuAAC reaction. Moreover the synthetic pathway towards TRGO-Cu<sub>2</sub>O catalyst was simpler, and could be produced in a large scale, whereas functionalization of r-GO with the imidazolium groups and anchoring the Cu(I) particles onto the NHC groups required a multi step reaction.

Therefore for the CuAAC crosslinking reaction and the production of the resin/graphene nanocomposite materials TRGO-Cu<sub>2</sub>O was chosen as the catalyst due to its high activity and simple producibility. In addition, for the formation of a covalent network, the sufficient molecular mobility is required, in order to keep the diffusion high while getting to a high monomer conversion together with a high molecular weight of the resulted polymer, therefore a low molecular weight trivalent azide and alkyne were synthesized.



The CuAAC crosslinking reaction was run using the trivalent azide and alkyne moieties and TRGO-Cu<sub>2</sub>O as a catalyst in bulk (Figure 37a) and followed *via in-situ* DSC and *in-situ* melt-rheology measurements. Furthermore the catalytic activity of TRGO-Cu<sub>2</sub>O and its effect on the physical properties of the final resin materials were compared with different commercial available homogenous (Cu(PPh<sub>3</sub>)<sub>3</sub>Br and Cu(PPh<sub>3</sub>)<sub>3</sub>F) and heterogeneous (copper on charcoal) Cu(I) catalysts.

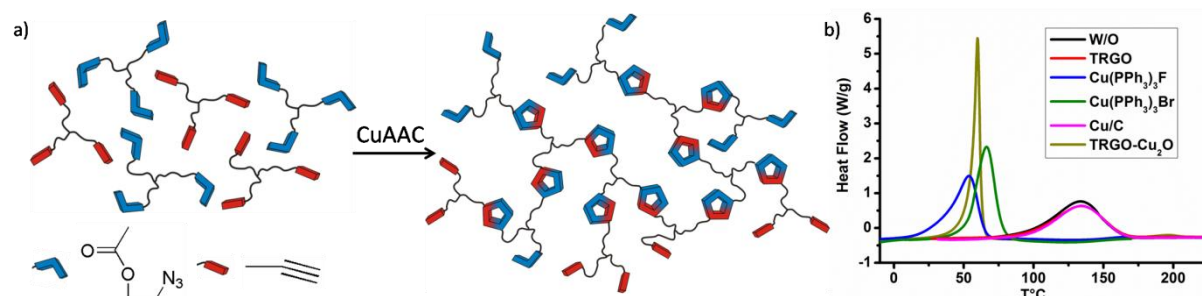


**Figure 37.** a) CuAAC crosslinking reaction between trivalent azide and alkyne moieties b) DSC results of crosslinking reaction using different Cu(I) catalysts

Crosslinking reactions were investigated either *via* DSC measurements using different heating rates or isothermally in a rheometer at different temperatures. The bulk CuAAC crosslinking reaction between the trivalent azide and trivalent alkyne moieties in DSC using 5 °C/*min* as heating rate (Figure 37b) without adding catalyst has occurred at 99.1 °C with 144 *kJ/mol* enthalpy of the reaction. Adding 1 *mol%* of TRGO-Cu<sub>2</sub>O per functional group reduced the reaction temperature to 55 °C and increased the enthalpy to 153 *kJ/mol* showing the superior catalytic activity together with higher crosslinking density in comparison to the reaction without catalyst. Furthermore the reaction temperature was reduced to 52 °C and 37 °C, using Cu(PPh<sub>3</sub>)<sub>3</sub>Br and Cu(PPh<sub>3</sub>)<sub>3</sub>F as homogenous catalysts, respectively. The enthalpy of the reaction has been increased to 158 *kJ/mol* in the case of Cu(PPh<sub>3</sub>)<sub>3</sub>Br, however it reduced to 139 *kJ/mol* for Cu(PPh<sub>3</sub>)<sub>3</sub>F. In addition, the heterogeneous Cu/C catalyst was completely inactive towards the CuAAC crosslinking reaction. Therefore, TRGO-Cu<sub>2</sub>O and Cu(PPh<sub>3</sub>)<sub>3</sub>Br were the suitable catalysts for the CuAAC crosslinking reaction exhibiting the lower reaction temperatures and higher enthalpies.

**Table 10.** Crossover study and physical-mechanical properties like storage modulus, viscosity, conductivity and decomposition temperature of final resin materials cured by different catalysts

Entry	Catalyst	mol%	mass%	crossover time [min]	G' [Pa]	G'' [Pa]	$ \eta^* $ [Pa.S]	Conductivity ( $\sigma_0$ ) (S/m)	T <sub>d</sub> (T°C)
1	Cu(PPh <sub>3</sub> ) <sub>3</sub> Br	1	3.5	270	7.4E+4	1.4E+4	7.5E+3	2.8E-11	296
2	Cu(PPh <sub>3</sub> ) <sub>3</sub> F	1	3.3	35	3.3E+5	2.3E+5	4.0E+4	1.5E-10	291
3	TRGO-Cu <sub>2</sub> O	1	7.6	-	8.6E+6	1.8E+6	8.7E+5	2.2E-4(1.6E-4) <sup>c</sup>	300
4	TRGO	-	7.4	-	3.2E+5	6.4E+4	3.2E+4	-	-
5	TRGO-Cu <sub>2</sub> O	0.1	0.8	409 <sup>a</sup>	1.9E+5	5.5E+4	1.9E+4	5.7E-11	-
6	TRGO-Cu <sub>2</sub> O	0.2	1.6	118 <sup>b</sup>	7.9E+5	5.9E+3	7.9E+4	5.0E-10	-
7	TRGO-Cu <sub>2</sub> O	0.3	2.5	10 <sup>b</sup>	1.5E+6	2.7E+4	1.4E+5	1.8E-10	-
8	TRGO-Cu <sub>2</sub> O	0.5	4.1	- <sup>b</sup>	1.4E+6	5.6E+4	1.4E+5	4.9E-6(4.5E-6) <sup>c</sup>	-
9	Cu/C	1	8.7	-	1.2E+1	1.3E+1	1.74	-	-

<sup>a</sup> 40 °C

<sup>b</sup> 70 °C

<sup>c</sup> 0 °C

Moreover the kinetic studies of the crosslinking reaction were investigated using fitting models with different equations. In the case of TRGO-Cu<sub>2</sub>O, Cu(PPh<sub>3</sub>)<sub>3</sub>Br, and Cu(PPh<sub>3</sub>)<sub>3</sub>F as catalysts, Prout

Tompkins equation (for autocatalytic reactions) was fitted very well with 2.7, 1.95, and 1.14 reaction order, respectively, proving the higher catalytic activity of TRGO-Cu<sub>2</sub>O.

The isothermal crosslinking reaction was performed using *in situ* melt-rheology technique at 20 °C investigating the crossover time using different catalysts (Table 10). The crossover time had happened at 270 *min* and 35 *min* for Cu(PPh<sub>3</sub>)<sub>3</sub>Br and Cu(PPh<sub>3</sub>)<sub>3</sub>F (1 *mol%* per functional group), respectively. However the investigation of the crossover time using 1 *mol%* (8.7 *wt%*) of TRGO-Cu<sub>2</sub>O was not possible since the storage modulus ( $G'$ ) was in the beginning higher than the loss modulus ( $G''$ ) exceeding the rheological percolation threshold of the graphene particles. Therefore the amount of TRGO-Cu<sub>2</sub>O was reduced to 0.1 *mol%* (0.8 *wt%*) showing the crossover time at 409 *min* which was comparable with commercial catalysts, although the amount was 10 times less. In order to investigate the rheological percolation threshold of the TRGO-Cu<sub>2</sub>O particles, the isothermal crosslinking reaction was performed by different amounts of the catalyst 0.1 *mol%* - 0.5 *mol%* (0.8 *wt%* - 4.1 *wt%*) calculating the rheological percolation threshold between 3-4 *wt%* (Table 10). Rheology measurements revealed that the resin which was cured by TRGO-Cu<sub>2</sub>O possessed higher storage modulus (8.6E+6) and viscosity (8.7E+5) comparing to the resins cured by Cu(PPh<sub>3</sub>)<sub>3</sub>Br ( $G' = 7.4E+4$ ,  $\eta^* = 7.5E+3$ ) and Cu(PPh<sub>3</sub>)<sub>3</sub>F ( $G' = 3.3E+5$ ,  $\eta^* = 4.0E+4$ ) proving the effect of r-GO on the final mechanical properties of the final cured resin (Figure 38a).

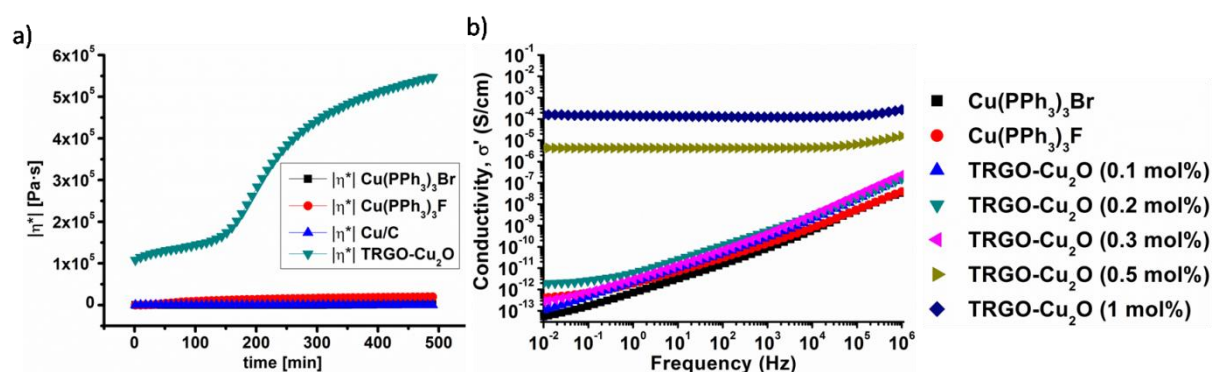


Figure 38. a) Rheology and b) BDS measurements of the final resin materials cured with different catalysts

Additionally, the BDS measurements showed that the resin curing by TRGO-Cu<sub>2</sub>O was conductive at 25 °C and 0 °C with  $2.2E-4$  S/m and  $1.6E-4$  S/m conductivity, respectively. Whereas the resins which were cured by Cu(PPh<sub>3</sub>)<sub>3</sub>Br and Cu(PPh<sub>3</sub>)<sub>3</sub>F were insulating (Figure 38b). By measuring the conductivity of the resins which were cured by different amounts of TRGO-Cu<sub>2</sub>O (0.8 *wt%* - 4.1 *wt%*), the electrical percolation threshold was calculated to be nearly 4 *wt%* (Table 10). Finally, TEM measurements revealed the high dispersion of the r-GO particles within the resin matrix (Figure 39). In conclusion, the innovation of an easy to synthesize and cheap Cu(I)/graphene catalyst (TRGO-Cu<sub>2</sub>O) which was highly active towards the CuAAC reactions led to the production of resin/graphene nanocomposite in a one facile step *via* the CuAAC crosslinking reaction between trivalent azide and



#### IV.SUMMARY

trivalent alkyne moieties. TRGO-Cu<sub>2</sub>O efficiently reduced the crosslinking reaction time and temperature, even exceeding those of the commercial homogenous catalysts. Furthermore by using 4 wt% (0.5 mol% per functional group) of TRGO-Cu<sub>2</sub>O, high performance resin composite material was achieved with high dispersion of graphene particles within the resin matrix which was conductive even at 0 °C, and exhibited improved mechanical properties.

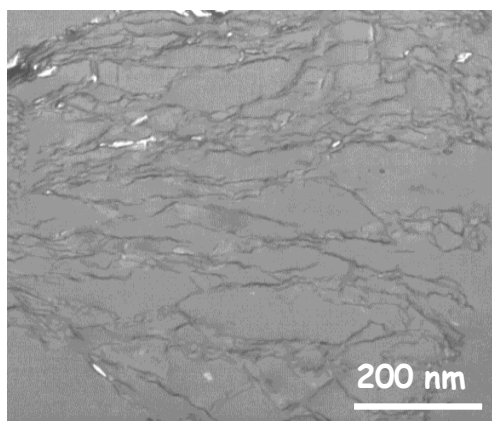


**Figure 39.** TEM image of TRGO-Cu<sub>2</sub>O (1 wt%) dispersion in cured resin materials

## V. REFERENCES

- [1] K. S. Novoselov, A. K. Geim, S. V. Morozov, D. Jiang, Y. Zhang, S. V. Dubonos, I. V. Grigorieva, A. A. Firsov, *Science* **2004**, *306*, 666.
- [2] A. A. Balandin, S. Ghosh, W. Bao, I. Calizo, D. Teweldebrhan, F. Miao, C. N. Lau, *Nano Lett.* **2008**, *8*, 902.
- [3] C. Lee, X. Wei, J. W. Kysar, J. Hone, *Science* **2008**, *321*, 385.
- [4] R. R. Nair, P. Blake, A. N. Grigorenko, K. S. Novoselov, T. J. Booth, T. Stauber, N. M. R. Peres, A. K. Geim, *Science* **2008**, *320*, 1308.
- [5] X. Huang, X. Qi, F. Boey, H. Zhang, *Chem. Soc. Rev.* **2012**, *41*, 666.
- [6] G. Yang, C. Zhu, D. Du, J. Zhu, Y. Lin, *Nanoscale* **2015**, *7*, 14217.
- [7] O. Penkov, H.-J. Kim, H.-J. Kim, D.-E. Kim, *Int. J. Precis. Eng. Manuf.* **2014**, *15*, 577.
- [8] a)J. Liang, Y. Huang, L. Zhang, Y. Wang, Y. Ma, T. Guo, Y. Chen, *Adv. Funct. Mater.* **2009**, *19*, 2297; b)Y. Xu, W. Hong, H. Bai, C. Li, G. Shi, *Carbon* **2009**, *47*, 3538.
- [9] a)H. Kim, C. W. Macosko, *Polymer* **2009**, *50*, 3797; b)G. Eda, M. Chhowalla, *Nano Lett.* **2009**, *9*, 814; c)M. Yoonessi, J. R. Gaier, *ACS Nano* **2010**, *4*, 7211.
- [10] A. K. Geim, K. S. Novoselov, *Nat. Mater.* **2007**, *6*, 183.
- [11] D. R. Dreyer, S. Park, C. W. Bielawski, R. S. Ruoff, *Chem. Soc. Rev.* **2010**, *39*, 228.
- [12] a)C. Huang, C. Li, G. Shi, *Energy Environ. Sci.* **2012**, *5*, 8848; b)S. Navalon, A. Dhakshinamoorthy, M. Alvaro, H. Garcia, *Chem. Rev.* **2014**, *114*, 6179; c)Y. Cheng, Y. Fan, Y. Pei, M. Qiao, *Catal. Sci. Technol.* **2015**, *5*, 3903; d)C. K. Chua, M. Pumera, *Chem. Eur. J.* **2015**, *21*, 12550; e)B. F. Machado, P. Serp, *Catal. Sci. Technol.* **2012**, *2*, 54.
- [13] C. N. R. Rao, A. K. Sood, K. S. Subrahmanyam, A. Govindaraj, *Angew. Chem. Int. Ed.* **2009**, *48*, 7752.
- [14] a)L. Hu, X. Hu, X. Wu, C. Du, Y. Dai, J. Deng, *Physica B* **2010**, *405*, 3337; b)K. Nakada, A. Ishii, *Solid State Commun.* **2011**, *151*, 13.
- [15] a)O. Leenaerts, B. Partoens, F. M. Peeters, *Phys. Rev. B* **2008**, *77*, 125416; b)C. Rajesh, C. Majumder, H. Mizuseki, Y. Kawazoe, *J. Chem. Phys.* **2009**, *130*, 124911.
- [16] a)X. Huang, Z. Yin, S. Wu, X. Qi, Q. He, Q. Zhang, Q. Yan, F. Boey, H. Zhang, *Small* **2011**, *7*, 1876; b)C. Soldano, A. Mahmood, E. Dujardin, *Carbon* **2010**, *48*, 2127.
- [17] C. Biswas, Y. H. Lee, *Adv. Funct. Mater.* **2011**, *21*, 3806.
- [18] a)X.-K. Kong, C.-L. Chen, Q.-W. Chen, *Chem. Soc. Rev.* **2014**, *43*, 2841; b)J. Albero, H. Garcia, *J. Mol. Catal. A: Chem.* **2015**, *408*, 296; c)J. Duan, S. Chen, M. Jaroniec, S. Z. Qiao, *ACS Catal.* **2015**, *5*, 5207.
- [19] a)D. R. Dreyer, C. W. Bielawski, *Chem. Sci.* **2011**, *2*, 1233; b)X. Fan, G. Zhang, F. Zhang, *Chem. Soc. Rev.* **2015**, *44*, 3023; c)H. Hu, J. H. Xin, H. Hu, X. Wang, Y. Kong, *Appl. Catal., A* **2015**, *492*, 1; d)C. Su, K. P. Loh, *Acc. Chem. Res.* **2013**, *46*, 2275; e)D. S. Su, S. Perathoner, G. Centi, *Chem. Rev.* **2013**, *113*, 5782; f)S. Zhu, J. Wang, W. Fan, *Catal. Sci. Technol.* **2015**, *5*, 3845.
- [20] a)D. Chen, H. Feng, J. Li, *Chem. Rev.* **2012**, *112*, 6027; b)Y. Zhu, S. Murali, W. Cai, X. Li, J. W. Suk, J. R. Potts, R. S. Ruoff, *Adv. Mater.* **2010**, *22*, 3906.
- [21] a)C. Mattevi, G. Eda, S. Agnoli, S. Miller, K. A. Mkhoyan, O. Celik, D. Mastrogiovanni, G. Granozzi, E. Garfunkel, M. Chhowalla, *Adv. Funct. Mater.* **2009**, *19*, 2577; b)H. A. Becerril, J. Mao, Z. Liu, R. M. Stoltenberg, Z. Bao, Y. Chen, *ACS Nano* **2008**, *2*, 463.
- [22] a)D. A. Dikin, S. Stankovich, E. J. Zimney, R. D. Piner, G. H. B. Dommett, G. Evmenenko, S. T. Nguyen, R. S. Ruoff, *Nature* **2007**, *448*, 457; b)S. Park, K.-S. Lee, G. Bozoklu, W. Cai, S. T. Nguyen, R. S. Ruoff, *ACS Nano* **2008**, *2*, 572.
- [23] a)C. E. Hamilton, J. R. Lomeda, Z. Sun, J. M. Tour, A. R. Barron, *Nano Lett.* **2009**, *9*, 3460; b)Y. Hernandez, V. Nicolosi, M. Lotya, F. M. Blighe, Z. Sun, S. De, I. T. McGovern, B. Holland, M. Byrne, Y. K. Gun'Ko, J. J. Boland, P. Niraj, G. Duesberg, S. Krishnamurthy, R. Goodhue, J. Hutchison, V. Scardaci, A. C. Ferrari, J. N. Coleman, *Nat. Nano.* **2008**, *3*, 563; c)U. Khan, P. May, A. O'Neill, J. N. Coleman, *Carbon* **2010**, *48*, 4035; d)U. Khan, A. O'Neill, M. Lotya, S. De, J. N. Coleman, *Small* **2010**, *6*, 864; e)M. Lotya, Y. Hernandez, P. J. King, R. J. Smith, V. Nicolosi, L. S. Karlsson, F. M. Blighe, S. De, Z. Wang, I. T. McGovern, G. S. Duesberg, J. N. Coleman, *J. Am.*

- Chem. Soc.* **2009**, *131*, 3611; f) M. Lotya, P. J. King, U. Khan, S. De, J. N. Coleman, *ACS Nano* **2010**, *4*, 3155; g) X. Lu, H. Huang, N. Nemchuk, R. S. Ruoff, *Appl. Phys. Lett.* **1999**, *75*, 193; h) M. Park, S. Seo, I. S. Lee, J. H. Jung, *Chem. Commun.* **2010**, *46*, 4478; i) Timothy J. Mason, J. P. Lorimer, Wiley-VCH, **2002**; j) Y. Zhang, J. P. Small, W. V. Pontius, P. Kim, *Appl. Phys. Lett.* **2005**, *86*, 073104.
- [24] a) B. C. Brodie, *Philos. Trans. R. Soc. London* **1859**, *149*, 249; b) P. Cui, J. Lee, E. Hwang, H. Lee, *Chem. Commun.* **2011**, *47*, 12370; c) J. Dong, B. Zeng, Y. Lan, S. Tian, Y. Shan, X. Liu, Z. Yang, H. Wang, Z. F. Ren, *J. Nanosci. Nanotechnol.* **2010**, *10*, 5051; d) S. Eigler, C. Dotzer, A. Hirsch, M. Enzelberger, P. Müller, *Chem. Mater.* **2012**, *24*, 1276; e) S. Eigler, M. Enzelberger-Heim, S. Grimm, P. Hofmann, W. Kroener, A. Geworski, C. Dotzer, M. Röckert, J. Xiao, C. Papp, O. Lytken, H.-P. Steinrück, P. Müller, A. Hirsch, *Adv. Mater.* **2013**, *25*, 3583; f) Z. Fan, K. Wang, T. Wei, J. Yan, L. Song, B. Shao, *Carbon* **2010**, *48*, 1686; g) M. J. Fernández-Merino, L. Guardia, J. I. Paredes, S. Villar-Rodil, P. Solís-Fernández, A. Martínez-Alonso, J. M. D. Tascón, *J. Phys. Chem. C* **2010**, *114*, 6426; h) J. Gao, F. Liu, Y. Liu, N. Ma, Z. Wang, X. Zhang, *Chem. Mater.* **2010**, *22*, 2213; i) W. Gao, L. B. Alemany, L. Ci, P. M. Ajayan, *Nat. Chem.* **2009**, *1*, 403; j) H. He, T. Riedl, A. Lerf, J. Klinowski, *J. Phys. Chem.* **1996**, *100*, 19954; k) U. Hofmann, R. Holst, *Ber. Dtsch. Chem. Ges. A and B* **1939**, *72*, 754; l) I. Janowska, K. Chizari, O. Ersen, S. Zafeiratos, D. Soubane, V. Costa, V. Speisser, C. Boeglin, M. Houllé, D. Bégin, D. Plee, M.-J. Ledoux, C. Pham-Huu, *Nano Res.* **2010**, *3*, 126; m) S. Kim, S. Zhou, Y. Hu, M. Acik, Y. J. Chabal, C. Berger, W. de Heer, A. Bongiorno, E. Riedo, *Nat. Mater.* **2012**, *11*, 544; n) D. C. Marcano, D. V. Kosynkin, J. M. Berlin, A. Sinitskii, Z. Sun, A. Slesarev, L. B. Alemany, W. Lu, J. M. Tour, *ACS Nano* **2010**, *4*, 4806; o) M. J. McAllister, J.-L. Li, D. H. Adamson, H. C. Schniepp, A. A. Abdala, J. Liu, M. Herrera-Alonso, D. L. Milius, R. Car, R. K. Prud'homme, I. A. Aksay, *Chem. Mater.* **2007**, *19*, 4396; p) I. K. Moon, J. Lee, R. S. Ruoff, H. Lee, *Nat. Commun.* **2010**, *1*, 73; q) A. V. Murugan, T. Muraliganth, A. Manthiram, *Chem. Mater.* **2009**, *21*, 5004; r) T. Nakajima, A. Mabuchi, R. Hagiwara, *Carbon* **1988**, *26*, 357; s) S. Pei, J. Zhao, J. Du, W. Ren, H.-M. Cheng, *Carbon* **2010**, *48*, 4466; t) G. Ruess, *Monatsh. Chem.* **1947**, *76*, 381; u) H. C. Schniepp, J.-L. Li, M. J. McAllister, H. Sai, M. Herrera-Alonso, D. H. Adamson, R. K. Prud'homme, R. Car, D. A. Saville, I. A. Aksay, *J. Phys. Chem. B* **2006**, *110*, 8535; v) W. Scholz, H. P. Boehm, *Z. Anorg. Allg. Chem.* **1969**, *369*, 327; w) H.-J. Shin, K. K. Kim, A. Benayad, S.-M. Yoon, H. K. Park, I.-S. Jung, M. H. Jin, H.-K. Jeong, J. M. Kim, J.-Y. Choi, Y. H. Lee, *Adv. Funct. Mater.* **2009**, *19*, 1987; x) S. Stankovich, D. A. Dikin, R. D. Piner, K. A. Kohlhaas, A. Kleinhammes, Y. Jia, Y. Wu, S. T. Nguyen, R. S. Ruoff, *Carbon* **2007**, *45*, 1558; y) L. Staudenmaier, *Ber. Dtsch. Chem. Ges.* **1898**, *31*, 1481; z) J. Zhang, H. Yang, G. Shen, P. Cheng, J. Zhang, S. Guo, *Chem. Commun.* **2010**, *46*, 1112; aa) W. S. Hummers, R. E. Offeman, *J. Am. Chem. Soc.* **1958**, *80*, 1339.
- [25] a) X. Li, G. Zhang, X. Bai, X. Sun, X. Wang, E. Wang, H. Dai, *Nat. Nano.* **2008**, *3*, 538; b) S. R. Dhakate, N. Chauhan, S. Sharma, J. Tawale, S. Singh, P. D. Sahare, R. B. Mathur, *Carbon* **2011**, *49*, 1946.
- [26] a) K. Parvez, Z.-S. Wu, R. Li, X. Liu, R. Graf, X. Feng, K. Müllen, *J. Am. Chem. Soc.* **2014**, *136*, 6083; b) S. Yang, S. Brüller, Z.-S. Wu, Z. Liu, K. Parvez, R. Dong, F. Richard, P. Samorì, X. Feng, K. Müllen, *J. Am. Chem. Soc.* **2015**, *137*, 13927.
- [27] a) M. Losurdo, M. M. Giangregorio, P. Capezuto, G. Bruno, *Phys. Chem. Chem. Phys.* **2011**, *13*, 20836; b) A. W. Robertson, J. H. Warner, *Nano Lett.* **2011**, *11*, 1182; c) A. T. Murdock, A. Koos, T. B. Britton, L. Houben, T. Batten, T. Zhang, A. J. Wilkinson, R. E. Dunin-Borkowski, C. E. Lekka, N. Grobert, *ACS Nano* **2013**, *7*, 1351; d) L. Wang, X. Zhang, H. L. W. Chan, F. Yan, F. Ding, *J. Am. Chem. Soc.* **2013**, *135*, 4476; e) Y. Zhang, L. Zhang, C. Zhou, *Acc. Chem. Res.* **2013**, *46*, 2329.
- [28] a) C. Berger, Z. Song, X. Li, X. Wu, N. Brown, C. Naud, D. Mayou, T. Li, J. Hass, A. N. Marchenkov, E. H. Conrad, P. N. First, W. A. de Heer, *Science* **2006**, *312*, 1191; b) C. Berger, Z. Song, T. Li, X. Li, A. Y. Ogbazghi, R. Feng, Z. Dai, A. N. Marchenkov, E. H. Conrad, P. N. First, W. A. de Heer, *J. Phys. Chem. B* **2004**, *108*, 19912; c) K. V. Emtsev, A. Bostwick, K. Horn, J. Jobst, G. L. Kellogg, L. Ley, J. L. McChesney, T. Ohta, S. A. Reshanov, J. Rohrl, E. Rotenberg, A. K. Schmid, D. Waldmann, H. B. Weber, T. Seyller, *Nat. Mater.* **2009**, *8*, 203.

- [29] a)X. Wang, L. Zhi, N. Tsao, Ž. Tomović, J. Li, K. Müllen, *Angew. Chem. Int. Ed.* **2008**, *47*, 2990; b)X. Yan, X. Cui, L.-s. Li, *J. Am. Chem. Soc.* **2010**, *132*, 5944.
- [30] a)A. Primo, P. Atienzar, E. Sanchez, J. M. Delgado, H. Garcia, *Chem. Commun.* **2012**, *48*, 9254; b)A. Dhakshinamoorthy, A. Primo, P. Concepcion, M. Alvaro, H. Garcia, *Chem. Eur. J.* **2013**, *19*, 7547.
- [31] C. N. R. Rao, K. Biswas, K. S. Subrahmanyam, A. Govindaraj, *J. Mater. Chem.* **2009**, *19*, 2457.
- [32] a)A. Lerf, H. He, T. Riedl, M. Forster, J. Klinowski, *Solid State Ionics* **1997**, *101–103, Part 2*, 857; b)A. Lerf, H. He, M. Forster, J. Klinowski, *J. Phys. Chem. B* **1998**, *102*, 4477.
- [33] A. C. Ferrari, J. C. Meyer, V. Scardaci, C. Casiraghi, M. Lazzeri, F. Mauri, S. Piscanec, D. Jiang, K. S. Novoselov, S. Roth, A. K. Geim, *Phys. Rev. Lett.* **2006**, *97*, 187401.
- [34] a)S. Eigler, S. Grimm, M. Enzelberger-Heim, P. Müller, A. Hirsch, *Chem. Commun.* **2013**, *49*, 7391; b)S. Eigler, A. Hirsch, *Angew. Chem. Int. Ed.* **2014**, *53*, 7720.
- [35] Z.-J. Fan, W. Kai, J. Yan, T. Wei, L.-J. Zhi, J. Feng, Y.-m. Ren, L.-P. Song, F. Wei, *ACS Nano* **2011**, *5*, 191.
- [36] a)G. M. Scheuermann, L. Rumi, P. Steurer, W. Bannwarth, R. Mülhaupt, *J. Am. Chem. Soc.* **2009**, *131*, 8262; b)Y. Li, X. Fan, J. Qi, J. Ji, S. Wang, G. Zhang, F. Zhang, *Mater. Res. Bull.* **2010**, *45*, 1413; c)A. R. Siamaki, A. E. R. S. Khder, V. Abdelsayed, M. S. El-Shall, B. F. Gupton, *J. Catal.* **2011**, *279*, 1; d)G. Xiang, J. He, T. Li, J. Zhuang, X. Wang, *Nanoscale* **2011**, *3*, 3737; e)J. Hu, Y. Wang, M. Han, Y. Zhou, X. Jiang, P. Sun, *Catal. Sci. Technol.* **2012**, *2*, 2332; f)Y. Nishina, J. Miyata, R. Kawai, K. Gotoh, *RSC Adv.* **2012**, *2*, 9380; g)X. Huo, J. Liu, B. Wang, H. Zhang, Z. Yang, X. She, P. Xi, *J. Mater. Chem. A* **2013**, *1*, 651; h)Ö. Metin, S. Ho, C. Alp, H. Can, M. Mankin, M. Gültekin, M. Chi, S. Sun, *Nano Res.* **2013**, *6*, 10; i)S. Santra, P. K. Hota, R. Bhattacharyya, P. Bera, P. Ghosh, S. K. Mandal, *ACS Catal.* **2013**, *3*, 2776; j)A. Shaabani, M. Mahyari, *J. Mater. Chem. A* **2013**, *1*, 9303; k)N. Shang, C. Feng, H. Zhang, S. Gao, R. Tang, C. Wang, Z. Wang, *Catal. Commun.* **2013**, *40*, 111; l)N. Shang, S. Gao, C. Feng, H. Zhang, C. Wang, Z. Wang, *RSC Adv.* **2013**, *3*, 21863; m)C. Bai, Q. Zhao, Y. Li, G. Zhang, F. Zhang, X. Fan, *Catal. Lett.* **2014**, *144*, 1617; n)K. Bhowmik, D. Sengupta, B. Basu, G. De, *RSC Adv.* **2014**, *4*, 35442; o)P. Fakhri, M. Nasrollahzadeh, B. Jaleh, *RSC Adv.* **2014**, *4*, 48691; p)Y.-S. Feng, X.-Y. Lin, J. Hao, H.-J. Xu, *Tetrahedron* **2014**, *70*, 5249; q)H. Firouzabadi, N. Iranpoor, M. Gholinejad, S. Akbari, N. Jeddi, *RSC Adv.* **2014**, *4*, 17060; r)S. Jafar Hoseini, M. Dehghani, H. Nasrabadi, *Catal. Sci. Technol.* **2014**, *4*, 1078; s)S. K. Movahed, M. Dabiri, A. Bazgir, *Appl. Catal., A* **2014**, *488*, 265; t)S. K. Movahed, R. Esmatpoursalmani, A. Bazgir, *RSC Adv.* **2014**, *4*, 14586; u)S. K. Movahed, N. F. Lehi, M. Dabiri, *RSC Adv.* **2014**, *4*, 42155; v)R. Nie, J. Shi, W. Du, Z. Hou, *Appl. Catal., A* **2014**, *473*, 1; w)J. H. Park, F. Raza, S.-J. Jeon, H.-I. Kim, T. W. Kang, D. Yim, J.-H. Kim, *Tetrahedron Lett.* **2014**, *55*, 3426; x)A. Saito, S.-i. Yamamoto, Y. Nishina, *RSC Adv.* **2014**, *4*, 59835; y)V. Sharavath, S. Ghosh, *RSC Adv.* **2014**, *4*, 48322; z)S. S. Shendage, A. S. Singh, J. M. Nagarkar, *Tetrahedron Lett.* **2014**, *55*, 857; aa)S.-i. Yamamoto, H. Kinoshita, H. Hashimoto, Y. Nishina, *Nanoscale* **2014**, *6*, 6501; ab)S. Diyarbakir, H. Can, Ö. Metin, *ACS Appl. Mater. Interfaces* **2015**, *7*, 3199; ac)H. A. Elazab, A. R. Siamaki, S. Moussa, B. F. Gupton, M. S. El-Shall, *Appl. Catal., A* **2015**, *491*, 58; ad)M. Gómez-Martínez, E. Buxaderas, I. M. Pastor, D. A. Alonso, *J. Mol. Catal. A: Chem.* **2015**, *404–405*, 1; ae)S. J. Hoseini, V. Heidari, H. Nasrabadi, *J. Mol. Catal. A: Chem.* **2015**, *396*, 90; af)S. J. Hoseini, H. G. Khozestan, R. H. Fath, *RSC Adv.* **2015**, *5*, 47701; ag)S. J. Hoseini, A. Zarei, H. Rafatbakhsh Iran, *Appl. Organomet. Chem.* **2015**, *29*, 489; ah)N. Hussain, A. Borah, G. Darabdhara, P. Gogoi, V. K. Azhagan, M. V. Shelke, M. R. Das, *New J. Chem.* **2015**, *39*, 6631; ai)D. Liu, C. Zhang, F. Wang, Z. Huang, N. Zhang, H. Zhou, Y. Kuang, *J. Mater. Chem. A* **2015**, *3*, 16583; aj)P. Mondal, N. Salam, A. Mondal, K. Ghosh, K. Tuhina, S. M. Islam, *J. Colloid Interface Sci.* **2015**, *459*, 97; ak)M. Nasrollahzadeh, A. Banaei, *Tetrahedron Lett.* **2015**, *56*, 500; al)C. Putta, V. Sharavath, S. Sarkar, S. Ghosh, *RSC Adv.* **2015**, *5*, 6652; am)R. K. Rai, K. Gupta, S. Behrens, J. Li, Q. Xu, S. K. Singh, *ChemCatChem* **2015**, *7*, 1806; an)S. Rana, S. Maddila, K. Yalagala, S. B. Jonnalagadda, *Appl. Catal., A* **2015**; ao)P. Wang, G. Zhang, H. Jiao, I. Liu, X. Deng, Y. Chen, X. Zheng, *Appl. Catal., A* **2015**, *489*, 188; ap)S. Wang, D. Hu, W. Hua, J. Gu, Q. Zhang, X. Jia, K. Xi, *RSC Adv.* **2015**, *5*, 53935; aq)Q. Yang, Z. Quan, S. Wu, B. Du,



- M. Wang, P. Li, Y. Zhang, X. Wang, *Tetrahedron* **2015**, *71*, 6124; ar)X. Zhang, C. Yu, C. Wang, Z. Wang, J. Qiu, *Mater. Res. Bull.* **2015**, *67*, 77.
- [37] a)M. Gopiraman, S. G. Babu, Z. Khatri, K. Wei, M. Endo, R. Karvembu, I. S. Kim, *Catal. Sci. Technol.* **2013**, *3*, 1485; b)R. Nie, J. Shi, W. Du, W. Ning, Z. Hou, F.-S. Xiao, *J. Mater. Chem. A* **2013**, *1*, 9037; c)N. Salam, A. Sinha, P. Mondal, A. S. Roy, N. R. Jana, S. M. Islam, *RSC Adv.* **2013**, *3*, 18087; d)W. Liu, D. Sun, J. Fu, R. Yuan, Z. Li, *RSC Adv.* **2014**, *4*, 11003; e)S. K. Movahed, M. Fakharian, M. Dabiri, A. Bazgir, *RSC Adv.* **2014**, *4*, 5243; f)N. Salam, A. Sinha, A. S. Roy, P. Mondal, N. R. Jana, S. M. Islam, *RSC Adv.* **2014**, *4*, 10001; g)W. Wang, J. Gu, W. Hua, X. Jia, K. Xi, *Chem. Commun.* **2014**, *50*, 8889; h)M. Gopiraman, D. Deng, S. Ganesh Babu, T. Hayashi, R. Karvembu, I. S. Kim, *ACS Sustainable Chem. Eng.* **2015**, *3*, 2478; i)B. Zahed, H. Hosseini-Monfared, *Appl. Surf. Sci.* **2015**, *328*, 536.
- [38] a)H. Su, S. Wu, Z. Li, Q. Huo, J. Guan, Q. Kan, *Appl. Organomet. Chem.* **2015**, *29*, 462; b)Q. Zhao, C. Bai, W. Zhang, Y. Li, G. Zhang, F. Zhang, X. Fan, *Ind. Eng. Chem. Res.* **2014**, *53*, 4232.
- [39] M. Blanco, P. Álvarez, C. Blanco, M. V. Jiménez, J. Fernández-Tornos, J. J. Pérez-Torrente, L. A. Oro, R. Menéndez, *Carbon* **2015**, *83*, 21.
- [40] a)J.-Y. Lee, T.-Y. Yung, L.-K. Liu, *Nanoscale Res. Lett.* **2013**, *8*, 1; b)D. Marquardt, C. Vollmer, R. Thomann, P. Steurer, R. Mülhaupt, E. Redel, C. Janiak, *Carbon* **2011**, *49*, 1326; c)Y. Wei, Z. Hao, F. Zhang, H. Li, *J. Mater. Chem. A* **2015**, *3*, 14779; d)J. Xu, M. Xu, J. Wu, H. Wu, W.-H. Zhang, Y.-X. Li, *RSC Adv.* **2015**, *5*, 72361; e)W. Zheng, R. Tan, S. Yin, Y. Zhang, G. Zhao, Y. Chen, D. Yin, *Catal. Sci. Technol.* **2015**, *5*, 2092.
- [41] X. Yu, Y. Huo, J. Yang, S. Chang, Y. Ma, W. Huang, *Appl. Surf. Sci.* **2013**, *280*, 450.
- [42] M. Nasrollahzadeh, F. Babaei, P. Fakhri, B. Jaleh, *RSC Adv.* **2015**, *5*, 10782.
- [43] J. Huang, L. Zhang, B. Chen, N. Ji, F. Chen, Y. Zhang, Z. Zhang, *Nanoscale* **2010**, *2*, 2733.
- [44] A. Pourjavadi, N. Safaie, S. H. Hosseini, C. Bennett, *Appl. Organomet. Chem.* **2015**, *29*, 601.
- [45] W. Zheng, R. Tan, L. Zhao, Y. Chen, C. Xiong, D. Yin, *RSC Adv.* **2014**, *4*, 11732.
- [46] Q. Zhao, Y. Li, R. Liu, A. Chen, G. Zhang, F. Zhang, X. Fan, *J. Mater. Chem. A* **2013**, *1*, 15039.
- [47] Z. Li, S. Wu, H. Ding, H. Lu, J. Liu, Q. Huo, J. Guan, Q. Kan, *New J. Chem.* **2013**, *37*, 4220.
- [48] S. Panigrahi, S. Kundu, S. Ghosh, S. Nath, T. Pal, *J. Nanopart. Res.* **2004**, *6*, 411.
- [49] a)M.-Q. Yang, X. Pan, N. Zhang, Y.-J. Xu, *CrystEngComm* **2013**, *15*, 6819; b)C. Ding, W. Wei, H. Sun, J. Ding, J. Ren, X. Qu, *Carbon* **2014**, *79*, 615; c)Y. Tian, Y. Liu, F. Pang, F. Wang, X. Zhang, *Colloids Surf., A: Physicochem. Eng. Aspects* **2015**, *464*, 96.
- [50] a)X. Li, X. Wang, S. Song, D. Liu, H. Zhang, *Chem. Eur. J.* **2012**, *18*, 7601; b)T. Truong-Huu, K. Chizari, I. Janowska, M. S. Moldovan, O. Ersen, L. D. Nguyen, M. J. Ledoux, C. Pham-Huu, D. Begin, *Catal. Today* **2012**, *189*, 77; c)M. Cano, A. M. Benito, E. P. Urriolabeitia, R. Arenal, W. K. Maser, *Nanoscale* **2013**, *5*, 10189; d)N. Morimoto, S.-i. Yamamoto, Y. Takeuchi, Y. Nishina, *RSC Adv.* **2013**, *3*, 15608; e)K. Szőri, R. Puskás, G. Szöllősi, I. Bertóti, J. Szépvölgyi, M. Bartók, *Catal. Lett.* **2013**, *143*, 539; f)G. Wu, X. Wang, N. Guan, L. Li, *Appl. Catal., B* **2013**, *136–137*, 177; g)J.-H. Yang, D. Ma, *RSC Adv.* **2013**, *3*, 10131; h)J. Sun, Y. Fu, G. He, X. Sun, X. Wang, *Catal. Sci. Technol.* **2014**, *4*, 1742; i)S. I. El-Hout, S. M. El-Sheikh, H. M. A. Hassan, F. A. Harraz, I. A. Ibrahim, E. A. El-Sharkawy, *Appl. Catal., A* **2015**, *503*, 176; j)Y. Hao, S. Wang, Q. Sun, L. Shi, A.-H. Lu, *Chin. J. Catal.* **2015**, *36*, 612; k)P. Liu, W.-T. Chang, M.-Y. Wu, Y.-X. Li, J. Wang, *React. Kinet. Mech. Catal.* **2015**, *1*; l)P. Liu, G. Li, W.-T. Chang, M.-Y. Wu, Y.-X. Li, J. Wang, *RSC Adv.* **2015**, *5*, 72785; m)M. Mirza-Aghayan, M. Molaee Tavana, R. Boukherroub, *Catal. Commun.* **2015**, *69*, 97; n)R. Nie, M. Miao, W. Du, J. Shi, Y. Liu, Z. Hou, *Appl. Catal., B* **2016**, *180*, 607.
- [51] a)Q. Huang, L. Zhou, X. Jiang, Y. Zhou, H. Fan, W. Lang, *ACS Appl. Mater. Interfaces* **2014**, *6*, 13502; b)S. K. Movahed, M. Dabiri, A. Bazgir, *Appl. Catal., A* **2014**, *481*, 79; c)I. Roy, A. Bhattacharyya, G. Sarkar, N. R. Saha, D. Rana, P. P. Ghosh, M. Palit, A. R. Das, D. Chattopadhyay, *RSC Adv.* **2014**, *4*, 52044; d)M. d'Halluin, T. Mabit, N. Fairley, V. Fernandez, M. B. Gawande, E. Le Grogneq, F.-X. Felpin, *Carbon* **2015**, *93*, 974; e)J. Yang, X. Shen, Z. Ji, H. Zhou, G. Zhu, K. Chen, *Ceram. Int.* **2015**, *41*, 4056.
- [52] a)Z. Ji, X. Shen, G. Zhu, H. Zhou, A. Yuan, *J. Mater. Chem.* **2012**, *22*, 3471; b)P. K. Sahoo, B. Panigrahy, D. Bahadur, *RSC Adv.* **2014**, *4*, 48563; c)Y.-g. Wu, M. Wen, Q.-s. Wu, H. Fang, *J.*

- Phys. Chem. C* **2014**, *118*, 6307; d)Q. Ling, M. Yang, C. Li, A. Zhang, *Mater. Res. Bull.* **2015**, *70*, 68.
- [53] X. Chen, G. Wu, J. Chen, X. Chen, Z. Xie, X. Wang, *J. Am. Chem. Soc.* **2011**, *133*, 3693.
- [54] R. Rajesh, E. Sujanthi, S. Senthil Kumar, R. Venkatesan, *Phys. Chem. Chem. Phys.* **2015**, *17*, 11329.
- [55] J. Mondal, K. T. Nguyen, A. Jana, K. Kurniawan, P. Borah, Y. Zhao, A. Bhaumik, *Chem. Commun.* **2014**, *50*, 12095.
- [56] S. Kumari, A. Shekhar, D. D. Pathak, *RSC Adv.* **2014**, *4*, 61187.
- [57] B. Sheng, L. Hu, T. Yu, X. Cao, H. Gu, *RSC Adv.* **2012**, *2*, 5520.
- [58] K. Matyjaszewski, T. P. Davis, *Handbook of Radical Polymerization*, John Wiley & Sons, New Jersey, **2002**.
- [59] a)T. Szabó, O. Berkesi, P. Forgó, K. Josepovits, Y. Sanakis, D. Petridis, I. Dékány, *Chem. Mater.* **2006**, *18*, 2740; b)F. Beckert, A. M. Rostas, R. Thomann, S. Weber, E. Schleicher, C. Friedrich, R. Mühlaupt, *Macromolecules* **2013**, *46*, 5488; c)R. Feng, W. Zhou, G. Guan, C. Li, D. Zhang, Y. Xiao, L. Zheng, W. Zhu, *J. Mater. Chem.* **2012**, *22*, 3982.
- [60] a)M. Kim, C. Lee, Y. D. Seo, S. Cho, J. Kim, G. Lee, Y. K. Kim, J. Jang, *Chem. Mater.* **2015**, *27*, 6238; b)Y. Li, X. Ni, S. Ding, *J. Mater. Sci. : Mater. Electron.* **2015**, *1*.
- [61] a)B. Wang, D. Yang, J. Z. Zhang, C. Xi, J. Hu, *J. Phys. Chem. C* **2011**, *115*, 24636; b)L. Ma, X. Yang, L. Gao, M. Lu, C. Guo, Y. Li, Y. Tu, X. Zhu, *Carbon* **2013**, *53*, 269; c)X. Zhao, P. Liu, *Langmuir* **2014**, *30*, 13699; d)A. Kumar, B. Behera, S. S. Ray, *RSC Adv.* **2015**, *5*, 39474.
- [62] a)Y. Yang, Y. Xie, L. Pang, M. Li, X. Song, J. Wen, H. Zhao, *Langmuir* **2013**, *29*, 10727; b)Y. Yang, M. Li, Y. Xie, X. Song, X. Qu, H. Zhao, *Mater. Lett.* **2014**, *118*, 184.
- [63] a)J. Liu, C. Chen, C. He, J. Zhao, X. Yang, H. Wang, *ACS Nano* **2012**, *6*, 8194; b)J. Liu, G. Song, C. He, H. Wang, *Macromol. Rapid Commun.* **2013**, *34*, 1002; c)K. Song, X. Zhao, Y. Xu, H. Liu, *J. Mater. Sci.* **2013**, *48*, 5750.
- [64] L. Tan, Y.-C. Zhang, B. Wang, H.-M. Luo, H.-X. Feng, *ChemPlusChem* **2014**, *79*, 929.
- [65] L. Tan, B. Wang, H. Feng, *RSC Adv.* **2013**, *3*, 2561.
- [66] K. Matyjaszewski, J. Xia, *Chem. Rev.* **2001**, *101*, 2921.
- [67] M. Kamigaito, T. Ando, M. Sawamoto, *Chem. Rev.* **2001**, *101*, 3689.
- [68] W. A. Braunecker, K. Matyjaszewski, *Prog. Polym. Sci.* **2007**, *32*, 93.
- [69] T. Kyotani, K.-y. Suzuki, H. Yamashita, A. Tomita, *TANSO* **1993**, *1993*, 255.
- [70] a)G. Fan, W. Huang, C. Wang, *Nanoscale* **2013**, *5*, 6819; b)G.-Y. Fan, W.-J. Huang, *Chin. Chem. Lett.* **2014**, *25*, 359; c)M. Gopiraman, S. Ganesh Babu, Z. Khatrri, W. Kai, Y. A. Kim, M. Endo, R. Karvembu, I. S. Kim, *J. Phys. Chem. C* **2013**, *117*, 23582; d)K. X. Yao, X. Liu, Z. Li, C. C. Li, H. C. Zeng, Y. Han, *ChemCatChem* **2012**, *4*, 1938; e)J. Zhao, W. Hu, H. Li, M. Ji, C. Zhao, Z. Wang, H. Hu, *RSC Adv.* **2015**, *5*, 7679.
- [71] a)M. Fang, K. Wang, H. Lu, Y. Yang, S. Nutt, *J. Mater. Chem.* **2009**, *19*, 7098; b)Y. Yang, J. Wang, J. Zhang, J. Liu, X. Yang, H. Zhao, *Langmuir* **2009**, *25*, 11808; c)M. Fang, K. Wang, H. Lu, Y. Yang, S. Nutt, *J. Mater. Chem.* **2010**, *20*, 1982; d)G. Goncalves, P. A. A. P. Marques, A. Barros-Timmons, I. Bdkin, M. K. Singh, N. Emami, J. Gracio, *J. Mater. Chem.* **2010**, *20*, 9927; e)R. K. Layek, S. Samanta, D. P. Chatterjee, A. K. Nandi, *Polymer* **2010**, *51*, 5846; f)S. H. Lee, H. W. Kim, J. O. Hwang, W. J. Lee, J. Kwon, C. W. Bielawski, R. S. Ruoff, S. O. Kim, *Angew. Chem. Int. Ed.* **2010**, *49*, 10084; g)L. Ren, X. Wang, S. Guo, T. Liu, *J. Nanopart. Res.* **2011**, *13*, 6389; h)A. Badri, M. R. Whittaker, P. B. Zetterlund, *J. Polym. Sci., Part A: Polym. Chem.* **2012**, *50*, 2981; i)L. Ren, S. Huang, C. Zhang, R. Wang, W. Tjiu, T. Liu, *J. Nanopart. Res.* **2012**, *14*, 1; j)J. Yang, X. Yan, F. Chen, P. Fan, M. Zhong, *J. Nanopart. Res.* **2012**, *15*, 1; k)S. Zhu, J. Li, Y. Chen, Z. Chen, C. Chen, Y. Li, Z. Cui, D. Zhang, *J. Nanopart. Res.* **2012**, *14*, 1; l)Z. Fang, A. Ito, A. C. Stuart, H. Luo, Z. Chen, K. Vinodgopal, W. You, T. J. Meyer, D. K. Taylor, *ACS Nano* **2013**, *7*, 7992; m)X. Sun, W. Wang, T. Wu, H. Qiu, X. Wang, J. Gao, *Mater. Chem. Phys.* **2013**, *138*, 434; n)W. Yuan, J. Wang, T. Shen, J. Ren, *Mater. Lett.* **2013**, *107*, 243; o)T. Kavitha, I.-K. Kang, S.-Y. Park, *Colloids Surf., B: Biointerfaces* **2014**, *115*, 37; p)T. Kavitha, I.-K. Kang, S.-Y. Park, *Langmuir* **2014**, *30*, 402; q)H. Roghani-Mamaqani, V. Haddadi-Asl, K. Khezri, M. Salami-Kalajahi, *RSC Adv.* **2014**, *4*, 24439; r)H. Roghani-Mamaqani, V. Haddadi-Asl, K. Khezri, M.

- Salami-Kalajahi, *Polym. Int.* **2014**, *63*, 1912; s)Y. Chen, S. Zhang, X. Liu, Q. Pei, J. Qian, Q. Zhuang, Z. Han, *Macromolecules* **2015**, *48*, 365; t)K. Qi, Y. Sun, H. Duan, X. Guo, *Corros. Sci.* **2015**, *98*, 500; u)H. Roghani-Mamaqani, *RSC Adv.* **2015**, *5*, 53357; v)H. Roghani-Mamaqani, V. Haddadi-Asl, Z. Sobhkhiz, M. Ghaderi-Ghahfarrokhi, *Colloid. Polym. Sci.* **2015**, *293*, 735.
- [72] K. Matyjaszewski, P. J. Miller, N. Shukla, B. Immaraporn, A. Gelman, B. B. Luokala, T. M. Siclovan, G. Kickelbick, T. Vallant, H. Hoffmann, T. Pakula, *Macromolecules* **1999**, *32*, 8716.
- [73] V. Percec, T. Guliashvili, J. S. Ladislav, A. Wistrand, A. Stjerndahl, M. J. Sienkowska, M. J. Monteiro, S. Sahoo, *J. Am. Chem. Soc.* **2006**, *128*, 14156.
- [74] A. Anastasaki, V. Nikolaou, G. Nurumbetov, P. Wilson, K. Kempe, J. F. Quinn, T. P. Davis, M. R. Whittaker, D. M. Haddleton, *Chem. Rev.* **2015**, *In press*.
- [75] a)S. H. Lee, D. R. Dreyer, J. An, A. Velamakanni, R. D. Piner, S. Park, Y. Zhu, S. O. Kim, C. W. Bielawski, R. S. Ruoff, *Macromol. Rapid Commun.* **2010**, *31*, 281; b)X. Chen, L. Yuan, P. Yang, J. Hu, D. Yang, *J. Polym. Sci., Part A: Polym. Chem.* **2011**, *49*, 4977; c)Y. Deng, Y. Li, J. Dai, M. Lang, X. Huang, *J. Polym. Sci., Part A: Polym. Chem.* **2011**, *49*, 4747; d)Y. Deng, J. Z. Zhang, Y. Li, J. Hu, D. Yang, X. Huang, *J. Polym. Sci., Part A: Polym. Chem.* **2012**, *50*, 4451; e)Z. Liu, S. Zhu, Y. Li, Y. Li, P. Shi, Z. Huang, X. Huang, *Polym. Chem.* **2015**, *6*, 311.
- [76] X. Jiang, B. M. Rosen, V. Percec, *J. Polym. Sci., Part A: Polym. Chem.* **2010**, *48*, 403.
- [77] a)D. J. Keddie, G. Moad, E. Rizzardo, S. H. Thang, *Macromolecules* **2012**, *45*, 5321; b)G. Moad, E. Rizzardo, S. H. Thang, *Aust. J. Chem.* **2005**, *58*, 379.
- [78] a)Y. Li, X. Li, C. Dong, J. Qi, X. Han, *Carbon* **2010**, *48*, 3427; b)H. M. Etmimi, M. P. Tonge, R. D. Sanderson, *J. Polym. Sci., Part A: Polym. Chem.* **2011**, *49*, 1621; c)B. Zhang, Y. Chen, L. Xu, L. Zeng, Y. He, E.-T. Kang, J. Zhang, *J. Polym. Sci., Part A: Polym. Chem.* **2011**, *49*, 2043; d)F. Beckert, C. Friedrich, R. Thomann, R. Mülhaupt, *Macromolecules* **2012**, *45*, 7083; e)L. Cui, J. Liu, R. Wang, Z. Liu, W. Yang, *J. Polym. Sci., Part A: Polym. Chem.* **2012**, *50*, 4423; f)K. Jiang, C. Ye, P. Zhang, X. Wang, Y. Zhao, *Macromolecules* **2012**, *45*, 1346; g)Y. Yang, X. Song, L. Yuan, M. Li, J. Liu, R. Ji, H. Zhao, *J. Polym. Sci., Part A: Polym. Chem.* **2012**, *50*, 329; h)Y.-S. Ye, Y.-N. Chen, J.-S. Wang, J. Rick, Y.-J. Huang, F.-C. Chang, B.-J. Hwang, *Chem. Mater.* **2012**, *24*, 2987; i)R. Gu, W. Z. Xu, P. A. Charpentier, *Polymer* **2014**, *55*, 5322; j)J. Liu, L. Cui, N. Kong, C. J. Barrow, W. Yang, *Eur. Polym. J.* **2014**, *50*, 9; k)M. Nikdel, M. Salami-Kalajahi, M. Salami Hosseini, *RSC Adv.* **2014**, *4*, 16743; l)P. Ding, J. Zhang, N. Song, S. Tang, Y. Liu, L. Shi, *Compos. Part A-Appl. Sci.* **2015**, *69*, 186; m)C. H. Park, H. Yang, J. Lee, H.-H. Cho, D. Kim, D. C. Lee, B. J. Kim, *Chem. Mater.* **2015**, *27*, 5288; n)Y. Zhao, S. Perrier, in *Controlled Radical Polymerization at and from Solid Surfaces, Vol. 270* (Ed.: P. Vana), Springer International Publishing, **2016**, pp. 77.
- [79] a)Y. I. Avila-Vega, C. C. Leyva-Porras, M. Mireles, M. Quevedo-López, J. Macossay, J. Bonilla-Cruz, *Carbon* **2013**, *63*, 376; b)O. García-Valdez, R. Ledezma-Rodríguez, E. Saldívar-Guerra, L. Yate, S. Moya, R. F. Ziolo, *Polymer* **2014**, *55*, 2347.
- [80] D. R. Dreyer, K. A. Jarvis, P. J. Ferreira, C. W. Bielawski, *Polym. Chem.* **2012**, *3*, 757.
- [81] B. Li, W. Hou, J. Sun, S. Jiang, L. Xu, G. Li, M. A. Memon, J. Cao, Y. Huang, C. W. Bielawski, J. Geng, *Macromolecules* **2015**, *48*, 994.
- [82] D. R. Dreyer, C. W. Bielawski, *Adv. Funct. Mater.* **2012**, *22*, 3247.
- [83] M. Zeng, J. Wang, R. Li, J. Liu, W. Chen, Q. Xu, Y. Gu, *Polymer* **2013**, *54*, 3107.
- [84] K. Yao, G. Zhang, Y. Lin, J. Gong, H. Na, T. Tang, *Polym. Chem.* **2015**, *6*, 389.
- [85] X. Zhang, X. Fan, H. Li, C. Yan, *J. Mater. Chem.* **2012**, *22*, 24081.
- [86] D. R. Dreyer, K. A. Jarvis, P. J. Ferreira, C. W. Bielawski, *Macromolecules* **2011**, *44*, 7659.
- [87] a)M. Mauro, M. R. Acocella, C. E. Corcione, A. Maffezzoli, G. Guerra, *Polymer* **2014**, *55*, 5612; b)T. M. Robert, D. Augustine, S. Chandran M, D. Mathew, C. P. R. Nair, *RSC Adv.* **2015**, *5*, 1198; c)J. W. Yu, J. Jung, Y.-M. Choi, J. H. Choi, J. Yu, J. K. Lee, N.-H. You, M. Goh, *Polym. Chem.* **2016**; d)X. Wang, J. Jin, M. Song, *Eur. Polym. J.* **2012**, *48*, 1034.
- [88] T. Jiang, Z.-Y. Sui, Q.-S. Yang, X. Zhang, B.-H. Han, *Soft Matter* **2015**, *11*, 3215.
- [89] Y. Huang, Y. Qin, Y. Zhou, H. Niu, Z.-Z. Yu, J.-Y. Dong, *Chem. Mater.* **2010**, *22*, 4096.
- [90] a)Y. Huang, Y. Qin, N. Wang, Y. Zhou, H. Niu, J.-Y. Dong, J. Hu, Y. Wang, *Macromol. Chem. Phys.* **2012**, *213*, 720; b)J.-Y. Dong, Y. Liu, *J. Organomet. Chem.* **2015**, *798*, Part 2, 311; c)H.



- Bahrami, A. Ramazani S. A, A. Kheradmand, M. Shafiee, H. Baniasadi, *Adv. Polym. Tech.* **2015**, 21508 (1).
- [91] M. Stürzel, F. Kempe, Y. Thomann, S. Mark, M. Enders, R. Mülhaupt, *Macromolecules* **2012**, 45, 6878.
- [92] M. Stürzel, Y. Thomann, M. Enders, R. Mülhaupt, *Macromolecules* **2014**, 47, 4979.
- [93] Z. Hu, C. Liu, *J. Polym. Res.* **2012**, 20, 1.
- [94] F. d. C. Fim, J. M. Guterres, N. R. S. Basso, G. B. Galland, *J. Polym. Sci., Part A: Polym. Chem.* **2010**, 48, 692.
- [95] B. Choi, J. Lee, S. Lee, J.-H. Ko, K.-S. Lee, J. Oh, J. Han, Y.-H. Kim, I. S. Choi, S. Park, *Macromol. Rapid Commun.* **2013**, 34, 533.
- [96] F. Kirschvink, M. Stürzel, Y. Thomann, R. Mülhaupt, *Polymer* **2014**, 55, 4547.
- [97] L. Zhang, E. Yue, B. Liu, P. Serp, C. Redshaw, W.-H. Sun, J. Durand, *Catal. Commun.* **2014**, 43, 227.
- [98] Q. Zhang, Q.-L. Li, S. Xiang, Y. Wang, C. Wang, W. Jiang, H. Zhou, Y.-W. Yang, J. Tang, *Polymer* **2014**, 55, 6044.
- [99] A. Mariconda, P. Longo, A. Agovino, L. Guadagno, A. Sorrentino, M. Raimondo, *Polymer* **2015**, 69, 330.
- [100] R. Huisgen, R. Grashey, P. Laur, H. Leitermann, *Angew. Chem.* **1960**, 72, 416.
- [101] W. H. Binder, R. Sachsenhofer, *Macromol. Rapid Commun.* **2007**, 28, 15.
- [102] a) J. Kaiser, S. S. Kinderman, B. C. J. van Esseveldt, F. L. van Delft, H. E. Schoemaker, R. H. Blaauw, F. P. J. T. Rutjes, *Org. Biomol. Chem.* **2005**, 3, 3435; b) Y. L. Angell, K. Burgess, *Chem. Soc. Rev.* **2007**, 36, 1674.
- [103] C. W. Tornøe, C. Christensen, M. Meldal, *J. Org. Chem.* **2002**, 67, 3057.
- [104] V. V. Rostovtsev, L. G. Green, V. V. Fokin, K. B. Sharpless, *Angew. Chem. Int. Ed.* **2002**, 41, 2596.
- [105] H. C. Kolb, M. G. Finn, K. B. Sharpless, *Angew. Chem. Int. Ed.* **2001**, 40, 2004.
- [106] T. R. Chan, R. Hilgraf, K. B. Sharpless, V. V. Fokin, *Org. Lett.* **2004**, 6, 2853.
- [107] M. Meldal, C. W. Tornøe, *Chem. Rev.* **2008**, 108, 2952.
- [108] C. Deraedt, N. Pinaud, D. Astruc, *J. Am. Chem. Soc.* **2014**, 136, 12092.
- [109] a) A. Cano-Odena, P. Vandezande, D. Fournier, W. Van Camp, F. E. Du Prez, I. F. J. Vankelecom, *Chem. Eur. J.* **2010**, 16, 1061; b) J. E. Macdonald, J. A. Kelly, J. G. C. Veinot, *Langmuir* **2007**, 23, 9543.
- [110] a) M. Lammens, J. Skey, S. Wallyn, R. O'Reilly, F. Du Prez, *Chem. Commun.* **2010**, 46, 8719; b) L. Bonami, W. Van Camp, D. Van Rijckegem, F. E. Du Prez, *Macromol. Rapid Commun.* **2009**, 30, 34; c) M. Chtchigrovsky, A. Primo, P. Gonzalez, K. Molvinger, M. Robitzer, F. Quignard, F. Taran, *Angew. Chem.* **2009**, 121, 6030; d) B. Dervaux, F. E. Du Prez, *Chem. Sci.* **2012**, 3, 959.
- [111] C. Girard, E. Önen, M. Aufort, S. Beauvière, E. Samson, J. Herscovici, *Org. Lett.* **2006**, 8, 1689.
- [112] B. H. Lipshutz, B. R. Taft, *Angew. Chem. Int. Ed.* **2006**, 45, 8235.
- [113] H. Sharghi, S. Ebrahimpourmoghaddam, M. M. Doroodmand, A. Purkhosrow, *Asian J. Org. Chem.* **2012**, 1, 377.
- [114] I. S. Park, M. S. Kwon, Y. Kim, J. S. Lee, J. Park, *Org. Lett.* **2008**, 10, 497.
- [115] F. Alonso, Y. Moglie, G. Radivoy, M. Yus, *Adv. Synth. Catal.* **2010**, 352, 3208.
- [116] a) T. Katayama, K. Kamata, K. Yamaguchi, N. Mizuno, *ChemSusChem* **2009**, 2, 59; b) K. Yamaguchi, T. Oishi, T. Katayama, N. Mizuno, *Chem. Eur. J.* **2009**, 15, 10464.
- [117] a) V. Bénétiau, A. Olmos, T. Boningari, J. Sommer, P. Pale, *Tetrahedron Lett.* **2010**, 51, 3673; b) S. Chassaing, M. Kumarraja, A. Sani Souna Sido, P. Pale, J. Sommer, *Org. Lett.* **2007**, 9, 883; c) S. Chassaing, A. Sani Souna Sido, A. Alix, M. Kumarraja, P. Pale, J. Sommer, *Chem. Eur. J.* **2008**, 14, 6713.
- [118] R. P. Jumde, C. Evangelisti, A. Mandoli, N. Scotti, R. Psaro, *J. Catal.* **2015**, 324, 25.
- [119] C. S. Radatz, L. d. A. Soares, E. R. Vieira, D. Alves, D. Russowsky, P. H. Schneider, *New J. Chem.* **2014**, 38, 1410.
- [120] I. Jlalía, F. Gallier, N. Brodie-Linder, J. Uziel, J. Augé, N. Lubin-Germain, *J. Mol. Catal. A: Chem.* **2014**, 393, 56.

- [121] R. Mirsafaei, M. M. Heravi, S. Ahmadi, M. H. Moslemin, T. Hosseinejad, *J. Mol. Catal. A: Chem.* **2015**, *402*, 100.
- [122] J.-M. Collinson, J. D. E. T. Wilton-Ely, S. Diez-Gonzalez, *Chem. Commun.* **2013**, *49*, 11358.
- [123] P. Li, L. Wang, Y. Zhang, *Tetrahedron* **2008**, *64*, 10825.
- [124] L. Wan, C. Cai, *Catal. Lett.* **2012**, *142*, 1134.
- [125] I. Jllia, H. Elamari, F. Meganem, J. Herscovici, C. Girard, *Tetrahedron Lett.* **2008**, *49*, 6756.
- [126] S. Mohammed, A. K. Padala, B. A. Dar, B. Singh, B. Sreedhar, R. A. Vishwakarma, S. B. Bharate, *Tetrahedron* **2012**, *68*, 8156.
- [127] K. Namitharan, M. Kumarraja, K. Pitchumani, *Chem. Eur. J.* **2009**, *15*, 2755.
- [128] K. Jacob, A. Stolle, B. Ondruschka, K. D. Jandt, T. F. Keller, *Appl. Catal., A* **2013**, *451*, 94.
- [129] a) A. Qin, J. W. Y. Lam, B. Z. Tang, *Macromolecules* **2010**, *43*, 8693; b) A. Qin, J. W. Y. Lam, B. Z. Tang, *Chem. Soc. Rev.* **2010**, *39*, 2522.
- [130] X. Sheng, D. M. Rock, T. C. Mauldin, M. R. Kessler, *Polymer* **2011**, *52*, 4435.
- [131] N. I. Kovtyukhova, P. J. Ollivier, B. R. Martin, T. E. Mallouk, S. A. Chizhik, E. V. Buzaneva, A. D. Gorchinskiy, *Chem. Mater.* **1999**, *11*, 771.
- [132] H. Feng, R. Cheng, X. Zhao, X. Duan, J. Li, *Nat Commun* **2013**, *4*, 1539.

## VI.APPENDIX

## 1-Synthesis of graphene oxide (GO) and reduced graphene oxide(r-GO)

## Graphene oxide (GO)

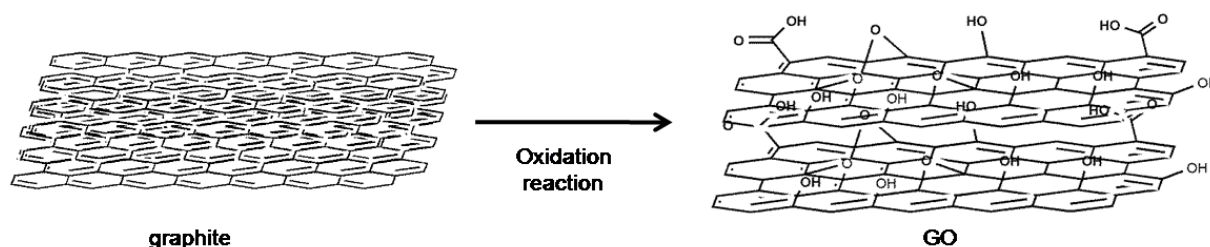


Figure 1. Exfoliation of graphite multilayer to graphene oxide (GO) with few number of layers

GO was synthesized by two different methods adopted from the previous reports<sup>[36a, 131]</sup>. In the first method the oxidation reaction was preceded like Hummers method in one step reaction (**GO1**), however in the second approach the oxidation was done in a two step reaction (**GO2**). In the first step, the graphite was preoxidized by  $K_2S_2O_8$  and  $P_2O_5$  in concentrated sulfuric acid at 80 °C, afterwards in the second step, the Hummers oxidation method was used for further oxidation of the surface.

XRD spectra of **GO1** exhibited two peaks at nearly 10° and 26° which related to GO and non-oxidized graphite, respectively. However in **GO2** only a main peak at 10° was presented related to GO sheets showing the complete oxidation of graphite sheets (Figure 2a). Lorentzian fitting of the (002) reflection peak at 10 ° for GO products calculated the number of layers for GO products which were 7 and 9 for **GO1** and **GO2**, respectively (Table 6, Entries 2 and 3). TGA showed 55 wt% and 71 wt% weight loss for **GO1** and **GO2**, respectively proving the existence of oxygen-containing functional groups on the surfaces of GO products in comparison to graphite (Figure 2b). Both XRD and TGA measurements proved that, oxidation of graphite in the second method (**GO2**) led to nearly complete oxidation of graphite sheets, hence the oxidation reaction in the first method (**GO1**) was not complete. Furthermore RAMAN spectra showed the  $I_D/I_G$  value of 0.576 and 0.896 for **GO1** and **GO2** respectively, proving less amount of defects on the surface of **GO1** in comparison to **GO2** (Figure 2c, Table 1, Entries 2 and 3,).

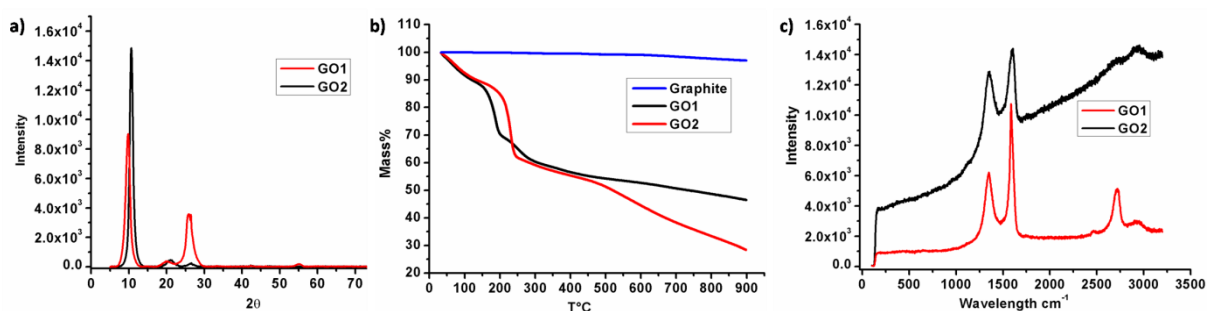


Figure 1. a) XRD, b) TGA, and c) RAMAN of GO achieved by two different approaches (**GO1** and **GO2**)

## Reduction reaction of GO to r-GO

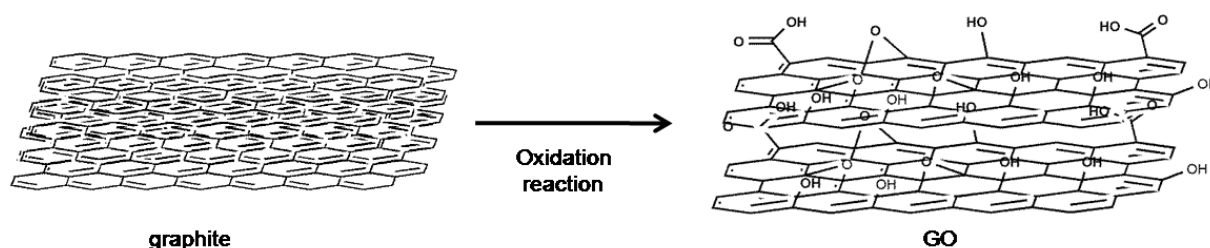


Figure 2. Reduction of graphene oxide (GO) to reduced graphene oxide(r-GO)

There are many methods for reduction of GO to r-GO based on thermal annealing, using microwave, and the application of different reducing agents such as hydrazine, ascorbic acid, hydrohalic acid, or sodium borohydride. Therefore GO was reduced utilizing different methods and the achieved r-GOs were characterized by XRD, TGA and RAMAN spectroscopy.

GO was reduced by  $\text{NaBH}_4$  (**r-GO1**), and the resulted reduction product from reaction by  $\text{NaBH}_4$  was further treated by  $\text{H}_2\text{SO}_4$  (**r-GO2**). In other chemical approaches GO was reduced by different reducing agents like hydrazine (**r-GO3**), mixture of ammonia with sodium (**r-GO4**), and vitamin C (**r-GO5**). Furthermore the thermal reduction of GO in oven was also probed (**r-GO6**).

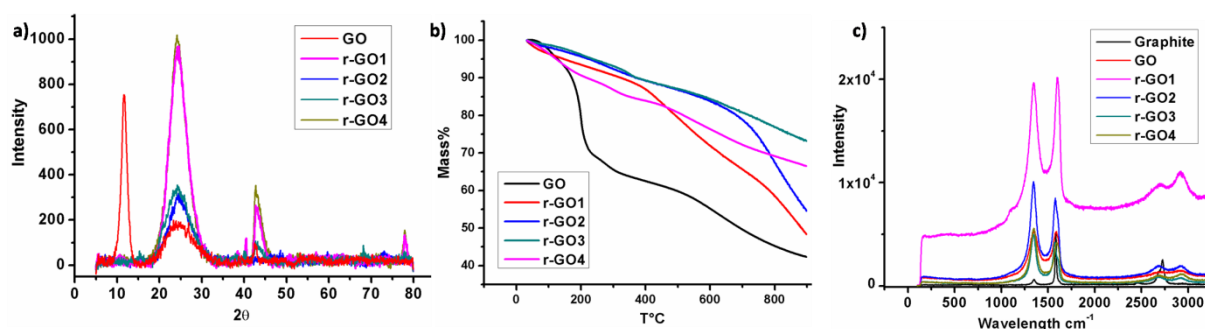
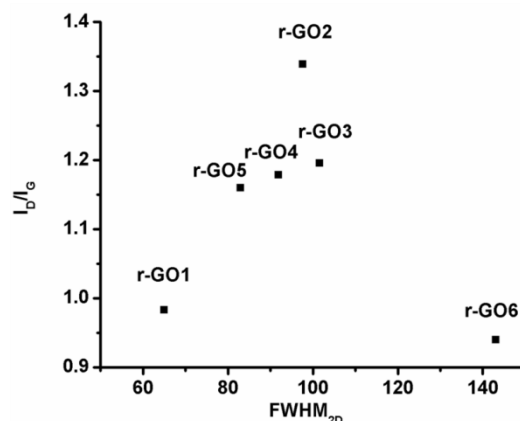


Figure 3. a) XRD, b) TGA, and c) RAMAN of r-GO achieved by different approaches

XRD measurements proved the successful reduction of GO with all of the methods by shifting the (002) reflection peak from  $10^\circ$  for GO to  $25^\circ$  for r-GO (Figure 4a), moreover the Lorentzian fitting of the (002) reflection showed the 4-5 number of layers for all of the methods (Table 1). TGA of r-GO products (Figure 4b), possessed no weight loss at  $200^\circ\text{C}$  (related to the water molecules connected *via* H-bonding to epoxy groups of GO) in turn removing of epoxy groups from the surface. However **r-GO1** (reduced by  $\text{NaBH}_4$ ) exhibited higher weight loss in comparison to other methods proving the existence of more oxygen-containing groups on the surface which reduced the conductivity of r-GO. RAMAN spectroscopy was performed for defect investigation of the surface of r-GO products, where  $I_D/I_G$  ratio for most of the r-GO products were between 1-1.3 which revealed that reduction reaction induced more defect on the surface in comparison to GO ( $I_D/I_G = 0.6 - 0.9$ ). For detailed study of defects on the surface of r-GO products, the  $I_D/I_G$  ratio of peaks plotted vs. FWHM of 2D band as

discussed earlier in introduction part (Figure 5). This plot showed that **r-GO1** and **r-GO5** exhibited less defect than other methods by shifting to left side of plot and possessing lower  $I_D/I_G$  ratio.



**Figure 4**  $I_D/I_G$  ratio vs. FWHM of 2D band in RAMAN spectra for different r-GO obtained by different methods

A crucial point in synthesis of r-GO methods is their ability for large amount production, which thermal reduction and chemical reduction by ascorbic acid showed promising properties by up scaling up to 1.5 g. The information regarding to characterization of GO and r-GO products are summarized in Table 1.

**Table 1.** characterization of GO and r-GO products with XRD, TGA and RAMAN spectroscopy

entry	material	XRD ( number of layers) <sup>[31]</sup>	RAMAN( $I_D/I_G$ )	TGA (residual mass%)	2D( $\Gamma_{2D}$ FWHM $\text{cm}^{-1}$ )	starting /final amount
1	graphite	213	-	96.98%	-	-
2	GO1	7	0.576	46.62%	-	10 g/10 g
3	GO2	9	0.896	28.37%	-	5 g/5 g
4	r-GO1	5	0.9833	48.38%	65	100 mg/90 mg
5	r-GO2	4	1.1785	54.58%	91.91	50 mg/45 mg
6	r-GO3	4	1.1955	73.17%	101.61	100 mg/78 mg
7	r-GO4	5	1.3387	66.48%	97.65	250 mg/210 mg
8	r-GO5	4	1.16	74.74%	82.94	1.5 g/700 mg
9	r-GO6	5	0.94	80.1%	143.14	500 mg/300 mg

## 2-Experimental part

### 2.1-Materials

All chemicals and solvents, which were used for the synthesis were purchased from Sigma-Aldrich and used as received unless otherwise stated. Graphite flakes (KFL 99.5, min 20% > 100  $\mu\text{m}$ ) was received from Kropfmühl AG. Toluene refluxed over sodium/benzophenone and freshly distilled under an argon atmosphere before use

### 2.2-Methods

#### XRD

Measurement were performed using a Bruker AXS D8 advanced X-ray diffractometer with  $\text{Cu}_{\text{K}\alpha}$  ( $\lambda = 0.15406 \text{ nm}$ ) radiation in the  $2\theta$  range between  $5\text{--}80^\circ$  with a scan rate of  $2^\circ \text{ min}^{-1}$ .

#### RAMAN

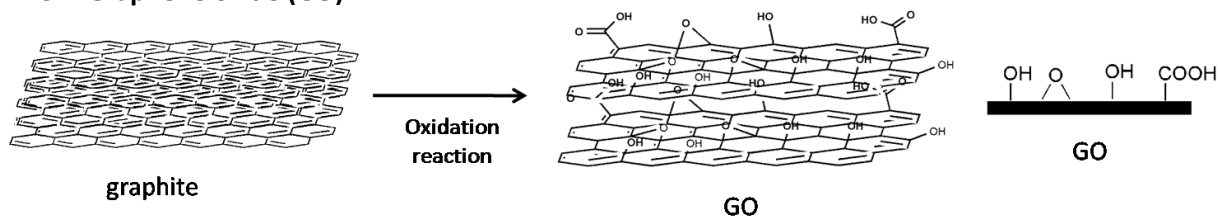
Raman spectra were obtained at room temperature with a Renishaw inVia spectrometer equipped with a Leica DM2500M confocal microscope using a Cobalt CW DPSS Laser. The RAMAN scattering was excited using 532 nm as excitation wavelength and detected with a CCD camera. Spectra was recorded in the  $100\text{--}3200 \text{ cm}^{-1}$  Raman shift range.

#### TGA

TGA was performed on a Netzsch TG tarsus 209 instrument. The samples were heated in a Pt pan under a dry flow of nitrogen ( $250 \text{ mL/min}$ ) over a temperature range of  $25\text{--}900^\circ\text{C}$ , with a heating rate of  $10^\circ\text{C/min}$ .

### 2.3-Synthesis

#### 2.3.1-Graphene oxide (GO)



**GO1**<sup>[36a]</sup> - In a 500 mL three-necked flask, the graphite powder (10 g) was stirred *via* mechanical stirrer in concentrated sulfuric acid (390 mL) at room temperature (RT), and sodium nitrate (5 g) was added, afterwards the mixture was cooled to  $0^\circ\text{C}$  and potassium permanganate (30 g) was added during 30 min to 1 h in order to avoid the increment in internal temperature of the reaction mixture. After 2 h, the green slurry was allowed to come to room temperature, and after being stirred for 3 h (during this time the viscosity of mixture was increased) the whole batch was carefully poured into a 2 L



beaker filled with ice-cold water (distilled). Subsequently, hydrogen peroxide (3 %) was added (250 mL) in excess and the mixture was stirred overnight and then filtered. Workup was accomplished by several washings with a mixture of HCl/H<sub>2</sub>O<sub>2</sub> (1:1, 5 %, 5×200 mL) and filtration was followed by several washings with water (5×200 mL) and centrifugation (5000 rpm, 10 min) until the supernatant did not show anymore precipitation with AgNO<sub>3</sub> solution. The obtained GO carefully was powdered in a ball mill, with pre cooling by liquid nitrogen, and further dried in high vacuum at 40 °C.

Yield: 9 g

XRD:  $2\theta = 10^\circ$ , calculated number of layers: 7.

RAMAN:  $I_D/I_G = 0.576$ ,

TGA: 53.38 % weight loss in comparison to graphite

**GO2**<sup>[131]</sup>- In a 50 mL one-necked flask, the graphite powder (5 g) was added into a 80 °C solution of concentrated H<sub>2</sub>SO<sub>4</sub> (7.5 mL), K<sub>2</sub>S<sub>2</sub>O<sub>8</sub> (2.5 g), and P<sub>2</sub>O<sub>5</sub> (2.5 g), and stirred for 6 h. Afterwards the reaction mixture was then carefully added to distilled water (1 L), filtered, and washed several times with water (5×200 mL) on the filter until the rinse water pH became neutral. The product was dried in desiccators (2 mbar) at ambient temperature overnight. As-preoxidized graphite was then subjected to oxidation by Hummers' method<sup>[24aa]</sup>. Therefore in a 250 mL three-necked flask, the as-oxidized graphite powder (5 g) was put at once into cold (0 °C) concentrated H<sub>2</sub>SO<sub>4</sub> (115 mL). KMnO<sub>4</sub> (15 g) was added gradually with stirring (mechanical stirrer) and cooling, so that the temperature of the mixture was not allowed to reach 20 °C (monitored with thermometer inside of reaction mixture). The reaction mixture was then stirred at 35 °C for 2 h. Afterwards the reaction mixture was allowed to come to room temperature, and after being stirred for 3 h the whole batch was carefully poured into a 2 L beaker filled with ice-cold water (distilled). Subsequently, hydrogen peroxide (3 %, 250 mL) was added in excess and the mixture was stirred overnight and then filtered. Workup was accomplished by several washings with a mixture of HCl/H<sub>2</sub>O<sub>2</sub> (1:1, 5 %, 5×200 mL) and filtration was followed by several washings with water (5×200 mL) and centrifugation (5000 rpm, 10 min) until the supernatant did not show anymore precipitation with AgNO<sub>3</sub> solution. The obtained GO was dried in desiccators (2 mbar) at room temperature overnight. Then GO was carefully powdered in a ball mill, with pre cooling by liquid nitrogen.

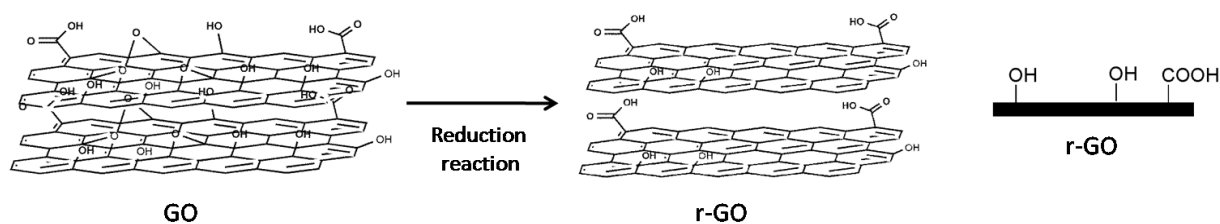
Yield: 8 g

XRD:  $2\theta = 10^\circ$ , calculated number of layers: 9.

RAMAN:  $I_D/I_G = 0.896$ ,

TGA: 71.63 % weight loss in comparison to graphite

### 2.3.2-Reduction reaction of GO to r-GO



#### Reduction by sodium borohydride ( $\text{NaBH}_4$ ) and sulfuric acid ( $\text{H}_2\text{SO}_4$ )<sup>[24i]</sup>

**r-GO1-** GO (100 mg) was dispersed by ultrasonicator (30 % amplitude, 30 min) in deionized water (100 ml). The GO solution was loaded to a 250 mL two-necked flask, afterwards the pH of this solution was adjusted to 9-10 by 5 wt% sodium carbonate solution. Sodium borohydride (800 mg) was directly added into the GO dispersion in water and the mixture was stirred at 80 °C for 1 h. The reduction product was separated by filtration and washed with large amounts of water several times (5×50 mL) by centrifugation (5000 rpm, 10 min) to remove most residual ions. The resulted product was dried overnight in a vacuum desiccator (2 mbar, 25 °C).

*Yield: 90 %.*

*XRD:  $2\theta = 25^\circ$ , calculated number of layers: 5.*

*RAMAN:  $I_D/I_G = 0.983$ ,  $\Gamma_{2D}$  (2D FWHM) = 65  $\text{cm}^{-1}$ .*

*TGA: 51.62 % weight loss in comparison to graphite*

**r-GO2-** The resulted product form the first step (r-GO1, 50 mg) redispersed by a bath sonicator in concentrated sulfuric acid (10 mL) and heated to 120 °C with stirring for 12 h. After cooling down, the dispersion was added to deionized water (200 mL). The final product was separated by centrifugation (5000 rpm, 10 min) and washed several times with water (5 × 50 mL) by centrifugation (5000 rpm, 10 min), finally the resulting product was dried overnight in a vacuum desiccator (2 mbar, 25 °C).

*Yield: 90 %.*

*XRD:  $2\theta = 25^\circ$ , calculated number of layers: 4.*

*RAMAN:  $I_D/I_G = 1.178$ ,  $\Gamma_{2D}$  (2D FWHM) = 91.91  $\text{cm}^{-1}$ .*

*TGA: 45.42 % weight loss in comparison to graphite*

#### Reduction reaction by hydrazine ( $\text{N}_2\text{H}_4$ )<sup>[24x]</sup>

**r-GO3-** GO (100 mg) was dispersed by ultrasonicator (30 % amplitude, 30 min) in deionized water (100 ml). Then the mixture was loaded in a three-necked 250 mL flask. The pH of the solution was set basic (9-10) by ammonium hydroxide. Hydrazine hydrate (76  $\mu\text{L}$ ) (The weight ratio of hydrazine to GO was about 7:10) was added to the solution and heated in an oil bath at 100 °C under a water-cooled condenser for 24 h over which the reduced GO gradually precipitated out as a black solid. This

product was isolated by washing with water (5× 50 mL) by centrifugation (500 rpm, 10 min), and dried overnight in a vacuum desiccator (2 mbar, 25 °C) and further drying was done in high vacuum at 40 °C.

*Yield: 78 %.*

*XRD:  $2\theta = 25^\circ$ , calculated number of layers: 4.*

*RAMAN:  $I_D/I_G = 1.195$ ,  $\Gamma_{2D}$  (2D FWHM) = 101.6  $cm^{-1}$ .*

*TGA: 26.83 % weight loss in comparison to graphite*

#### **Reduction reaction using mixture of ammonia and sodium (NH<sub>3</sub>+Na)<sup>[132]</sup>**

**r-GO4-** In a 250 ml three-necked flask, 220 mg of GO was dispersed in 80 mL of liquid NH<sub>3</sub> (ammonia gas was condensed in a three-necked flask by acetone-liquid nitrogen bath ( -40 °C - -50 °C) and added to GO). This dispersion was stirred for 20 min, afterwards sodium (800 mg, cutting into small pieces) was added and the mixture was stored in acetone- liquid nitrogen bath ( -40 °C - -50 °C) for 30 min with constant stirring. Then the acetone-liquid nitrogen bath was removed, and ammonia volatize to remove. Subsequently the mixture of *iso*-propanol and water (1:1, 150 mL) was added to remove the sodium, and the product was washed with water (2×100 mL) and ethanol (2×100 mL), and dried overnight in a vacuum desiccator (2 mbar, 25 °C).

*Yield: 84 %.*

*XRD:  $2\theta = 25^\circ$ , calculated number of layers: 5.*

*RAMAN:  $I_D/I_G = 1.33$ ,  $\Gamma_{2D}$  (2D FWHM) = 97.65  $cm^{-1}$ .*

*TGA: 33.52 % weight loss in comparison to graphite*

#### **Thermal reduction in oven<sup>[36a]</sup>**

**r-GO5-** GO (1 g) was placed in a quartz flask of the rotating oven and flashed for 30 min with nitrogen. Afterwards it was heated to 600 °C (heating rate: 10 k/min) and kept at that temperature for 2 min. Then it cooled down to room temperature under nitrogen atmosphere.

*Yield: 84 %.*

*XRD:  $2\theta = 25^\circ$ , calculated number of layers: 5.*

*RAMAN:  $I_D/I_G = 1.33$ ,  $\Gamma_{2D}$  (2D FWHM) = 97.65  $cm^{-1}$ .*

*TGA: 33.52 % weight loss in comparison to graphite*

#### **Reduction by vitamin C (ascorbic acid)<sup>[24g]</sup>**

**r-GO6-** GO (500 mg) was dispersed in 50 mL deionized water by ultrasonicator (30 % amplitude, 30 min) and placed in a 200 mL three-neck flask. Afterwards 500 mg of ascorbic acid was added to the GO dispersion and the mixture was allowed to react under nitrogen at 100 °C for 24 h. The r-GO

powders slowly precipitated as a black solid. This product was washed with deionized water (5×50 mL) by centrifugation (5000 rpm, 10 min) and finally dried at 60 °C for 24 h in high vacuum.

*Yield: 84 %.*

*XRD:  $2\theta = 25^\circ$ , calculated number of layers: 5.*

*RAMAN:  $I_D/I_G = 1.33$ ,  $\Gamma_{2D}$  (2D FWHM) =  $97.65 \text{ cm}^{-1}$ .*

*TGA: 33.52 % weight loss in comparison to graphite*

# Ali Shaygan Nia

**Address:** Oleariusstr 11, 06108-D, Halle (Saale), Germany  
**E-mail:** [ali.shaygan-nia@chemie.uni-halle.de](mailto:ali.shaygan-nia@chemie.uni-halle.de)  
**Mobile:** +4917670759735  
**Phone (office):** +493455525936  
**Date of birth:** 24.03.1985  
**Marital status:** Single  
**Nationality:** Iranian



## Research experience

- 2012-2015**      **IASS project**
- Title: IASS (Improving the Aircraft Safety by Self-Healing Structure and Protecting Nanofillers)** <http://www.iass-project.eu/>
- Funded by: European Commission under the 7<sup>th</sup> Framework Programme
- 2009-2015**      **Martin Luther University Halle-Wittenberg, institute of chemistry, macromolecular chemistry department**

## Education

- 2011-2015**      **Ph.D. degree in polymer chemistry**
- Martin Luther University of Halle-Wittenberg, Halle (Saale), Germany
- Title: Graphene supported Cu(I) nanocatalysts for application in CuAAC reactions and production of resin/graphene nanocomposites**
- 2008-2011**      **M.Sc. degree in polymer material science**
- Martin Luther University of Halle-Wittenberg, Halle (Saale), Germany
- Title: Synthetic and spectroscopic properties of oligothiophenes**
- 2003-2008**      **B.Sc. degree in chemical engineering in branch of polymer technology**
- Isfahan University of Technology, Isfahan, Iran

## Training

- 2012**      **Alles für die Chromatographie (Everything about chromatography)**
- VWR international, Halle, Germany

## Skills

<b>Language</b>	<b>English</b>	Fluent
	<b>German</b>	Advanced
	<b>Farsi</b>	Native
<b>Computer</b>	<b>OS</b>	MS Windows
	<b>Applications</b>	MS Office, Chem Draw, Origin, Mathematica, Bruker Data Analysis, MestRec, Coreldraw

**Laboratory**

**Synthesis, modification and characterization of graphene-oxide and reduced-graphene oxide, organic synthesis and purification, polymerization techniques.**

Conducting ESI-TOF-MS, MALDI-TOF-MS, HPLC, GC, LC-MS coupling, XRD, RAMAN, DSC, TGA, GPC and IR measurements

Data interpretation (GPC, MALDI, HPLC, ESI-MS, DSC, TGA, XRD, RAMAN, NMR, IR, TEM)

**Additional skills**

Team work, Communication, Time management, Flexibility

**Personal interest**

music (playing Persian instrument in a professional level), literature

**Publications**

- **Shaygan Nia, A.,** Enders, C. and Binder, W. H. (2012) **Hydrogen-bonded perylene/terthiophene-materials: synthesis and spectroscopic properties.** Tetrahedron, 68, 722-729.
- **Shaygan Nia, A.,** Rana, S., Döhler, D., Noirfalise, X., Belfiore, A. and Binder, W. H. (2014) **Click chemistry promoted by graphene supported copper nanomaterials.** Chem. Commun., 50, 15374-15377.
- **Shaygan Nia, A.,** Rana, S., Döhler, D., Jirsa, F., Meister, M., Guadagno, L., Koslowski, E., Bron, M., and Binder, W. H. (2015) **Carbon Supported Copper Nanomaterials: Recyclable Catalysts for Huisgen [3+2] Cycloaddition Reaction.** Chem. Eur. j., 21, 10763-10770
- **Shaygan Nia, A.,** Rana, S., Döhler, D., Osim, W., and Binder, W. H. (2015) **Nanocomposites via a direct graphene-promoted "click"-reaction.** polymer., 2015. 79, 21-28
- **Shaygan Nia, A.,** and Binder, W. H. (2016) **Graphene as initiator/catalyst in polymerization chemistry.** Submitted

**Conferences (Proceeding)**

- **Shaygan Nia, A.,** Enders, C. and Binder, W. H. **Hydrogen bonded oligo (poly)-thiophene and perylene based derivatives as donor and acceptor materials in BHJ solar cell technology.** 15<sup>th</sup> International Conference in Polymeric materials, 12<sup>th</sup>-14<sup>th</sup> september **2012**, Halle(saale), Germany. Oral presentation
- **Shaygan Nia, A.,** Rana, S., Döhler, D., Osim, W. and Binder, W. H. **Graphene Supported Copper (I) Nanoparticels for self-healing nanocomposites.** 5th International conference on self-healing materials (ICSHM), 22<sup>nd</sup>-24<sup>th</sup> june **2015**, Durham, NC, USA. Oral presentation



### EIGENSTÄNDIGKEITSERKLÄRUNG

Ich erkläre an Eides statt, dass ich die vorliegende Dissertation mit dem Titel " Graphene supported Cu(I) nanocatalysts for application in CuAAC reactions and production of resin/graphene nanocomposites " selbstständig und ohne fremde Hilfe verfasst, keine anderen als die von mir angegebenen Quellen und Hilfsmittel benutzt und die den zitierten Werken wörtlich oder inhaltlich entnommenen Stellen als solche kenntlich gemacht habe.

Außerdem erkläre ich, dass ich die vorliegende Dissertation an keiner anderen wissenschaftlichen Einrichtung zur Erlangung eines akademischen Grades eingereicht zu haben.

Halle (Saale),

---

Ali Shaygan Nia